NASA Contractor Report 4041

On the Modelling of Non-Reactive and Reactive Turbulent Combustor Flows

Mohammad Nikjooy and Ronald M. C. So

GRANTS NAG3-167 and NAG3-260
APRIL 1987

NASA

NASA Contractor Report 4041

On the Modelling of Non-Reactive and Reactive Turbulent Combustor Flows

Mohammad Nikjooy and Ronald M. C. So
Arizona State University
Tempe, Arizona

Prepared for
NASA Lewis Research Center
and Defense Advanced Research Project Agency
under Grants NAG3-167 and NAG3-260

NASA
National Aeronautics
and Space Administration

**Scientific and Technical
Information Branch**

1987

TABLE OF CONTENTS

NOMENCLATURE

A	area of control volume surface
C_1	coefficient in modelled form of $\Pi_{ij,1}$, Eq. (2.13)
C_2	coefficient in modelled form of $\Pi_{ij,2}$,Eqs. (2.14-2.16)
C_{R1}	constant in eddy break-up model, Eq. (2.71)
C_{R2}	constant in eddy break-up model, Eq. (2.72)
C_p	specific heat at constant pressure
C_s	coefficient in equations (2.18) and (2.19)
C_μ	coefficient in equation (2.27)
C_ε	coefficient in equation (2.24)
$C_{\varepsilon 1}$	coefficient in modelled production of ϵ, Eq. (2.24)
$C_{\varepsilon 2}$	coefficient in modelled destruction of ϵ, Eq. (2.24)
$C_{1\theta}$	coefficient in equation (2.22)
$C_{2\theta}$	coefficient in equation (2.23)
$C_{\theta 2}$	coefficient in equation (2.25)
$C_{D\theta 2}$	coefficient in equation (2.25)
$C_{s\theta}$	coefficient in equation (2.20)
E_1	activation energy
$\overset{*}{E}$	roughness parameter
f	mixture fraction

$F(\tilde{\theta})$ assumed density weighted pdf of $\tilde{\theta}$

h stagnation enthalpy

H_c heat of combustion

j_i diffusion flux of scalar in the x_i direction

k turbulent kinetic energy

k_1 pre-exponential constant for Arrhenius reaction rate

k_2 pre-exponential constant for Arrhenius reaction rate

ℓ characteristic turbulence length scale

ℓ_m mixing length

m mass fraction of species

p static pressure

p' fluctuating pressure

P_{ij} production rate of Reynolds stress tensor, Eq. (2.15)

P_k production rate of turbulent kinetic energy, Eq.(2.15)

r polar radius in axisymmetric flows

R universal gas constant

R_T turbulent Reynolds number $k^2/\nu\epsilon$

S_{ij} strain rate tensor, Eq. (2.14)

t time

T averaging time

T temperature

$\tilde{u}_i$ instantaneous velocity component (i=1,2,3)

$\overline{u^2}$ streamwise component of Reynolds normall stress

u_τ friction velocity $(\tau_w/\rho)^{.5}$

U Favre-averaged streamwise velocity

$\overline{v^2}$ radial component of Reynolds normall stress

V Favre-averaged radial velocity

$\overline{w^2}$ azimuthal component of Reynolds normall stress

W azimuthal component of Reynolds normall stress

x streamwise direction

y distance from wall

y^+ dimensionless wall distance

Greek Symbols

α coefficient in modelled form of $\Pi_{ij,2}$, Eq. (2.16)

β coefficient in modelled form of $\Pi_{ij,2}$, Eq. (2.16)

γ coefficient in modelled form of $\Pi_{ij,2}$, Eq. (2.16)

Γ gamma function

Γ_{false} false (numerical) diffusion coefficient, Eq. (3.2)

δ_{ij} Kronecker delta

ϵ dissipation rate of turbulent kinetic energy

ϵ_{ij} dissipation rate tensor of Reynolds stresses

κ the von Karman constant

θ scalar fluctuation

Θ Favre-averaged of scalar

μ dynamic viscosity of fluid

μ_t turbulent viscosity, Eq. (2.27)

ν kinematic viscosity of fluid

Π_{ij} pressure-strain term

$\Pi_{ij,1}$ fluctuating velocity part of Π_{ij}

$\Pi_{ij,2}$ mean strain part of Π_{ij}

$\Pi_{i\theta}$ pressure-scalar-gradient correlation

$\Pi_{i\theta,1}$ turbulence interaction part of $\Pi_{i\theta}$

$\Pi_{i\theta,2}$ mean strain part of $\Pi_{i\theta}$

ρ density of fluid

σ_k turbulent Prandtl number for k

σ_ε turbulent Prandtl number for ϵ

τ_w wall shear stress

τ_{ij} viscous stress tensor

Φ any dependent variable

Subscripts

E	value at node east of P
EBU	denotes eddy break-up model
fu	fuel
F	fuel stream
N	value at node north of P
ox	oxidant
O	oxidant stream
pr	product
st	denotes stoichiometric value
S	value at node south of P
t	turbulent
W	value at node west of P

SUMMARY

A numerical study of non-reactive and reactive axisymmetric combustor flows with and without swirl is presented. Closure of the Reynolds equations is achieved by three different levels of models: k-ϵ, algebraic stress and Reynolds stress closure. Performance of two locally non-equilibrium and one equilibrium algebraic stress models is analyzed assuming four different pressure-strain models. A comparison is also made of the performance of a high and a low Reynolds number model for combustor flow calculations using Reynolds stress closures. Effects of diffusion and pressure-strain models on these closures are also investigated. Two different models for the scalar transport are presented. One employes the second-moment closure which solves the transport equations for the scalar fluxes, while the other solves the algebraic equations for the scalar fluxes. In addition, two cases of non-premixed and one case of premixed combustion are considered. Fast- and finite-rate chemistry models are applied to non-premixed combustion. Both models show promise for application in gas turbine combustors. However, finite rate chemistry models, which are more realistic, need to be further examined to establish a suitable coupling of the heat release effects on the turbulence field and the rate constants.

CHAPTER 1

INTRODUCTION

1.1 BACKGROUND

The calculation of turbulent combusting flows has received considerable attention in recent years. This is due to different reasons. Some of these are: demands for higher efficiency combustors, higher cost of measurement instruments, rapid growth of computer technology, limitation of fossil fuel resources, and a better understanding of pollutant formations which jeopardize the ecology in industrial societies. As a result, an increased interest in combustion modelling has been generated by researchers in this area.

At first, attention is only given to the handling of the complexities of real chemical reactions, which involve scores of individual species (Lavoie, et al.,1970). In reality, fifty to one hundred elementary reactions, involving ten to fifty chemical species, are required for a complete description of the kinetic process. Typical examples are concerned with the accurate calculation of the equilibrium composition of the gases in a rocket nozzle, followed by the kinetically-influenced variation of the composition of the gases as they flow through the nozzle.

Later, two- and three-dimensional variations in space and variations in time are taken into account (Butler and O'Rouke, 1977; Griffin et al., 1978), and the development of "turbulence models" permits realistic representation of the flow patterns and chemical reactions.

In order to construct a comprehensive combustion model, the problem may be broadly grouped into three categories: numerical methods, turbulence models, and chemical kinetics. There are some serious numerical obstacles involved in a comprehensive combustion model. Time scales associated with molecular transport and chemical reactions are vastly different, and there are sharp gradients in the temperature and density fields. Simulation of such a process would involve a set of partial differential equations that include mass, momentum, energy and species conservation. This set of equations describing the combustion flow field are coupled and generally they cannot be easily solved by conventional procedures because of extremely disparate physical scales introduced by steep gradients involved in the reaction processes. For example, in the work done by Dwyer and Sanders (1977), a numerical technique known as operator splitting was used to compensate for the vastly different time scales associated with molecular transport, chemical transport and unsteady wave propagation. The fluid dynamics portion of the model problem was solved using explicit finite difference scheme, while the split reaction terms

were solved by an ordinary differential equation technique. Otey (1978) has presented a review of different numerical methods. His work retained the essential features of chemical flows and allowed insight into the numerical difficulties involved in the solution of such a complex system.

However, among the most important questions in current combustion research are those regarding the role of interaction between the fluid mechanics and the chemical reactions (Smoot and Hill,1983). Chemical reactions take place in the molecular level. On the other hand, turbulent motion plays an important role in the mixing of the reacting species. Local turbulence controls the time and frequency that each of the reactants and products are mixed together, thus allowing reaction to proceed. In turn, the local instantaneous reaction processes themselves, often associated with local heat release or absorption, density and volume changes,etc. can impact the local turbulent fluid mechanics.

In practice, the fluid mechanics and chemical kinetics are so complex that various modelling assumptions are required to render the solution of the conservation equations possible. These assumptions which combine physical reality with ease of formulation are concerned with the turbulent nature of the flow, the flame, the combustion characteristics, and the radiative heat transfer from the

products of combustions. Improper models result in erroneous prediction of combustion efficiency, temperature distribution in the combustion system and pollutant formations.

Numerous turbulence models have successfully been devised for constant properties flows (Launder et al.,1975; Lumley,1975a; Reynolds,1976). These provide the basis for extension to flows with variable properties and combustion. However, one of the main problem in devising physically valid models for reactive flows lies in the characterization of the time-mean net rate of formation or destruction of the molecular species due to chemical reactions (Pratt,1979 ;Bilger,1980). Although the kinetic mechanisms are not always known and kinetic rate constants are difficult to identify, the major problem lies not in these areas but in obtaining the proper time-mean rate of formation or destruction of molecular species due to the presence of turbulence (Borghi,1974). Analytical expressions relating the instantaneous reaction rates to associated flow quantities are always highly non-linear functions of the temperature and species concentrations, and thus the knowledge of the mean values of these latter quantities is insufficient to allow the evaluation of the mean formation rates (Pratt,1979). In order to express the mean formation rate in a correct manner, it is convenient to use the technique of Reynolds decomposition and express the

Arrhenius term in terms of an infinite series involving the mean values of the scalars and their higher statistics and cross-correlations. This series is not always convergent because the correlation terms can be of comparable magnitude with the mean quantities (Borghi,1974). Depending on the type of reactions considered and on the chemical species involved, Borghi (1974) estimated that at least seven terms, involving third and lower order moments of the scalars, in the expansion have to be considered. For any realistic combustion scheme, many equations of this type are present. Therefore, it is clear that closure of turbulent reacting flow is a formidable problem. This problem was recognized by various researchers and different alternate paths have been suggested. A review of the state of the art of different combustion models for turbulent diffusion flames has been given by Bilger (1976).

The effects of these chemistry-turbulence interactions are quite different for different types of chemical reactions. To help identify these effects, it is convenient to identify two hypothetical time scales: the reaction time scale and the turbulent time scale. The reaction time scale is defined as a typical time for the reacting species of interest to react completely to its equilibrium value. The turbulence time scale is chosen to be a typical fine-scale mixing time for scale reduction by turbulent breakup of large eddies. This time scale must be adequate for molecular

interaction to take place (micromixing). The turbulence time scale then is the time required for mixing to proceed to the molecular level before reaction can occur. The reaction time scale is the time required for these reacting species, once contacted, to react completely to form their products. Approaches for incorporating chemical reactions in turbulent systems can be characterized by examining the relationship between these two time scales.

If the reaction time scale, t_r, is much greater than the turbulent time scale, t_t, then the reactions are very slow compared to changes in the local turbulence. In this case, if the fluctuations of any variable are very small, the chemistry is unaware of the presence of the turbulent fluid mechanics, and the effect of the fluctuations on the reaction rate can be ignored. However, the mean reaction rate is highly sensitive to temperature fluctuations. Thus, even though reaction rates are slow but significant temperature fluctuations exist, still the mean reaction rate should account for turbulence effects. Therefore, only in the very special case is the mean reaction rate equal to the reaction rate calculated from the mean variables. Although this approximation has been used by many researchers, it has been shown to be valid only in a very limited number of cases. When reaction rates are not suffeciently slow compared to the local turbulence, the use of this approximation produces appreciable error (Pratt, 1979).

When the reaction time scale is of the same order of magnitude as the turbulent time scale, both the chemical kinetics and the turbulent fluctuations must be accounted for. It is this area that has been identified by combustion researchers as the area that has the most need of specific research advances (Smoot and Hill, 1983). Recently, Bilger (1978) reported an important experimental observation relating to chemistry/turbulence interaction in a diffusion flames. Over a broad region of a given non-equilibrium, laminar, hydrocarbon diffusion flame, the molecular species composition was only a function of the equivalence ratio, even though the products were not in thermodynamic equilibrium. He concluded that the species reaction rate seems to be only a function of the mixture fraction in these flames. This observation holds great significance for the interactions between kinetically limited chemistry and the turbulent flow field. If the expeimental data base could be extended to turbulent flames with similar relationships between local instantaneous chemical composition and the local instantaneous conserved scalar, then statistical techniques for calculating mean composition could be extended to non-equilibrium combustion (Bilger, 1980).

However, reactions associated with heat release in the high temperature oxidation of hydrocarbon fuels have time scales very short compared to the time scale of the turbulent micromixing process (Libby and Williams,1980). In

this case, the reactions occur quickly once the reacting species are mixed together. The fast chemistry assumption can then be applied. Unfortunately this assumption can be applied only to situatioins where the fuel and oxidant enter in separate streams. In this type of turbulent reacting flows, the assumption can be made that the micromixing process is rate limiting and not the chemical kinetic process. Thus, as far as the overall flame is concerned, the chemistry is fast enough to be considered in local instantaneous equilibrium. Therefore, fuel and oxidant cannot both exist at the same point. Once the reactants are mixed through turbulent motions, the reactions proceed to equilibrium instantaneously. If the assumptions are made that all species and heat diffuse at the same rate and the heat loss to the surrounding is negligible compared with the heat release, then the instantaneous chemical composition and temperature can be determined in terms of a single conserved scalar quantity. For these cases, the conventional conserved scalar or mixture fraction is defined to identify the degree of "mixedness" at a point. With these simplifications, the reacting flow problem is reduced to an equivalent non-reacting mixing problem (Bilger, 1980). A significant weakness in this approach is that no details concerning the formation and emission of carbon monoxide, nitric oxide, and unburnt fuel are available. All these require consideration of finite rate chemistry. However,

this method is sufficient even when equilibrium cannot be assumed, but the reaction rates are sufficiently fast that chemical composition is only a function of the local equivalance ratio, and thus only a function of the mixture fraction. Physically, this implies that the reactions proceed quickly to some condition that approximates the equilibrium condition (Smith and Smoot, 1981).

The mean density can be evaluated once the scalar probability density function (PDF) is known. With appropriate incorporation of the intermittency of pure fuel or oxidant streams, some effects of turbulence on the chemical reactions can be accounted for. The approach adopted involves specifying a two-parameter PDF. The mean and variance of the conserved scalar which are determined from solutions of their respective transport equations can be used to determine the unknowm parameters. Different two-parameter PDF's have been proposed and tested by a number of researchers (Spalding,1971 ; Lockwood and Naguib,1975 ; Rhode,1975). However, evidence in support of the beta-distribution has been provided by Jones (1977) in his calculation of diffusion flames.

Despite the rapid advances made in computer technology, a direct solution of the time-dependent conservation equations for turbulent flows is not currently practical. For example, the calculation of the diurnal cycle by Deardorf (1974) using a sub-grid-scale scheme required a

week's computing time using the whole resources of a CDC 7600 computer. The conventional technique is to solve the time-averaged equations. In this way, the equations become identical to the instantaneous form of the equations only in the time-mean variable, but there are a large number of extra terms involving the fluctuating components (Borghi, 1974). Terms such as $\rho\overline{u_i u_j}$, $U\overline{\rho' u_i}$, etc. appear. A constant density flow simplifies these problems greatly since $\rho'=0$. For variable density flow, more often, it is assumed that ρ' is not correlated with u_i, thus, terms involving ρ' are neglected and the equations reduce to those for the constant density flow. However, some measurements cited by Bilger (1976) indicate that terms such as $U\overline{\rho' v}$ can be of the same order as $\rho\overline{u_i u_j}$ and sometimes greater than the turbulent momentum flux $\overline{\rho uv}$. However, there is a way to circumvent this difficulty. Bilger (1975;1976) points out how Favre averaging can be applied to deal with this problem. In Favre averaging, quantities are weighted by the instantaneous density before averaging. The resulting partial differential equations are identical in form to the uniform density flow equations, except Favre-averaged variables replace the conventional Reynolds-averaged ones (Favre, 1969). Furthermore, the density remaining in the equation is still the time mean density.

In the fluid mechanics area, a survey of the mean-turbulence-field closure models by Mellor and Herring (1973)

gives an excellent discussion of what has been achieved in the mathematical modelling of turbulence up to 1973. Spalding (1975) gives a discussion of solved and unsolved problems in turbulence modelling. He focuses on the k-ϵ model and enumerates its advantages and shortcomings. It is the deficiencies in the k-ϵ model which have encouraged developments in more advanced turbulence modelling. Different classes of turbulence models have been developed such as Reynolds stress closures (Hanjalic and Launder,1972), algebraic stress/scalar flux closures (Mellor and Yamada,1974 ; Rodi, 1976; Gibson and Launder, 1976), sub-grid-scale scheme (Deardorff, 1973,1975; Schumann,1975 ; Kwak et al., 1975), etc. All of these focus on the non-isotropic nature of the eddy viscosity.

In Reynolds stress closures, the stress components are no longer related to the local mean strain rates but are determined from their transport equations (Launder,1979). A similar approach is used to determine the turbulent scalar fluxes. Models employing transport equations for the individual turbulent stress and flux components simulate the turbulent processes most realistically and are therefore potentially better than simpler models. However, they are not thoroughly tested and computationally more expensive, and hence at the present state of development not very suitable for practical applications. However, they are important as a starting point for deriving algebraic

expressions for the turbulent stresses and fluxes (Rodi,1976; Mellor and Yamada,1974). It seems that such expressions, together with k and ϵ equations, are sufficient for most engineering problems and that there are hardly any cases where a full transport equation model is needed. They combine, at least to some extent, the numerical simplicity of the k-ϵ model with the generality of the Reynolds stress closures when it comes to accounting for the effect of body forces such as buoyancy and rotation. Finally, a completely different turbulence modelling approach is to solve the Navier-Stokes equations directly by simulation and modelling only the sub-grid-scale turbulence. The present computers are too small and too slow to resolve the small-scale turbulent motion in a numerical solution. However, the computer capacity is sufficient to solve the time-dependent equations for the large scale motions; the small-scale turbulence that cannot be resolved with the chosen numerical grid must then be approximated by a model. The small-scale turbulence is much less problem-dependent than the large scale turbulence so that the sub-grid-scale turbulence can be represented by relatively simple models. This approach appears very promising for solving three-dimensional time-dependent problems. Kim (1985) used 128x129x128 computational grid points for direct numerical simulation of turbulent flow in a channel. He used the temperature as a passive scalar to investigate the interaction of the wall-

layer structure with the outer layer. Herring (1979) gives a short introduction and overview to subgrid modelling and Love and Leslie (1979) give more details. The greatest drawback with this approach is the huge amount of computing time involved. For this reason, they are being looked upon as methods of improving the modelling approximations of simpler closures.

In view of the similarity of the density-weighted averaged equations to those for uniform-density flow, the idea has emerged that existing uniform density models may be adapted to non-uniform density turbulent flows simply by substituting the density-weighted variables for the standard average variables in a particular model. Bilger (1976, 1977, 1979) advocates this hypothesis of turbulent model similarity. However, not much work has been done in this area. Therefore, our present objective is to try to establish the validity of constant-density models for variable density flows.

1.2 OBJECTIVES

The main objectives of this research are:

A. To evaluate and identify the most general and efficient model for turbulent momentum exchange in swirling and non-swirling combustor flow calculations. The evaluations will include k-ϵ model, algebraic stress models and full Reynolds stress models.

B. To provide a review of the existing turbulent scalar flux models and to evaluate and identify the most general and efficient scalar flux model for swirling and non-swirling combustor flows.

C. The validity of these models for variable-density flows is examined and their applicability is demonstrated by comparison with measurements.

D. The turbulence models identified above will be applied to calculate premixed and non-premixed reacting flows using both fast and finite rate chemistry models. Their validity will be examined in detail.

E. Finally, the effect of heat release on the turbulent flow field is examined, and the validity and extent of constant-density turbulence models for reacting flow calculations is assessed.

1.3 OUTLINE OF THE REPORT

The remainder of the report consists of five chapters and the accompanying appendices.

In chapter 2, the problem of calculating turbulent flows is posed more precisely by introducing and discussing the density-weighted averaged equations governing the mean-flow quantities. The appearance of turbulent transport terms

in these equations makes apparent the necessity of introducing turbulence models. The heart of this chapter is the actual review of models in the sections 2.3 to 2.4; the models are discussed in order of increasing complexity. Section 2.5 considers the extension of the turbulence models to include the low Reynolds number region that is always found in the immediate vicinity of a smooth wall. Although this region usually occupies less than 1% of the flow domain, it is of significant importance because 50% of the change in mean velocity occurs across it. Section 2.6 turns the attention to the modelling of combustion processes. It will discuss the cases of non-premixed and premixed reactants, respectively.

Chapter 3 presents the details of the solution procedure adopted for the highly coupled and non-linear governing equations. This chapter briefly discusses numerical (false) diffusion which may or may not seriously affect the accuracy of the solution. A scheme is introduced to reduce this source of error.

In chapter 4, the effects of four different pressure-strain models on three different algebraic stress closures (ASM) for swirling and non-swirling turbulent flows are investigated. The results are compared with the standard k-ϵ model. Having demonstrated the effect of the pressure-strain correlation and determined its suitable model, attention is turned to the performance of the Reynolds stress closure

(RSM). A comparison is made of the performance of a high and a low Reynolds number Reynolds stress closure. Effects of two different turbulent diffusion models on RSM are also analysed and the results are compared with the standard k-ϵ model and some algebraic stress closures. For swirling flows, comparison of standard k-ϵ model, ASM and RSM are made using the diffusion model and pressure-strain model which are found to perform the best for non-swirling flow calculations. As for the scalar field calculations, effects of two pressure-scalar-gradient models on two different algebraic scalar flux models (AFM) are analysed and the results are compared with the full Reynolds stress/flux closure. Finally, comparison of three different ASM and the k-ϵ model are made for variable-density swirling flows and the results are discussed.

Chapter 5 discusses the results of non-premixed and premixed combustion models. Both fast and finite rate chemistry models are applied to non-premixed combustion. However, in contrast to non-premixed flames, premixed flames require the consideration of finite rate reaction only. In this case, a two-step reaction process is used and the mean formation rates are calculated from the Arrhenius reaction rates and also the eddy break-up model.

Finally, chapter 6 summarises the main conclusions emerged from this study and put forward some recommendations for future work.

CHAPTER 2

GOVERNING EQUATIONS FOR VARIABLE-DENSITY FLOWS

2.1 MEAN EQUATIONS IN FAVRE-AVERAGED FORM

In this section, the equations which govern the distribution of the mean flow quantities are presented. These equations are derived from the conservation laws of mass, momentum and scalar which can be expressed in Cartesian tensor notation as:

mass conservation :

$$\frac{\partial \rho}{\partial t} + \frac{\partial \rho \tilde{u}_i}{\partial x_i} = o, \tag{2.1}$$

momentum conservation :

$$\rho \frac{\partial \tilde{u}_i}{\partial t} + \rho \tilde{u}_j \frac{\partial \tilde{u}_i}{\partial x_j} = - \frac{\partial \tilde{p}}{\partial x_i} + \frac{\partial \tilde{\tau}_{ij}}{\partial x_j} \quad , \tag{2.2}$$

scalar conservation :

$$\rho \frac{\partial \tilde{\theta}}{\partial t} + \rho \tilde{u}_j \frac{\partial \tilde{\theta}}{\partial x_j} = - \frac{\partial \tilde{J}_i}{\partial x_i} \tag{2.3}$$

where $\tilde{u}_i$ is the component of instantaneous velocity in the x_i direction, $\tilde{p}$ is the instantaneous static pressure, $\tilde{\theta}$ is an instantaneous scalar quantity, $\tilde{j}_i$ is the diffusion flux of scalar $\tilde{\theta}$ in the x_i direction, and $\tilde{\tau}_{ij}$ is the instantaneous viscous stress tensor.

Turbulent flows contain motions which are much smaller than the extent of the flow domain. In order to resolve these motions in a numerical procedure, the mesh size of the numerical grid would have to be even smaller. Storing the flow variables at so many grid points is beyond the capacity of present computers. For this reason, turbulent flow is normally analysed using statistical methods. Following Reynolds, the instantaneous quantities are separated into mean values and their fluctuations. For variable density flows two types of decomposition can be used; either the unweighted form conventionally used for constant density flows or the density-weighted decomposition suggested by Favre (1969). The unweighted decomposition and averaging of flow variables are represnted by

$$\tilde{u}_i = \bar{U}_i + u_i'$$

where

$$\bar{U}_i = \lim_{T \to \infty} \frac{1}{T} \int_t^{T+t} \tilde{u}_i \, dt \qquad \text{and} \quad \bar{u}_i' = 0$$

which the density-weighted decomposition and averaging are defined as:

$$\tilde{u}_i = U_i + u_i$$

where

$$U_i = \lim_{T \to \infty} \frac{1}{T} \int_t^{T+t} \frac{\tilde{\rho}\tilde{u}_i}{\rho} \, dt$$

Since by definition $\overline{\rho u}_i \equiv 0$, it can be shown that $\overline{u}_i \neq 0$ and $\overline{\rho}\overline{u}_i = -\overline{\rho' u'_i}$. The averaging time T is long compared with the largest turbulence time scales, but shorter than the period over which the average flow quantities may vary. In general, the averaging process should involve ensemble averaging, but for stationary flows, time averaging and ensemble averaging are the same (Lumley, 1970). For high Reynolds number flows, after noting that density weighting is not to be applied to either the pressure or density , the Favre-averaged forms of the equations of continuity and conservation of momentum and scalar may be written as

$$\frac{\partial \bar{\rho}}{\partial t} + \frac{\partial}{\partial x_i}(\bar{\rho}\bar{U}_i) = 0 \ , \tag{2.4}$$

$$\frac{\partial \bar{\rho}\bar{U}_i}{\partial t} + \frac{\partial}{\partial x_j}(\bar{\rho}U_iU_j) = - \frac{\partial \bar{P}}{\partial x_i} - \frac{\partial}{\partial x_j}(\bar{\rho}\overline{u_iu_j}) \ , \tag{2.5}$$

$$\frac{\partial \bar{\rho}\bar{\Theta}}{\partial t} + \frac{\partial}{\partial x_i}(\bar{\rho}\bar{U}_i\Theta) = -\frac{\partial}{\partial x_i}(\bar{\rho}\,\overline{u_i\theta}) \ . \tag{2.6}$$

The unweighted averaging technique results in similiar equations but with two differences. Firstly, the density-weighted quantities are replaced by unweighted quantities. Secondly, correlations such as $\overline{\rho' u'}$ and $\overline{\rho' \theta'}$ appear in the equations.

There are some advantages for selecting the Favre averaged forms of the equations. It provides equations describing the mean values of those quantities which are conserved. For example, the component of mean momentum per unit volume in the x_i-direction is $\bar{\rho}U_i$ and not $\bar{\rho}\bar{U}_i$. In addition, the equations which arise from the application of the density-weighted averaging technique are of a much simpler form and are more easily interpreted than those obtained from unweighted averaging. For the reasons stated above, we will concern ourselves only with the density-weighted averaged forms of the governing conservation equations from now on.

As a consequence of the non-linearity of the equations (2.2) and (2.3), the averaging process used introduces unknown correlations. As a result, the equations are no longer closed and closure assumptions are necessary before solution is possible. The problem of calculating these correlations can be approached at different levels of complexity. It is the intention of this chapter to discuss in detail the appropriate turbulence closures for variable density flows. These include both turbulent viscosity and full Reynolds stress models.

2.2 REYNOLDS EQUATIONS IN FAVRE-AVERAGED FORM

For high Reynolds number turbulent flows, the equations that govern the transport of the Reynolds-stress tensor may be concisely expressed in Cartesian tensor form as

$$\bar{\rho}\frac{\partial}{\partial t}(\overline{u_i u_j}) + \bar{\rho}U_k\frac{\partial}{\partial x_k}(\overline{u_i u_j}) = \underbrace{-\frac{\partial}{\partial x_k}(\bar{\rho}\,\overline{u_i u_j u_k})}_{(a)} \underbrace{- \left(\overline{u_i \frac{\partial p'}{\partial x_j}} + \overline{u_j \frac{\partial p'}{\partial x_i}}\right)}_{(b)}$$

$$\underbrace{- \bar{\rho}\left(\overline{u_i u_k}\frac{\partial U_j}{\partial x_k} + \overline{u_j u_k}\frac{\partial U_i}{\partial x_k}\right)}_{(c)}$$

$$\underbrace{- \left(\overline{\tau'_{ki}\frac{\partial u_j}{\partial x_k}} + \overline{\tau'_{kj}\frac{\partial u_i}{\partial x_k}}\right)}_{(d)} \qquad (2.7)$$

Equation (2.7) is obtained by subtracting equation (2.5) from (2.2), multiplying the result by u_j and adding to it the same equation with subscripts i and j interchanged, then averaging the resultant equation. It expresses the rate of change of the Reynolds stresses as the sum of four different processes: (a) diffusion by the action of velocity fluctuations, (b) transport by fluctuating velocity-pressure gradient correlations, (c) generation of Reynolds stresses through the interaction of stresses with the mean strain rate, and (d) dissipation of Reynolds stresses through viscous action. The contraction of this equation, that is when the equations for the three normal stresses (i=j=1,2,3) are summed up, yields the turbulent kinetic energy equation.

The density-weighted averaged form of the equation for the scalar flux, $\overline{\rho u_i \theta}$ may be obtained by multiplying the fluctuating velocity equation by the fluctuating scalar,θ; then adding to it the equation for θ multiplied by u_i and averaging the result. Neglecting the influence of buoyant force and viscous diffusion, the result is expressed as:

$$\bar{\rho}\frac{\partial}{\partial t}(\overline{u_i\theta}) + \bar{\rho}\,U_m\frac{\partial}{\partial x_m}(\overline{u_i\theta}) = -\frac{\partial}{\partial x_m}(\bar{\rho}\,\overline{u_i u_m\theta} + \overline{p'\theta}\,\delta_{im}) + \overline{p'\frac{\partial\theta}{\partial x_i}}$$

(A) (B)

$$-\bar{\rho}(\overline{u_m\theta}\frac{\partial U_i}{\partial x_m} + \overline{u_i u_m}\frac{\partial\Theta}{\partial x_m}) - (\overline{\tau'_{ij}\frac{\partial\theta}{\partial x_j}} - \overline{j'_m\frac{\partial u_i}{\partial x_m}}) \qquad (2.8)$$

(C) (D)

The physical interpretion of the terms on the right hand side of (2.8), from left to right, is: (A) the diffusive transport due to velocity and pressure fluctuations, (B) transport due to the fluctuating pressure-scalar-gradient correlations, (C) the generation of scalar flux due to the mean gradients of the velocity and scalar fields, and (D) viscous dissipation.

2.3 MODELLING OF THE REYNOLDS EQUATIONS

2.3.1 MODELLING OF THE $\overline{u_i u_j}$-EQUATION

Of the terms on the right-hand side of equation (2.7), only the production term (c) can be calculated directly in a flow field where the velocities, Reynolds stresses and dissipation rate are known. Others, however, need to be modelled because they either include higher order correlations (term a) or correlations between turbulence quatities that are not known. The objective of this section

is to discuss each of these terms separately and to suggest approximate models for closure. In order to accomplish this task we shall make extensive use of models developed for uniform density flows and assume that the use of density-weighted averaging will partially account for the influence of density fluctuations (Jones, 1980).

The viscous dissipation correlation (d) is the least difficult term to model. This term represents the destruction of Reynolds stresses through viscous action. At high Reynolds number, the small scale structure of turbulence tends to be independent of any orientation effects introduced by the mean shear. Under these conditions, the small scale strucure of turbulence is in a state of local isotropy and the dissipation correlation as suggested by Kolmogorov (1941) can be expressed as

$$\bar{\rho}\,\epsilon_{ij} = \overline{\tau'_{ki}\,\frac{\partial u_j}{\partial x_k}} + \overline{\tau'_{kj}\,\frac{\partial u_i}{\partial x_k}} = \frac{2}{3}\,\delta_{ij}\,\bar{\rho}\,\epsilon \qquad (2.9)$$

where

$$\bar{\rho}\,\epsilon = \overline{\tau_{km}\,\frac{\partial u_m}{\partial x_k}}$$

is the dissipation rate of turbulent kinetic energy per unit volume. This model introduces another unknown into the problem; namely ϵ, the turbulent kinetic energy dissipation rate. Therefore, an equation for the dissipation rate must be solved in conjunction with the set of Reynolds-stress equations.

Term (b) is conventionally partition into two parts

$$\overline{u_i \frac{\partial p'}{\partial x_j}} + \overline{u_j \frac{\partial p'}{\partial x_i}} = \frac{\partial}{\partial x_k}(\delta_{jk}\,\overline{p'u_i} + \delta_{ik}\,\overline{p'u_j}) - \overline{p'\left(\frac{\partial u_i}{\partial x_j} + \frac{\partial u_j}{\partial x_i}\right)} \qquad (2.10)$$

where the first term on the right hand side of (2.10) is conventionaly identified as diffusive transport of $\overline{u_i u_j}$ due to p' and the second term is usually referred to as the pressure-strain term. This term is redistributive if the flow is incompressible, because the trace of this term is identically zero.

For variable density flows, the conventional partitioning of (2.10) does not result in a redistributive term since $\partial u_i/\partial x_i \neq 0$. An alternate partition which gives a

redistributive term has been suggested by Lumley (1975 b).It can be written as

$$\overline{u_i \frac{\partial p'}{\partial x_j}} + \overline{u_j \frac{\partial p'}{\partial x_i}} = \left(\overline{u_i \frac{\partial p'}{\partial x_j}} + \overline{u_j \frac{\partial p'}{\partial x_i}} - \frac{2}{3} \overline{u_m \frac{\partial p'}{\partial x_m}} \delta_{ij}\right)$$

$$+ \frac{2}{3} \overline{u_m \frac{\partial p'}{\partial x_m}} \delta_{ij} \qquad (2.11)$$

It can be seen that the first term on the right-hand-side of (2.11) gives a zero trace whether the flow is incompressible or not. The primary function of this term is to change the relative levels of the normal stresses, and to redistribute the turbulence energy in the stress equations.

From a practical point of view, all these arguments are quite immaterial, since none of the terms can be measured (Jones 1980). However, from the view point of turbulence modelling, the difference may be important. Thus if we want to apply the constant density models (which are redistributive) for variable density flows the latter decomposition (2.11) is recommended.

In order to gain further insight into the modelling of the redistributive term, a Poisson equation for the fluctuating pressure is derived. This is done by taking the

divergence of the equation for the fluctuating velocity u_i. The result is expressed as:

$$\frac{\partial^2}{\partial x_i^2} p' = -\frac{\partial^2}{\partial t^2} (\rho u_i + \rho' U_i) - \frac{\partial^2}{\partial x_i \partial x_j} (\rho u_i u_j - \overline{\rho u_i u_j} + \rho u_i U_j + \rho u_j U_i)$$

$$+ \frac{\partial^2 \tau'_{ij}}{\partial x_i \partial x_j} \qquad (2.12)$$

Equation (2.12) is much more complicated than its constant density version because $\partial U_i / \partial x_i \neq 0$. According to Jones (1980) some of the influence of density fluctuations could be partially accounted for by considering the Favre-averaged equations rather than the Reynolds-averaged equations. Besides, since the complete modelling of variable-density flows is, at present, hindered by a lack of credible data, therefore, it is more practical to apply constant density models.

Following Chou (1945) the redistributive part of the velocity-pressure gradient correlation, Π_{ij} , is divided into two types of terms: one containing fluctuating quantities alone ($\Pi_{ij,1}$) and the second due to mean strain effects, ($\Pi_{ij,2}$). Each contribution is ususally modelled separately. The term $\Pi_{ij,1}$ has long been recognized as the only mechanism in the stress transport equation (2.7) that could promote a return to isotropy. Rotta's (1951) proposal

for the modeling of $\Pi_{ij,1}$ has generally been adopted and is used in most Reynolds-stress equation models:

$$\Pi_{ij,1} = - C_1 \bar{\rho} \frac{\epsilon}{k} (\overline{u_i u_j} - 2 \delta_{ij} k/3) \qquad (2.13)$$

where ϵ/k defines a time scale and C_1 is a constant to be determined from experimental considerations.

A model to represent the interaction of mean strain and fluctuating velocities ($\Pi_{ij,2}$) was first devised by Rotta (1972). In the absence of external forces this can be written as:

$$\Pi_{ij,2} = -C_2 \bar{\rho} k \left(S_{ij} - \frac{2}{3} \delta_{ij} \frac{\partial U_m}{\partial x_m}\right) \qquad (2.14)$$

where

$$S_{ij} = \left(\frac{\partial U_i}{\partial x_j} + \frac{\partial U_j}{\partial x_i} \right)$$

Later, Naot et al. (1973) proposed that the effect of mean strain rate is to promote a similar return to isotropy in the Reynolds stress production tensor, i.e.

$$\Pi_{ij,2} = - C_2 \left(P_{ij} - \frac{2}{3} \bar{\rho} \overline{u_i u_j} \frac{\partial U_m}{\partial x_m} - \frac{2}{3} \delta_{ij} P_k \right) \qquad (2.15)$$

where

$$P_{ij} \equiv - \bar{\rho} \left(\overline{u_i u_k} \frac{\partial U_j}{\partial x_k} + \overline{u_j u_k} \frac{\partial U_i}{\partial x_k} \right),$$

$$P_k \equiv \frac{P_{ii}}{2}$$

Launder, Reece and Rodi (1975) suggested a model which takes into account effects due to both the symmetric and antisymmetric parts of the rate of strain tensor. Their model takes the form

$$\begin{aligned} \Pi_{ij,2} = & -\alpha \left(P_{ij} - \frac{2}{3} \delta_{ij} P_k - \frac{2}{3} \bar{\rho} \overline{u_i u_j} \frac{\partial U_m}{\partial x_m} \right) \\ & -\beta \left(D_{ij} - \frac{2}{3} \delta_{ij} P_k - \frac{2}{3} \bar{\rho} \overline{u_i u_j} \frac{\partial U_m}{\partial x_m} \right) \\ & -\gamma \bar{\rho} k \left(S_{ij} - \frac{2}{3} \delta_{ij} \frac{\partial U_m}{\partial x_m} \right) \end{aligned} \qquad (2.16)$$

where

$$D_{ij} \equiv \bar{\rho} \left(\overline{u_i u_k} \frac{\partial U_k}{\partial x_j} + \overline{u_j u_k} \frac{\partial U_k}{\partial x_i} \right),$$

$$\alpha = \frac{C_2 + 8}{11},$$

$$\beta = \frac{8C_2 - 2}{11},$$

$$\gamma = \frac{30C_2 - 2}{55}.$$

The remaining part of the fluctuating velocity-pressure gradient correlations is not redistributive and can be written as

$$\frac{2}{3}\,\delta_{ij}\,\overline{u_m\,\frac{\partial p'}{\partial x_m}} = -\,\frac{2}{3}\,\delta_{ij}\,\overline{p'\,\frac{\partial u_m}{\partial x_m}} + \frac{2}{3}\,\delta_{ij}\,\frac{\overline{\partial p' u_m}}{\partial x_m} \qquad (2.17)$$

Bilger (1976) has argued that the first term is associated with noise generation and is small. In constant density flows and in situations where the Boussinesq approximation is appropriate this term vanishes. The second term can be lumped into the diffusive transport terms. Hence, the diffusive transport of turbulent stresses includes three mechanism: (1) transport through fluctuating velocities, (2) transport through pressure fluctuations, and (3) molecular transport, which is negligible at high Reynolds number. Irwin's (1973) measurements of self preserving wall jets in an adverse pressure gradient show that the transport due to pressure fluctuations is negligible compared with that due to velocity fluctuations. Within these assumptions, the diffusive transport term reduces to the triple-velocity correlation only. Daly and Harlow (1970) modelled this term as

$$- \overline{u_i u_j u_k} = C_s \frac{k}{\epsilon} \overline{u_k u_m} \frac{\partial}{\partial x_m} (\overline{u_i u_j}) \qquad (2.18)$$

The left-hand-side of equation (2.18) is tensor-invariant but the right-hand-side alters under permutation of the indicies i,j and k. In order to have a model that is consistent tensorially, Hanjalic and Launder (1972) propose the following form for this correlation

$$-\overline{u_i u_j u_k} = C_s \frac{k}{\epsilon} [\overline{u_k u_m} \frac{\partial}{\partial x_m} (\overline{u_i u_j}) + \overline{u_i u_m} \frac{\partial}{\partial x_m} (\overline{u_j u_k}) + \overline{u_j u_m} \frac{\partial}{\partial x_m} (\overline{u_i u_k})] \qquad (2.19)$$

This formulation contains the Daly and Harlow modelling as its first term and possesses the correct tensor properties. Both (2.18) and (2.19) imply gradient transport of Reynolds stresses but whereas in (2.18) the diffusivities are the same for each stress component, the diffusivities evaluated from (2.19) are different for each stress component.

2.3.2 MODELLING OF THE $\overline{u_i \theta}$ -EQUATION

The mean field production term (C) in equation (2.8) is due to the combined action of mean velocity and mean scalar

gradients, the former tending to increase the scalar fluctuations and the latter the velocity fluctuations. This term is exact and does not need to be modeled. At high Reynolds number, the fine scale motions are assumed to be isotropic. Since there is no first-order isotropic tensor, the dissipative term (D) is zero. Consequently, model approximations have to be proposed for the diffusion term (A) and for the fluctuating pressure-scalar-gradient correlation term (B).

By neglecting pressure transport, Launder (1976) proposed the following gradient approximation for term (A):

$$-\overline{u_i u_m \theta} = C_{s\theta} \frac{k}{\epsilon} \left[\overline{u_m u_k} \frac{\partial}{\partial x_k} \overline{(u_i \theta)} + \overline{u_i u_k} \frac{\partial}{\partial x_k} \overline{(u_m \theta)} \right] \qquad (2.20)$$

where the coefficient $C_{s\theta}$ has been taken as 0.11 in conformity with the value of C_s in equation (2.19).

The most important process requiring approximation is the pressure-scalar-gradient correlation $\Pi_{i\theta}$. This term is the counterpart of the pressure-strain term in the Reynolds stress transport equations. This is the main term to counteract the production of the scalar flux and thus to limit its growth. With the aid of the Poisson equation for the fluctuation pressure, two different mechanisms which contribute to $\Pi_{i\theta}$ can be identified. One is due to pure

turbulence interaction, and the other arising from mean strain effect. Therefore, $\Pi_{i\theta}$ can again be partitioned into

$$\Pi_{i\theta} = \Pi_{i\theta,1} + \Pi_{i\theta,2} \tag{2.21}$$

The most widely used model for the first part is due to Monin (1965)

$$\Pi_{i\theta,1} = - C_{1\theta} \bar{\rho} \frac{\epsilon}{k} \overline{u_i \theta} \tag{2.22}$$

Equation (2.22) is a direct counterpart of Rotta's return to isotropy approximation (2.13) for the pressure-strain term $\Pi_{ij,1}$. Analogous to the pressure-strain model (2.15), Launder (1975) proposed that the second part should be proportional to the scalar flux production due to the mean strain, or

$$\Pi_{i\theta,2} = C_{2\theta} \overline{u_\ell \theta} \frac{\partial U_i}{\partial x_\ell} \tag{2.23}$$

2.3.3 THE DISSIPATION RATE TRANSPORT EQUATION

In anticipation of the fact that the quantity ϵ is required in turbulent flow calculations, we need to solve a transport equation for ϵ. For high-Reynolds-number variable

density flows, the transport equation for turbulent kinetic energy dissipation rate is given by Jones (1980)as:

$$\bar{\rho}\frac{\partial \epsilon}{\partial t} + \bar{\rho} U_m \frac{\partial \epsilon}{\partial x_m} = \frac{\partial}{\partial x_k}\left(C_\varepsilon \bar{\rho} \frac{k}{\epsilon} \overline{u_k u_m} \frac{\partial \epsilon}{\partial x_m}\right) - C_{\varepsilon 1} \bar{\rho} \frac{\epsilon}{k} \overline{u_i u_j} \frac{\partial U_i}{\partial x_j} - C_{\varepsilon 2} \bar{\rho} \frac{\epsilon^2}{k} \qquad (2.24)$$

Additional terms could be added to equation (2.24) for variable density flows. These terms are:

$$\frac{\epsilon}{k} \frac{\overline{\rho' u_i}}{\bar{\rho}} \frac{\overline{\partial p'}}{\partial x_i} \quad \text{and} \quad \bar{\rho}\epsilon \frac{\partial U_i}{\partial x_i}$$

However, this introduces more empiricism into the equation and there are no reliable means to determine the additional empirical constants. As a result, the additional terms for (2.24) are commonly neglected.

Equation (2.24) shows that the rate of change of ϵ is balanced by the diffusive transport, the generation of vorticity due to vortex stretching connected with the energy cascade, and viscous destruction of vorticity.

2.3.4 THE SCALAR FLUCTUATION TRANSPORT EQUATION

In connection with variable-density flow calculations, it is necessary to determine the scalar fluctuation quantities (Spalding, 1971). For high-Reynolds-numbers, the transport equation for the scalar fluctuation is given by Jones (1980) as:

$$\bar{\rho}\frac{\partial\overline{\theta^2}}{\partial t} + \bar{\rho}U_j\frac{\partial\overline{\theta^2}}{\partial x_j} = -2\bar{\rho}\,\overline{u_j\theta}\frac{\partial\Theta}{\partial x_j} + \frac{\partial}{\partial x_j}\left(C_{\theta^2}\bar{\rho}\frac{k^2}{\epsilon}\frac{\partial\overline{\theta^2}}{\partial x_j}\right) - 2C_{D\theta^2}\,\bar{\rho}\frac{\epsilon}{k}\overline{\theta^2} \qquad (2.25)$$

(AA) (BB) (CC)

The equation expresses the fact that the level of $\overline{\theta^2}$ following a mean stream-line will change through an imbalance of the generation rate of the scalar fluctuation by gradient in Θ (AA), through diffusive transport produced by turbulent velocity fluctuations (BB) and the dissipation of fluctuations due to molecular diffusion in the fine scale motions (CC). Equation (2.25) is the most straightforward of all turbulence transport equations; it resembles the turbulence kinetic energy equation except that pressure transport is absent from (2.25).

2.4 DIFFERENT LEVELS OF CLOSURE MODELS

The task of turbulence closure is to determine the turbulent flux terms in the mean-flow equations so that these can be substituted into the equations and thus allow the velocity, temperature and concentration fields to be solved. Turbulence models may be classified according to whether the turbulent momentum and heat/mass fluxes are assumed to be locally determined or whether they are obtained from their transport equations. The former approach is known as mean flow closure while the latter is called Reynolds stress closure.

In mean flow closures, turbulent viscosity relates the Reynolds stresses to the local strain field by an expression similar to that for laminar flow. However, the turbulent viscosity is a function of the properties of the turbulence and not of the fluid. A wide variety of models are available in the literature. However, these have only been applied to particular classes of thin shear flows. Since these models are not discussed in detail in later sections, it may be helpful to briefly mention some of the more pertinent work here. The simplest model that provides information about the distribution of the eddy viscosity, is the mixing-length hypothesis, generally attributed to Prandtl (1925). Prandtl, stimulated by kinetic gas theory, assumed that the eddy viscosity ν_t is proportional to a mean fluctuating velocity

ϑ and a mixing length ℓ_m. Considering shear layers with only one significant turbulent stress ($\overline{uv}$) and velocity gradient ($\partial U/\partial y$), he then postulated that ϑ is equal to the mean velocity gradient times the mixing length. The closure problem is then reduced to a determination of the mixing length ℓ_m. Prandtl found that simple algebraic prescription ℓ_m leads to fairly good results for simple shear flows.

Recognizing that the level of turbulence at a point in the flow is determined not just by local events but by convective and diffusive behavior too, Prandtl (1945) proposed that the square root of the turbulence kinetic energy, k should be adopted as the characteistic fluctuating velocity and that its value should be determined from a transport equation. The mixing-length ℓ_m is typically described with the aid of empirical information. The general form of the equation he proposed is still in use today in models of the "one-equation" type. Two further one-equation models also deserve mention. Nee and Kovasznay (1969) devised a transport equation for the turbulent viscosity itself while Bradshaw et al. (1967) developed a simplified transport equation for the shear stress. The latter model was suitable for calculating thin shear flows where the shear stress did not change sign; it has been extended to allow reversal in the shear stress across the layer (Bradshaw et al. , 1974). Unlike boundary-layer flows on a smooth wall, there are no simple rules that can serve to

give the length scale in a separated flow. The only way to obtain a reasonably accurate estimate of the length scale distribution is to calculate it, like the turbulent kinetic energy, from a simulated length scale equation.

Two-equation models are the simplest models that are suitable for complex flows in which the length-scale cannot be prescribed empirically in an easy way. The various length-scale equations proposed in the literature have very similar performance; the ϵ-equation become most popular because of its relative simplicity. The standard k-ϵ model is based on the assumption that the eddy viscosity is the same for all Reynolds stresses $\overline{u_i u_j}$. However, in certain flow situations the assumption of an isotropic eddy viscosity is too crude; for example it does not produce the turbulence-driven secondary motions in square ducts which have been observed experimentally (Meroney, 1976). To allow for the non-isotropic behavior of the eddy viscosity and to account for the effect of body forces (buoyancy , rotation), the k-ϵ model is refined by introducing algebraic stress model. This model is based on a simplification of the Reynolds stress equations that allows the equations to be reduced to algebraic equations for $\overline{u_i u_j}$. Since the quantities k and ϵ are present in these equations, their transport equations also have to be solved.

In the Reynolds stress closure, the stress components are no longer coupled to the local mean strain rates but are

determined from their transport equations. Models employing transport equations for the individual turbulent stress and flux components simulate the turbulent processes more realistically and are therefore potentially more general than the simple models.

Combustor flows are very complicated. They contain different flow regions such as: (1) inviscid core region, (2) recirculation zone, (3) shear region between regions (1) and (2), (4) reattachment region, (5) recovery region and ordinary boundary layer along the wall. Each region has its particular turbulence characteristics. Therefore, any proposed model has to be general enough to predict all these different regions if it is to be successful in combustor flow calculations. It is not possible to specify empirically the length-scale distribution in such complex flows. As a result, attention is given to turbulent transport models in which at least one turbulent velocity and length-scale is found from the solution of approximated transport equations. Only turbulence models of at least this degree of complexity are suitable for complex combustor flow calculations. Therefore, the standard k-ϵ model, algebraic stress model and Reynolds stress model are the only qualified models for combustor flow calculations.

2.4.1 k-ϵ MODEL

The k-ϵ model developed by Jones and Launder (1972) is the simplest model which is suitable for recirculating flow calculations. This model achieves closure by using a gradient transport model for $\overline{u_i u_j}$, or

$$- \bar{\rho}\, \overline{u_i u_j} = - \frac{2}{3} \delta_{ij} \left(\bar{\rho}\, k + \mu_t \frac{\partial U_m}{\partial x_m} \right) + \mu_t S_{ij} \qquad (2.26)$$

The effective (turbulent or eddy) viscosity μ_t appearing in (2.26), is defined in terms of a characteristic length and velocity. If this length is taken as the turbulence length scale $k^{3/2}/\epsilon$,and the velocity is approximated by $k^{1/2}$, μ_t can be expressed as

$$\mu_t = C_\mu \bar{\rho} \frac{k^2}{\epsilon} \qquad (2.27)$$

where C_μ is a constant of proportionality.

The k-ϵ model is the simplest model that allows the characteristic length scale of a wide range of complex flow fields to be determined. It has been applied to the calculation of various free shear flows (Launder et al., 1973), recirculating flows (Sindir, 1983a, 1983b), and

confined reacting flows with and without swirl (Smith and Smoot, 1981). In direct comparison of the k-ϵ model predictions with experimental data, the model is successful in predicting the basic features of turbulent flows. When significant streamline curvatures are introduced into the flow field, the k-ϵ model does not adequately account for the enhanced turbulence diffusion caused by the extra strain rates associated with streamline curvature. The standard k-ϵ model is based on the isotropic eddy viscosity assumption. However, in the calculation of simple thin shear layers where only the shear stress, $\overline{uv}$, appears in the equations, the closure is not influenced by the isotropic assumption. In other flow situations where such simplifications are not realized, models based on isotropic turbulent viscosity often lead to unsatisfactory flow predictions. To allow for the non-isotropic behavior of the eddy viscosity in such cases, the k-ϵ model is often modified by introducing the algebraic stress model to replace the isotropic eddy viscosity assumption. The axisymmetric form of the turbulent flow equations is given in appendix A for the k-ϵ model.

2.4.2 THE ALGEBRAIC STRESS/FLUX MODELS

The algebraic stress model (ASM) is a special case of the Reynolds stress model. It relates the individual stresses to mean velocity gradient, turbulent kinetic energy

and its dissipation rate by way of algebraic expressions. Algebraic stress models, hereafter denoted by ASM for short, can be classified into two categories. The first is based on a local equilibrium assumption for the turbulence field, whereby the turbulence transport terms are neglected compared to the local production and dissipation of turbulence. A second class of ASM is based on the local non-equilibrium assumption. Approaches of this kind, where the convection and diffusion transport of turbulent stresses are approximated, have been developed by Mellor and Yamada (1974,1982) and Rodi (1976).

The equilibrium ASM, hereafter denoted by ASM/E, is obtained when the convective and diffusive transport terms in the Reynolds stress transport equation (2.7) are assumed to be zero. With this simplification, (2.7) reduces to

$$P_{ij} - \frac{2}{3}\delta_{ij}\epsilon + \Pi_{ij} \simeq 0. \qquad (2.28)$$

With suitable modelling for Π_{ij}, (2.28) becomes algebraic in $\overline{u_i u_j}$ and can be solved in terms of k, ϵ and S_{ij}. Many flows, in particular thin shear layers, evolve so slowly that neglecting the convection and diffusion of turbulent stresses and fluxes can be justified. It should be mentioned however, that these simplified relations lead to an inconsistancy in the normal stresses when dissipation is not

balanced by production, because the resulting normal stresses do not sum up to 2k as they should.

Mellor and Yamada propose to simplify the Reynolds transport equations through an order-of-magnitude argument based on $a^2 = O(a_{ij})^2$, where a_{ij} is a non-dimensional measure of anisotropy and is given by

$$a_{ij} = \frac{\overline{u_i u_j}}{2k} - \frac{\delta_{ij}}{3} \tag{2.29}$$

The order-of-magnitude argument is performed on an equation for $(2a_{ij}k)$ which is obtained by subtracting the product of $\delta_{ij}/3$ and the transport equation for turbulent kinetic energy from the transport equation for $\overline{u_i u_j}$. The resultant equation becomes

$$\mathcal{L}(\overline{u_i u_j} - \frac{2}{3}\delta_{ij}k) = \mathcal{L}(2a_{ij}k) = P_{ij} - \frac{2}{3}\delta_{ij}P_k + \Pi_{ij} \tag{2.30}$$

where the differential operator $\mathcal{L}$ is used to denote the combined convective and diffusive transport operators. Terms in (2.30) are evaluated in powers of a and terms of order a^2 and higher are neglected. The result is

$$P_{ij} - \frac{2}{3}\delta_{ij}P_k + \Pi_{ij} \simeq 0 \tag{2.31}$$

Rodi's (1976) approach is to eliminate the transport terms in the governing equations by assuming

$$\mathcal{L}(\overline{u_i u_j}) = \left(\frac{\overline{u_i u_j}}{k}\right) \mathcal{L}(k) \tag{2.32}$$

This assumption is correct when $\overline{u_i u_j}/k$ is constant over the whole flow field. However, its validity for flows with varying $\overline{u_i u_j}/k$ ratios has not been demonstrated. Another point to note is that $\overline{u_i u_j}/k$ is constant only for flows that are in local or near equilibrium (Mellor and Yamada, 1982). Nevertheless, this assumption leads to

$$\overline{u_i u_j}(P_k - \bar{\rho}\epsilon) = k(P_{ij} - \frac{2}{3}\delta_{ij}\,\bar{\rho}\,\epsilon + \Pi_{ij}) \tag{2.33}$$

which gives a set of algebraic equations for $\overline{u_i u_j}$ after Π_{ij} has been appropriately modeled.

The approaches of Mellor and Yamada, and Rodi are essentially similiar to the same order a^2. This can be seen by considering assumption (2.32), which can be written with the help of (2.29) as

$$\mathcal{L}(\overline{u_i u_j} - \frac{2}{3}\,\delta_{ij}\,k) = \frac{\overline{u_i u_j}}{k}\,\mathcal{L}(k) - \mathcal{L}(\frac{2}{3}\,\delta_{ij}\,k) \tag{2.34}$$

Since $\mathcal{L}(k) = P_k - \rho\epsilon$, and by virtue of (2.29)

$$\mathcal{L}(\overline{u_i u_j} - \frac{2}{3}\delta_{ij} k) = 2(P_k - \bar{\rho}\epsilon)a_{ij} \qquad (2.35)$$

The term $2(P_k-\rho\epsilon)a_{ij}$ is of order a^2 and (2.35) would again lead to the results of (2.31). Rodi's assumption also leads to the neglect of terms of order a^2 in the Reynolds transport equations, and the two different approaches are essentially similiar to the same order, a^2.

If the two non-equilibrium ASM are denoted by ASM/MY and ASM/R, then ASM/MY is given by (2.31) and ASM/R is given by (2.33). The three ASM yield a set of algebraic equations for $\overline{u_i u_j}$ once a suitable model is proposed for the pressure-strain terms, Π_{ij}. Therefore, the performance of the ASM will be influenced greatly by the model adopted for Π_{ij}.

A similar approach can be applied to model the scalar-flux equations. As a result, no explicit statement about the form of diffusive transport in the scalar flux equation (2.8) is needed. The resultant model is the scalar-flux counterpart of the algebraic-stress-modelling (ASM) method. According to the order-of-magnitude analysis of Mellor and Yamada (1974)the turbulent scalar equation (2.8) reduces to

$$\overline{\frac{p'}{\rho}\frac{\partial\theta}{\partial x_i}} - \overline{u_i u_j}\frac{\partial\Theta}{\partial x_j} - \overline{u_j\theta}\frac{\partial U_i}{\partial x_j} = 0 \qquad (2.36)$$

where local isotropy of fine scale turbulence have been assumed. Note that (2.36) does not imply local balance of production and dissipation of $\overline{\theta^2}$.

Gibson and Launder (1976) proposed to approximate the turbulent scalar flux equation in a parallel manner to (2.33). Their result gives

$$\bar{\rho}U_m\frac{\partial\overline{u_i\theta}}{\partial x_m} + \frac{\partial}{\partial x_m}(\bar{\rho}\,\overline{u_i u_m\theta} + \delta_{im}\overline{p\theta}) = \frac{\overline{u_i\theta}}{2k}(P_k - \bar{\rho}\epsilon) - \frac{\overline{u_i\theta}}{\overline{\theta^2}}(P_\theta - \bar{\rho}\epsilon_\theta) \qquad (2.37)$$

where P_θ and ϵ_θ are respectively the production and dissipation of the scalar fluctuation $\overline{\theta^2}$. Gibson and Launder (1976) then argue that since there is only a weak coupling between the $\overline{\theta^2}$ and $\overline{u_i\theta}$ equations the assumption of local equilibrium for $\overline{\theta^2}$ is suffeciently accurate. Then (2.37) may be further simplified and written as:

$$-\bar{\rho}\left(\overline{u_i u_j}\frac{\partial\Theta}{\partial x_j} + \overline{u_j\theta}\frac{\partial U_i}{\partial x_j}\right) + \overline{p\frac{\partial\theta}{\partial x_i}} + \bar{\rho}\frac{\overline{u_i\theta}}{2k}\left(\overline{u_i u_j}\frac{\partial U_i}{\partial x_j} + \epsilon\right) = 0 \qquad (2.38)$$

Relations (2.36,2.38) and (2.31,2.33) together with the k- and ϵ-equations form a two-equation model which can account for the different production or destruction processes acting on the Reynolds stress and flux components, and to a certain approximation also for the transport of these components. This model is therefore cosiderably more general than the standard k-ϵ model which employs an isotropic eddy viscosity. These governing equations in the axisymmetric coordinate system are given in appendices B through D.

2.4.3 REYNOLDS STRESS MODELS

The models reviewed so far assume that the local state of turbulence can be characterized by one velocity scale and that the individual Reynolds stresses can be related to this scale by the eddy-viscosity expression. This relation often implies that the transport of the individual stresses is not adequately accounted for, even if the transport of the characterizing velocity scale is. In order to allow for the different development of the various Reynolds stresses representing various velocity scales in complex flows and to account properly for their transport, models which employ transport equations for the individual stresses $\overline{u_i u_j}$ must be applied. Analogous transport equations are required for the

turbulent heat/mass fluxes $\overline{u_i\theta}$, and the models based on these equations are often referred to as Reynolds stress models. The derivation of $\overline{u_iu_j}$- and $\overline{u_i\theta}$- equations (2.7,2.8) and their modelling to obtain a closed system were explained in previous sections. In general, there are six components of the Reynolds stresses and three components of the turbulent scalar fluxes. The modelled equations for these components, the turbulence dissipation rate ϵ, the scalar fluctuations $\overline{\theta^2}$ and the mean flow equations (2.4-2.6) allow the calculation of non-reacting variable density flows. However, for turbulent reacting flows, a combustion model must also be added. A complete set of the Reynolds equations in cylindrical coordinate are presented in appendices E and F.

2.5 NEAR-WALL FLOW MODELLING

2.5.1 WALL FUNCTION

At a solid boundary the no-slip condition applies. This means that both mean and fluctuationg velocities are zero. In contrast, the dissipation rate ϵ is finite and requires special attention. When the boundary conditions are specified right at the wall, the equations must be integrated through the viscous sublayer. This is undesirable because the high-Reynolds-number turbulence models

introduced above are not applicable in this region. However, integration through the sublayer can be avoided by using the law-of-the-wall function to connect the wall conditions to the dependent variables just outside the viscous sublayer. The value of k at the first grid point which is selected to be outside the viscous sublayer is determined from the k-balance for a control volume adjacent to the wall and with diffusive and convective transport through the wall set equal to zero. On the other hand, ϵ at the first grid point is calculated from the equilibrium condition. When turbulent transport equations are solved, the individual stresses (relative to friction velocity) are specified at the first grid point (Launder et al. ,1975). More discussion regarding the wall functions are presented in appendix G.

2.5.2 DIRECT CALCULATION

All the models described so far imply negligible viscosity effect on the energy containing motions and negligible effect of the mean strain field on the dissipative phenomena. These assumptions are generally valid for high Reynolds-number turbulent flows except very close to a wall. Here, the no slip condition at the wall ensures that viscous effect will always be important in the immediate vicinity of the wall. Although the viscosity

affected zone has a thickness of two or more order of magnitude less than the characteristic dimension of the flow, almost 50% of the velocity change from the wall to the free stream occurs in this region (Launder,1984). Fortunately, it is practical to ignore many of the complexities inside the viscosity dominated layer by noting the fact that the important mean and turbulent flow quantities highly depend on the normal distance from the wall. In high-Reynolds-number modelling, the calculations are carried out to the vicinity of the wall and all the dependent variables are then matched to their corresponding values determined from approximate wall functions. Transpiration through the wall, swirl, steep temperature or streamwise pressure gradients are just a few examples that may cause the near-wall region to differ from its so called universal behavior. To account for these various influences it is necessary to extend the calculation right up to the wall itself.

In order to provide predictions of the flow within the viscous sublayer, the form of the models given for high Reynolds number flows must be modified in three ways. These are: (1) retain the viscous diffusion of k, ϵ and $\overline{u_i u_j}$, (2) constants in ϵ and eddy viscosity equations become dependent on the turbulence Reynolds number, ($R_T=k^2/\nu\epsilon$), (3) further terms are required due to the fact that the dissipation

processes are not isotropic and this effect must be accounted for.

Several two-equation, low-Reynolds-number turbulence models have been proposed by different researches (Launder and Sharma, 1974; Hassid and Poreh, 1978; Chien, 1980; Reynolds, 1976; Lam and Bremhorst, 1981). A systematic evaluation of these models has been performed by Patel et al. (1985). From an overall examination of the results for all the test cases, the model of Chien (1980) performs relatively better than the others. Therefore, this model has been selected here to calculate the turbulence energy and dissipation rate. The final modified form of the k and ϵ equations proposed by Chein (1980) are

$$\bar{\rho}\frac{Dk}{Dt} = \frac{\partial}{\partial x_k}\left(C_S\,\bar{\rho}\,\frac{k}{\epsilon}\,\overline{u_k u_m}\,\frac{\partial k}{\partial x_m}\right) - \bar{\rho}\,\overline{u_i u_j}\,\frac{\partial U_i}{\partial x_j} - \bar{\rho}\left(\epsilon + \frac{2\nu k}{y^2}\right) \tag{2.39}$$

$$\bar{\rho}\frac{D\epsilon}{Dt} = \frac{\partial}{\partial x_k}\left(C_\epsilon\,\bar{\rho}\,\frac{k}{\epsilon}\,\overline{u_k u_m}\,\frac{\partial \epsilon}{\partial x_m}\right) + C_{\epsilon 1}\,\frac{\epsilon}{k}\left(-\bar{\rho}\,\overline{u_i u_j}\,\frac{\partial U_i}{\partial x_j}\right)$$

$$- \frac{\epsilon}{k}\left(C_\epsilon\,\epsilon\,f_2 + \frac{2\nu k}{y^2}\,e^{-c_4 y^+}\right) \tag{2.40}$$

where

$$f_2 = 1 - \frac{2}{9}\,e^{-R_T^2/36}$$

and y is the normal distance from the wall.

Recently, So and Yoo (1986) applied asymptotic analysis technique in a way parallel to Chien (1980) to modify the viscous dissipation term in the Reynolds stress transport equations to account for viscous behavior near a wall.

2.6 TURBULENT COMBUSTION MODELS

Turbulent reactive flows are difficult to predict for the simple reason that neither turbulent transport nor chemical kinetics are adequately understood. Specific problems of particular interest are the evaluation of the mean formation rates and the effects of heat release on the turbulence structure and, in turn, on the turbulence flux closure models. In order to illustrate the effect of turbulence on the mean formation rates, consider a simple irreversible reaction such as

$$A + B \xrightarrow{k1} C \tag{2.41}$$

The instantaneous formation rate of C is represented by the Arrhenious equation, or

$$R_C = k_0 \rho^2 m_A m_B \exp(-E1/RT) \tag{2.42}$$

where m_i is the instantaneous mass fraction of species i, E1 is the activation energy and k_0 is the pre-exponential rate constant

In order to evaluate the mean formation rate $\bar{R}_C$, it is necessary to decompose each of the fluctuating variables into their mean and fluctuating components. It is emphasized that the time-mean rate expression is not simply the reaction rate calculated from the time-mean variables. For example

$$\bar{R}_C = \overline{m_A m_B \rho^2 k_0 \exp(-E1/RT)} \neq \bar{m}_A \bar{m}_B \bar{\rho}^2 k_0 \exp(-E1/R\bar{T}) \qquad (2.43)$$

Instead, after applying Reynolds decomposition and appropriate simplification we obtain:

$$\bar{R}_C = \bar{\rho}^2 \bar{m}_A \bar{m}_B k_0 \exp(-\frac{E1}{R\bar{T}}) [1 + \frac{(\overline{\rho'})^2}{\bar{\rho}^2} + \frac{\overline{m_A' m_B'}}{\bar{m}_A \bar{m}_B} + 2\frac{\overline{\rho' m_A'}}{\bar{\rho}\,\bar{m}_A} + 2\frac{\overline{\rho' m_B'}}{\bar{\rho}\,\bar{m}_B} +$$

$$\frac{E1}{R\bar{T}} (\frac{\overline{m_A' T'}}{\bar{m}_A \bar{T}}) + (\frac{E1}{2R\bar{T}} - 1)(\frac{\overline{T'^2}}{\bar{T}^2} + ..] \qquad (2.44)$$

which is an infinite series in terms of $\overline{m_A' m_B'}$, $\overline{\rho' m_A'}$, $\overline{m_A' T'}$, etc. For $\bar{R}_C$ to be evaluated correctly, an infinite number of these moments containing the variables T', m_A' and m_B' would have to be determined. This rate expression is for the

simple example given by equation (2.44). For any realistic combustion scheme, many of these equations have to be considered. It is ideal to be able to handle reacting flows in which combustion may occur via a large number of finite-rate reaction steps. However, this would necessitate the solution of conservation equations for the mean value of each of the independent species, which in turn requires the evaluation of the mean formation rate of each species. It is clear that closure of turbulent reacting flow is a formidable problem.

At present, only PDF transport equation formulation offers the possibility of handling large numbers of reacting species (Pope,1976), but in view of computer storage requirements, run times and multidimensionality of the approach, their suitability requires further investigations. Fortunately, most of the reactions associated with the high temperature oxidation of hydrocarbon and hydrogen fuels usually have time scales very short compared with those characteristics of the turbulence field and the assumption of fast chemistry thus provides a reasonable description of the equilibrium composition, temperature and mixture density. However, the estimation of unburnt fuel, formation of pollutants, and the study of such phenomena as ignition and blow out require consideration of finite rate reactions. The fast chemistry assumption can only be applied to non-premixed combustion systems where fuel and oxidant are

injected separately. However, in premixed combustion system, where fuel and oxidant have been mixed prior to reaction, only finite-rate chemistry assumption can be invoked because the species are allowed to come into contact without burning occurring at the same time. In view of these differences the following discussion of combustion models will be divided into non-premixed and premixed combustion. Under non-premixed combustion, both the fast and finite-rate chemistry models are discussed.

2.6.1 FAST CHEMISTRY MODEL FOR NON-PREMIXED COMBUSTION

A practical idealized approach in non-premixed combustion (two-feed) system is based on the assumption that the chemistry is fast. Its first principal feature is the neglect of all intermediate reactions so that pure fuel and pure oxidant will react to form the products the moment they are in contact. Its second main feature is the assumption that the effective diffusivity coefficient of all species is the same. The first is justifiable only by the need to simplify. The second cannot be very far from reality for a turbulent flow.

When the chemistry can be simplified to a one-step reaction such as

1 Kg fuel + i Kg oxidant → (1+i) Kg product

we have

$$R_{fu} = R_{ox}/i$$

where R_{fu} and R_{ox} stand for the rates of creation by chemical reaction of fuel and oxidant ,respectively.

The consequence of these assumptions is that a suitably chosen linear combination of the equations describing the conservation of two-unpremixed reactants yields an equation whose form is identical to that describing the convection and diffusion of chemically inert species. The equation which results will have no source term. The dependent variable of the resultant equation is usually taken to be the mixture fraction and is defined as

$$\Theta \equiv \frac{(\gamma - \gamma_O)}{(\gamma_F - \gamma_O)} \qquad (2.45)$$

where γ is given by

$$\gamma \equiv m_{fu} - m_{ox}/i \qquad (2.46)$$

or

$$\gamma \equiv m_{fu} + m_{pr}/i+1 \qquad (2.47)$$

or

$$\gamma \equiv m_{ox} + i\, m_{pr}/1+i \tag{2.48}$$

Here m_{fu}, m_{ox}, m_{pr} ,and i are the mass fraction of the fuel, oxidant, product and the stoichiometric oxidant requirement per unit mass of fuel. Subscript F and O stand for fuel and oxidant stream, respectively.

Let us now presume that the reaction is every where complete. This gives the following conditions for Θ:

$$0 \le \Theta \le \Theta_{st} \qquad \begin{cases} m_{fu} = 0 \\ m_{ox} = m_{ox,O}\left(1 - \dfrac{\Theta}{\Theta_{st}}\right) \end{cases} \tag{2.49}$$

and

$$\Theta_{st} \le \Theta \le 1 \qquad \begin{cases} m_{fu} = m_{fu,F}\dfrac{(\Theta - \Theta_{st})}{(1 - \Theta_{st})} \\ m_{ox} = 0 \end{cases} \tag{2.50}$$

where Θ_{St} is the stoichiometric value of the mixture fraction and is characterized by:

$$\Theta_{st} = \frac{1}{1 + i(m_{fu,F}/m_{ox,O})} \tag{2.51}$$

The mass fraction of the products of combustion can then be obtained from

$$m_{pr} = 1 - m_{fu} - m_{ox} \qquad (2.52)$$

Equations (2.49,2.50) are the result of the fact that thermodynamic equilibrium is supposed to prevail throughout. This means that finite values of both fuel and oxidant concentration cannot prevail at the same point.

For adiabatic operation of gaseous flame, the standard enthalpy is a conserved scalar and thus with the assumption of equal diffusivity of heat and mass,the local enthalpy,h, may be calculated directly from

$$h = \Theta\, h_F + (1-\Theta)\, h_O \qquad (2.53)$$

where

$$h = \int_0^T C_p\, dT + H_c\, m_{fu} \qquad (2.54)$$

H_c and C_p are the heat of combustion and specific heat of the mixture at constant pressure, respectively. If the specific heat is assumed to be independent of temperature, then the temperature can be calculated as

$$T = \frac{h - H_c\, m_{fu}}{C_p} \qquad (2.55)$$

As has already been discussed throughout this chapter, solution of the turbulent, variable-density, differential equations requires a properly averaged density. It can be seen from equations (2.4-2.6) that the conventional mean density is required. However, according to these equations the Favred-averaging mixture fraction (scalar) is predicted along with the variance for the Favre-averaged probability density function (PDF). By using the local instantaneous equilibrium approximation and convoluting over the PDF, the Favre-averaged density would result. On the other hand, if it is realized that the Favre-averaged of the inverse density is equal to the inverse of the Reynolds-averaged of the density, Then,

$$\frac{1}{\rho} = \int_0^1 \frac{\tilde{F(\theta)}}{\rho} \, d\tilde{\theta} \qquad (2.56)$$

where $F(\tilde{\theta})$ is the Favre probability density function of the mixture fraction and is unknown. A straightforward approach to determine this PDF is to assume a PDF with two parameters. The two parameters are determined from the first two moments of the PDF which are obtained by solving their respective transport equations. Different two-parameter PDF's have been proposed and tested by a number of

researchers (Spalding,1971 ; Lockwood and Naguib,1975 ; Rhodes,1975). However, evidence in support of the β-distribution has been provided by Jones (1977) in his calculation of diffusion flames. We shall assume a β-distribution function for $F(\tilde{\theta})$ so that

$$F(\tilde{\theta}) = \frac{\Gamma(a+b)}{\Gamma(a)\Gamma(b)} \tilde{\theta}^{a-1}(1-\tilde{\theta})^{b-1} \qquad (2.57)$$

where $0 \leq \tilde{\theta} \leq 1$ and $a > 0$, $b > 0$.
since

$$\Theta = \int_0^1 \tilde{\theta}\, F(\tilde{\theta})\, d\tilde{\theta} = \frac{a}{a+b} \qquad (2.58)$$

$$\overline{\theta 2} = \int_0^1 (\tilde{\theta} - \Theta)^2\, F(\tilde{\theta})\, d\tilde{\theta} = \frac{a}{(a+b+1)(a+b)^2} \qquad (2.59)$$

constants a, b can be found from (2.58) and (2.59) and are given by

$$a = \Theta \left[\frac{\Theta\,(1-\Theta)}{\overline{\theta^2}} - 1 \right] , \qquad (2.60)$$

$$b = \frac{a\,(1-\Theta)}{\Theta} \qquad (2.61)$$

Therefore, once Θ and $\overline{\theta^2}$ are known from the solution of their transport equations, a and b can be determined and consequently the mean density can be calculated at each node point.

2.6.2 FINITE-RATE CHEMISTRY MODEL FOR NON-PREMIXED COMBUSTION

An important problem in finite-rate chemistry is choosing an appropriate level of complexity, in view of the large number of species and chemical reactions taking place. One solution to this problem is the use of a global approach that reduces chemistry to the specification of an overal global oxidation scheme. Both m_{fu} and m_{ox} can have non-zero values at the same point at the same time. This model can predict quantities of interest: fuel consumption and heat release rates. However, it is the evaluation of the mean formation rate which presents problems. If fluctuation terms are neglected and the rate evaluated in terms of the mean values of the quantities involve in the reaction rate, the result may be in serious error. To reduce this error, the eddy breakup model of Spalding (1971) is included. This model can be written as

$$S_{\Theta} = C_{EBU} \frac{\epsilon}{k} \overline{\rho}\, \Theta \qquad (2.62)$$

which is based on the idea that the mean reaction rate is determined completely by the rate of scale reduction via a process of turbulence vortex stretching. Generally, one uses the smaller of these two expressions at a given point in the flow field. The eddy dissipation rate often slowing chemical reaction. This basic model has had several refinements, culminating in the Eulerian - Lagrangian theory of turbulent combustion (Spalding, 1977).

The one-step reaction model of section 2.6.1 (popular in the simulation of heat release) may be replaced by a slightly more sophisticated kinetics model which allows prediction of local mass fractions of hydrocarbon fuel, carbon dioxide and nitrogen. Consider the two step mechanism:

$$C_X H_Y + (\frac{X}{2} + \frac{Y}{4})(O_2 + nN_2) \rightarrow X\ CO + \frac{Y}{2}\ H_2O + (\frac{X}{2} + \frac{Y}{4})\ nN_2 \tag{2.63}$$

$$X\ CO + \frac{X}{2}\ (O_2 + nN_2) \rightarrow X\ CO_2 + \frac{X}{2}\ nN \tag{2.64}$$

The mass fractions of all chemical species obey the general differential equation. These transport equations are all similar and contain terms for convection, diffusion and source S_ϕ of a general variable ϕ (which contains terms

describing the generation and consumption of ϕ). In fact, they all conform to

$$\frac{\partial}{\partial x_i}(\rho U_i \phi) - \frac{\partial}{\partial x_i}(\Gamma_\phi \frac{\partial \phi}{\partial x_i}) = S_\phi \qquad (2.65)$$

and the equations differ not only in their effective diffusive flux but also, and primarily, in their final source terms as defined in Table 2.1.

Table 2.1 Source terms for chemical species

ϕ	S_ϕ
m_{fu}	S_{fu}
m_{CO}	$S_{CO} - r_2 S_{fu}$
m_{ox}	$r_1 S_{fu} + r_4 S_{CO}$
m_{CO_2}	$- r_5 S_{CO}$
m_{H_2O}	$- r_3 S_{fu}$
$\phi_A \equiv m_{ox} - (r_1 + r_2 r_4) m_{fu} - r_4 m_{CO}$	0
$\phi_B \equiv m_{CO_2} + r_5 m_{CO} + r_2 r_5 m_{fu}$	0
$\phi_C \equiv m_{H_2O} + r_3 m_{fu}$	0

where

$$r_1 = \left(\frac{X}{2} + \frac{Y}{4}\right) W_{O_2}/W_{fu}$$

$$r_2 = X\, W_{CO}/\, W_{fu}$$

$$r_3 = (Y/2) W_{H_2O}/W_{fu} \qquad (2.66)$$

$$r_4 = 0.5\, W_{O_2}/W_{CO}$$

$$r_5 = W_{CO_2}/W_{CO}$$

Further, the diffusion coefficient for all species are related to the turbulent viscosity via the turbulent prandtl number. For the last entries in Table 2.1, a single values Θ with a zero source term and values 0 and 1 in the air and fuel stream, respectively can provide the solutions for ϕ_A, ϕ_B and ϕ_C via the following relationships

$$\Theta = \frac{\phi_A - \phi_{A,air}}{\phi_{A,fu} - \phi_{A,air}} = \frac{\phi_B - \phi_{B,air}}{\phi_{B,fu} - \phi_{B,air}} = \frac{\phi_C - \phi_{C,air}}{\phi_{C,fu} - \phi_{C,air}} \qquad (2.67)$$

Using Equation (2.66) and assuming that the mass fraction of fuel in the primary stream is 1 and the mass fraction of oxidant in the secondary stream is R, we have

$$m_{ox} = r_4\, m_{CO} + R(1-\Theta) + (r_1 + r_2 r_4)(m_{fu} - \Theta) \qquad (2.68)$$

$$m_{CO_2} = r_2\, r_5\, (-m_{fu} + \Theta) - r_5\, m_{CO} \qquad (2.69)$$

$$m_{H_2O} = r_3 (-m_{fu} + \Theta) \qquad (2.70)$$

This scheme involves the solution of the conservation equations for unburnt fuel, CO and mixture fraction. The reaction rates of fuel and carbon monoxide are given by the following relations

$$S_{fu} = - \min \left[C_{R1} \rho \, m_{fu} \frac{\epsilon}{k} , \; k_1 \rho^{a} m_{fu}^{b} m_{ox}^{c} \exp(-E1/R\bar{T}) \right] \qquad (2.71)$$

$$S_{CO} = - \min \left[C_{R2} \rho \, m_{CO} \frac{\epsilon}{k} , \; k_2 \rho^{a'} m_{CO}^{b'} m_{ox}^{c'} m_{H_2O}^{d'} \exp(-E2/R\bar{T}) \right] \qquad (2.72)$$

where C_{R1} , C_{R2} are the eddy breakup constants and k_1 , k_2 are the pre-exponential constants for Arrhenius rate equations.

Many chemical reaction phenomena posses stiff kinetics; that is, they involve a multitude of species with widely different reaction rate coefficient. Their equations have to be solved along with the more usual fluid dynamics equations. Special computational techniques for handling the source terms are required. One often solving the associated time - dependent problem even when the steady state solution is required. Of course, different time steps are chosen for the fluid dynamics and chemical kinetic portions of the problems. An efficient technique for steady state solution of stiff kinetic problems has been developed by Pratt (1976)

and shows considerable promise for practical engineering situations.

2.6.3 MODEL FOR PREMIXED COMBUSTION

In many combustion systems, fuel and oxidant are premixed prior to reaction. Premixed flames, spreading downstream of flame-holders, have been the subject of many previous investigations concerned with the development of ram jets and afterburners. In contrast to unpremixed flames which can be analysed with fast or finite-rate chemistry, premixed turbulent flames are kinetically controlled and the rate of flame propagation, called the burning velocity, is dependent upon chemical composition and rate of chemical reaction. Completely premixed flames are seldom found in practice for reasons of safety, (for example flashback and blow off) and stability. For this reason, and may be these type of flames occur less frequently in practical systems, they appear to have received less attention than have unpremixed flames. It is only in recent years, however, that detailed attempts to understand the flow characteristics, with the aid of local measurements, have been reported (Stevenson et al. ,1983). A detailed discussion of premixed turbulent flames is given by Bray (1980) and a review of various methods developed for calculating premixed turbulent flames is given by Jones and Whitelaw (1982).

In general, most work on premixed flames has assumed that combustion can be characterized by a global single step reaction of the type shown by equation (2.41). In terms of the three - component mixture undergoing a simple one step reaction, partial differential equations are set up for m_{fu}, mixture fraction and stagnation enthalpy, with the first of these for mass fraction of fuel requiring the specification of its source, the mean formation rate of fuel. In earlier sections the Arrhenius expression was introduced, but clearly its mean value should not be calculated merely from mean values of components in its expression. If fluctuations are neglected and the rate evaluated in terms of the mean values of temperature and mass fraction, the result can be in error by typically one order of magnitude and will exhibit a strong dependence on temperature, pressure and mixture strength (Jones and Whitelaw, 1982). In practice, experimental results for premixed turbulent flames are only weakly dependent on mass fractions, pressure and temperature. This fact led to the turbulence dominated mean reaction expression called the eddy breakup reaction model described earlier. It is based on the idea that the mean reaction rate is determined solely by the rate of scale reduction via a process of turbulence vortex stretching. The model, thus takes no explicit account of chemical kinetics and relates to combustion which is entirely mixing controlled (Jones and Whitelaw, 1982). In this situation, it

has been shown to be in good accord with the available evidence for premixed flames. The model has also been used occasionally for non-premixed flames, but it is generally inappropriate in this situation and Pope (1977) has shown that it does not necessarily provide unique solution. A more logical basis for expressions of the eddy breakup type is provided by the Bray-Moss (1977) model for premixed flames. The Bray-Moss model for premixed combustion has been extended by Libby and Bray (1980a, 1980b), who utilize the concept of laminar flamelets in order to derive models for turbulent transport and dissipation processes in one dimensional planer flames.

For two-step reaction rate,the solution of the conservation equations for unburnt fuel and carbon dioxide CO_2 (or carbon monoxide CO) is involved . The mass fraction of intermidiate species are determined by the following algebraic relations

$$m_{co} = Z_{co} - r_2 m_{fu} - (m_{co_2})/r_5 \tag{2.73}$$

$$m_{H_2o} = Z_{H_2o} - r_3 m_{fu} \tag{2.74}$$

$$m_{o_2} = Z_{o_2} + r_1 m_{fu} - (r_4 m_{co_2})/r_5 \tag{2.75}$$

where

$$Z_{co} = r_2 m_{fu,p} \tag{2.76}$$

$$Z_{o_2} = m_{o_2,p} - r_1 m_{fu,p} \tag{2.77}$$

$$Z_{H_2O} = r_3 m_{fu,p} \tag{2.78}$$

and $m_{fu,p}$ and $m_{O2,p}$ are mass fractions of fuel and oxidant in primary stream, respectively. The mean reaction rates are calculated from the minimum of the Arrhenius reaction rates and the eddy breakup model similar to (2.71) and (2.72).

CHAPTER 3

NUMERICAL PROCEDURE

The governing partial differential equations described in the preceeding chapter are coupled and non-linear. At the present time, it is not possible to obtain analytical solutions to these equations and numerical technique has to be used. A computer program has been developed to solve axisymmetric elliptic partial differential equations through an iterative procedure based on an integral control volume analysis with hybrid upwind finite differencing or quadratic upwind differencing and staggered grids. The logic behind this program is briefly described below.

3.1 GRID AND ITERATION SEQUENCE

Before integrating the standard equations over the flow domain, a satisfactory grid is required. For hybrid differencing purposes the program uses a staggered grid in which the velocities are evaluated at the boundaries of scalar variable (P,k,ϵ, etc) cells. Hence separate grids define the locations of the U- and V-velocities. A portion of these three grids is shown in Figure 3.1 . The solution domain is arranged so that the outer surfaces of the

boundary scalar cell coincide with the physical boundaries of the flow field (Figure 3.2).

The iteration sequence consists of two major parts: the SIMPLE solution algorithm of Patankar and Spalding (1972), and the solution of transport equations for the turbulence quantities. The SIMPLE algorithm solves for a fixed pressure field, by line iteration, sets of difference equations for the x and r momentum equations. After each such sweep over the solution domain, adjustments are made to the pressure field to satisfy continuity along each line of cells. These adjustments in turn destrory the compliance of the velocity and pressure field with the momentum equations. Transport equations for the turbulence quantities are then solved using the calculated velocity field . Finally, closure is achieved by evaluating the Reynolds stresses using the new mean velocity, turbulent kinetic energy, and dissipation rate fields. Iterations are carried out until the momentum and continuity equations are simultaneously satisfied to the required degree of accuracy.

3.2 FALSE DIFFUSION

It is a well-known fact that all upwind scheme, although numerically very stable, introduce false diffusion into the formulation. It is this false diffusion that acts to stablize the numerical solution as it becomes larger than

the physical diffusion for $P_e>2$. The exact value of false diffusion for one dimensional convection-diffusion equation is (Patankar, 1980):

$$\Gamma_{x,f} = \frac{|U|\ \Delta x}{2} = \frac{|P_e|\ \Gamma}{2} \qquad (3.1)$$

This is not serious when the streamlines are aligned with the grid lines, because, in this case, false diffusion occures in the direction of the velocity vector and is of little consequence for larger P_e numbers. However, when the streamlines are at an angle to the grid lines, false diffusion in the x and r directions combine to give a diffusive flux normal to the velocity vector which can lead to large errors when the variable considered has a significant gradient in this normal direction. That the upwind scheme must lead to errors in such a situation becomes clear immediately from Figure 3.3 which shows that it is not the value Φ_W that is convected across the west face but the value Φ_{W-SW} indicated in this figure. An approximate expression for the false diffusion coefficient for a two dimensional situation has been givened by de Vahl Davis and Mallinson (1972). It is

$$\Gamma_{false} = \frac{\rho U \Delta x \Delta r \sin(2\theta)}{4(\Delta r \sin^3\theta + \Delta x \cos^3\theta)} \qquad (3.2)$$

where U is the resultant velocity, and θ is its angle to the x axis. It is seen from this equation that the false diffusion is most serous when the flow direction makes an angle of 45° with the grid lines. False diffusion can be reduced by using smaller grid size and by orienting the grid such that the grid lines are more or less aligned with the flow direction or using higher order schemes.

The recently developed skew-upwind and quadratic-interpolation schemes have been shown to perform better in all situations where streamline skewness causes numerical diffusion. Both schemes produce similar results. According to Leschziner (1980), the quadratic scheme requires no more computing time than the hybrid scheme, but the skew-upwind scheme needs about 50 percent more time. For this reason and also because it is easier to implement, the quadratic scheme became more popular and is explained in the next section.

3.3 QUADRATIC UPWIND DIFFERENCING SCHEME

Upwind differencing scheme, although very stable, is only first-order accurate and suffers from false diffusion. A promising new technique proposed by Leonard (1979), which

is known as QUICK (Quadratic Upstream Interpolation for Convective Kinematic), aims at combining the relatively high accuracy of the central difference scheme with the stability of the upwind scheme. QUICK uses a three-point upstream-wighted quadratic interpolation for each cell's wall value, two located on either side of the face and the third being the next node in the upstream direction.

Using quadratic interpolation for the dependent variable Φ, it can be shown that the finite difference form of any convective-diffusive equation is reduced to

$$A_P \Phi_P = A_E \Phi_E + A_W \Phi_W + A_N \Phi_N + A_S \Phi_S + A_{EE} \Phi_{EE} + A_{WW} \Phi_{WW} + A_{NN} \Phi_{NN} + A_{SS} \Phi_{SS} \qquad (3.3)$$

The derivation of Φ_w is given in detail below and the derivation of Φ at the other faces are similiar.

A general second degree polynomial for the calculation of Φ_w is

$$\Phi_w = C_0 + C_1 x + C_2 x^2 \qquad (3.4)$$

The mathematically equivalent but more convenient quadratic form is

$$\Phi = C_0 + C_1(x-x_P) + C_2(x-x_P)(x-x_W) \tag{3.5}$$

where the constants C_0, C_1, and C_2 are determined from the neighbouring points. Consider the situation for positive axial velocity in which case calculation of Φ_w is biased toward the upwind node at X_{WW} , then :

$$C_0 = \Phi_P \ , \tag{3.6}$$

$$C_1 = \frac{\Phi_W - \Phi_P}{x_W - x_P} \ , \tag{3.7}$$

$$C_2 = \left(\frac{\Phi_{WW} - \Phi_P}{x_{WW} - x_P} - \frac{\Phi_W - \Phi_P}{x_W - x_P}\right)\left(\frac{1}{x_{WW} - x_W}\right) \tag{3.8}$$

and for the case when the axial velocity is negative, the coefficient in Eq.(3.5) are calculated using the values of Φ at the grid node W, P, and E so that:

$$C_0 = \Phi_P \ , \tag{3.9}$$

$$C_1 = \frac{\Phi_W - \Phi_P}{x_W - x_P} \ , \tag{3.10}$$

$$C_2 = \left(\frac{\Phi_E - \Phi_P}{x_E - x_P} - \frac{\Phi_W - \Phi_P}{x_W - x_P}\right)\left(\frac{1}{x_E - x_W}\right) \qquad (3.11)$$

The quadratic interpolation scheme is therefore third-order accurate; requires 9-point and must take the sign of all face velocities into account. This algorithm was extended to two dimension by applying a similiar procedure in the cross-stream direction. Like the central-difference scheme, the quadratic scheme does not produce diffusion-type truncation error, but it may suffer from some unboundedness. Han et al. (1981) further report that, unlike the upwind scheme, the quadratic scheme is not unconditionally stable and may require certain special measures to produce stability.

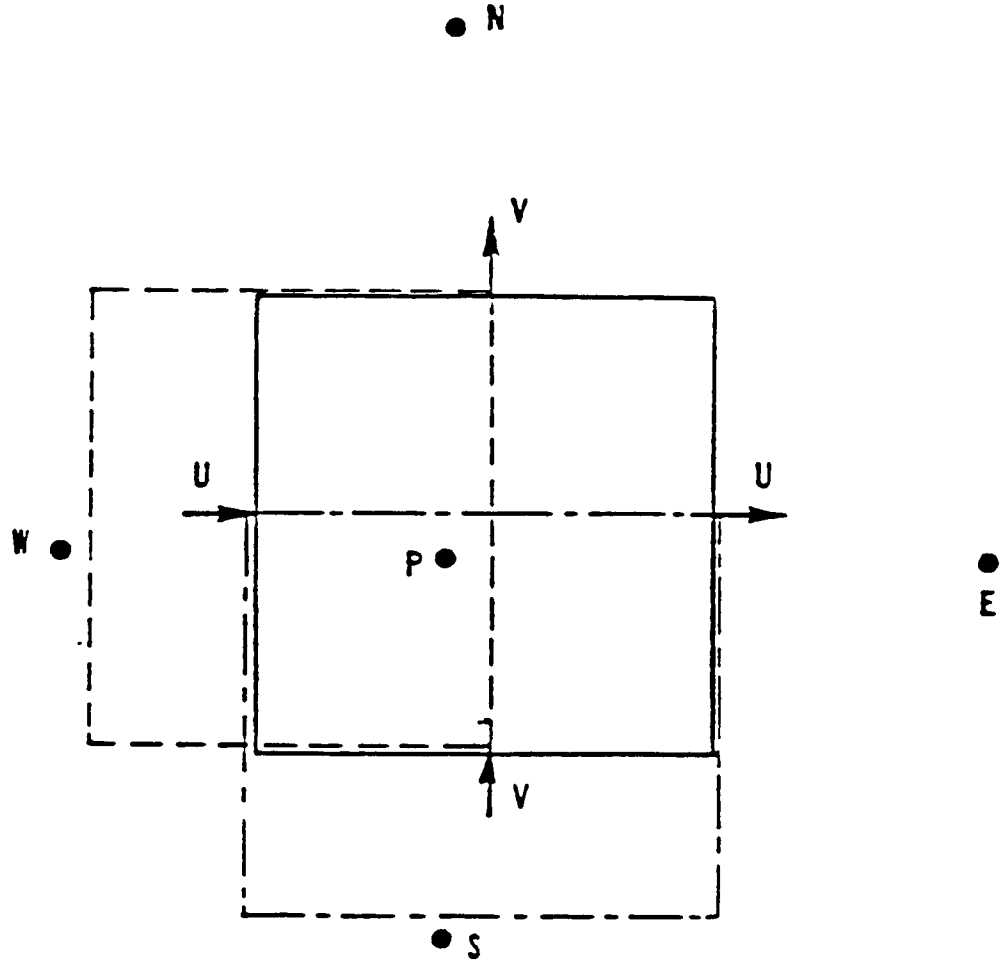

Figure 3.1 Typical non-uniform grid portion

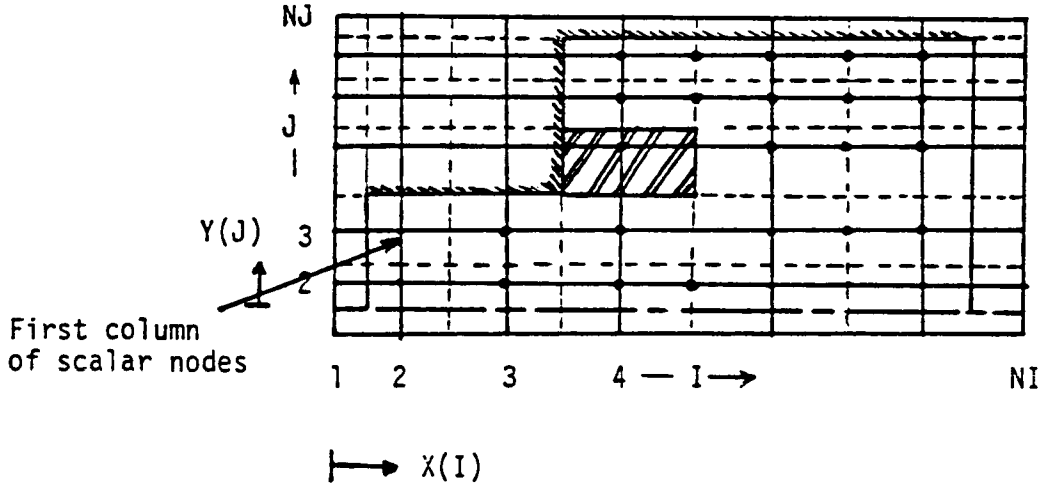

Figure 3.2 Solution domain used in backward-facing step flow computations

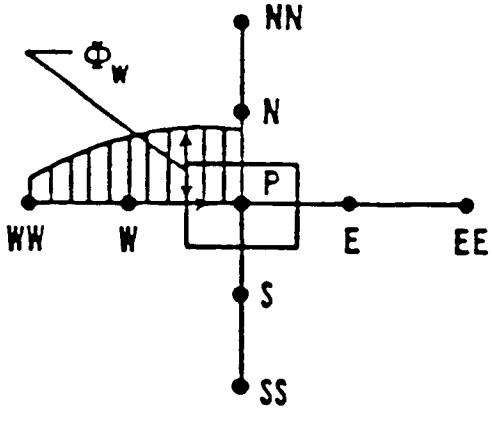

Figure 3.3 Quadratic upstream-weighted difference scheme

CHAPTER 4

MODEL EVALUATIONS

This chapter presents the results of the comparisons of the various models for isothermal, constant and variable density turbulent recirculating flows. Predictions obtained with each of the turbulence models are discussed and, when available, compared with experimental data. The goals of this study require a careful selection of the test cases. They have to provide reliable mean flow and turbulence data in the recirculation and recovery regions. A detailed specification of the flow parameters in the upstream region is also essential since these are used as inlet conditions to start the computations. However, the most common shortcoming is found to be the lack of well-defined inlet boundary conditions. The importance of these quantities has not been fully appreciated (Sturgess et al. ,1983). Incorrect specification of inlet turbulence quantities could have a further adverse effect if the flow is a reacting one. This is because the eddy break-up combustion model relates the reaction rate of the fuel to the eddy lifetime, k/ϵ. An incorrect specification of k and ϵ at the inlet therefore results in an incorrect density field. Since density is strongly coupled to the mean flow field, an incorrect

density changes the mean flow field completely. Finally, all data sets have to meet the criteria set by Eaton and Johnson(1980) for acceptable measurements in terms of adequate experimental facility, appropriate instrumentation, and agreement with generally accepted flow trend.

After reviewing some of the available data sets the following three are chosen as the test cases:

1. Johnson and Bennett (1981); confined coaxial non-swirling suddenly-expanded jets

2. Roback and Johnson (1983); confined coaxial swirling suddenly-expanded jets

3. Brum and Samuelsen (1982); CO_2 into air (three coaxial streams with middle stream swirling)

Only a portion of the predictions and comparisons with measurements are presented. These are chosen to illustrate specific points concerning the turbulence models and their performance.

4.1 THE BASIC EXPERIMENTAL FLOW FIELDS

The cases of Johnson and Bennett (1981), and Roback and Johnson (1983) are selected for comparison with the calculated mean and turbulence quantities in a constant density flow. The experiments are carried out in a water rig that resembles closely a gas turbine engine (can) combustor (Figure 4.1). The flow conditions selected for this study have Reynolds numbers of 15900 and 47500 for the inner and annular streams, respectively. These Reynolds numbers are factors of 5 to 20 greater than the transitional Reynolds number range occurring in aircraft gas turbines. Mean velocity and turbulence fluctuations were measured with a Laser Doppler Velocimeter (LDV). The scalar transport measurements were made using a Laser-Induced Fluorescence (LIF) technique. Fluorescein dye was introduced as a tracer into the water flow of the central jet to give constant density, variable species, mixing of the two concentric jets. This permitted the modelling of turbulent mass transport to be investigated. Sketches of the flow regions occurring for the swirling and non-swirling flow conditions are shown in Figure 4.2. For the non-swirling flow, four major shear flow regions can be identified. These are: a wake region immediately downstream of the inner jet inlet duct, a shear region further downstream between the inner and annular jets, a recirculation zone, and a reattachment

region. A three-dimensional counter-rotating corner eddy is also observed and extends only a short distance, less than one step height downstream of the step. The large primary eddy occupies the rest of the recirculation zone. For swirling flow, a second recirculation cell occurs along the centerline and the length of the annular recirculation cell is decreased. One other difference between the swirling and non-swirling experiments should be noted. This is the observation that, once reattachment of the annular jet occurred, the axial velocity profile tended to flatten with momentum transport from the outside inward for the swirling flow case whereas the velocity profile tended to flatten with momentum transport from the inside outward for the nonswirling flow case.

For variable-density flow analysis, the isothermal, non-reacting flow inside a dilute swirl combustor provided by Brum and Samuelsen (1982) is selected. The dilute swirl combustor is designed with a cone-annular gas injector, a swirling stream and a non-swirling stream of dilute air. The complex model laboratory flow combustor (Figure 4.3) has an aerodynamically controlled, swirl-stabilized recirculation zone. It consists of an 80 mm I.D. cylindrical stainless steel tube 50 cm long with rectangular optical windows mounted vertically on either side of the combustor tube. These flat windows provide for clear optical access necessary for laser anemometry measurements. A set of swirl

vanes (57 mm O.D.) is concentrically located within the combustor tube around a 19 mm O.D. centrally positioned fuel/CO_2 delivery tube. The combustor was operated at atmospheric pressure with an overall equivalence ratio of 0.2 and a bulk reference velocity of 15 m/s.

4.2 EVALUATION OF DIFFERENT CLOSURE MODELS FOR COMBUSTOR FLOW CALCULATIONS WITHOUT SWIRL

In this section the comparison is made of the performance of the k-ϵ closure, algebraic stress closures and Reynolds stress closure in calculating the combustor flows. Effects of different pressure-strain models and turbulent diffusion models are also analysed. Predictions of the mean and turbulence quantities using high and low Reynolds number models are compared. Finally, the efficient models for turbulent momentum exchange in combustor flow calculations are identified.

4.2.1 THE k-ϵ MODEL RESULTS

The mean and turbulence quantities predicted by the standard k-ϵ model and the measured values are illustrated in Figures 4.4 - 4.6. The model constants used in this calculation are listed in Table 4.1. The overall agreement is good and the calculated velocity and maxima and their locations closely reproduce the experimental results. The recirculation zone and the reattachment length has been

reasonably predicted (Tables 4.2-4.3). There are however, some discrepancies in the region of the center line with the velocities being under-predicted by about 5% - 30% at the downstream locations. The change in the axial velocity profile from x = 13 mm to successive locations downstream document the development of the various shear regions within the combustor. The shear layer between jets occurred between x=51 mm and 203 mm. In this shear region, the annular jet flow accelerated the inner jet flow but the predicted result does not show such a behavior and the centerline velocity is contineously decreased (Figure 4.7). The under-prediction for a centerline velocity stems from the incorrect representation of the turbulent diffusion process. As shown by Ribeiro (1976), the radial normal stress is particularly important in the upstream region and, as a consequence, the isotropic viscosity hypothesis is inadequate.

Comparison of the predicted turbulent kinetic energy with data are shown in Figure 4.5. The predicted k values are in good agreement with the data near the inlet plane. However, the k-ϵ model under-predicts the k values further downstream near the centerline. The discrepancy near the centerline is due to: (1) under-prediction of the corresponding maximum in the mean velocity, (2) inadequacy of the eddy viscosity hypothesis, and (3) over-prediction of turbulent kinetic energy dissipation rate, ϵ. The inlet distribution of length scale has a significant effect on the

ϵ distribution in the upstream region where the diffusion terms have a large effect on the mean velocity; it has no significant effect in the downstream region where the diffusion effects are smaller. The k-ϵ model tends to connect the dissipation rate too strongly to the local mean velocity field (Habib and Whitelaw, 1979) which is inappropriate since the dissipation occurs in the finest scales of motion and these do not reflect the local mean strain field. These connection tends to increase the local level of ϵ. The predicted turbulent shear stress ,$\overline{uv}$, profiles are also in very good agreement with the data (Figure 4.6). At x = 13 mm, the negative peak value for $\overline{uv}$ near the axis corresponds to the shear layer between the inner and annular streams and the positive peak corresponds to the shear layer associated with the pipe expansion.

4.2.2 THE ALGEBRAIC STRESS MODEL RESULTS

Prediction results for non-swirling flow using Π_{ij} model given by eq. (2.13) are shown in Figures 4.8-4.13, while the comparisons of different Π_{ij} models given by eqs.(2.13,2.14), (2.13,2.15) and (2.13,2.16) are presented in Figures 4.14-15. The various models used in this investigation and the recommended values for the constants appearing in these models are presented in Tables 4.4-4.6. The details of these calculations have been discussed by Nikjooy et al. (1985).

For a fixed pressure-strain model, the calculated mean and turbulence fields obtained from the three different ASM are essentially identical and are in good agreement with measurements. Some slight differences can be identified; however, they are not substantial enough to lead one to conclude that one ASM is better or worse than another. In general, the flow is very well predicted in the near and far field but not so well calculated in the mid-field. This is especially true of the flow near the combustor core, where the calculated mean axial velocity and turbulent normal stresses are consistently lowered than the measurements (Figures 4.8,4.11-4.13). The recirculation zone is very well predicted by all ASM. One surprising result of the present study is given by the calculations of the k-ϵ closure (Figures 4.8-4.10). Essentially the same calculated distributions of U, k and $\overline{uv}$ are obtained when the k-ϵ closure is used instead of the ASM. Indeed, the k-ϵ closure gives a k distribution that is in as good an agreement with measurement as that given by ASM/E (Figure 4.9).

A second interesting result of the present study can be found in the comparison of the different Π_{ij} models. Here, the effects of the four Π_{ij} models are discussed. Instead of giving rise to improved correlations with measurements as anticipated, some of the calculations are actually in worse agreement with measured data for ASM/MY and ASM/R (Figures 4.14,4.15). As for the ASM/E, very little differences are

noted for the four Π_{ij} considered, except in the prediction of the reattachment length. Also, the choice of the mean strain model has a great effect on the calculated turbulence field. The results shown in Figures 4.14 and 4.15 for the Π_{ij} given by (2.13,2.14), (2.13,2.15) and (2.13,2.16), respectively, are selected to illustrate the points made above. In general, the comparisons for other stream locations are quite similar to those shown in Figures 4.14 and 4.15. Depending on the non-equilibrium ASM used for closure of the flow equations, $\Pi_{ij,2}$ modelling given by (2.14) or (2.15) will lead to prediction of double peaks behavior for the turbulence field (Figure 4.14), which are not observed in the experimental flow. Such behavior is not found in ASM/E calculations, though. One reason for this could be due to the fact that the constant C_2 used is not suitable for complex turbulent flows. Since C_2 is determined for simple turbulent flows in local equilibrium, it would be more appropriate for ASM/E than for ASM/MY and ASM/R. Another reason could be the incorrect modelling of the mean strain part of the pressure-strain terms by (2.14) and (2.15). The results shown in part (c) of Figures 4.10 and 4.11 illustrate the importance of accounting for the anti-symmetric contributions of the mean strain tensor as given by (2.16). With this improvement, the anomalies seen in parts (a) and (b) of Figures 4.14 and 4.15 disappear with the exception of the calculated $\sqrt{\overline{v^2}}$ using ASM/R closure.

Therefore, it is very important to model the mean strain tensor correctly. Either the mean strain effects are not modelled at all, as in (2.13), or they should be accounted for properly, as in (2.16).

Another measure of the performance of the different turbulence models is in the calculation of the reattachment length. This length is determined by locating the point of zero shear at the combustor wall. Factors which influence the reattachment length may be classified in one of two groups: (1) system geometry, (2) upstream conditions. System geometry has a significant effect on reattachment length. The two primary geometric parameters influencing the sudden expansion flow are: (a) d_2/d_1, the expansion ratio, where d_1 is the diameter at the inlet to the sudden expansion and d_2 is the diameter of the downstream tube. (b) $d_2/(d_2-d_1)$,the aspect ratio. Upstream conditions which have an effect on reattachment length in the sudden expansion flow are: (a) the inlet flow Reynolds number, (b) centerline turbulence level, (c) inlet Mach number. So (1986) has examined the effects of these parameters on reattachment length in an axisymmetric sudden-expansion flow. Based on his analysis, it was reported that the single most important parameter that influences the reattachment length is the centerline turbulence level. The results of the fifteen different calculations are listed in Table 4.3 together with the measured reattachment length determined from Johnson and

Bennett (1981). It can be seen that the best estimate of the reattachment length is given by the k-ϵ and ASM/E closures, while the worst is given by the ASM/R with Π_{ij} deduced from (2.15).

An Attempt is made to assess the lack of differences shown by the calculations of the three ASM closures (Figures 4.8-4.13). The calculated turbulent viscosities of the three ASM closures are compared with the numerical viscosity (Figure 4.16). It can be seen that the turbulent viscosities are quite a bit smaller than the numerical viscosity in the inlet region of the combustor and are of the same order at or near the dividing streamline of the recirculation zone. Consequently, calculations in the near field and the recirculation region are being masked by the numerical viscosity and the errors would propagate through the whole field. Unless the numerical viscosity is significantly reduced, the improvements afforded by more sophisticate turbulence closures will not be realized for complex turbulent flow calculations. In addition to hybrid differencing scheme, the Quadratic Upwind Differencing (QUD) scheme of Leonard (1979) was also explored. The results are very much similar to the hybrid scheme predictions. It should be pointed out that QUD reduces false diffusion, but does not eliminate it entirely (Figure 4.17)

4.2.3 REYNOLDS STRESS MODEL RESULTS

Having demonstrated the effect of the pressure-strain correlation and compared the k-ϵ model with ASM, attention is now turned to the performance of the Reynolds-stress model (RSM). It seems somewhat paradoxical that the more advanced types of turbulence model have been least successful in the complex flows associated with flow recirculation for which (in theory) they have the most to offer compared with eddy viscosity based closures. The difficulty in clearly demonstrating calculations free of numerical errors has hampered the real testing of Reynolds stress closures in such flows due to the practice of using upwind differencing for discreption of the convection terms. This practice is resulted in the phenomenon of numerical diffusion and to produce a scheme which is slow to respond to grid refinement. Although local selective mesh refinement can be used to obtain numerical error-free predictions when using eddy viscosity based models, this become totally impracticable when considering Reynolds stress transport closures where the lack of an eddy viscosity increases the local cell Peclet numbers and the associated numerical diffusion coeffiecients by orders of magnitude. Unless numerically accurate solutions are developed, the improvements afforded by advanced turbulence models will not be realized for complex recirculating flows.

Effects of two different turbulent diffusion models (2.18,2.19) on the Reynolds stress closure are investigated (Figures 4.18-4.21). The predicted results of the mean velocity and turbulent shear stress, $\overline{uv}$ fields obtained from these two models are very similar. However, some differences are observed in the prediction of the peak values of the normal stresses. In the fully developed region, the model developed by Daly and Harlow (2.18) performs better, especially near the centerline. Despite the superiority of Hanjalic and Launder's model (2.19) in a theoretical sense, it does not appear to give better predictions.

For a fixed diffusion model (2.19), two different pressure-strain models are employed to predict the mean and turbulence quantities. In one case, mean strain rate effects are not considered and in another, these effects are accounted for using the Launder et al. model (2.16). The predicted results of mean velocity and turbulent stresses are illustrated in Figures 4.22-4.25. It can be seen that, both models performed similarly. However, Rotta's model (2.13), gives a better prediction of the normal stresses.

In comparison with other simple closures (k-ϵ and ASM), it can be seen that the major discrepancy arises in the prediction of reattachment length (Table 4.3) and centerline values (Figures 4.26-4.30). In spite of its higher class of sophistication, RSM under-predicts the size of the recirculation region. A question arises here on the mass

flow rate in the combustor displayed by the measured data; this seems larger than in the calculations, which certainly conserve mass between inlet and exit from the solution domain. This feature is also to be seen in the comparisons shown by Mansour et al. (1983) and Hackman et al. (1984), where the area under the predicted velocity curves is clearly less than under the measured data. It is possible that transverse side-wall boundary layer growth in the experiment caused acceleration on the centerline of the combustor, but it is difficult to do more than speculate.

It is speculated by McGuirk et al. (1985) that the k-ϵ deficiency is caused by the model's inability to represent the normal stress-normal strain production terms properly. This feature still remains in the RSM calculations, as is shown by the distribution of the two contributions to the production of k from shear and normal stress terms in the profiles drawn in Figure 4.31 at an axial station near reattachment. Although positive values of the normal stress term are obtained near the axis, they represent only about 10% of the maximum shear stress production. Estimate made from the measurements of recirculating flow reported by Taylor and Whitelaw (1984) show that the maximum values should be of the same order, so that even in the RSM calculations the normal stress production is too small by an order of magnitude.

So far computations have been performed by using a high Reynolds number model and 51x41 non-uniform grid system. The conventional wall law has been adopted to connect adjacent grid lines to the wall boundary. However, results do not show any trace of the secondary circulation observed experimentally. The switchover to a fine-grid (51x50), low-Reynolds-number analysis has had a significant effect on the predicted flow pattern in this region. An appreciable secondary eddy is now formed which extends almost one-step height downstream and one-tenth of a step height normal to the wall (Figure 4.32). It is because of the thinness of this secondary eddy that the wall-function approach failed to predict its existence. Comparison of the calculations with a high and a low Reynolds number model results show that outside the viscosity dominated region, the two models performed with just about equal success (Figures 4.33-4.34). However, transpiration through the wall and steep temperature gradients due to large imposed wall heat fluxes or frictional heating are just a few of the cases that may cause the near wall region to have more influence on the core region. Despite the limitations of the turbulence model, the replacement of wall function by a fine-grid treatment has allowed a more realistic modelling of the flow just downstream of the step.

4.2.4 CONCLUSIONS

Based upon the preceding discussion, Several main conclusions can be summarized as follows.

1. As far as the mean field prediction is concerned, k-ϵ closure performs just as well as any ASM closure in the calculation of combustor flow.
2. The reattachment length is reasonably predicted by the k-ϵ closure.
3. The effects of pressure-strain modelling on the calculations are large compared to the effects of different ASM closures.
4. If the mean strain effects on the pressure-strain terms are to be accounted for, they should be modeled by the Launder et al. (1975) model.
5. The simplest pressure-strain model (2.13) gives as good a correlation with measurements as the model given by (2.13, 2.16)
6. The best correlation with measurements for combustor flow calculations is given by the ASM/E closure with Π_{ij} determined from (2.13).
7. The best prediction of normal stresses is given by the ASM/E closure with Π_{ij} determined from (2.13).
8. The best prediction of shear stress is given by the ASM/E closure with Π_{ij} determined from (2.13) or the k-ϵ closure.

9. Turbulent diffusion model developed by Daly and Harlow (1970) results in better predictions than the Hanjalic and Launder (1972) model.

10. Reynolds stress models do not seem to yield better predictions than the algebraic stress models.

11. Low-Reynolds-number model prediction of the near wall region is more realistic and show the corner recirculation region.

4.3 MODEL EVALUATIONS FOR COMBUSTOR FLOW CALCULATIONS WITH SWIRL

In this section, performance of the k-ϵ closure, algebraic stress model (ASM) and Reynolds stress model (RSM) are evaluated and compared with data. In the previous section, it was concluded that the turbulent diffusion model developed by Daly and Harlow (1970) results in better predictions than the Hanjalic and Launder (1972). Therefore, this model is employed for RSM calculations. Based on some preliminary calculations, it was found that the mean strain rate effects have to be accounted for. Otherwise, predicted results of the normal stresses show negative values in some regions of the flow fields. Therefore, these effects are approximated by the Launder et al. model (2.16)

The data of Roback and Johnson (1983) represent a carefully measured turbulent water case with a 30 degree,

free swirler. Inasmuch as inlet profiles were not provided, Calculations were started at the first measurement location, which was just downstream of the expansion plane (5 mm). This approach is unsatisfactory because the input length scales of turbulence used to calculate dissipation rate are unknown and the effect of area expansion on the flow has not been properly accounted for. The ability to predict the existence and location of the central recirculation zone in this combustor is a good indication of the suitability of the model.

4.3.1 THE k-ϵ MODEL RESULTS

The centerline plot of the axial velocity is provided in Figure 4.35. The k-ϵ model mimics the data trend reasonably well along the symmetry axis, however, the rate of recovery is under-predicted. The reason is not easily resolved. Comparison of the calculated mean axial and tangential (azimuthal) velocity profiles with the experimental data are presented in Figures 4.36 and 4.37. In this case, the k-ϵ model fails to display the size and strength of the experimental recirculation zone. The predicted axial profile is skewed tward the wall in accordance with the data trend, although the maximum value decreases slightly with a corresponding increase in the near-wall region. At the farthest downstream locations, the k-ϵ model produces a decreased axial velocity near the

centerline, indicative of its lagging characteristics and apparent slow recovery. The k-ϵ model prediction of tangential velocity is excellent up to a station of 152 mm from the expansion. At subsequent downstream locations, calculation of the azimuthal velocity decays prematurely to a forced vortex profile, while the experimental data still shows a combined vortex profile. Over most of the radius, the measured tangential velocity is approximately constant and only rapidly approaches zero at the centerline from a radius of about 2 cm (r/R= 0.33). Further downstream from 305 mm (x/R=5), the calculated flow approximates a forced vortex while the measured flow approximates a free vortex in the outer region, with a forced vortex core.

4.3.2 THE ALGEBRAIC STRESS MODEL RESULTS

For a pressure correlation model given by Launder et al.(2.16), three different ASM's are compared. Results show that the calculated mean and turbulence fields are very similar for all the ASM's and are in good agreement with measurements at most of the locations (Figures 4.38-4.41). The tangential velocities obtained from the three ASM's are also very similar and in very good agreement with the data. The algebraic stress models provide profile shapes which are remarkably similar to the exhibited data trend, although the swirl velocity predictions are reduced in magnitude from the measurements. The discrepancy in tangential velocity

profiles is probably generated in part by incorrect inlet radial velocity profile. The measurements of mean axial and radial velocities at downstream stations indicate that the tangential velocity profile at 405 mm is in equilibrium. A free vortex is not a stable profile, and viscosity effects at the core modify the profile to the stable forced vortex form locally, as indicated at 405 mm. Therefore, the discrepancy in tangential profiles could also be due in part to an inadequate calculation of eddy viscosity across the radius.

Figure 4.40 displays the fluctuating axial velocity at various locations. All the algebraic stress predictions are similar to the exhibited data trend with a slight under prediction of stress magnitudes. This may be due to the modelling of the terms in the pressure-strain correlation and the constants used. Consequently, it cannot be implied that the algebraic stress model exhibits a superior prediction capability. The lack of agreement between the predictions and the data may be attributed to experimental error, boundary conditions, numerical diffusion, and oscillatory phenomena. However, it is difficult to separate the relative effects and apportion to each its respective contribution to error.

4.3.3 REYNOLDS STRESS MODEL RESULTS

Results of the mean and turbulence field obtained from the k-ϵ model and the ASM were compared with the Reynolds stress model (Figures 4.42-4.45). A wide disparity exists between the models prediction of the axial velocity near the centerline. It is evident that there are substantial differences in the capability of the various models to promote or hinder formation of the recirculation zone relative to the k-ϵ model. The comparison of the calculated and measured locations of the forward and rear stagnation points along the centerline for five different models is presented in Table 4.7. It is clear that the proper turbulence model is dependent on the location within the flow field. With regard to the comparison between measurements and calculations, the predictions by RSM seem to be slightly better than ASM for tangential velocity, while those by k-ϵ model are closer to experimental data for the central recirculation. An examination of the calculated Reynolds stresses indicates that the relative performance of the model is strongly dependent on the flow region.

4.3.4 CONCLUSIONS

Based upon the preceding discussion, The main conclusions can be summarized as follows.

1. As far as the mean field prediction is concerned, algebraic stress model (ASM) and Reynolds stress model (RSM) perform better than the k-ϵ closure in predicting the tangential velocity profiles.

2. The mean strain effects on the pressure-strain terms must be accounted for.

3. The central recirculation region is over-predicted by the ASM and the RSM; however, it is under-predicted by the k-ϵ closure.

4. The Reynolds stress model does not yield any better predictions compared to the algebraic stress model calculations.

5. Inlet conditions are the most important factor in determining the location, size, and the strength of the central recirculation region.

4.4 SCALAR TRANSPORT MODELLING AND COMPARISON

In the present study, the experiments of Johnson and Bennett (1981) and Roback and Johnson (1983) are chosen to compare with the calculation results. These experiments are selected because of their unique turbulent mass transport measurements.

4.4.1 NON-SWIRLING FLOW CALCULATIONS

In the present study, the mean velocities and Reynolds stresses predicted by Reynolds stress closure are used to calculate the mean mixture fraction, Θ, the RMS of the fluctuating mixture fraction and turbulent mass flux for non-swirling flow (Figures 4.46-4.50). The various models used for turbulent scalar flux and the recommended values for the constants appearing in these models are listed in Table 4.8-4.10. In the present study, firstly, the effect of the two algebraic flux closures (2.36,2.37) with two different pressure-scalar gradient models on combustor flow mass transfer are analysed (Figures 4.46-4.48). Secondly, the components of the scalar flux are obtained directly from solution of their respective modelled transport equations. The effect of pressure-scalar gradient models are also investigated. All the model predictions are essentially identical and are in good agreement with measurements. Some slight differences can be identified, however, they are not substaintial. In the case of mean concentrations, the calculated profiles at x=51 mm, x=102 mm and x=305 mm, are in close agreement with those measured. Between x=152 mm and x=254 mm where the transport in the axial direction is comparable to or larger than the radial, some discrepancies near the axis of the tube are seen. Here, the turbulent diffusion rates are anisotropic. Although this effect has been considered in the modelling, the model did not respond

effectively in the non-isotropic region of the flow field. The shapes and thickness of the concentration profiles are in reasonable agreement with measured values, however, the calculated concentrations at and in the vicinity of the center line are over-predicted by around 20% . This is consistent and at least in part a consequence of the low mean velocities calculated in this region. The error is probably due to experimental errors, because the predicted levels of the mixture fraction are required to conserve the mass flux of dye. The fluctuation profiles show that the models under-predict the peak values almost at all the locations. These predictions suggest that the constant associated with the dissipation of fluctuations should be lower than the present choice in some portions of the flow field.

The results of the transport equations for turbulent scalar fluxes (Figures 4.49-4.50) show that the predicted mean concentration are in better agreement with the data although the turbulent mass flux has been over-predicted near the centerline. It seems reasonable to increase the diffusion rate of the turbulent mass flux through its constant.

Finally, it should be pointed out that Mellor and Yamada's model gives a linear set of algebraic equations for $\overline{u_i u_j}$ and $\overline{\theta u_i}$. This is much more easy to solve and less time consuming than the set of non-linear algebraic equations

obtained from Rodi's model (2.33) ,and Launder and Gibson's model (2.37).

4.4.2 SWIRLING FLOW CALCULATIONS

For swirling flows, effects of two pressure-scalar gradient correlation models (2.22,2.23) on two Algebraic Flux Models (AFM) are also investigated (Figures 4.51-4.53). The calculated mean and turbulence fields obtained from these closure models are very similar. Some minor differences are observed. However, they are not significant. The agreement between the predicted and the measured mean concentration profiles at most of the locations are excellent, except near the axis at the central recirculation zone (x=51 mm). The discrepancy could be due in part to an inadequate calculation of the centerline velocity. The radial turbulent mass transport rate profiles indicate that radial transport occurred at axial locations of x= 13, 25, 50 mm and essentially zero mass turbulent transport between x=102 mm to x=203 mm. The peak rates for x=13 mm and 25 mm correspond to the location of the interface between the inner jet and annular jet, and the location where the axial velocities were negative, respectively. At these two stations the turbulent mass rates have been under-predicted which could be the results of the inlet condition or velocity field. The discrepancy between the model predictions and the measurement is more clear at 51 mm.

There is considerable scatter in the measurements, however, this location is near the upstream end of the central recirculation region where the flow may not be axisymmetric. Finally, the β-probability density function for concentration at location x = 25 mm is calculated from the known mean and variance. The results obtained are very similar and in close agreement with the measured profiles (Figure 4.54).

4.4.3 CONCLUSIONS

The main conclusions emerged from the preceding discussion can be summarized as follows:

1. The two algebraic flux model predictions are very similar.
2. The effect of mean strain modelling on the pressure-scalar gradient terms is not significant.
3. The transport model for scalar fluxes does not have any advantage over the algebraic flux model.
4. The β-distribution is sufficient to give the correct behaviour of the instantaneous scalar distribution.

4.5 EXTENSION OF CONSTANT DENSITY MODELLING TO VARIABLE DENSITY CALCULATIONS

The preceding models are extended to the variable-density swirling flow conditions studied by Brum and Samuelsen (1982). For this case, mean velocity and turbulence intensity measurements were provided in the flow field for the axial and tangential velocity components. However, inlet velocity profiles were not measured. Consequently, the axial velocity profile used to initiate computations was regarded to an idealized, turbulent, annular pipe flow distribution. The tangential mean velocity component and turbulence quantities were taken from the downstream measured profiles. The turbulence length scale at inlet was assumed to be 1.6 mm. It may be argued that the independent specification of the velocity distributions for separate jet streams, the use of idealized profiles, or the use of profile shapes from the measurements is not entirely justifiable. Nevertheless, the predictions are still useful in demonstrating some of the differences between the various turbulence models. The injection velocity of propane/CO_2 was estimated based upon the mass flow and nozzle area. It is quite high (28.1 m/s) and such velocities would tend to eliminate or change the position of the recirculation region. Therefore, accurate inlet injection velocity measurements are required to correctly predict the flow field in the recirculation zone.

4.5.1 k-ϵ MODEL VERSUS ALGEBRAIC STRESS MODEL

Computations are started from the swirler exit, extending 300 mm downstream. A non-uniform grid of 51x50 with more nodes concentrated from the centerline to the nozzle opening is used. Axial grid spacing starts with 0.5 mm at the inlet and expands geometrically to the exit. A total of four different sets of calculations are performed for the non-reacting case. The calculations and their comparisons with measurement for Π_{ij} model given by (2.13,16) are presented in Figures 4.55-4.58. The results of the three ASM predictions of mean and turbulence fields are very similar. In the outer flow region, the predicted axial velocities are in agreement with the data; however, the calculations reveal substantial differences between the ASM's and the k-ϵ model near the centerline. The differences appear to be more significant for the present case than the previous ones, because of the large impact on the primary jet by the surrounding, swirling flow field. All the models induce a recirculation zone along the symmetry axis but maximum flow reversal velocities are smaller than the measurement. A comparison between predicted and measured swirl velocity profiles show that the algebraic stress model promotes fairly rapid decay of the mean velocities relative to the k-ϵ model. The use of the algebraic stress model, which are destabilized with forced vortex flow, may not be sound. The predicted turbulence profiles demonstrate a

pronounced relaminarization effect, reducing the turbulence intensities to unrealistically low values. The discrepancy between the prediction and the measurement is probably generated in part by incorrect inlet condition and to some extent by using constant-density models for variable-density flow. However, this is minor, since the variations in density flow field are not significant enough to affect the momentum field (air flow rate/CO_2 flow rate = 117.6). It is recognized that by selecting only three examples, it is difficult to generalize about the performance of these models under all conditions. It should be noted that this particular set of constants for the ASM cannot be lightly dismissed. The unusual characteristics adopted by the predictions prompts the inquiry as to the necessity of the full convection and diffusion terms for strongly swirling flow.

4.5.2 CONCLUSIONS

The previously discussed comparisons have demonstrated the relative merits of various turbulence models for the calculation of swirling, recirculating flows. It should be noted that the effectiveness of turbulence model predictions may be obscured to some extent by competing factors such as: inlet and boundary conditions, oscillatory phenomena, and numerical scheme. A significant contribution from any of the

aforementioned factors tends to invalidate conclusions regarding the superiority or inferiority of a given turbulence model. Even the most advanced turbulence model cannot compensate for inadequacy in this area.

Although little confidence is expressed in the ability of current generation turbulence models to simulate swirling flow aerodynamics, the k-ϵ model performs competitively. None of the ASM's could satisfactorily predict the Reynolds stresses, but alteration of the constants in pressure-strain model is a viable option to improve the capability of the ASM's for strongly swirling flows. The derivation and validation of higher-order closure schemes hold the greatest potential for turbulence model improvement for strongly swirling flows. In view of the current numerics, the additional computational time associated with higher order closure, and the lack of a well validated turbulence model, the k-ϵ model remains the model of choice and should be used to calculate reactive flows in practical combustors.

Table 4.1 Values of constants in k-ϵ model.

C_{μ}	$C_{\varepsilon 1}$	$C_{\varepsilon 2}$	σ_k	σ_{ε}
0.09	1.44	1.92	1.0	1.3

Table 4.2 Various models used in Reynolds stress and algebraic stress closures

MODEL	MODEL NUMBER	EQUATION NUMBER
REDISTRIBUTION	1	(2.13)
	2	(2.13) + (2.14)
	3	(2.13) + (2.15)
	4	(2.13) + (2.16)
DIFFUSION	5	(2.18)
	6	(2.19)
DISSIPATION	7	(2.24)
	8	(2.40)

Table 4.3 Comparison of calculated and measured reattachment lengths in mm.

		MODEL NUMBER			
		1	2	3	4
k-ϵ	258				
ASM/E		245	242	227	246
ASM/MY		245	254	222	246
ASM/R		240	229	158	201
RSM					242
DATA	254				

Table 4.4 Various algebraic stress models (ASM) used in this investigation

MODEL	MODEL NUMBER	EQUATION NUMBER
ASM/E	9	(2.28) + (model-1)
	10	(2.28) + (model-2)
	11	(2.28) + (model-3)
	12	(2.28) + (model-4)
ASM/MY	13	(2.31) + (model-1)
	14	(2.31) + (model-2)
	15	(2.31) + (model-3)
	16	(2.31) + (model-4)
ASM/R	17	(2.34) + (model-1)
	18	(2.34) + (model-2)
	19	(2.34) + (model-3)
	20	(2.34) + (model-4)

Table 4.5 Various Reynolds stress models (RSM) used in this investigation

MODEL	MODEL NUMBER	EQUATION NUMBER
high-Reynolds number model	21	(2.7) + (model-1) + (model-5) + (model-7)
	22	(2.7) + (model-4) + (model-5) + (model-7)
	23	(2.7) + (model-4) + (model-6) + (model-7)
low-Reynolds number model	24	(E.1-E.6) + (model-4) (model-5) + (model-8)
	25	(E.1-E.6) + (model-4) (model-6) + (model-8)

Table 4.6 Values of constants used in Reynolds stress and algebraic stress closures

MODEL	CONSTANT	ASSIGNED VALUES	MODEL NUMBER
REDISTRIBUTION	C1	5.0	1
	C1	3.7	2
	C2	-0.09	
	C1	1.5	3
	C2	0.6	
	C1	1.5	4
	C2	0.5	
DIFFUSION	C_S	0.22	5
	C_S	0.11	6
DISSIPATION	C_ε	0.15	
	$C_{\varepsilon 1}$	1.44	7
	$C\varepsilon 2$	1.92	

Table 4.7 Comparison of calculated and measured locations of the stagnation points along the centerline in mm

MODEL	FORWARD	REAR
$k-\epsilon$	31.4	147.9
ASM/MY	50.8	267
ASM/R	49.5	242.7
ASM/E	49.7	269
RSM	91	275
DATA	38	170

Table 4.8 Various models used in flux transport and algebraic flux models

MODEL	MODEL NUMBER	EQUATION NUMBER
REDISTRIBUTION	26	(2.22)
	27	(2.22) + (2.23)
DIFFUSION	28	(2.20)
VARIANCE	29	(2.25)

Table 4.9 Various flux transport and algebraic flux models (AFM) used in this investigation

MODEL	MODEL NUMBER	EQUATION NUMBER
AFM/MY	30	(2.36) + (model-26)
	31	(2.36) + (model-27)
AFM/LAUNDER	32	(2.38) + (model-26)
	33	(2.38) + (model-27)
FLUX TRANSPORT MODEL	34	(2.8) + (model-26) + (model-28)
	35	(2.8) + (model-27) + (model-28)

Table 4.10 Values of constants used in scalar flux models

MODEL	CONSTANT	ASSIGNED VALUES	MODEL NUMBER
REDISTRIBUTION	$C_{1\theta}$	3.63	26
	$C_{1\theta}$	3.0	27
	$C_{2\theta}$	0.33	
DIFFUSION	$C_{s\theta}$	0.11	28
VARIANCE	$C_{D\theta^2}$	1.3	29
	C_{θ^2}	1.5	

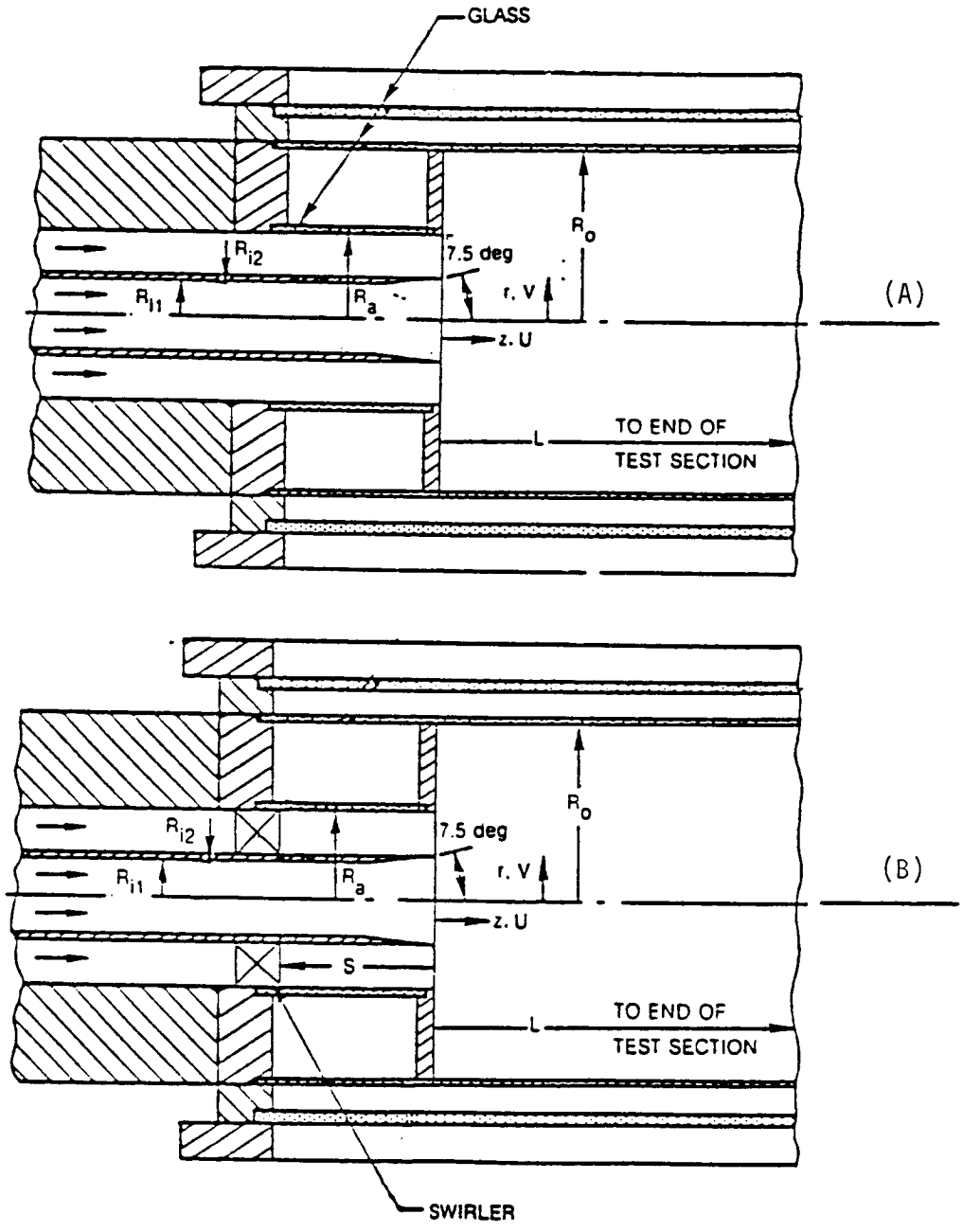

DIMENSION	R_{i1}	R_{i2}	R_a	R_o	S	L
LENGTH (mm)	12.5	15.3	29.5	61.0	51	1016
LENGTH (in.)	0.492	0.601	1.162	2.402	2.0	40
RADIUS RATIO, r/R_o	0.205	0.251	0.484	1.0	–	–

Figure 4.1 Sketch of inlet and test section A: Johnson and Bennett (1981), B: Roback and Johnson (1983)

a) SWIRLING FLOW

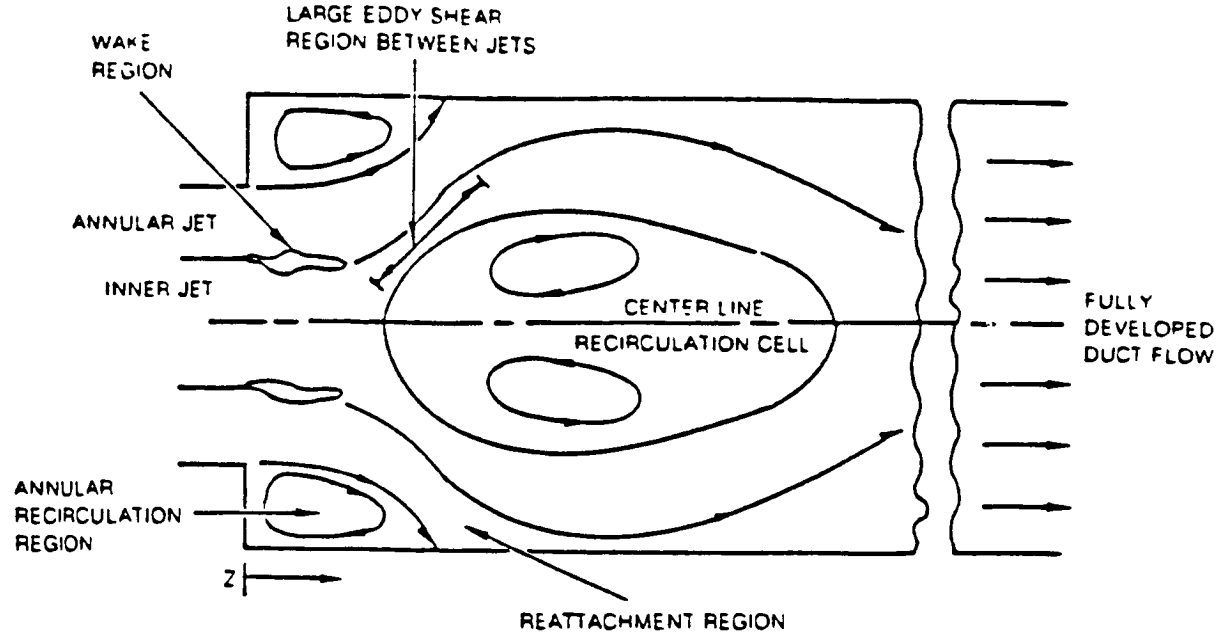

b) NONSWIRLING FLOW

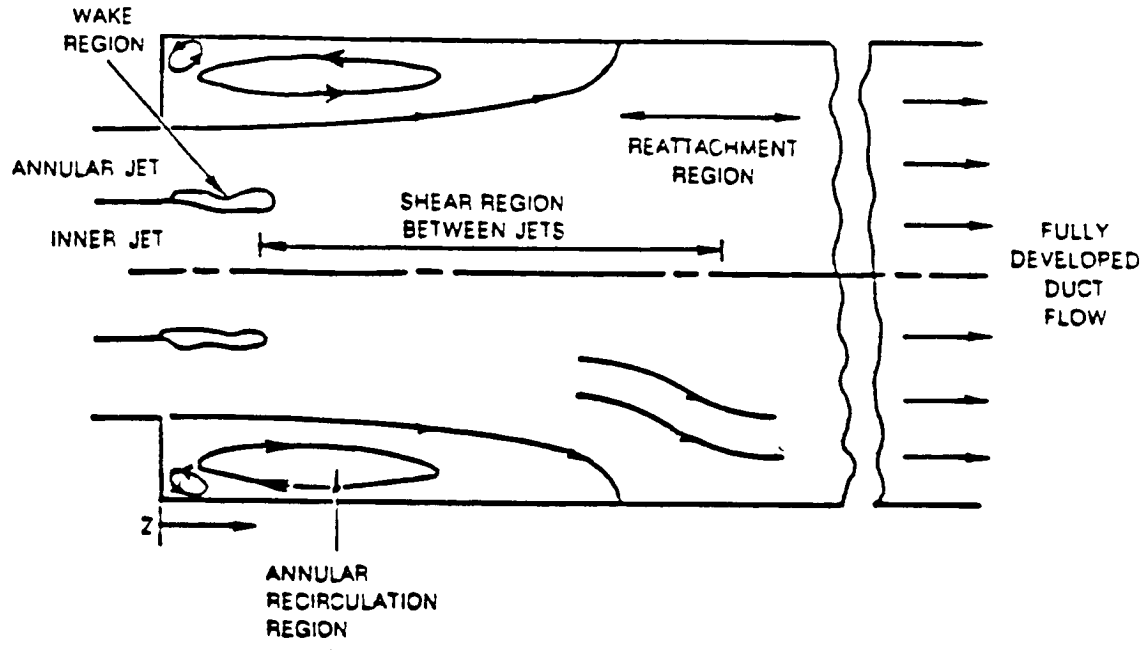

Figure 4.2 Sketches of flow regions for swirling and non-swirling flow conditions A: Johnson and Bennett (1981), B: Roback and Johnson (1983)

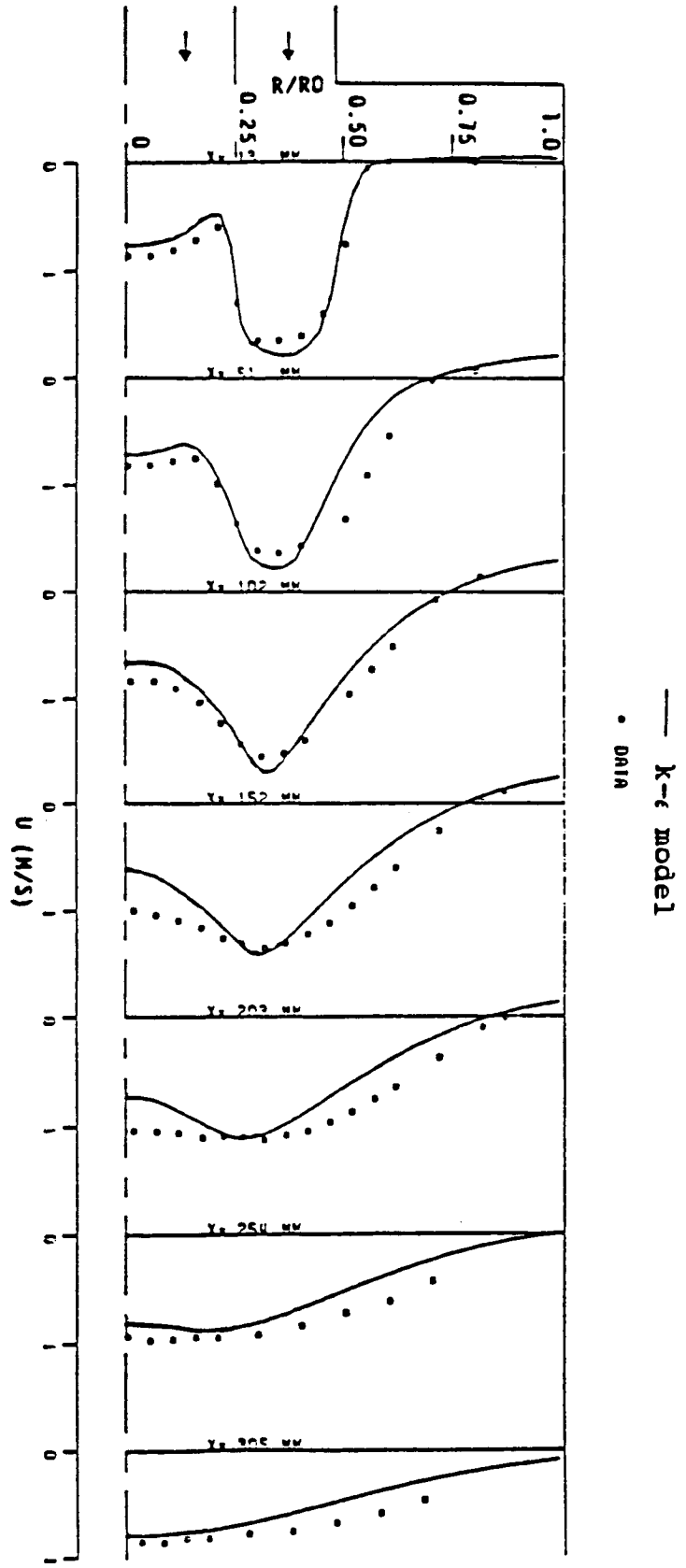

Figure 4.4 Comparison of predicted & measured axial velocity profile using k-ε model (Johnson and Bennett (1981))

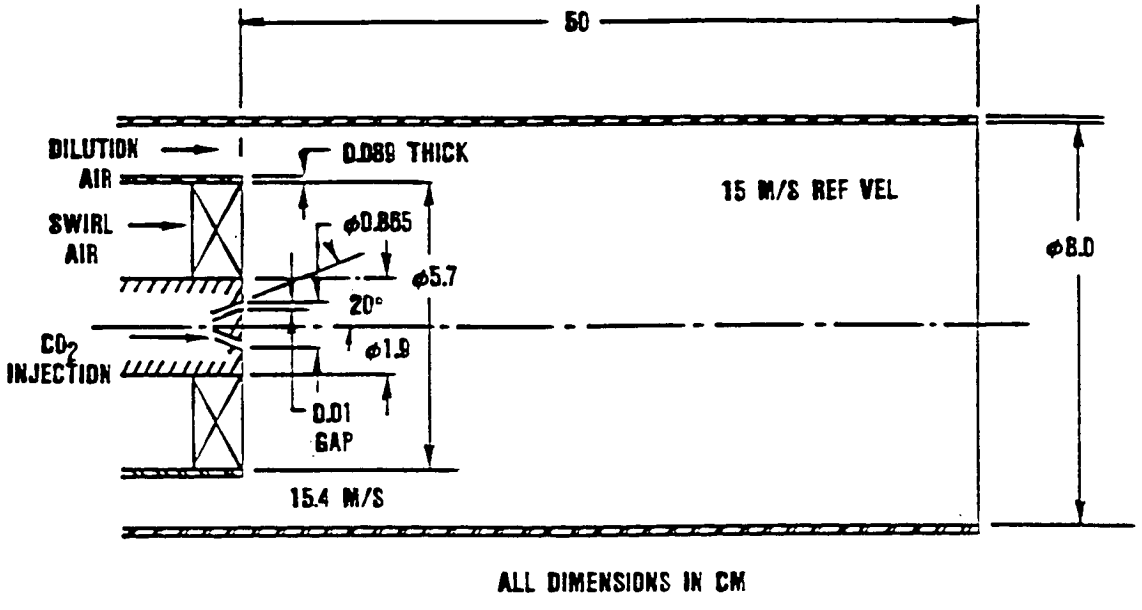

Figure 4.3 Sketch of inlet and test section (Brum & Samuelsen (1982))

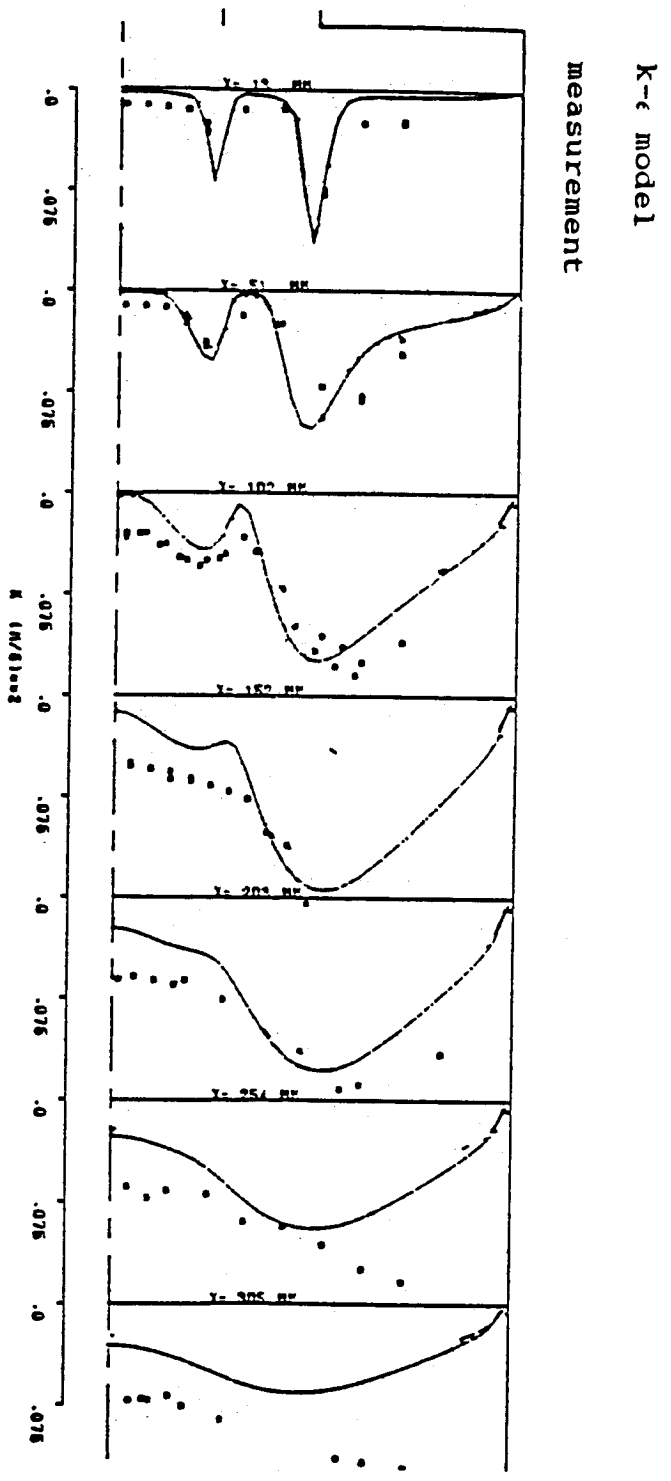

Figure 4.5 Comparison of predicted & measured turbulent kinetic energy profile using k-ε model (Johnson and Bennett (1981))

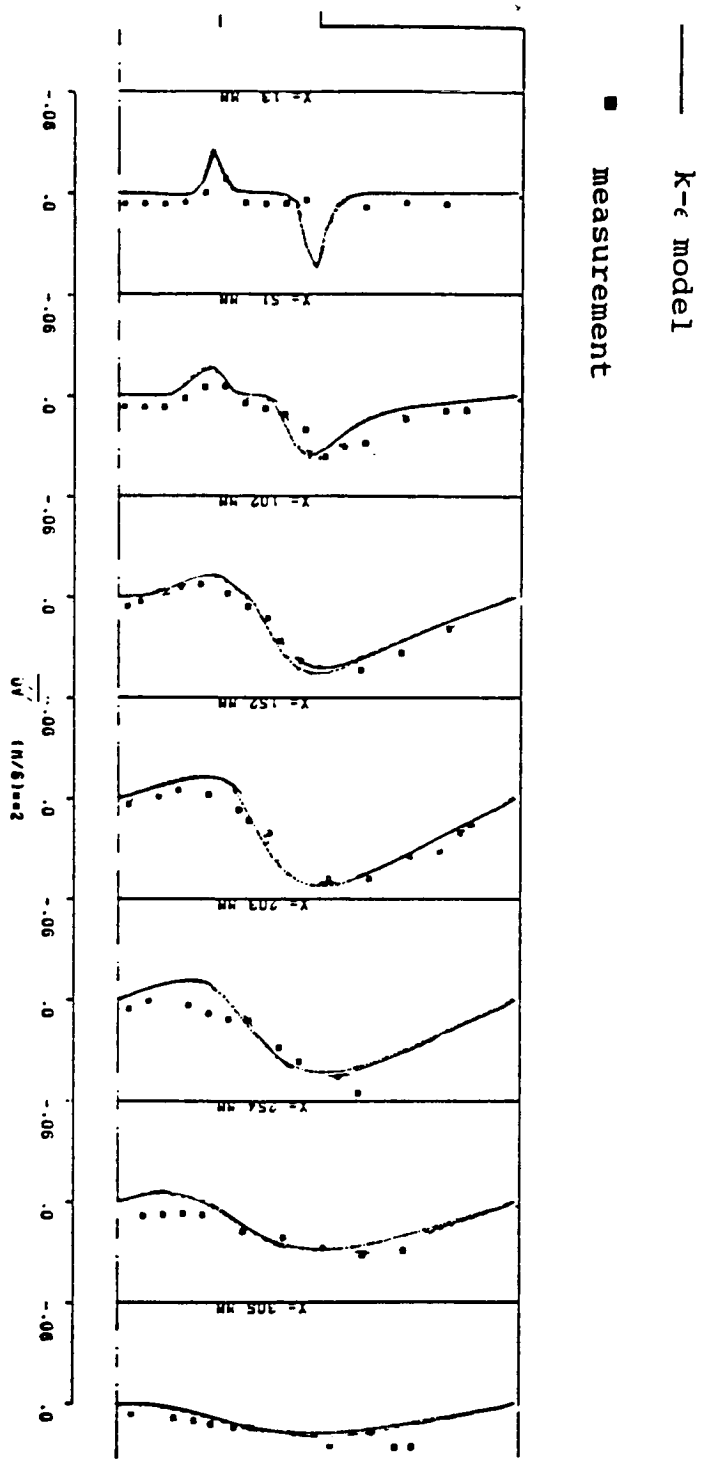

Figure 4.6 Comparison of predicted & measured turbulent shear stress profile using k-ε model (Johnson and Bennett (1981))

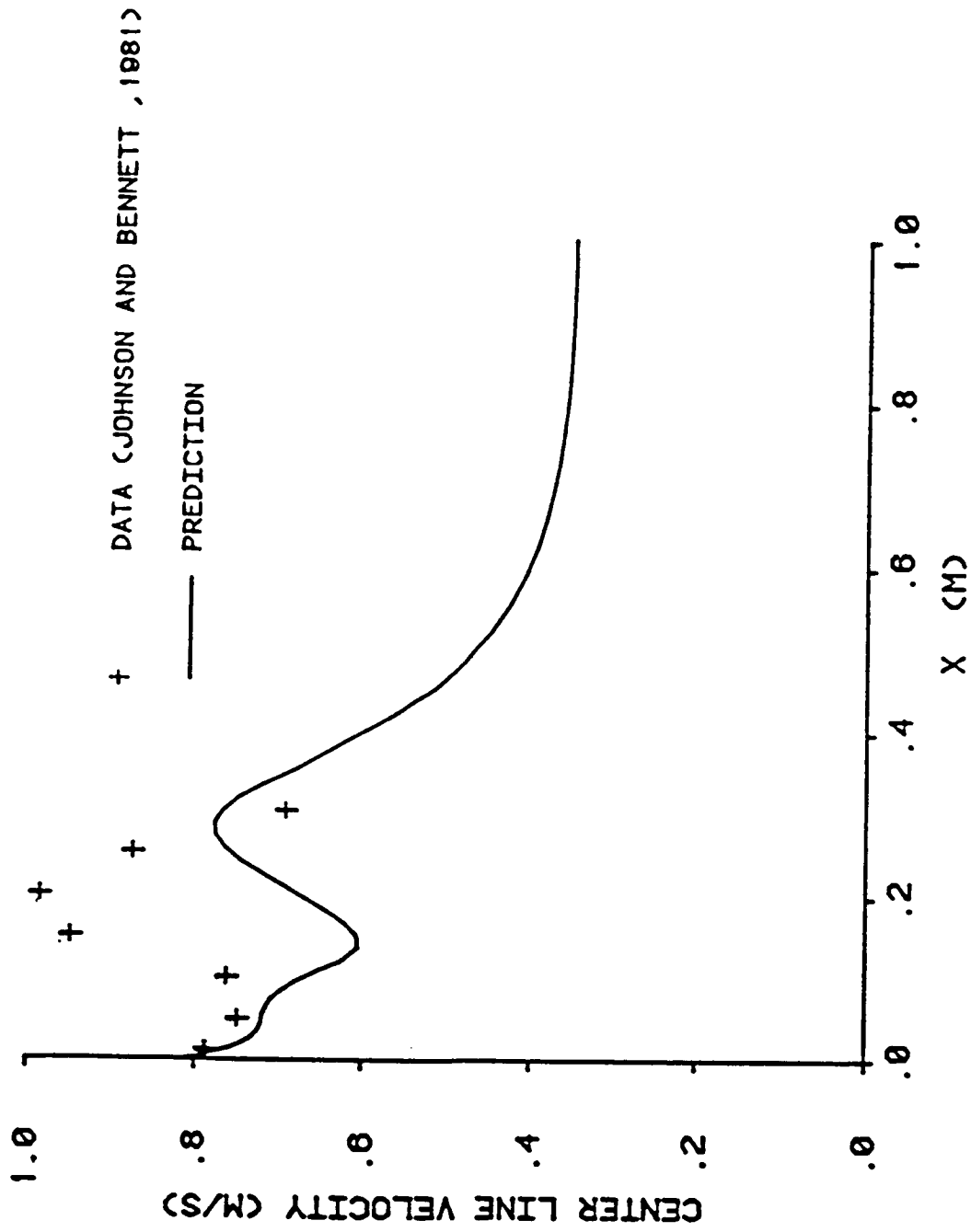

Figure 4.7 Comparison of predicted & measured centerline axial velocity profile (Johnson and Bennett (1981))

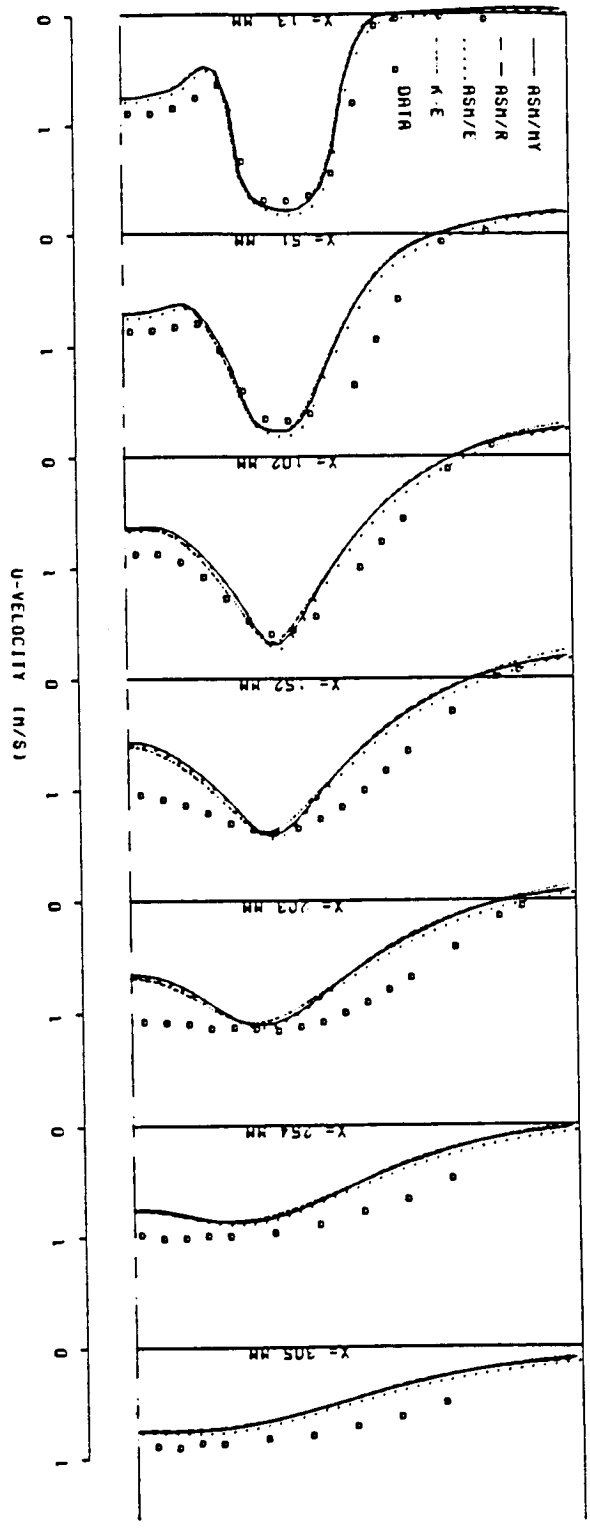

Figure 4.8 Comparison of measurements with mean axial velocity calculations using Π_{ij} from eq. (2.13) (Johnson and Bennett (1981))

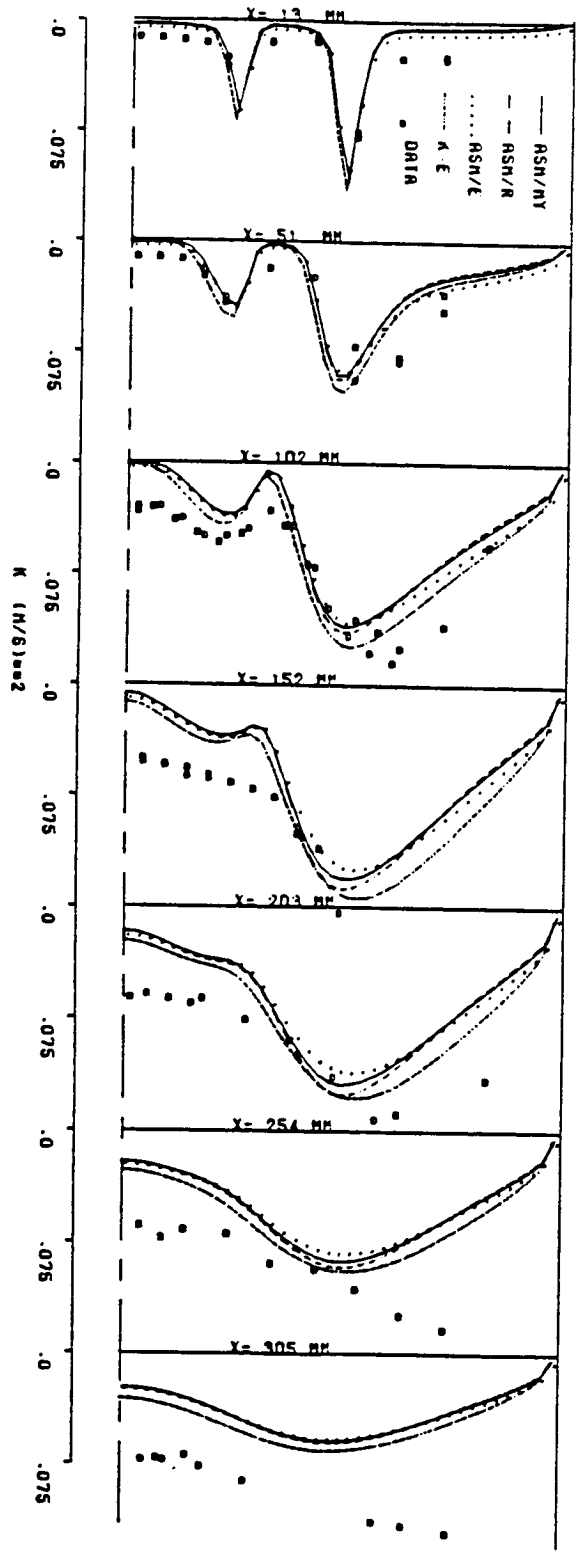

Figure 4.9 Comparison of measurements with k calculations using Π_{ij} from eq. (2.13) (Johnson and Bennett (1981))

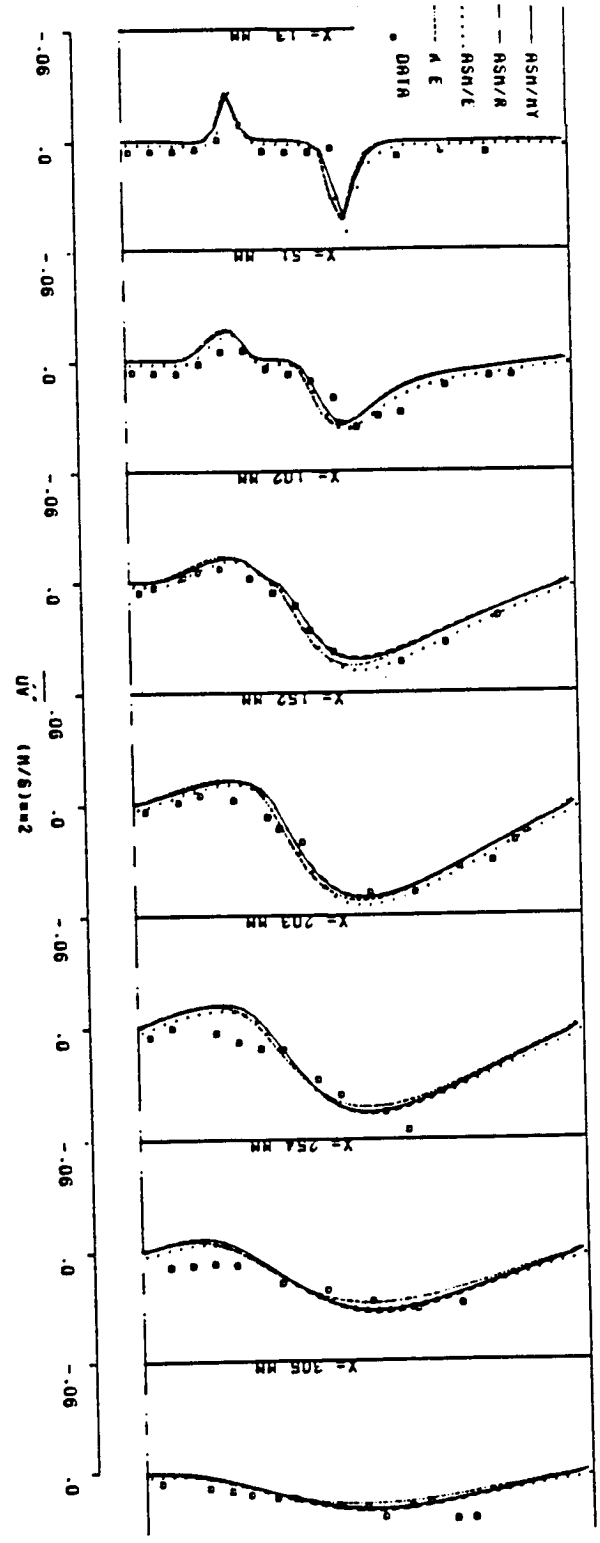

Figure 4.10 Comparison of measurements with $\overline{uv}$ calculations using Π_{ij} from eq. (2.13) (Johnson and Bennett (1981))

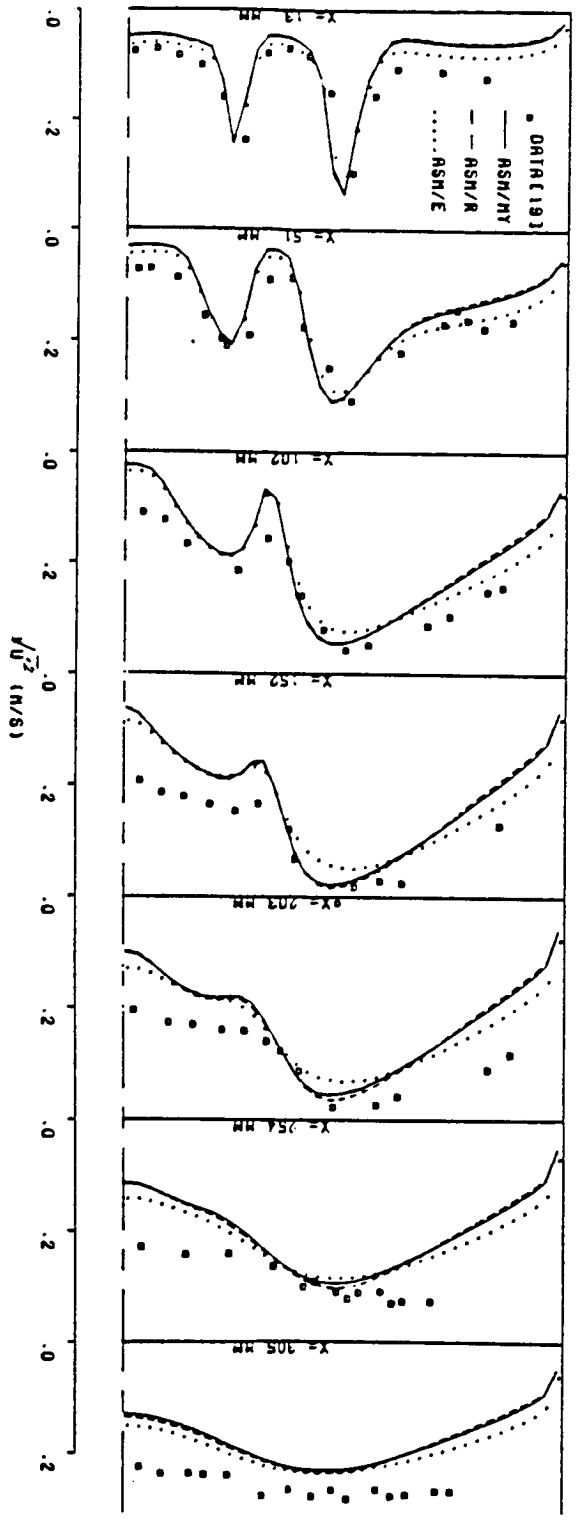

Figure 4.11 Comparison of measurements with $\sqrt{u'^2}$ calculations using Π_{ij} from eq. (2.13) (Johnson and Bennett (1981))

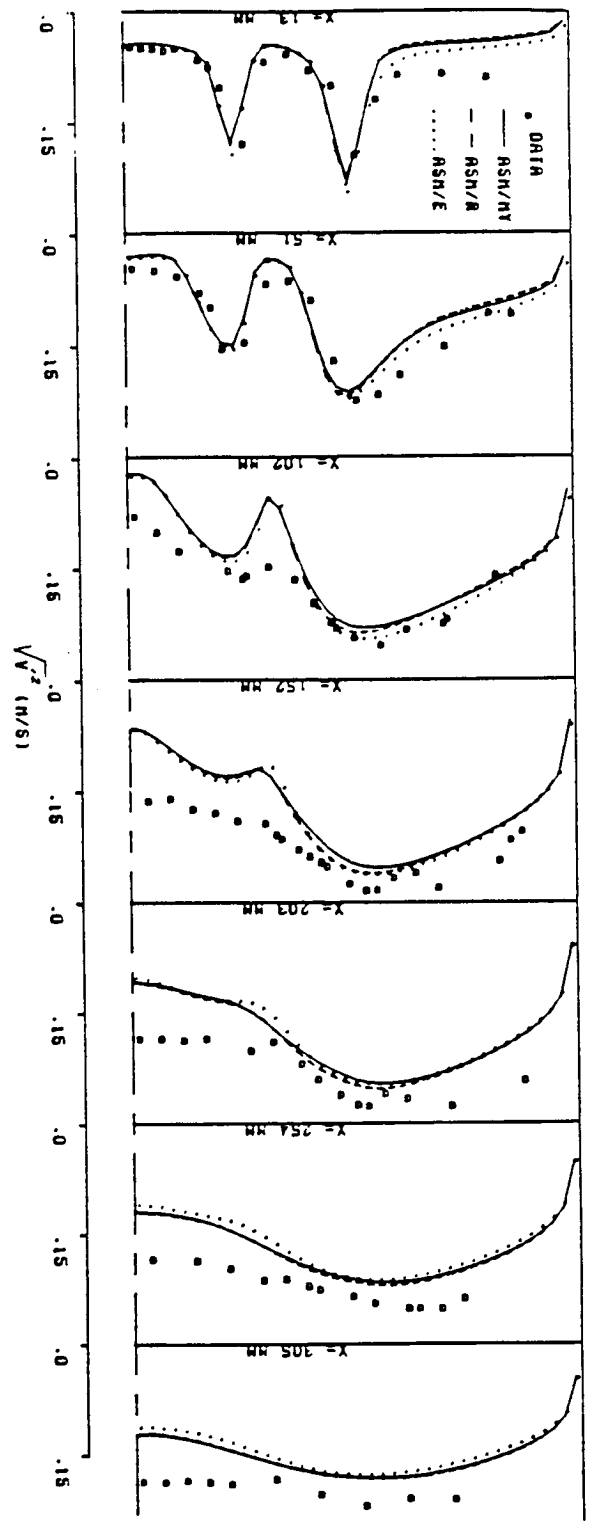

Figure 4.12 Comparison of measurements with $\sqrt{\overline{v^2}}$ calculations using Π_{ij} from eq. (2.13) (Johnson and Bennett (1981))

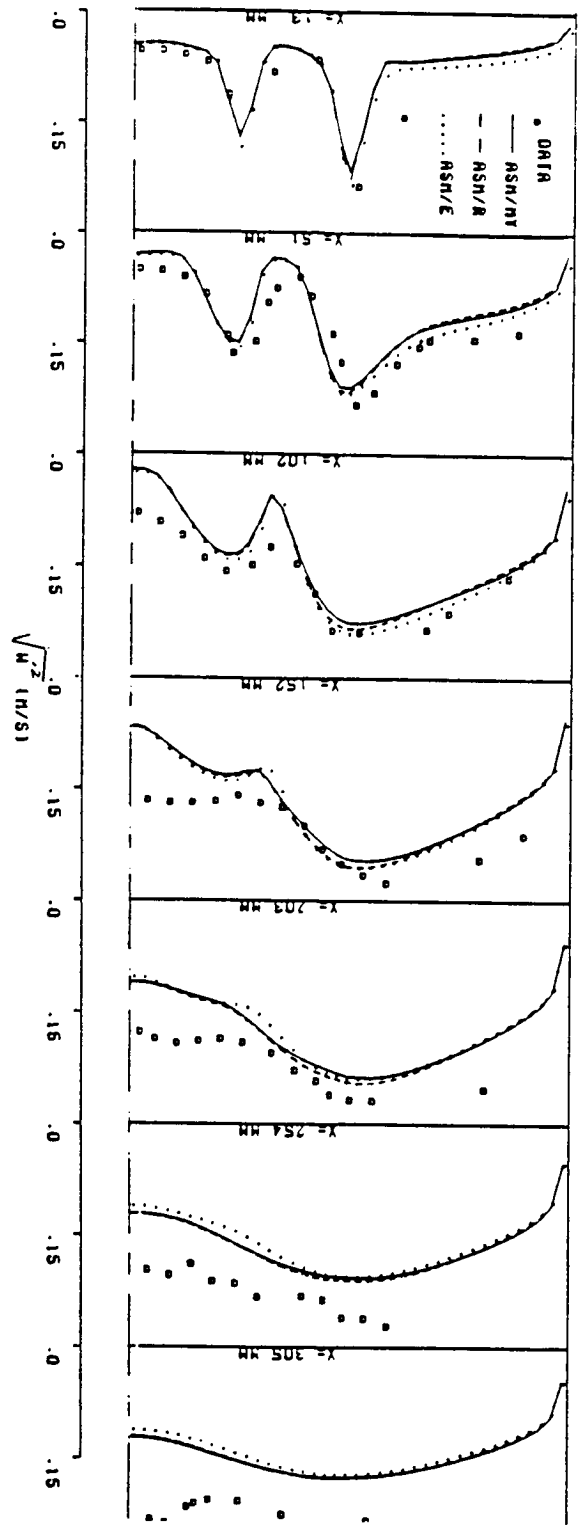

Figure 4.13 Comparison of measurements with $\sqrt{w^2}$ calculations using Π_{ij} from eq. (2.13) (Johnson and Bennett (1981))

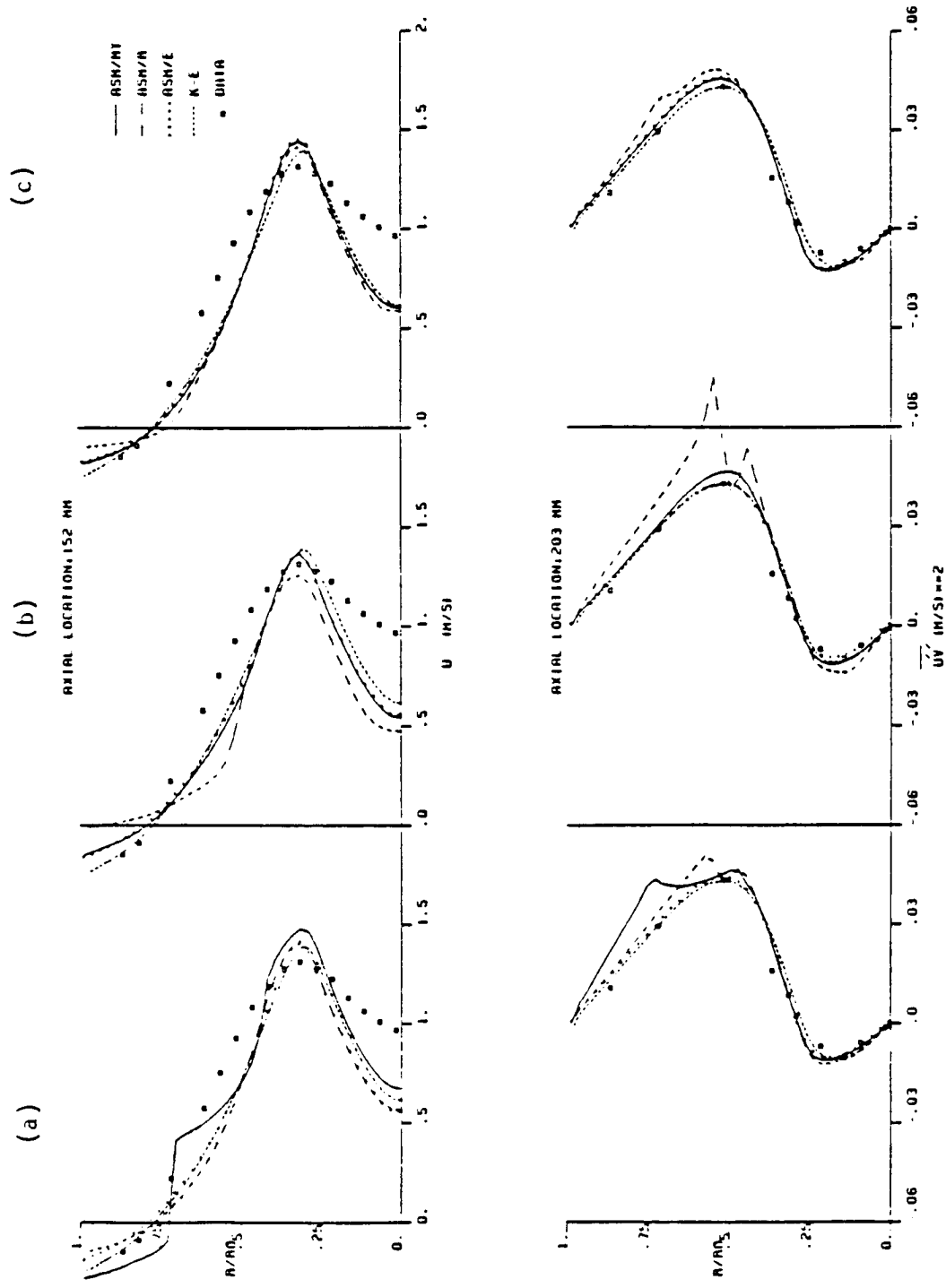

Figure 4.14 Comparison of measurements with U and $\overline{uv}$ calculations using $\Pi_{ij} = \Pi_{ij,1} + \Pi_{ij,2}$
(a) eqs. (2.13,2.14), (b) eqs. (2.13,2.15),
(c) eqs. (2.13,2.16) (Johnson and Bennett (1981))

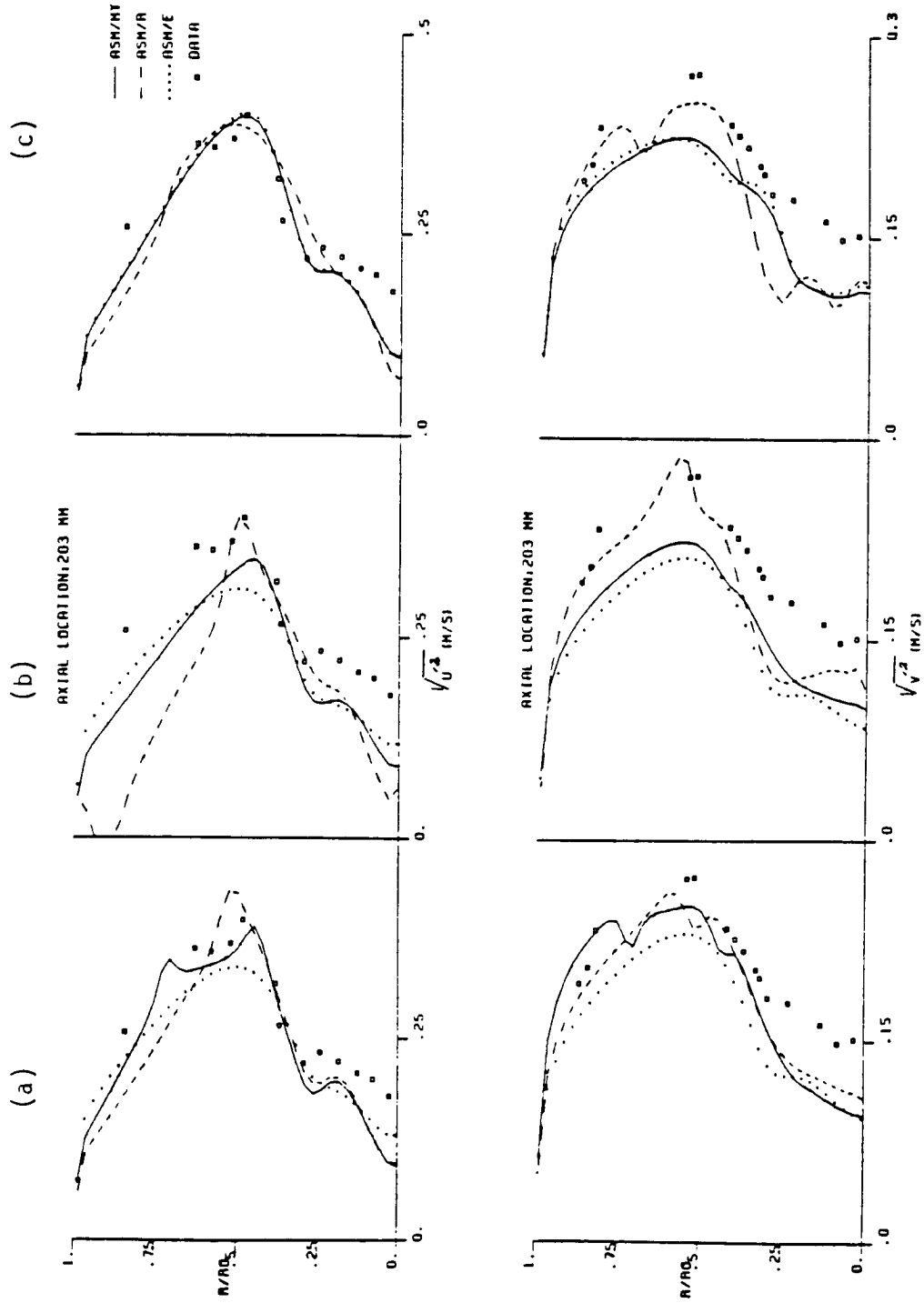

Figure 4.15 Comparison of measurements with $\sqrt{\overline{u'^2}}$ and $\sqrt{\overline{v'^2}}$ calculations using $\Pi_{ij} = \Pi_{ij,1} + \Pi_{ij,2}$
(a) eqs. (2.13,2.14), (b) eqs (2.13,2.15),
(c) eqs.(2.13,2.16) (Johnson & Bennett (1981))

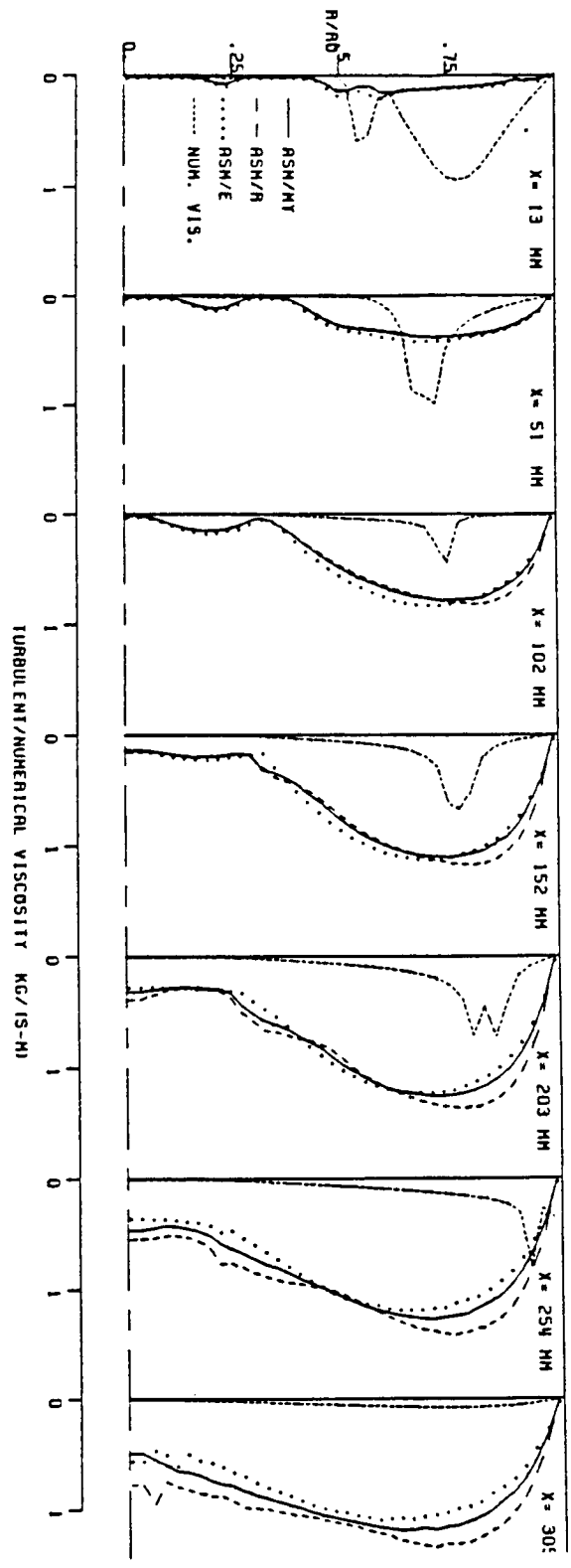

Figure 4.16 Comparison of the distributions of numerical viscosity with turbulent viscosities at different locations along combustor

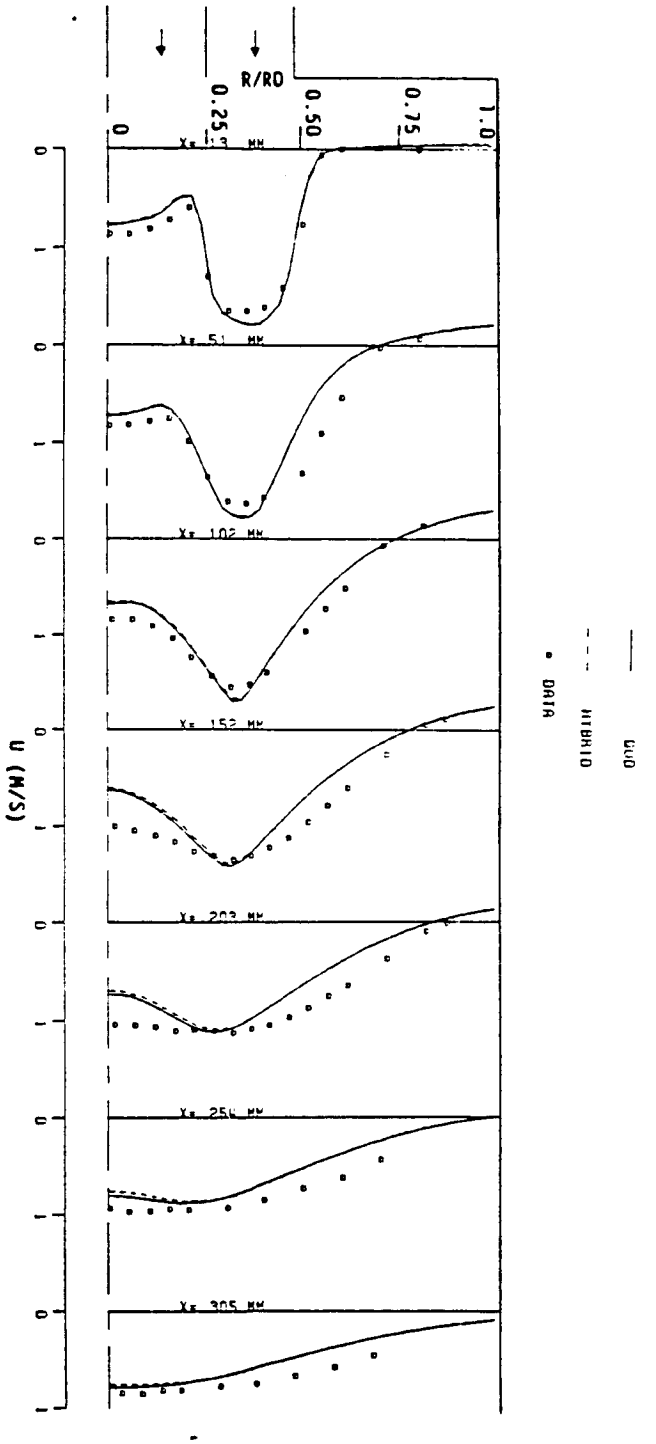

Figure 4.17 Comparison of hybrid differencing scheme with quadratic upwind differencing scheme on mean axial velocity

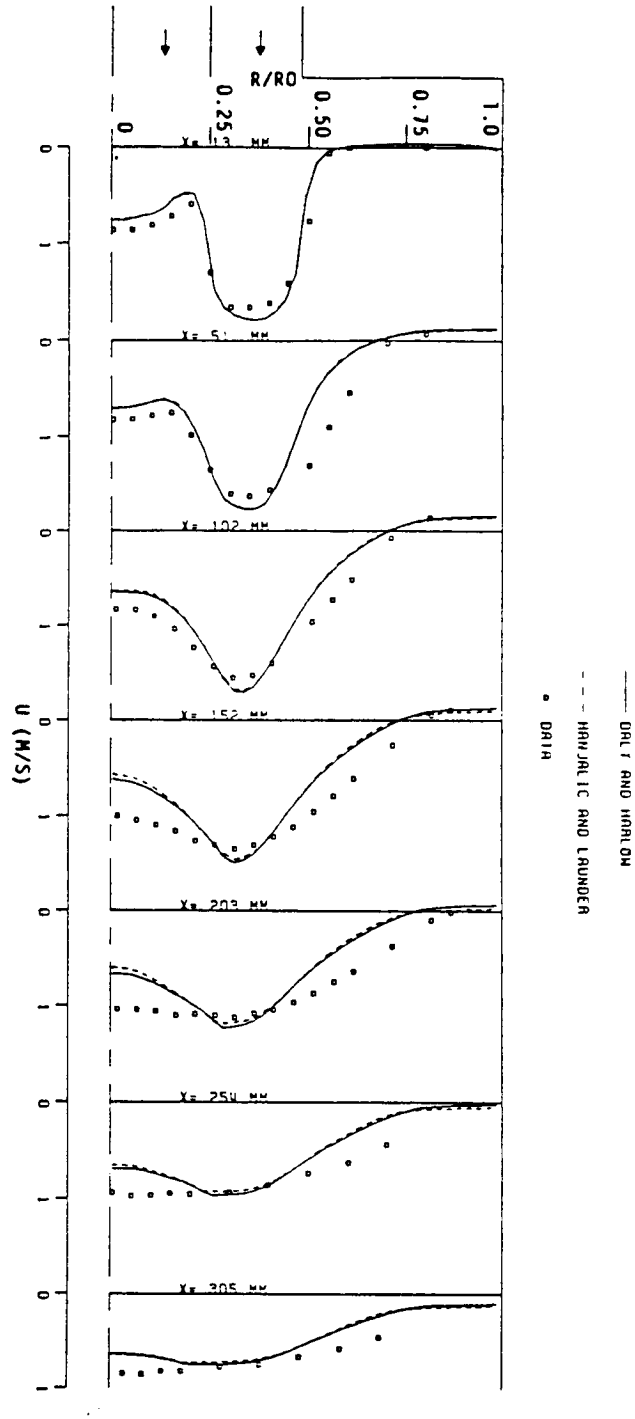

Figure 4.18 Comparison of measurements with mean axial velocity calculations using two turbulent diffusion models (2.18,2.19)

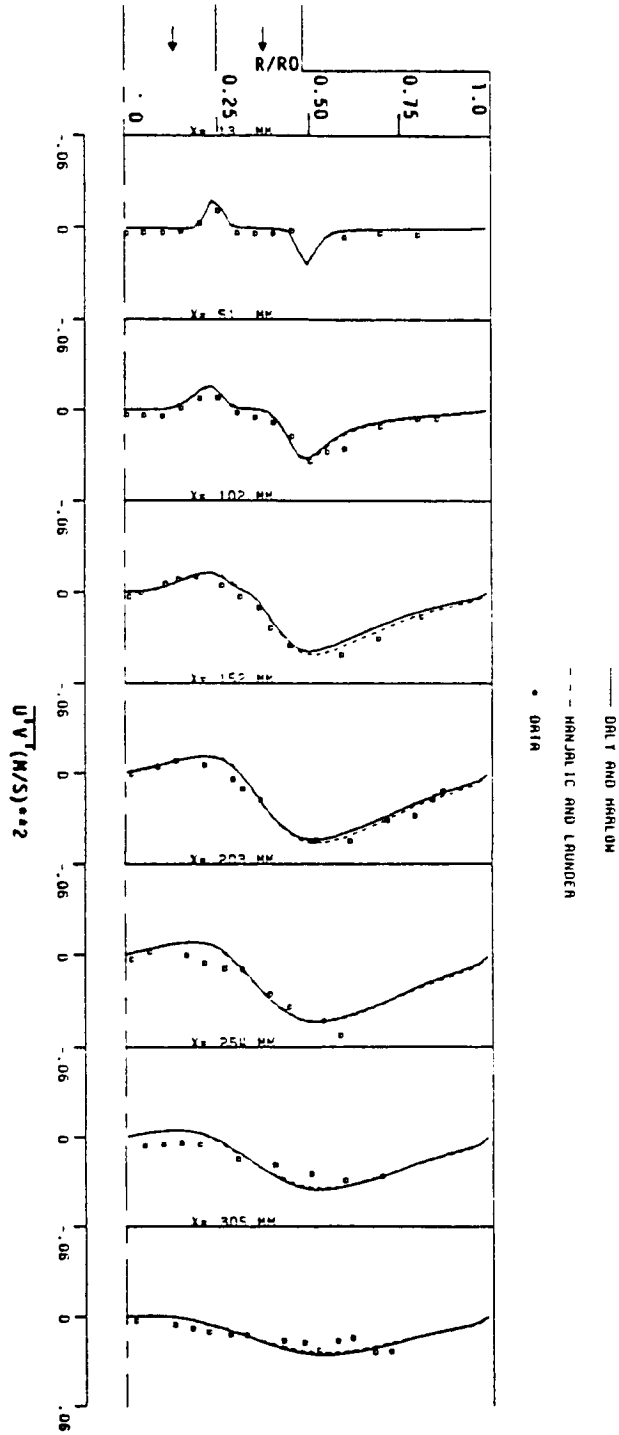

Figure 4.19 Comparison of measurements with $\overline{uv}$ calculations using two turbulent diffusion models (2.18,2.19)

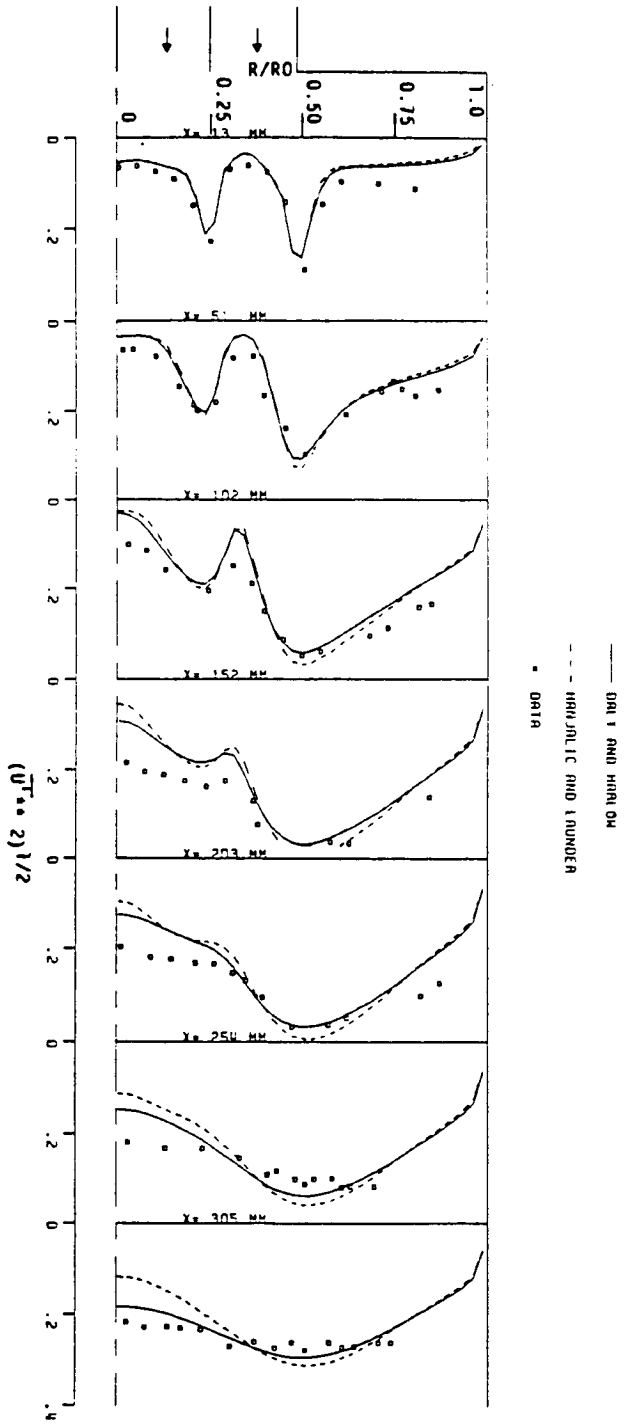

Figure 4.20 Comparison of measurements with $\sqrt{u'^2}$ calculations using two turbulent diffusion models (2.18,2.19)

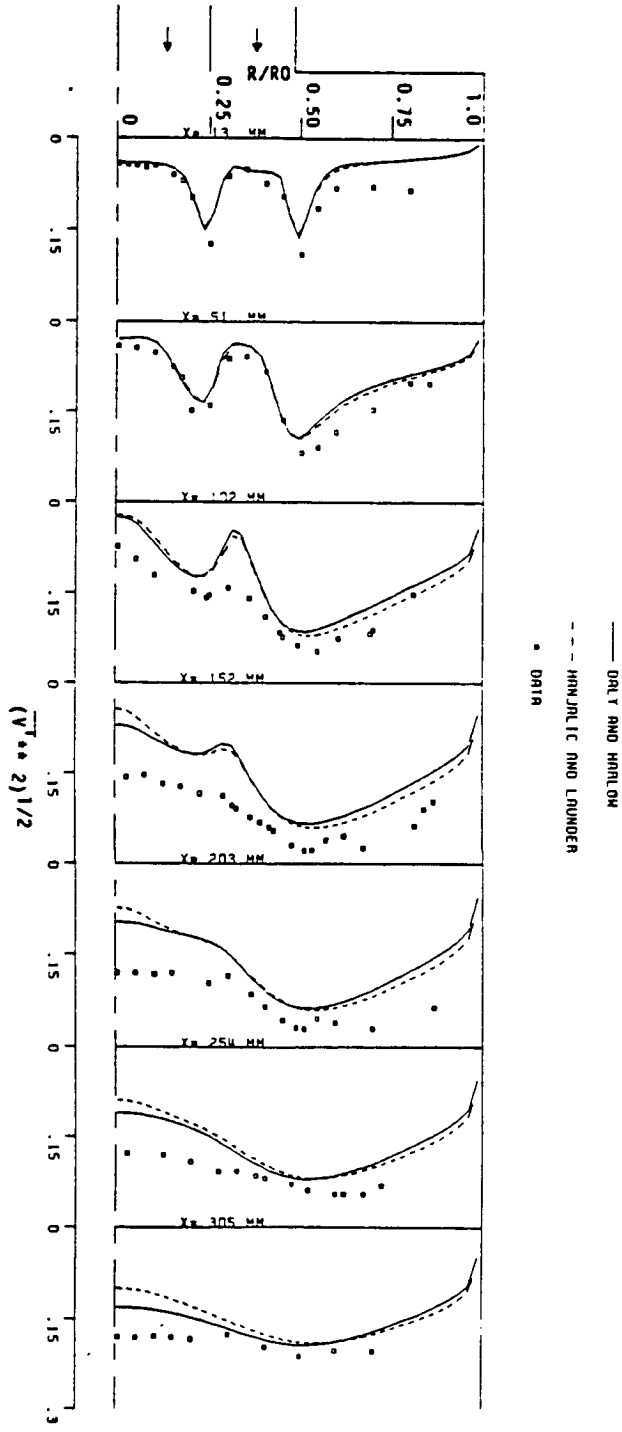

Figure 4.21 Comparison of measurements with $\sqrt{\overline{v^2}}$ calculations using two turbulent diffusion models (2.18,2.19)

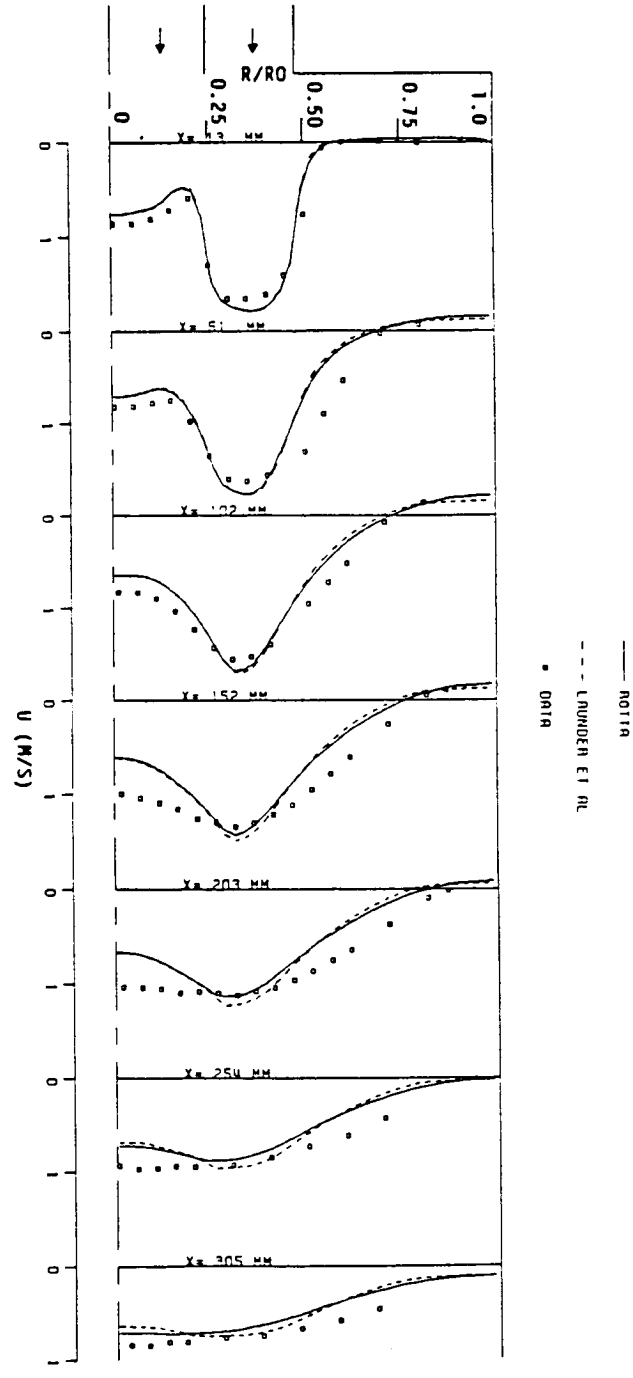

Figure 4.22 Comparison of measurements with mean axial velocity calculations using Reynolds stress closure and two different Π_{ij} models (a) eq. (2.13), (b) esq.(2.13,2.16)

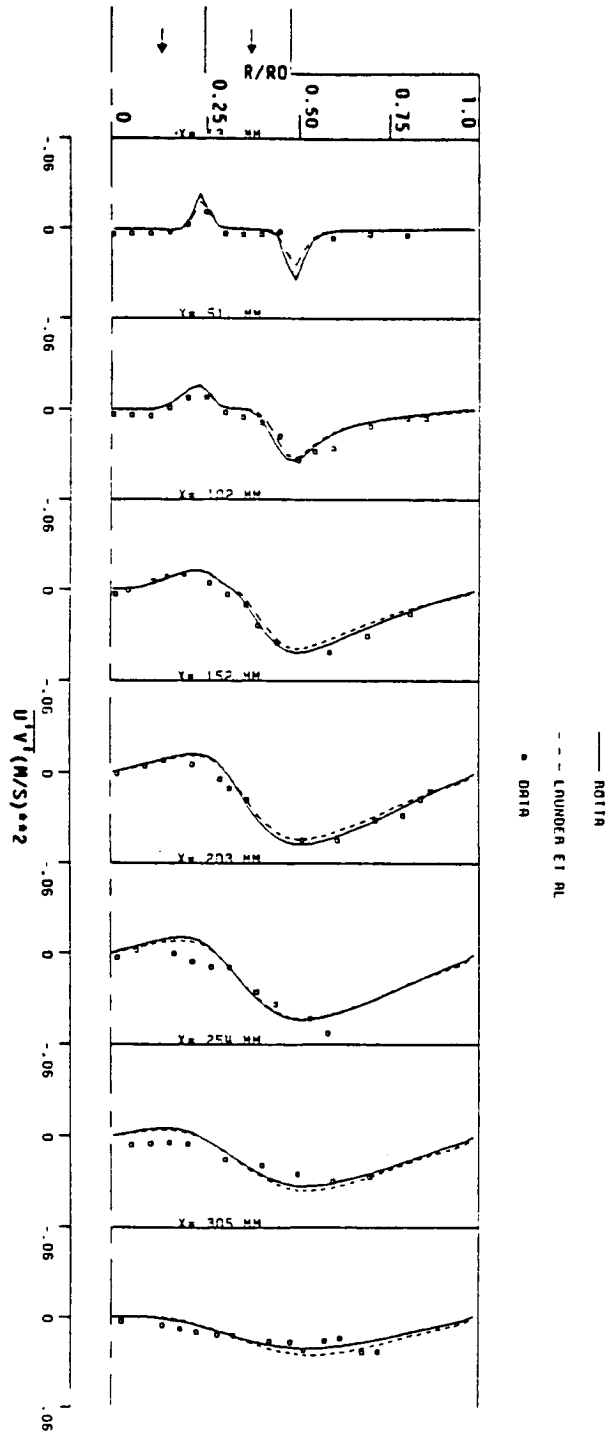

Figure 4.23 Comparison of measurements with $\overline{uv}$ calculations using Reynolds stress closure and two different Π_{ij} models (a) eq. (2.13), (b) esq.(2.13,2.16)

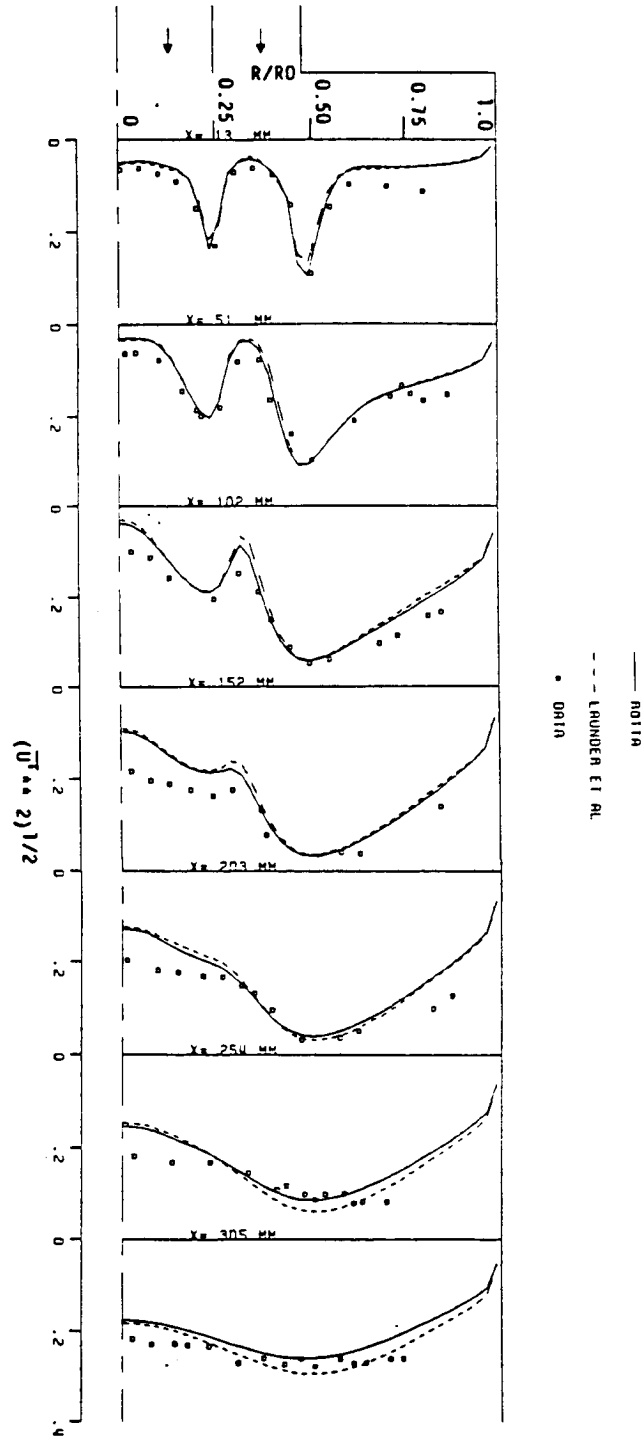

Figure 4.24 Comparison of measurements with $\sqrt{u^2}$ calculations using Reynolds stress closure and two different Π_{ij} models (a) eq. (2.13), (b) esq.(2.13,2.16)

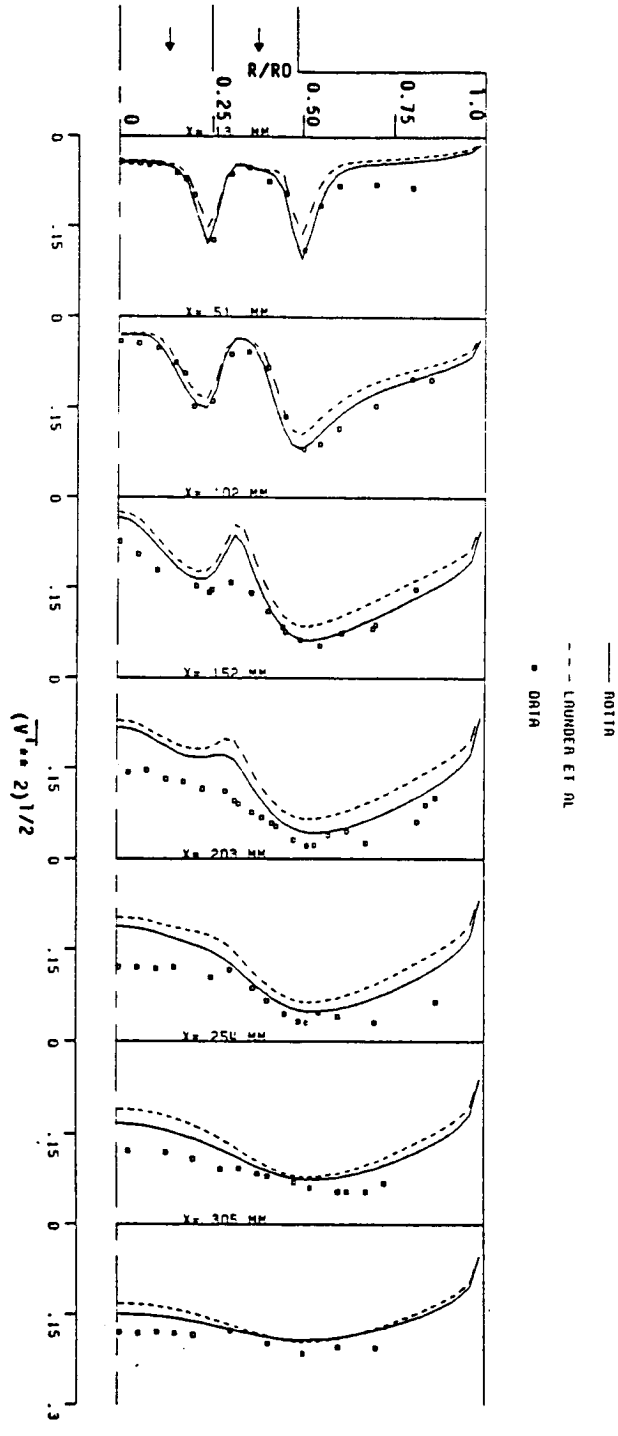

Figure 4.25 Comparison of measurements with $\sqrt{\overline{v^2}}$ calculations using Reynolds stress closure and two different Π_{ij} models (a) eq. (2.13), (b) esq.(2.13,2.16)

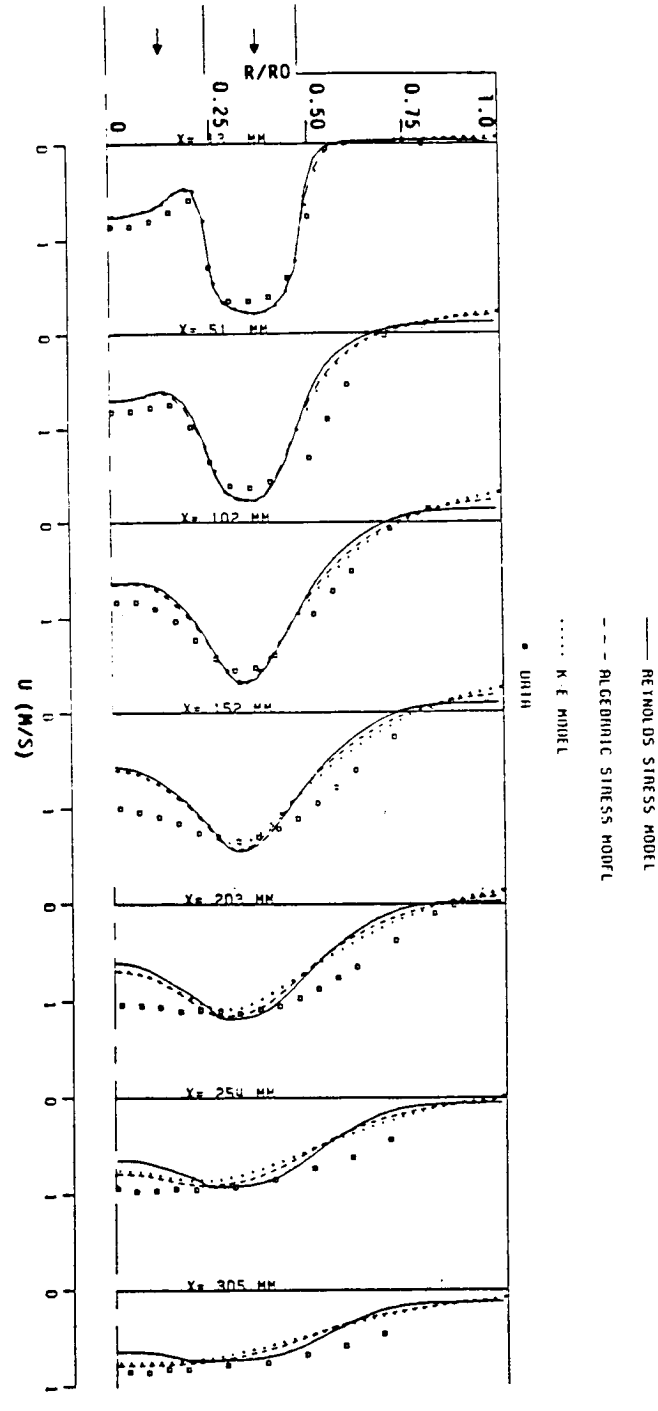

Figure 4.26 Comparison of measurements with mean axial velocity calculations (Johnson & Bennett (1981) ,k-ϵ, ASM, RSM)

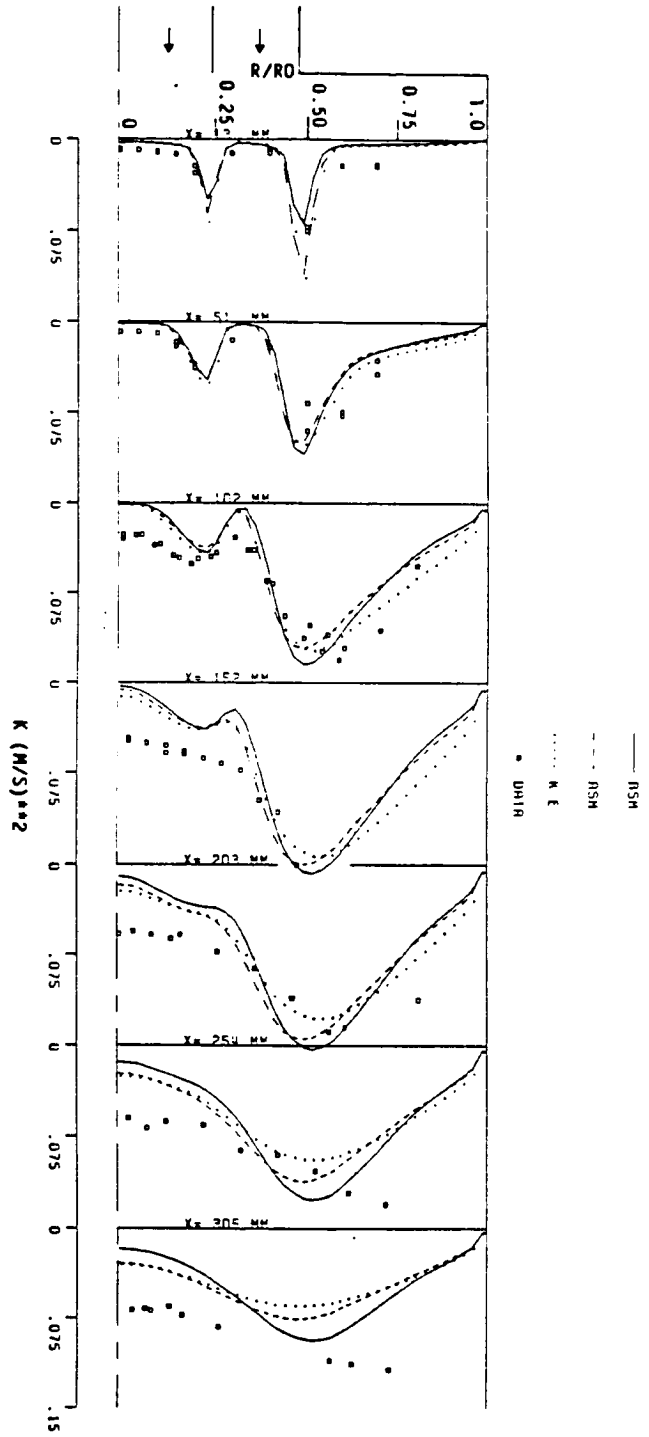

Figure 4.27 Comparison of measurements with k calculations (Johnson & Bennett (1981), k-ϵ, ASM, RSM)

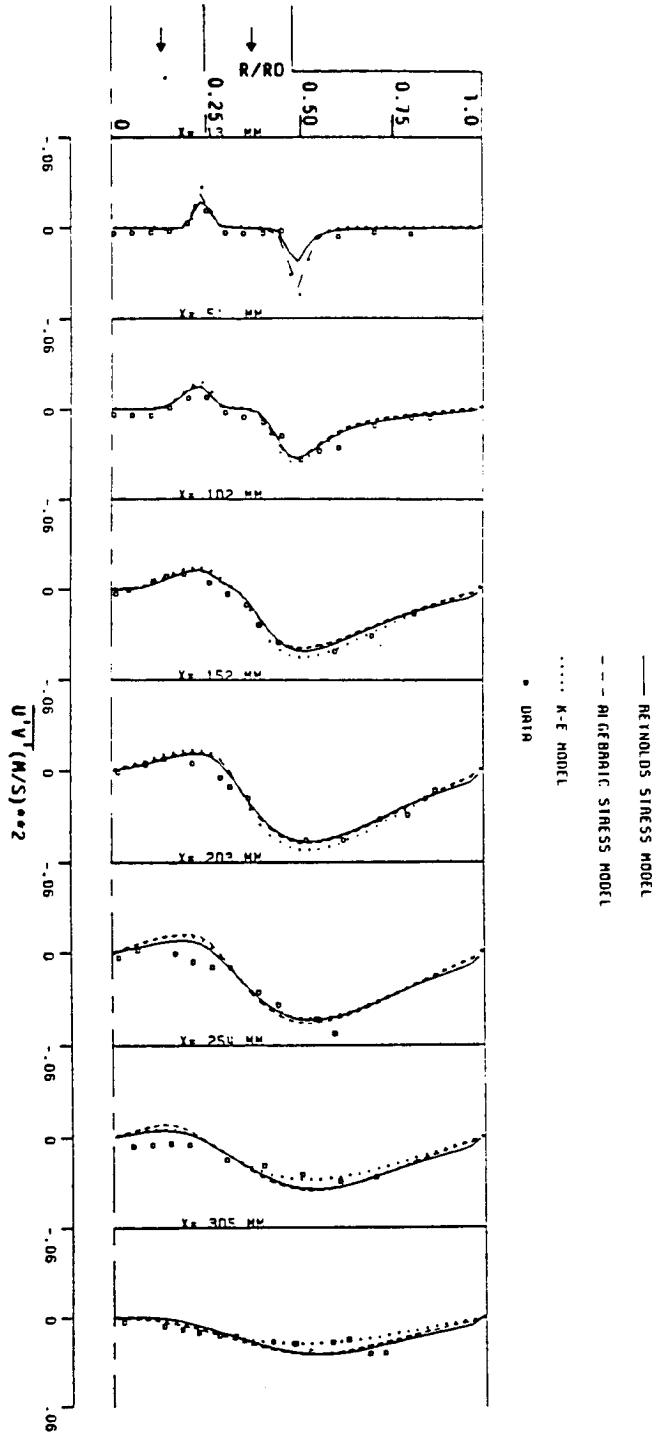

Figure 4.28 Comparison of measurements with $\overline{u'v'}$ calculations (Johnson & Bennett (1981), k-ϵ, ASM, RSM)

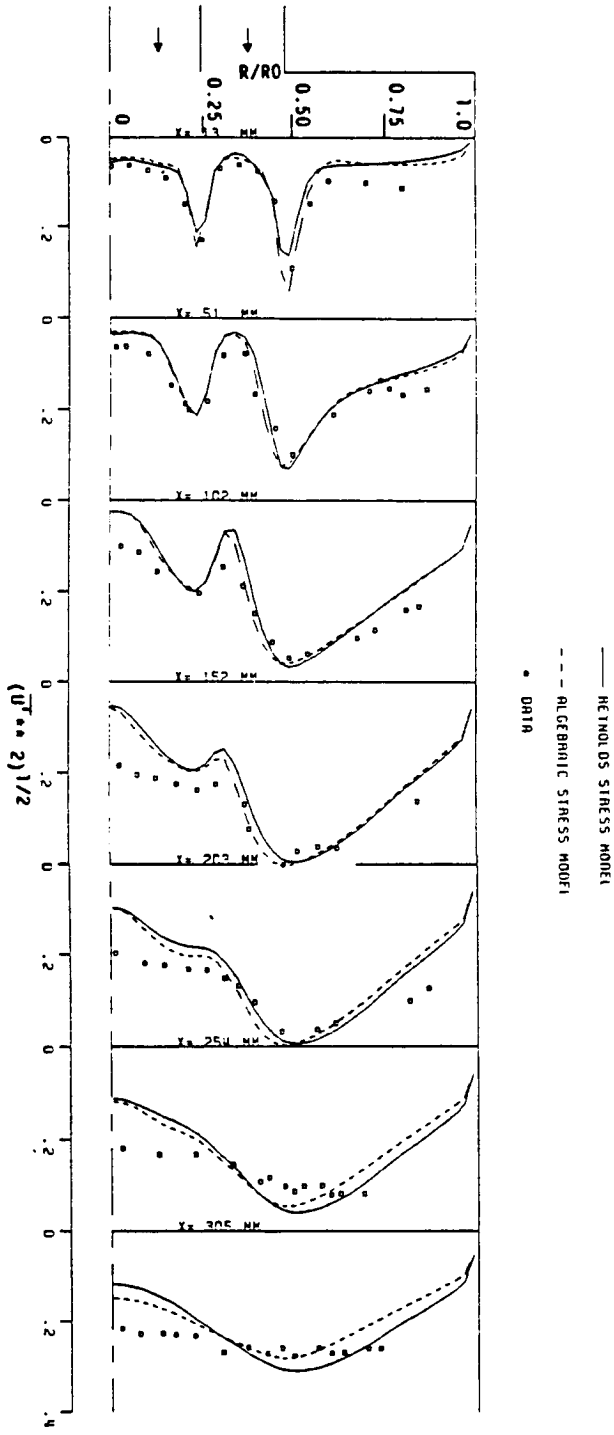

Figure 4.29 Comparison of measurements with $\sqrt{u^2}$ calculations (Johnson & Bennett (1981), ASM, RSM)

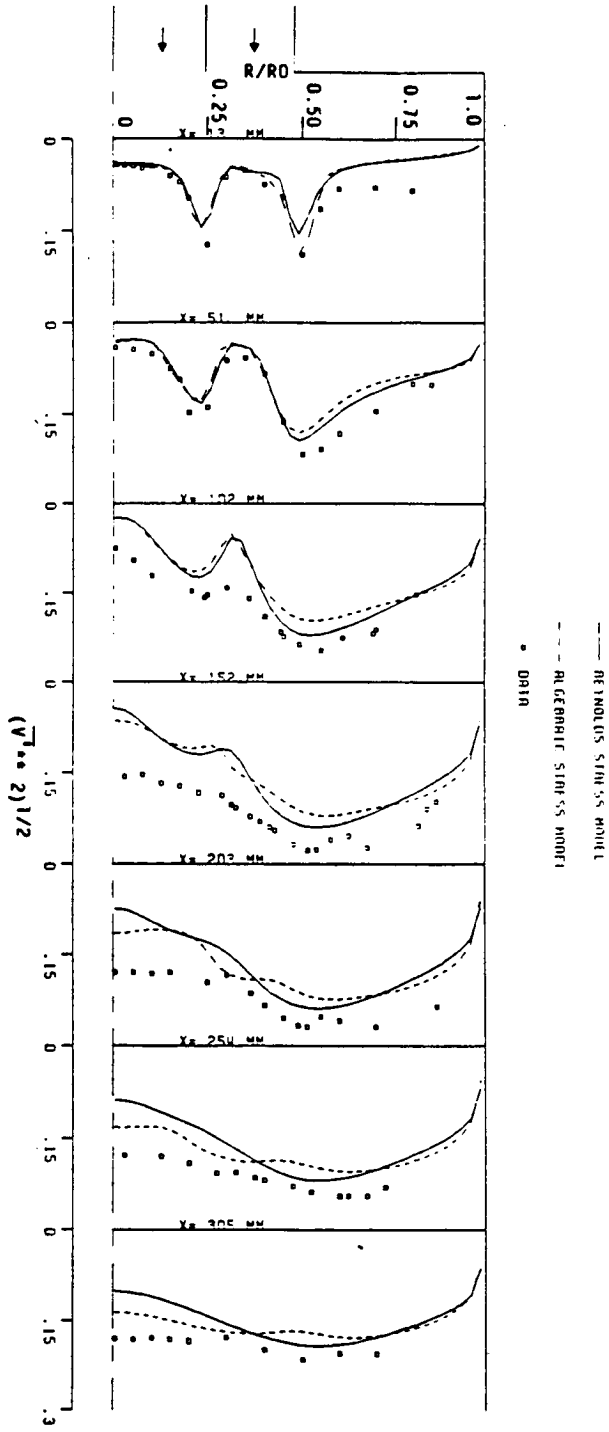

Figure 4.30 Comparison of measurements with $\sqrt{v^2}$ calculations (Johnson & Bennett (1981), ASM, RSM)

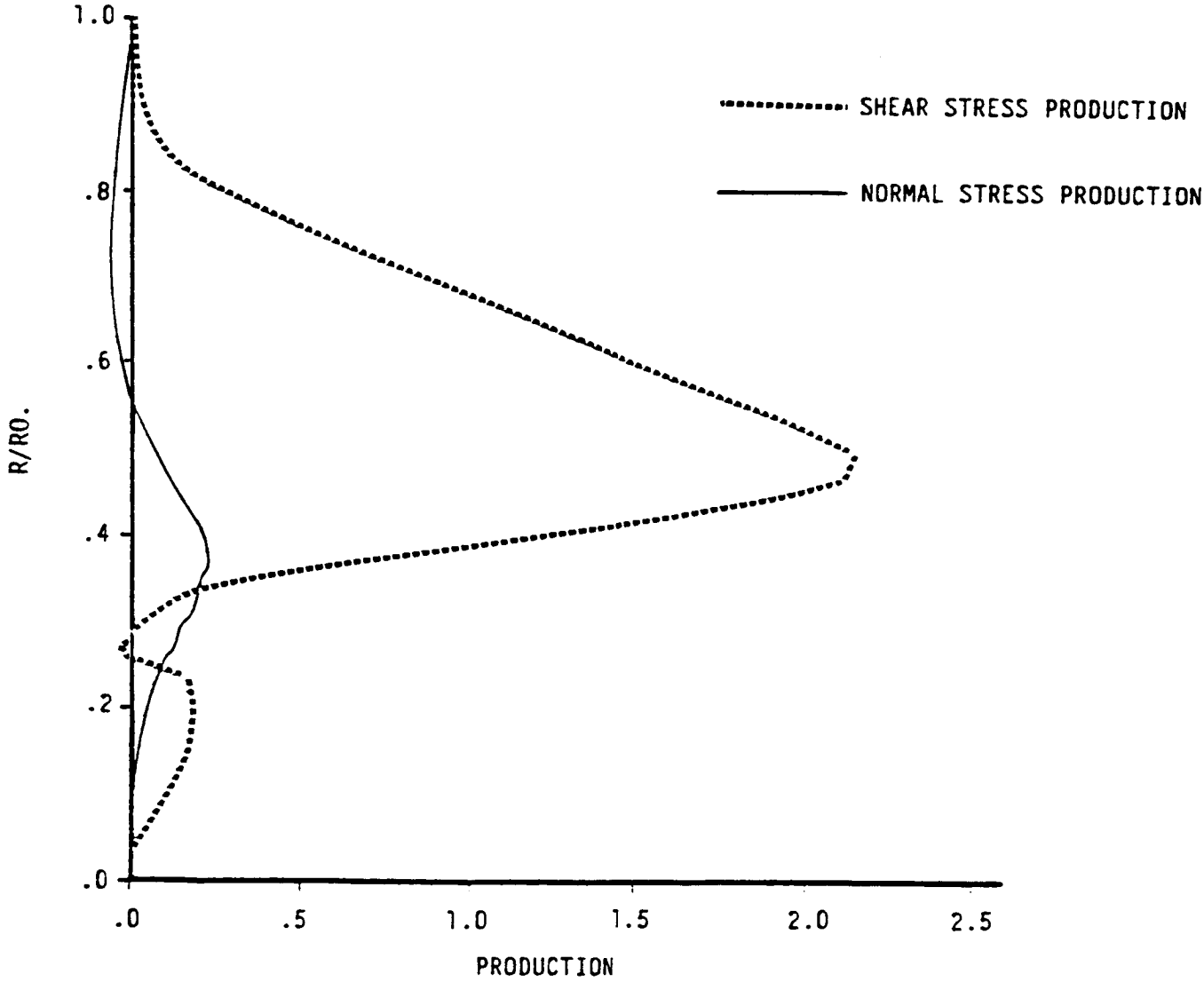

Figure 4.31 Shear stress and normal stress production of turbulent kinetic energy

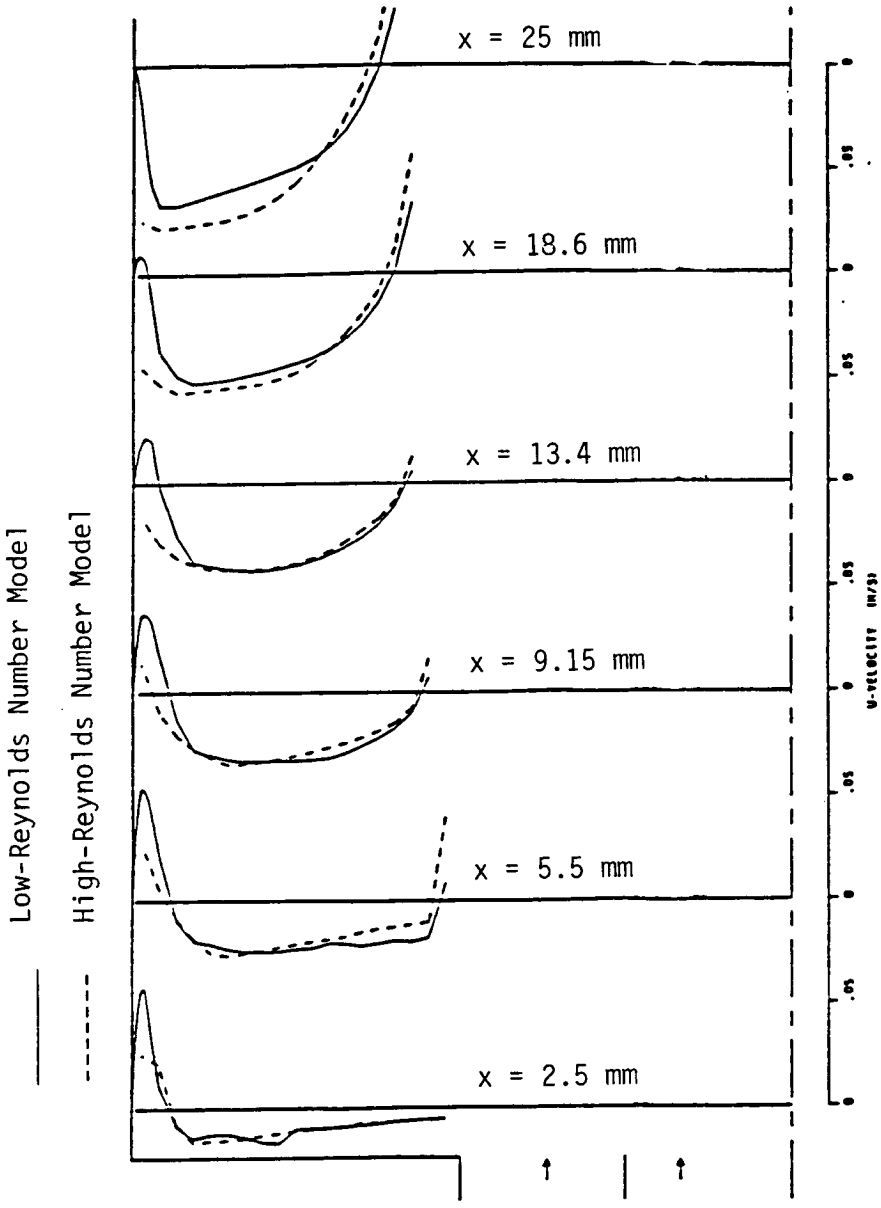

Figure 4.32 Secondary recirculation in the corner region using a high and a low Reynolds stress closure

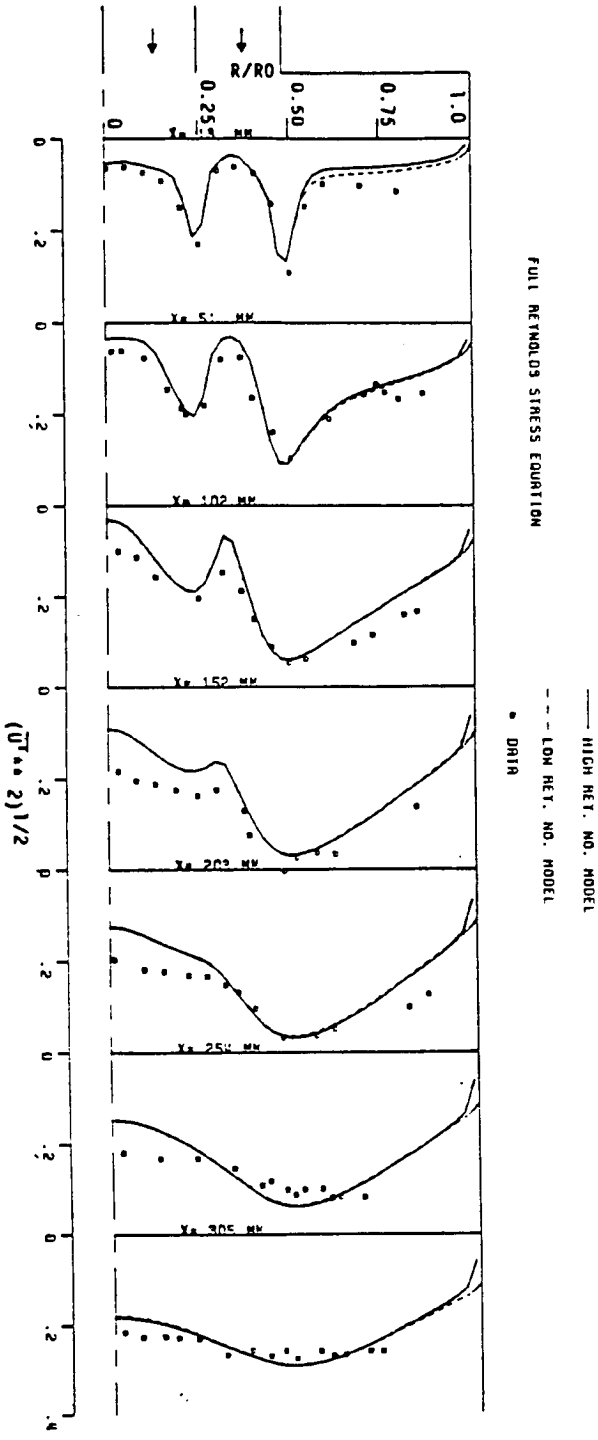

Figure 4.33 Comparison of measurements with $\sqrt{\overline{u^2}}$ calculations using a high and a low Reynolds number model (RSM)

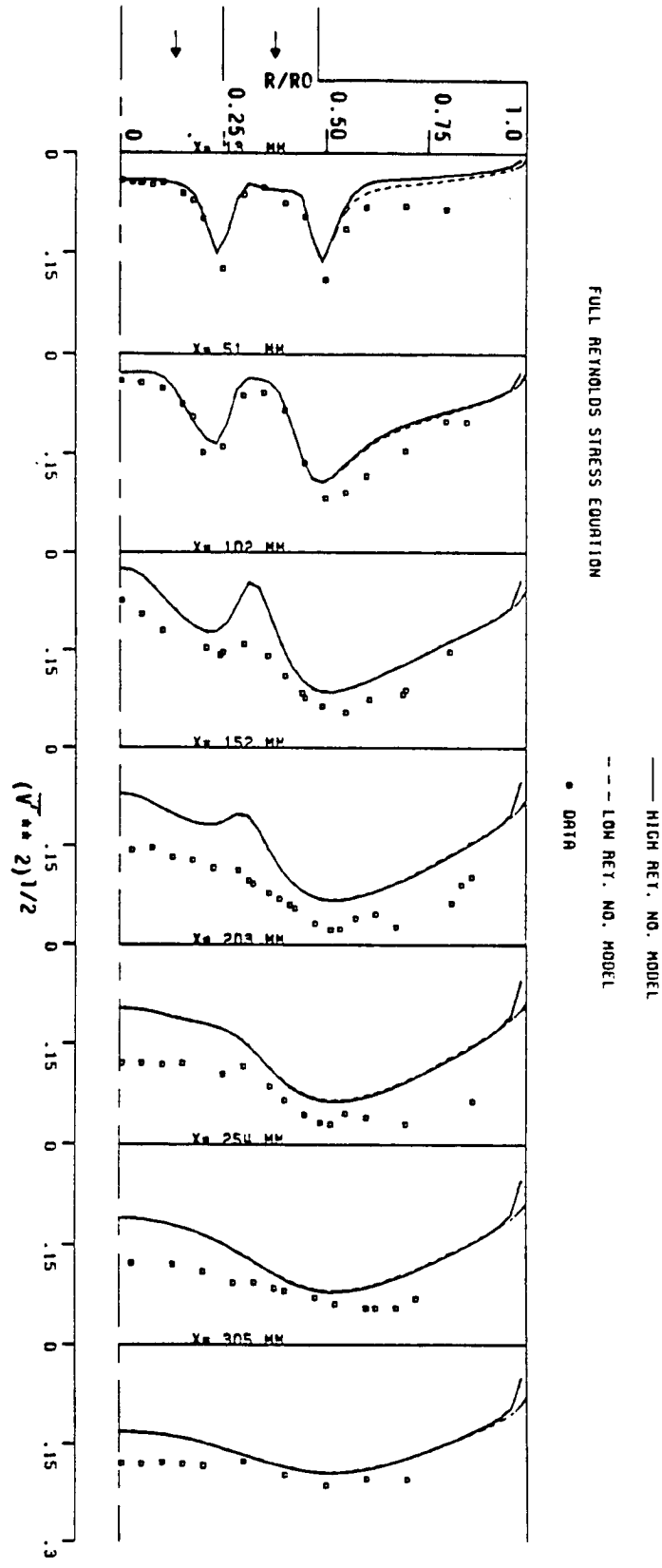

Figure 4.34 Comparison of measurements with $\sqrt{\overline{v^2}}$ calculations using a high and a low Reynolds number model (RSM)

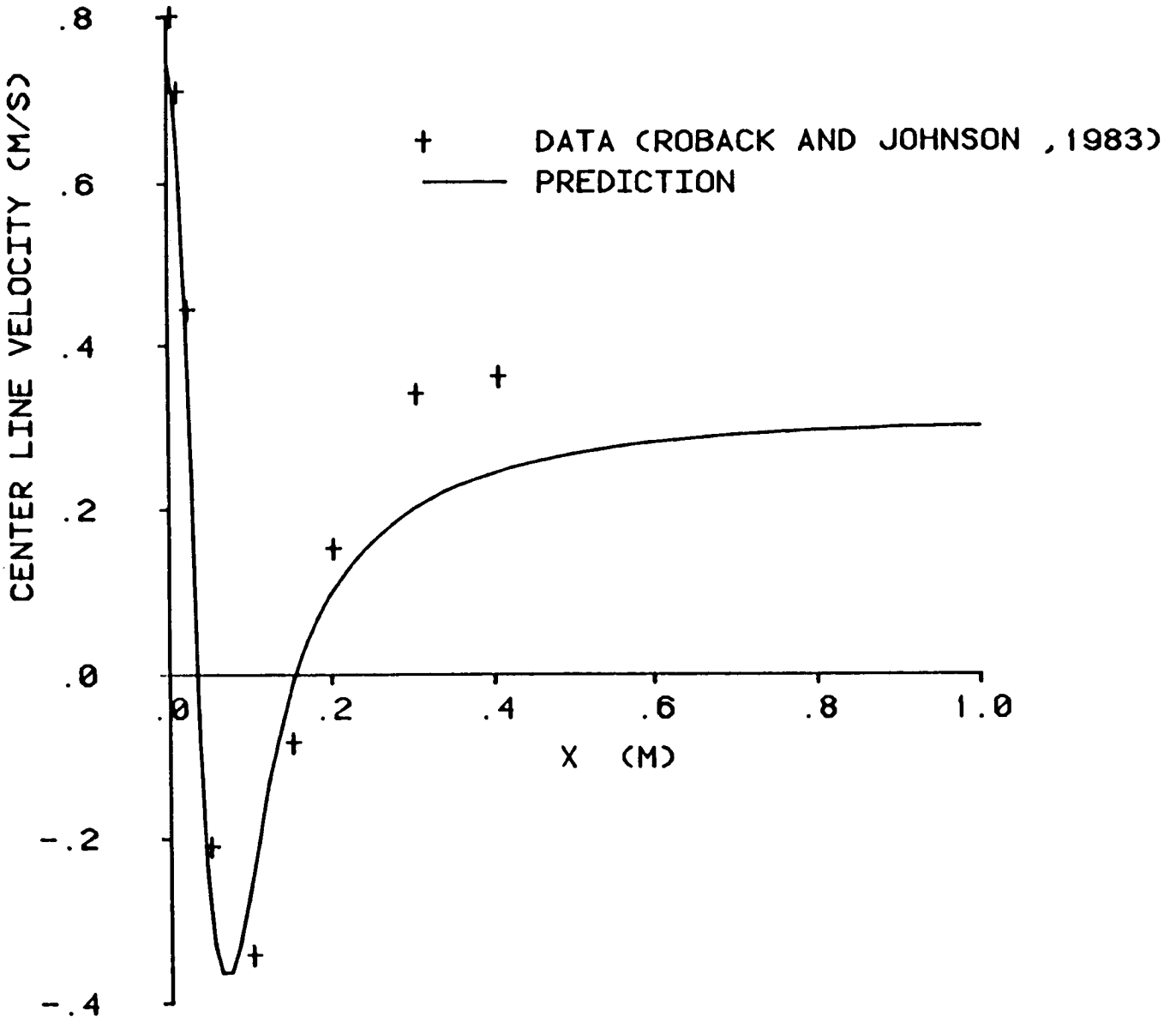

Figure 4.35 Comparison of predicted & measured centerline axial velocity profile (Roback & Johnson (1983))

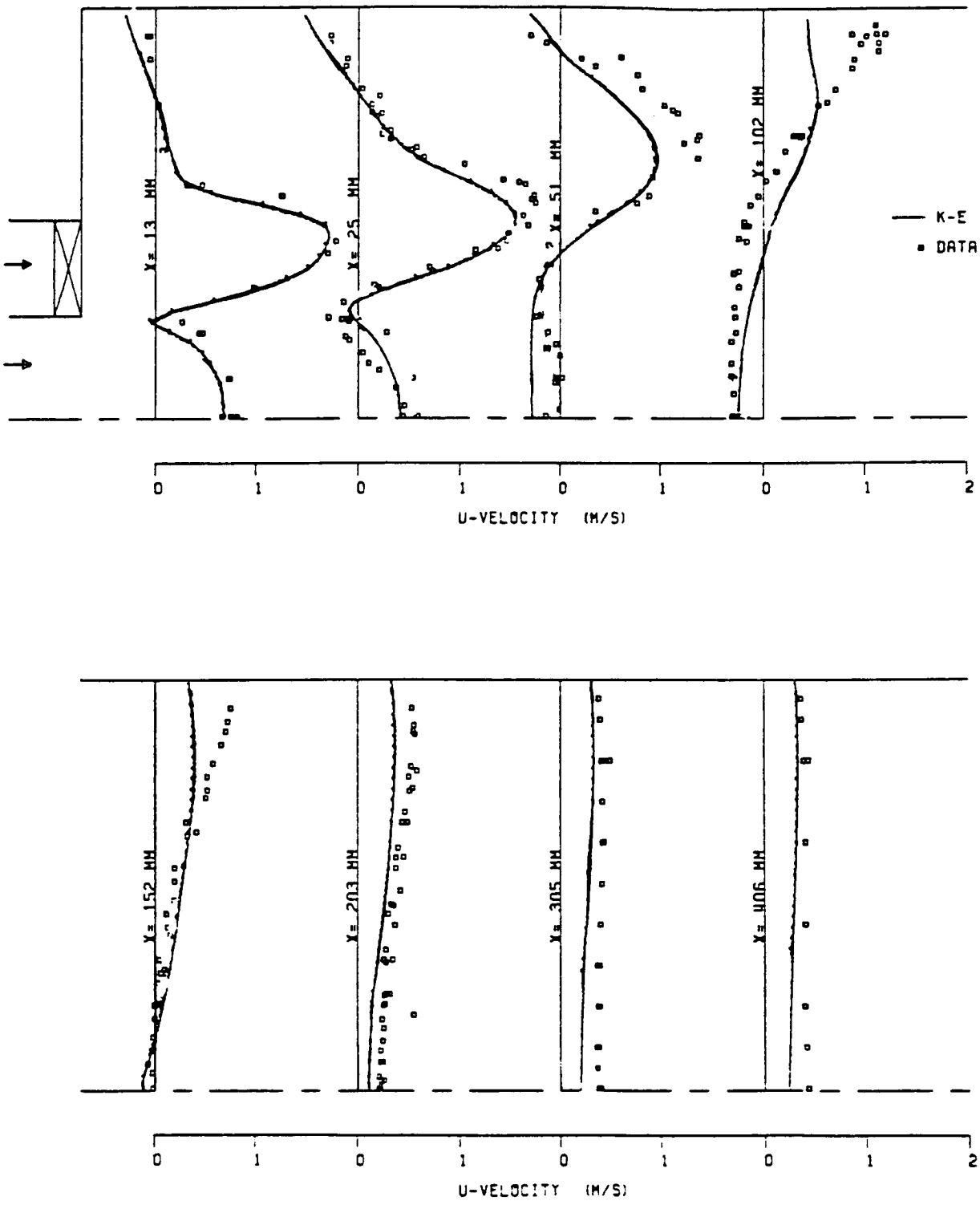

Figure 4.36 Comparison of predicted & measured axial velocity profile using k-ϵ model (Roback & Johnson (1983))

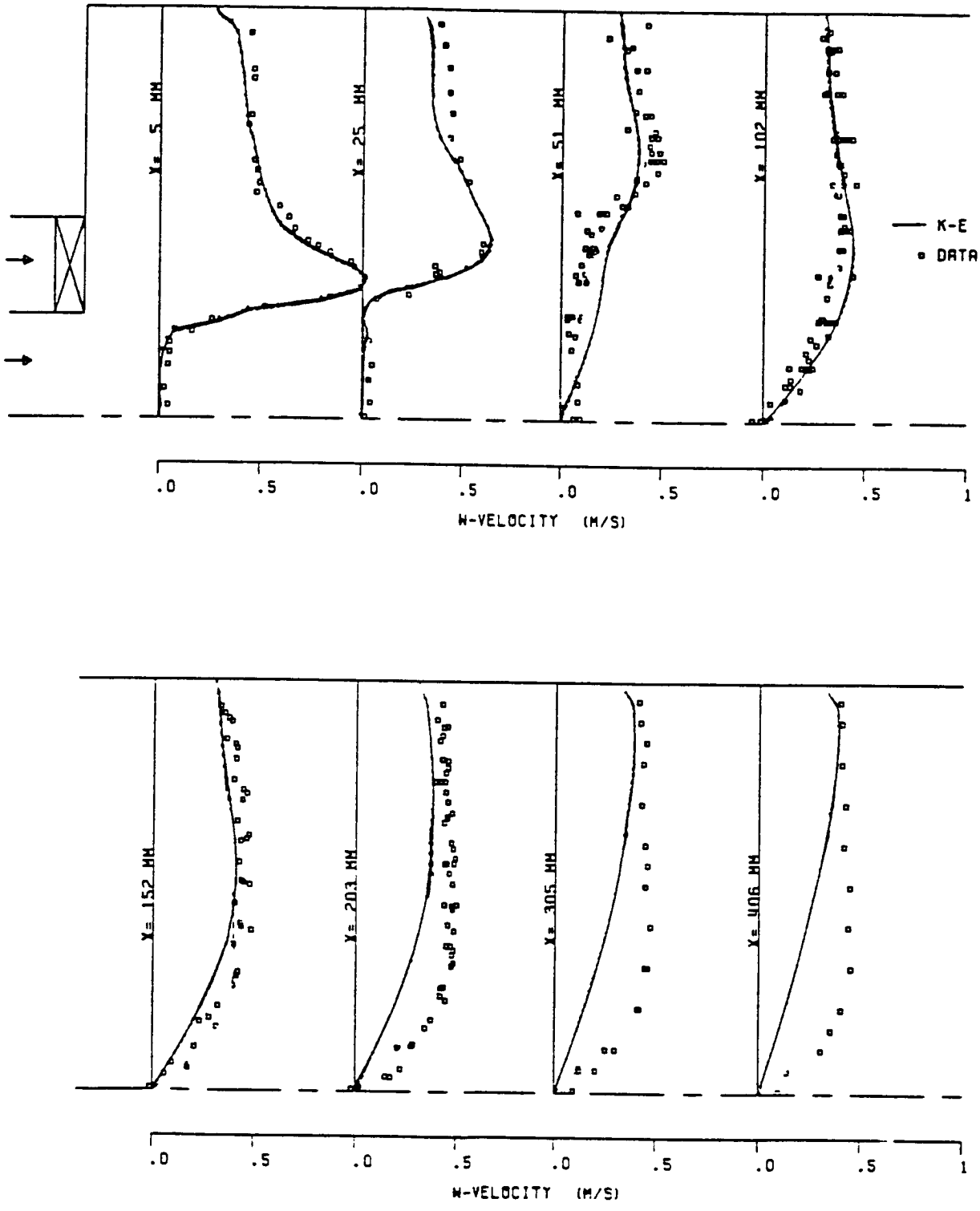

Figure 4.37 Comparison of predicted & measured tangential velocity profile using k-ϵ model (Roback & Johnson (1983))

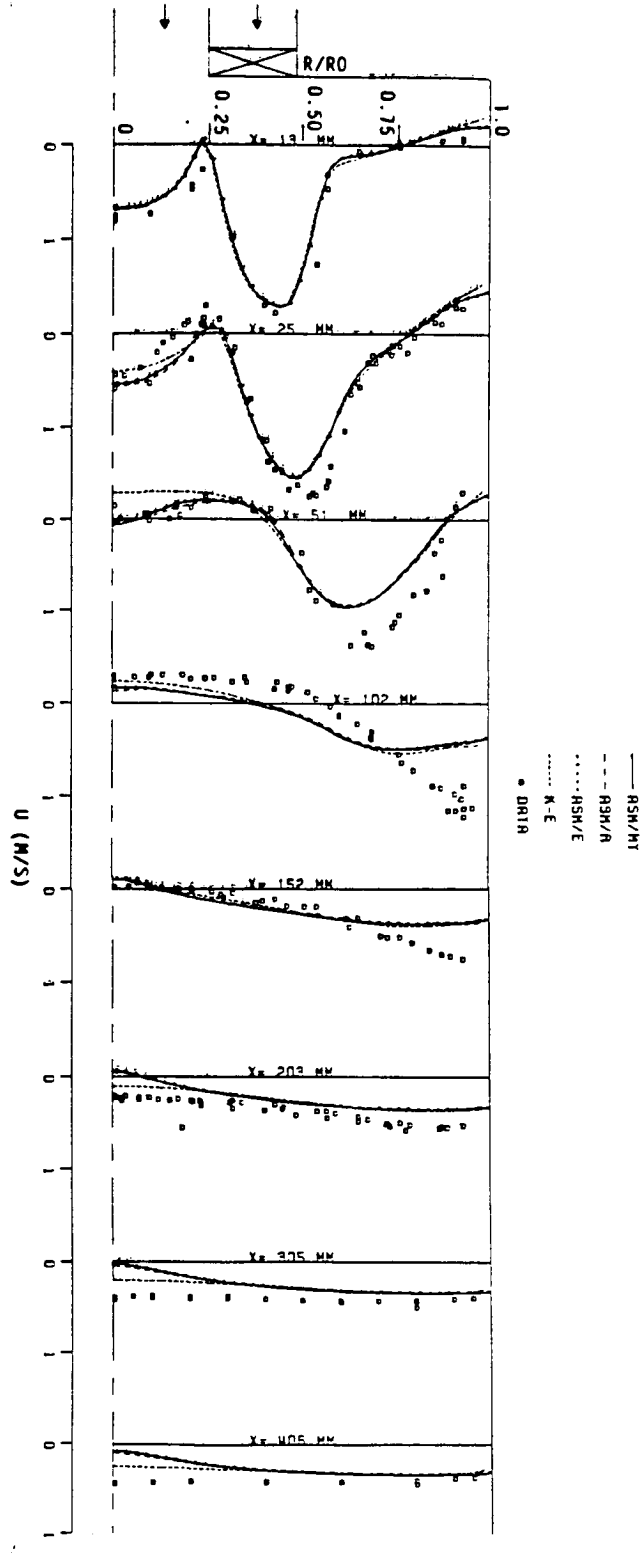

Figure 4.38 Comparison of measurements with mean axial velocity calculations (Roback & Johnson (1983), ASM, k-ϵ)

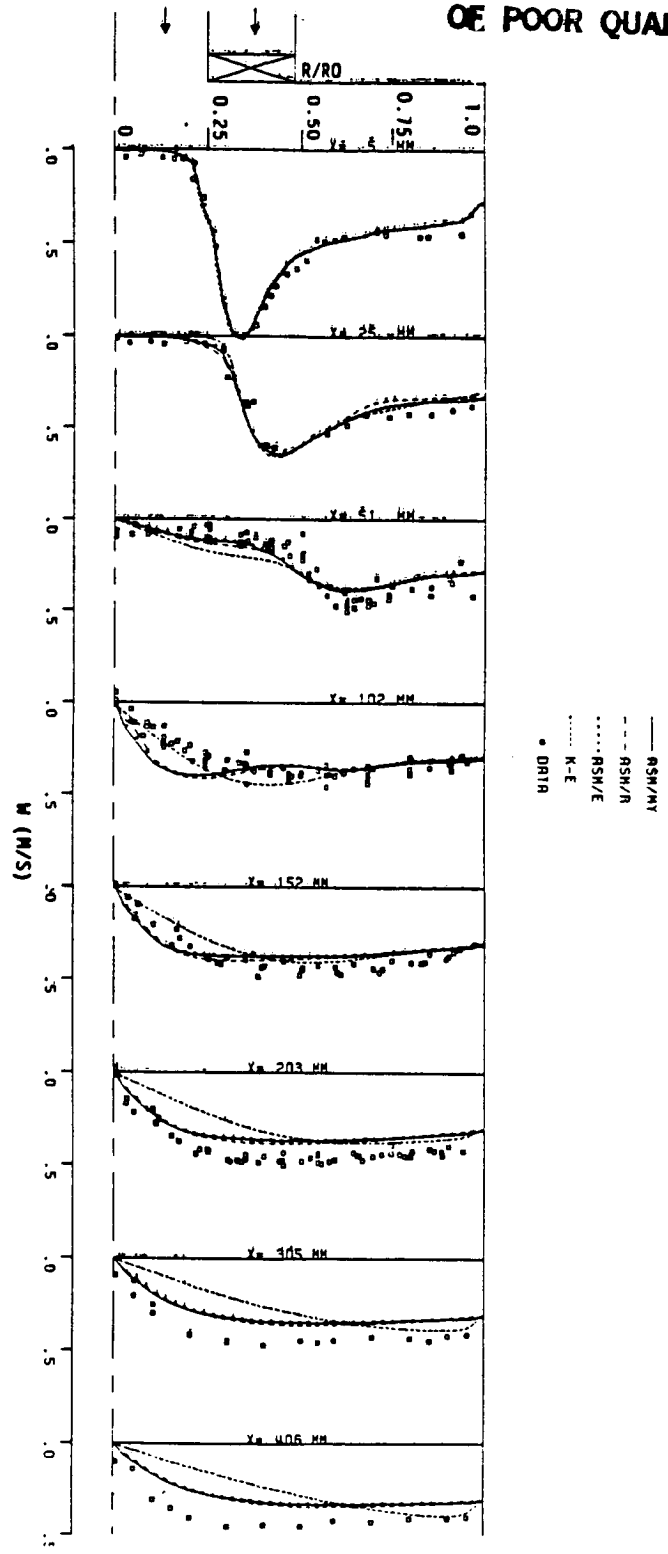

Figure 4.39 Comparison of measurements with mean tangential velocity calculations (Roback & Johnson (1983), ASM, k-ϵ)

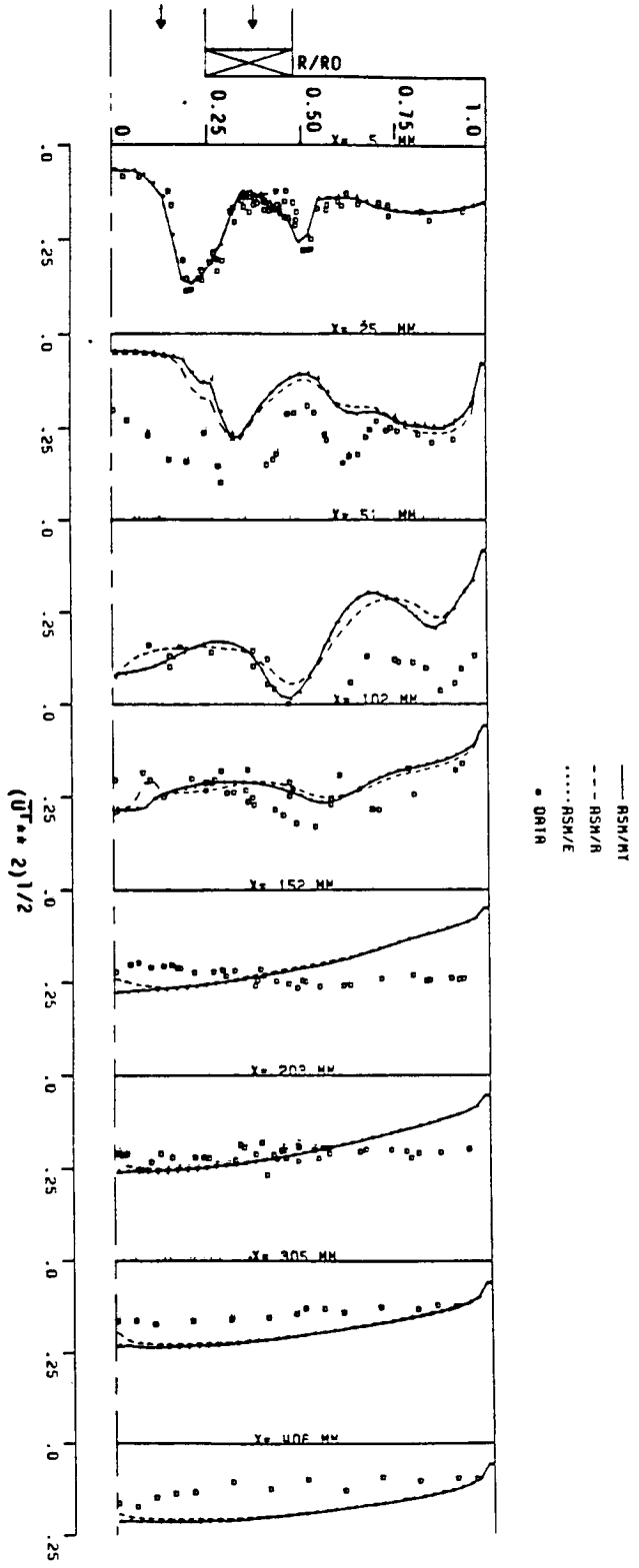

Figure 4.40 Comparison of measurements with $\sqrt{\overline{u^2}}$ calculations (Roback & Johnson (1983) ASM)

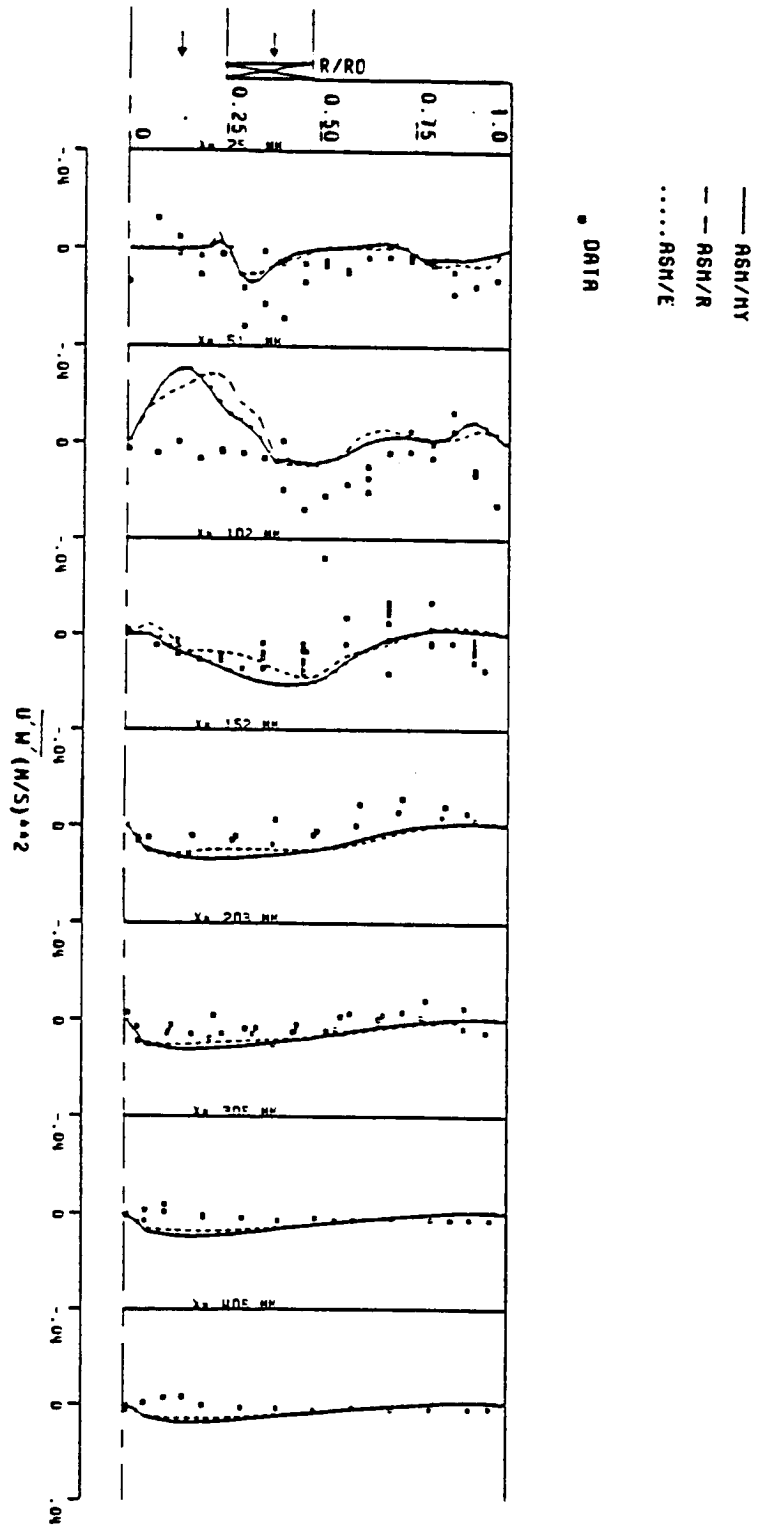

Figure 4.41 Comparison of measurements with $\overline{uw}$ calculations (Roback & Johnson (1983), ASM)

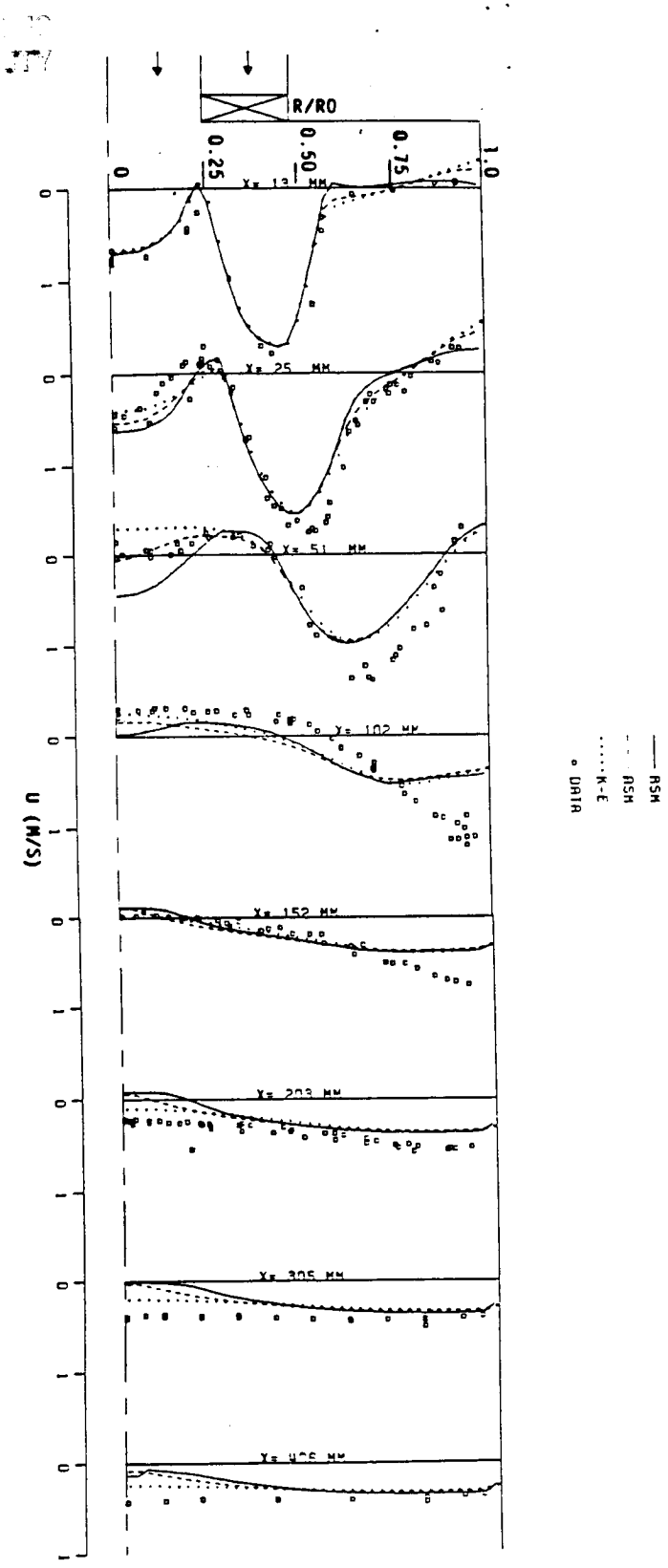

Figure 4.42 Comparison of measurements with mean axial velocity calculations (Roback & Johnson (1983), k-ϵ, ASM, RSM)

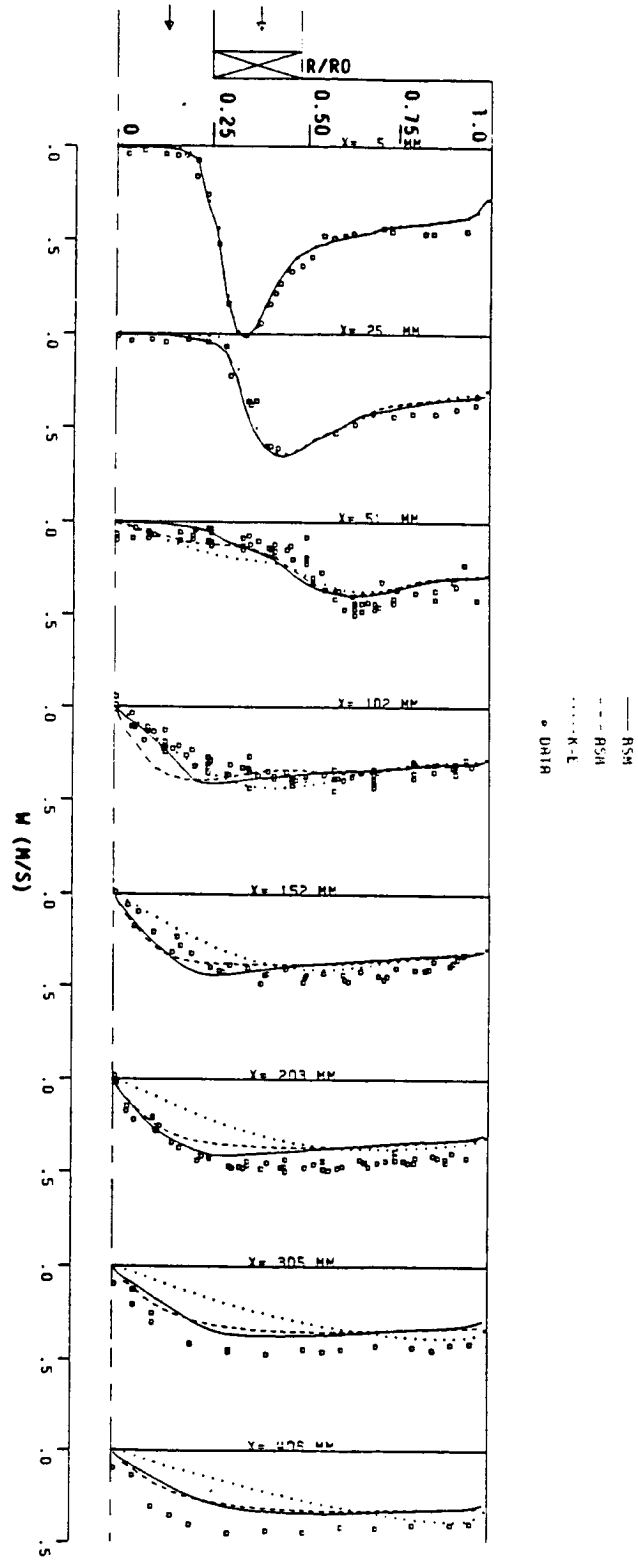

Figure 4.43 Comparison of measurements with mean tangential velocity calculations (Roback & Johnson (1983), k-ϵ, ASM, RSM)

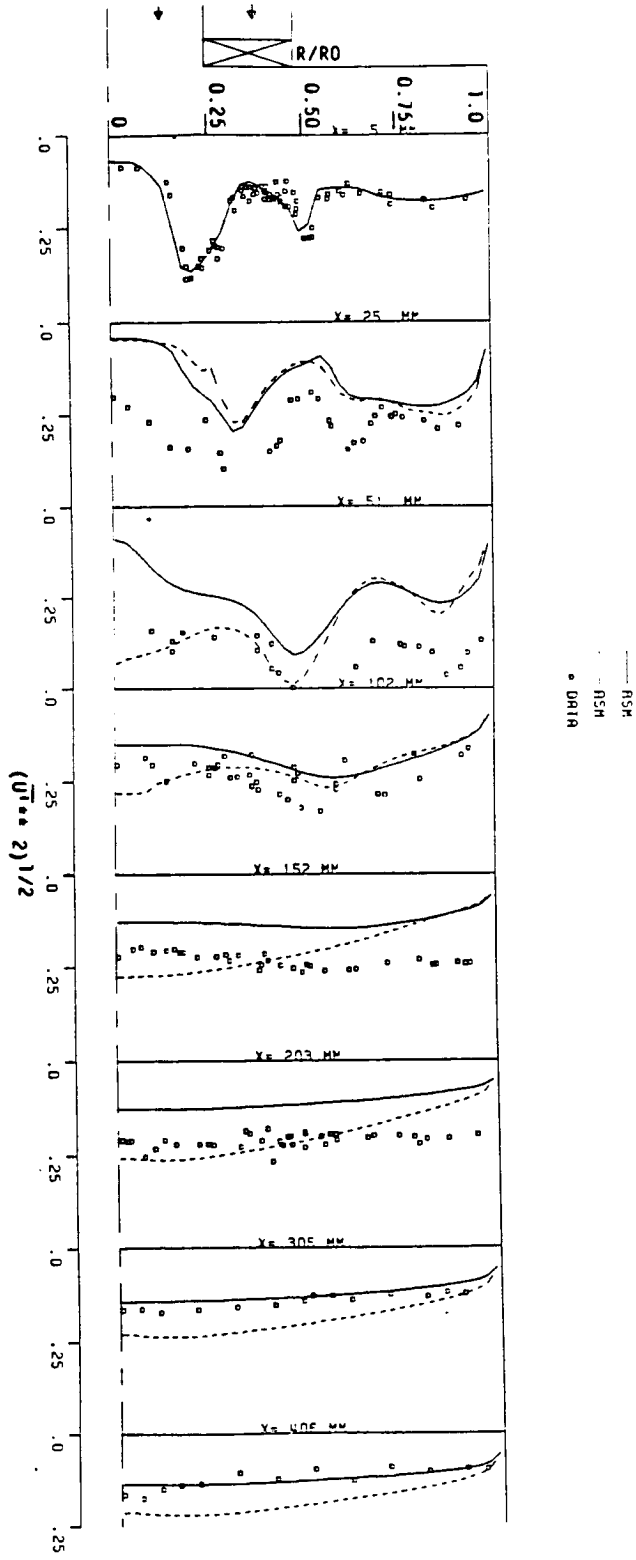

Figure 4.44 Comparison of measurements with $\sqrt{\overline{u'^2}}$ calculations (Roback & Johnson (1983), ASM,RSM)

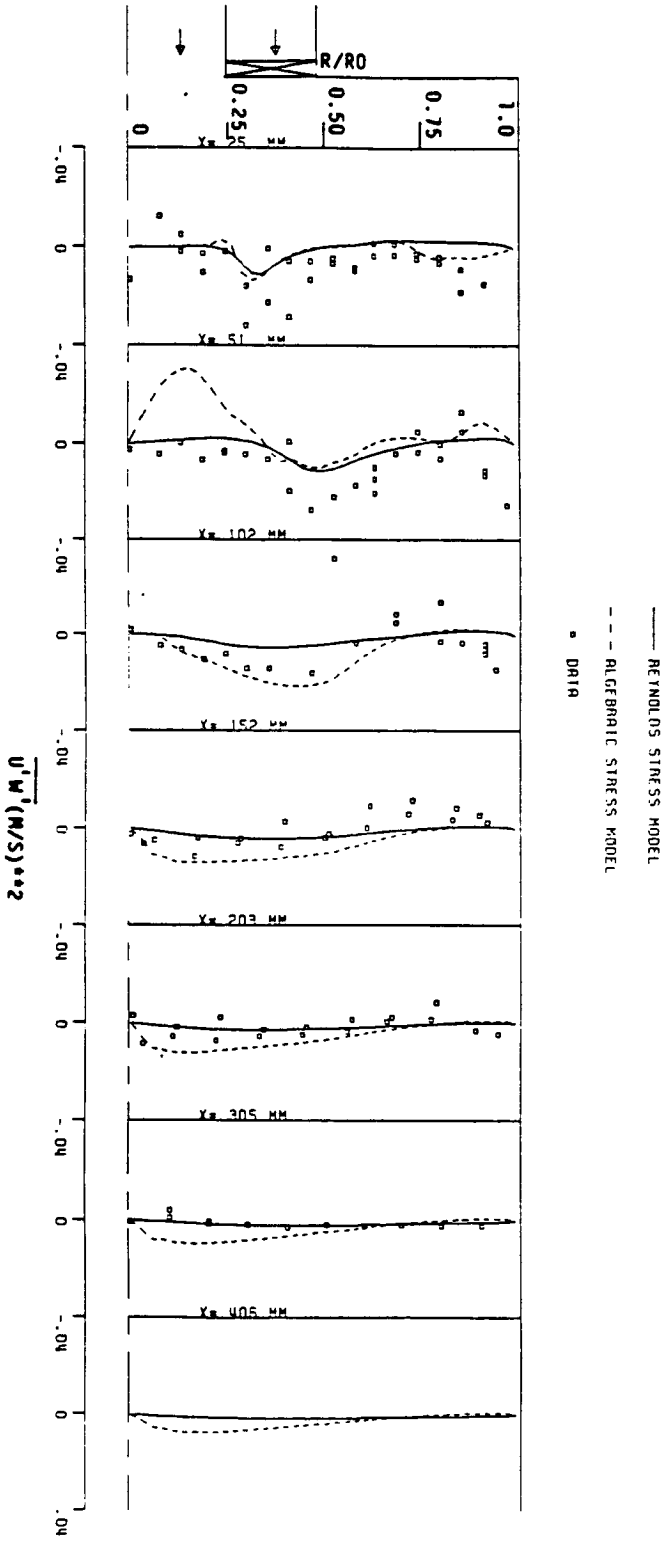

Figure 4.45 Comparison of measurements with $\overline{u'w'}$ calculations (Roback & Johnson (1983), ASM,RSM)

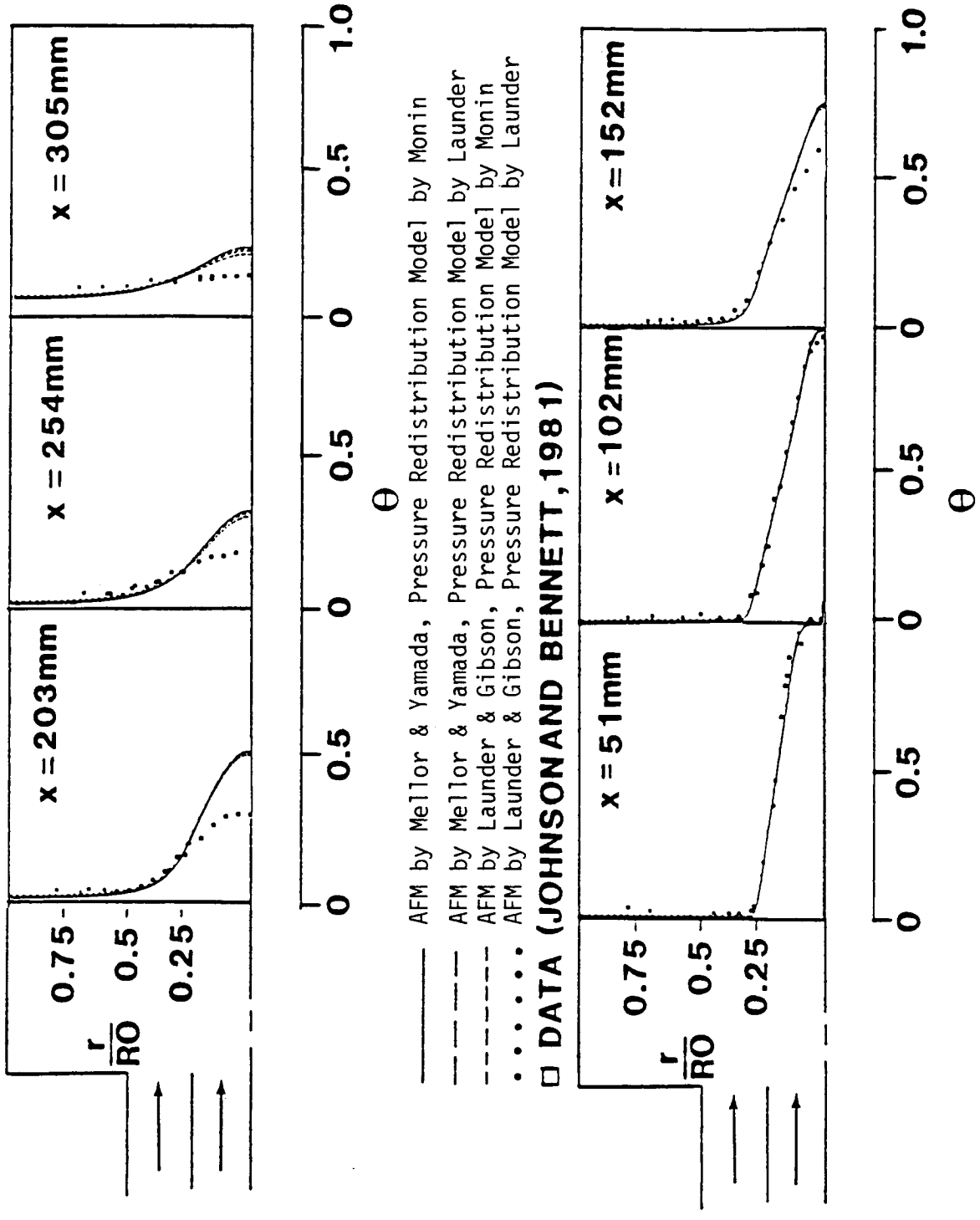

Figure 4.46 Comparison of measurements with mean scalar calculations using AFM (Johnson & Bennett,1981)

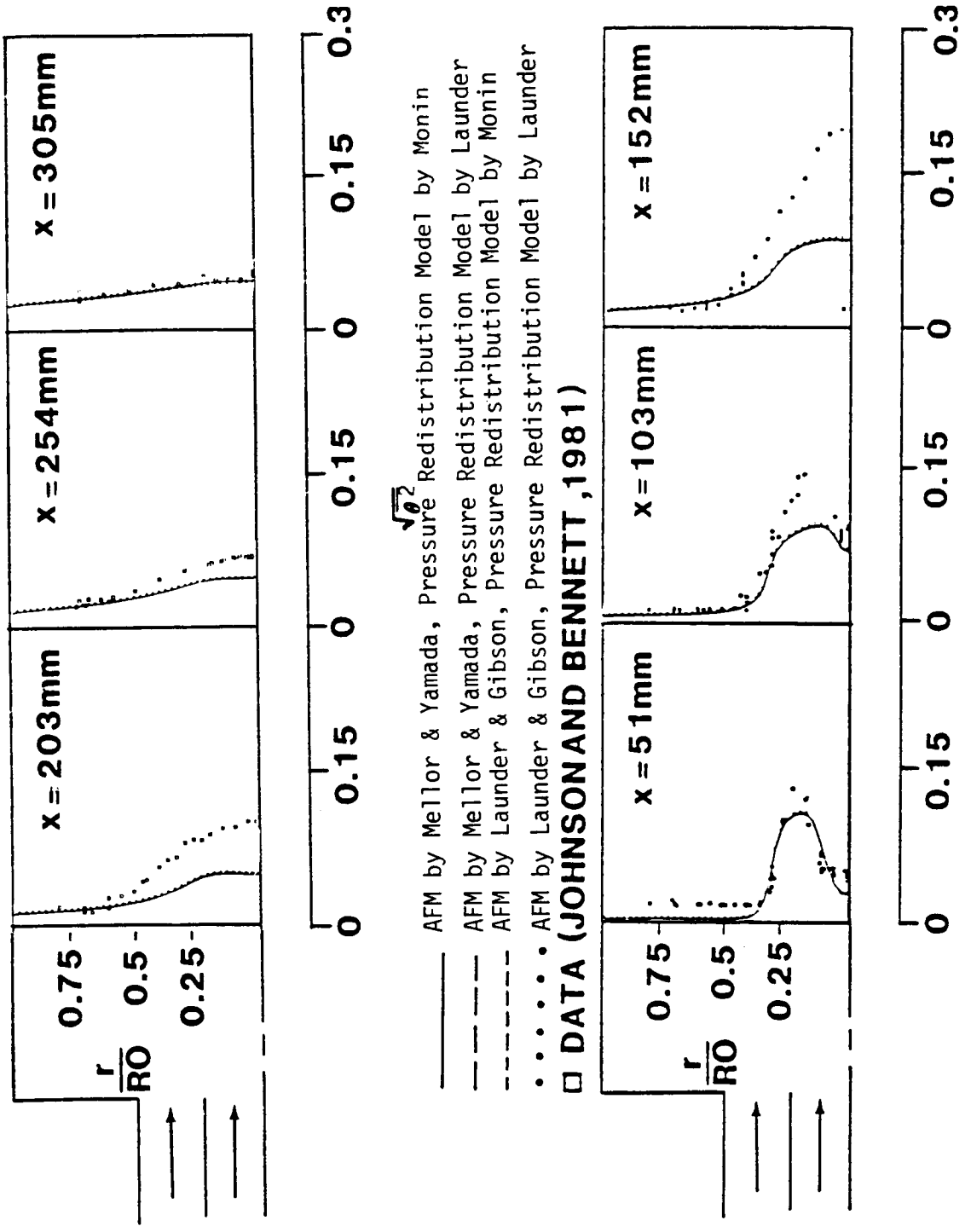

Figure 4.47 Comparison of measurements with $\sqrt{\theta^2}$ calculations using AFM (Johnson & Bennett,1981)

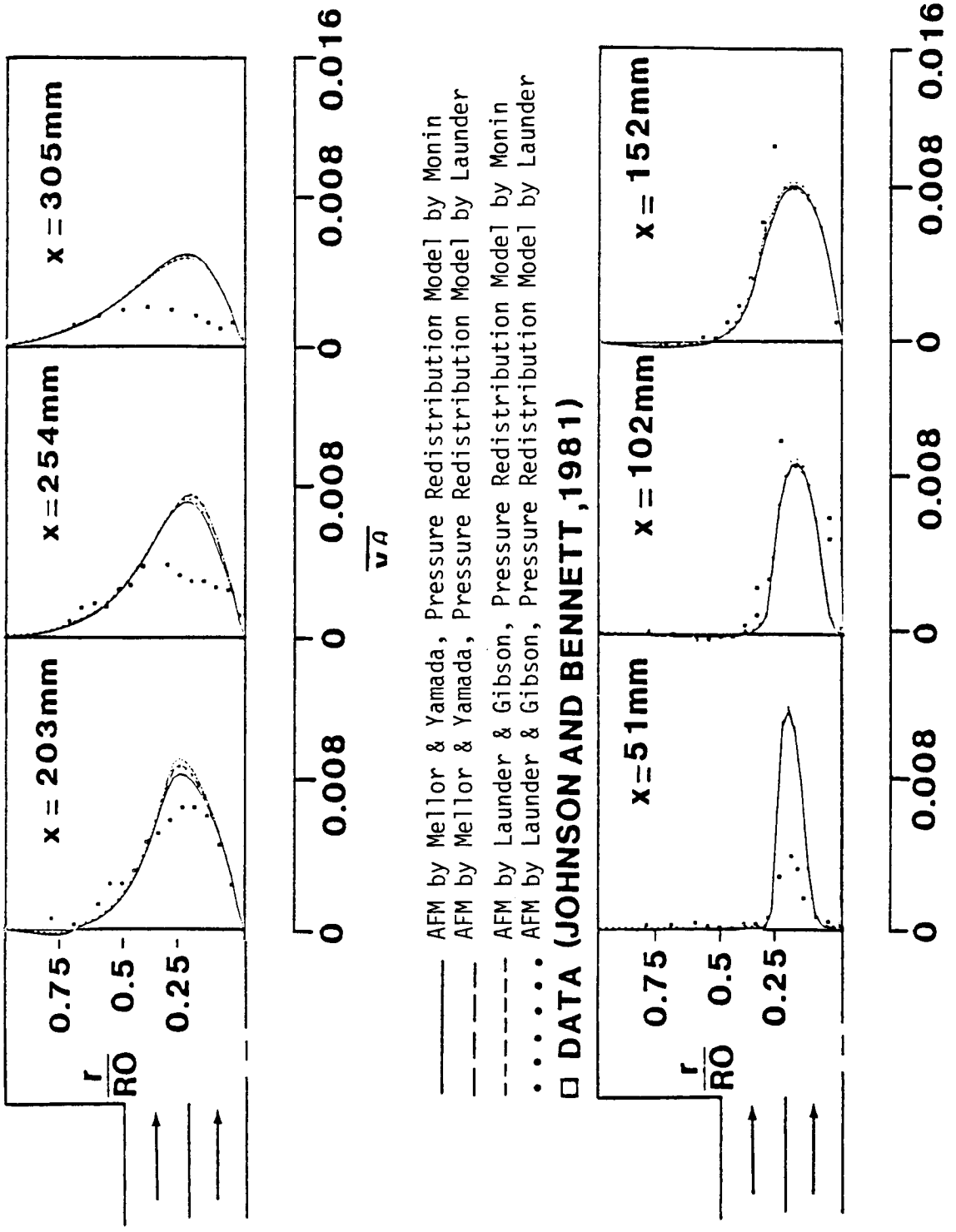

Figure 4.48 Comparison of measurements with $\overline{v\theta}$ calculations using AFM (Johnson & Bennett, 1981)

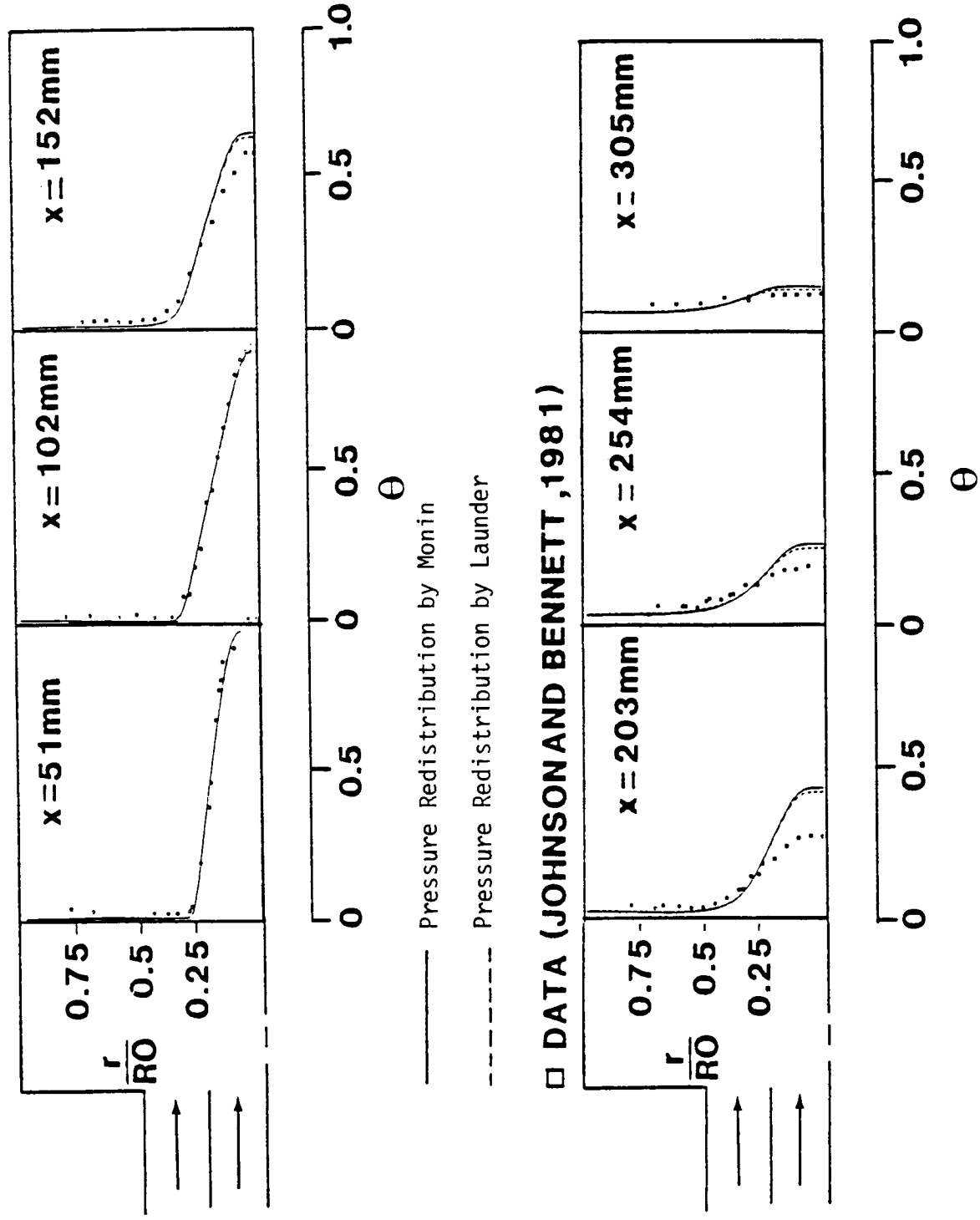

Figure 4.49 Comparison of measurements with mean scalar calculations using second-moment closure (Johnson and Bennett , 1981)

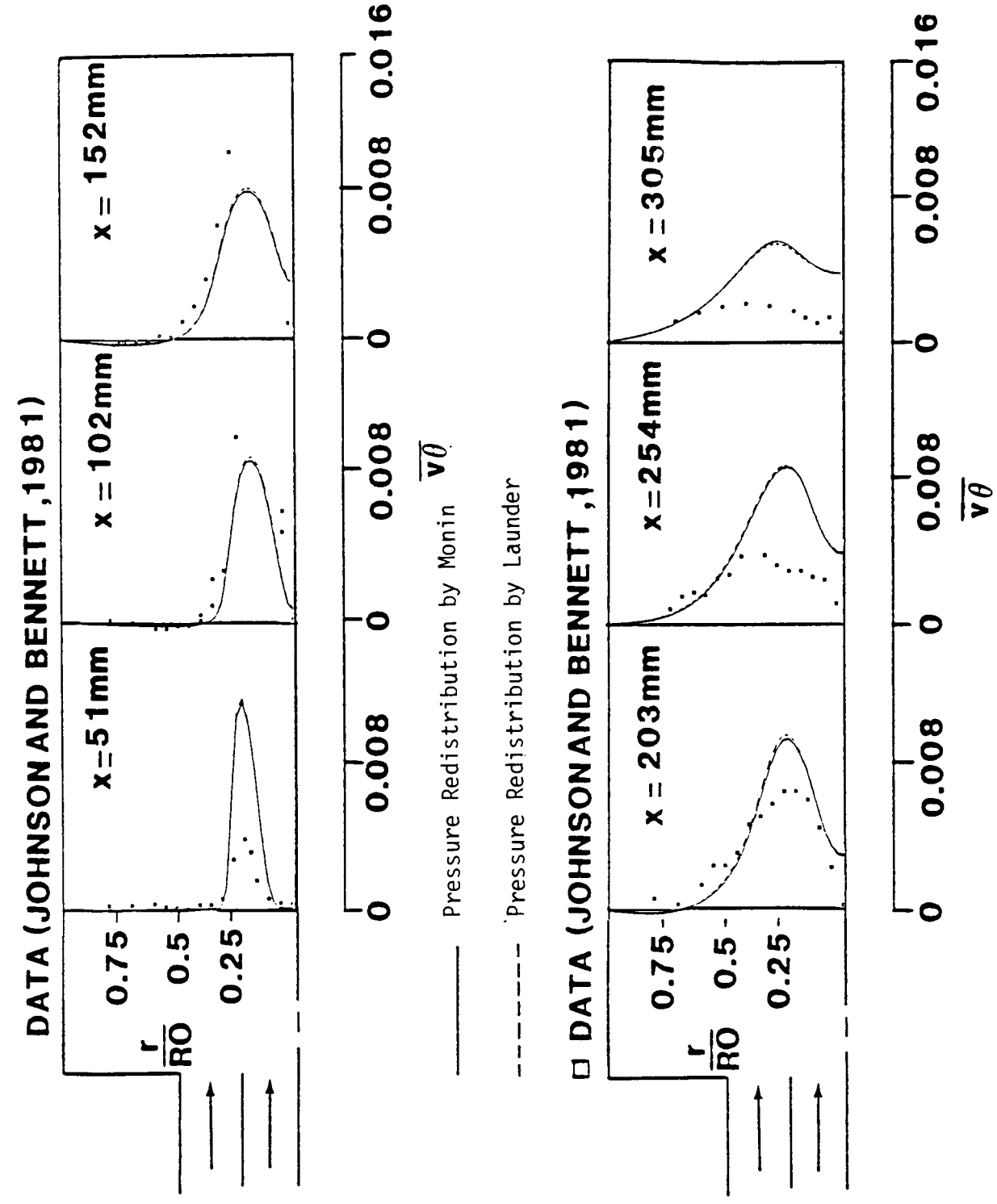

Figure 4.50 Comparison of measurements with $\overline{v\theta}$ calculations using second-moment closure (Johnson and Bennett , 1981)

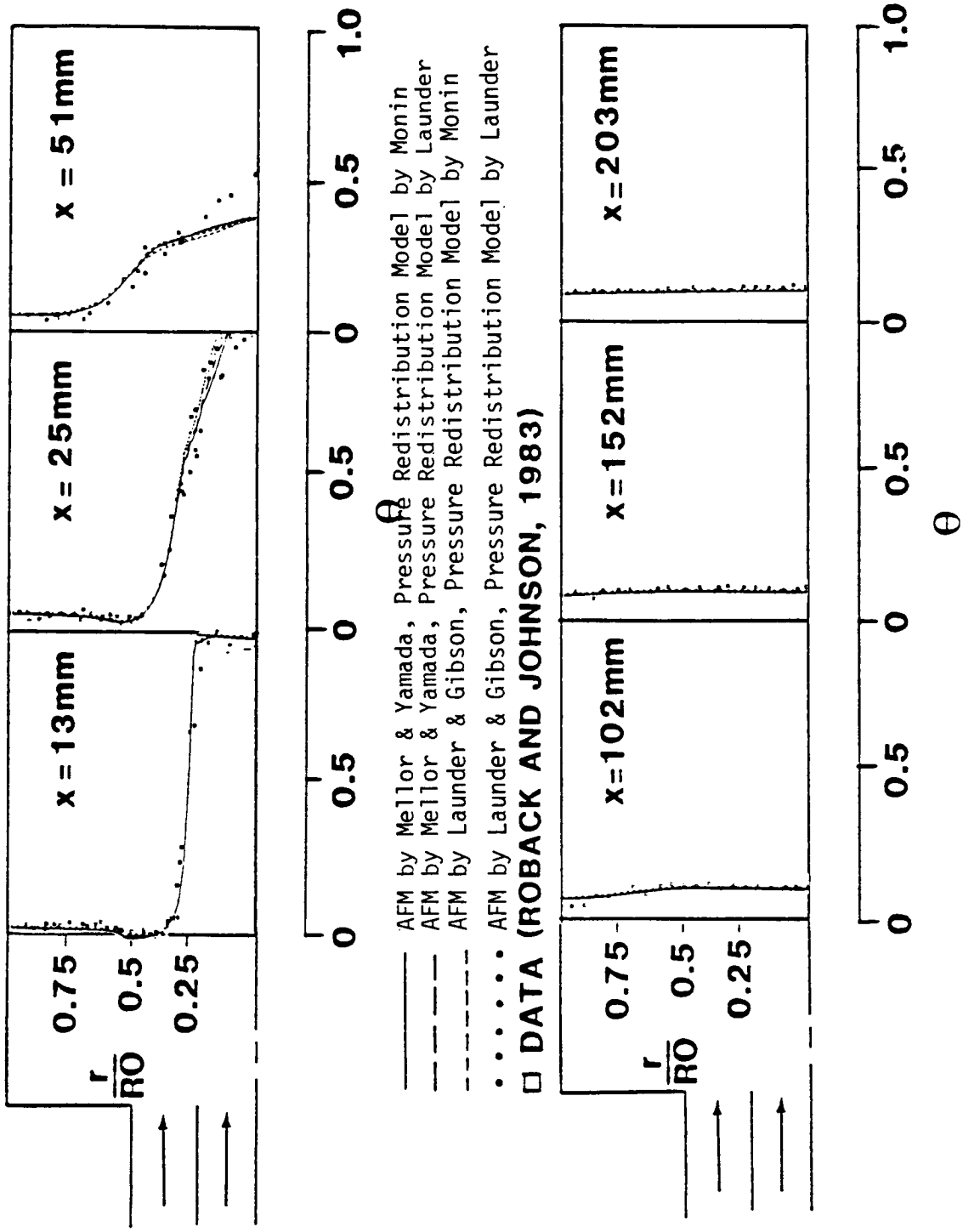

Figure 4.51 Comparison of measurements with mean scalar calculations using AFM (Roback & Johnson,1983)

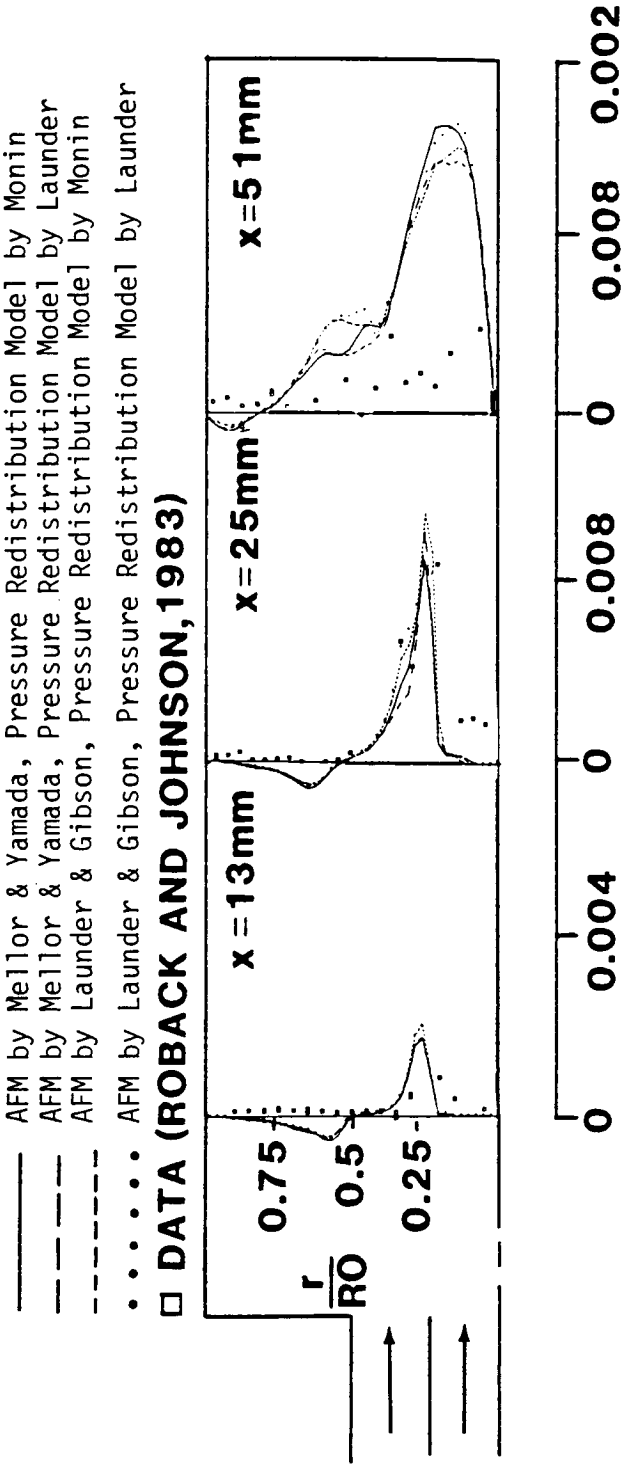

Figure 4.52 Comparisons of measurements with $\overline{v\theta}$ calculations using AFM (Roback & Johnson,1983)

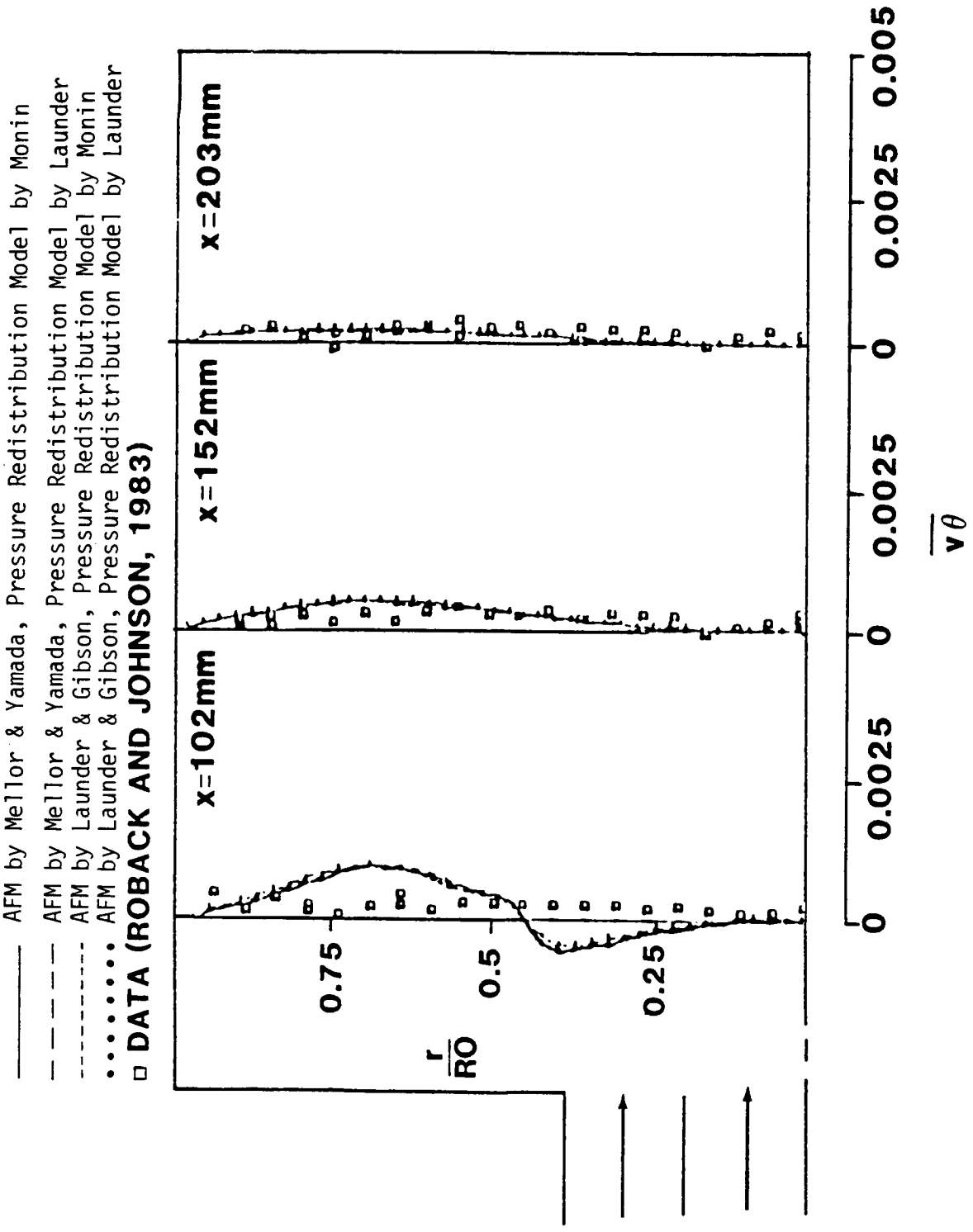

Figure 4.53 Comparisons of measurements with $\overline{v\theta}$ calculations using AFM (Roback & Johnson,1983)

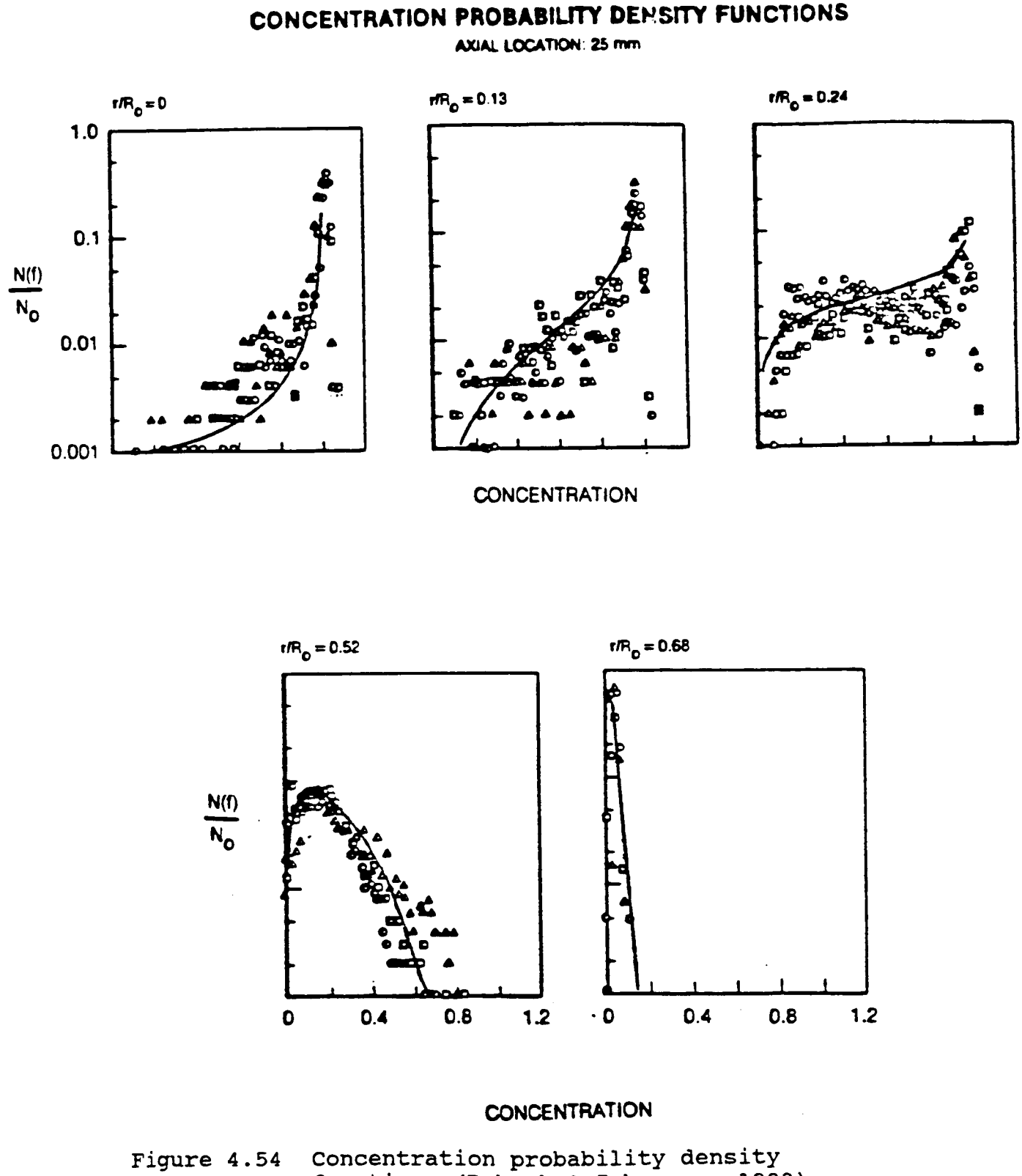

Figure 4.54 Concentration probability density functions (Roback & Johnson , 1983)

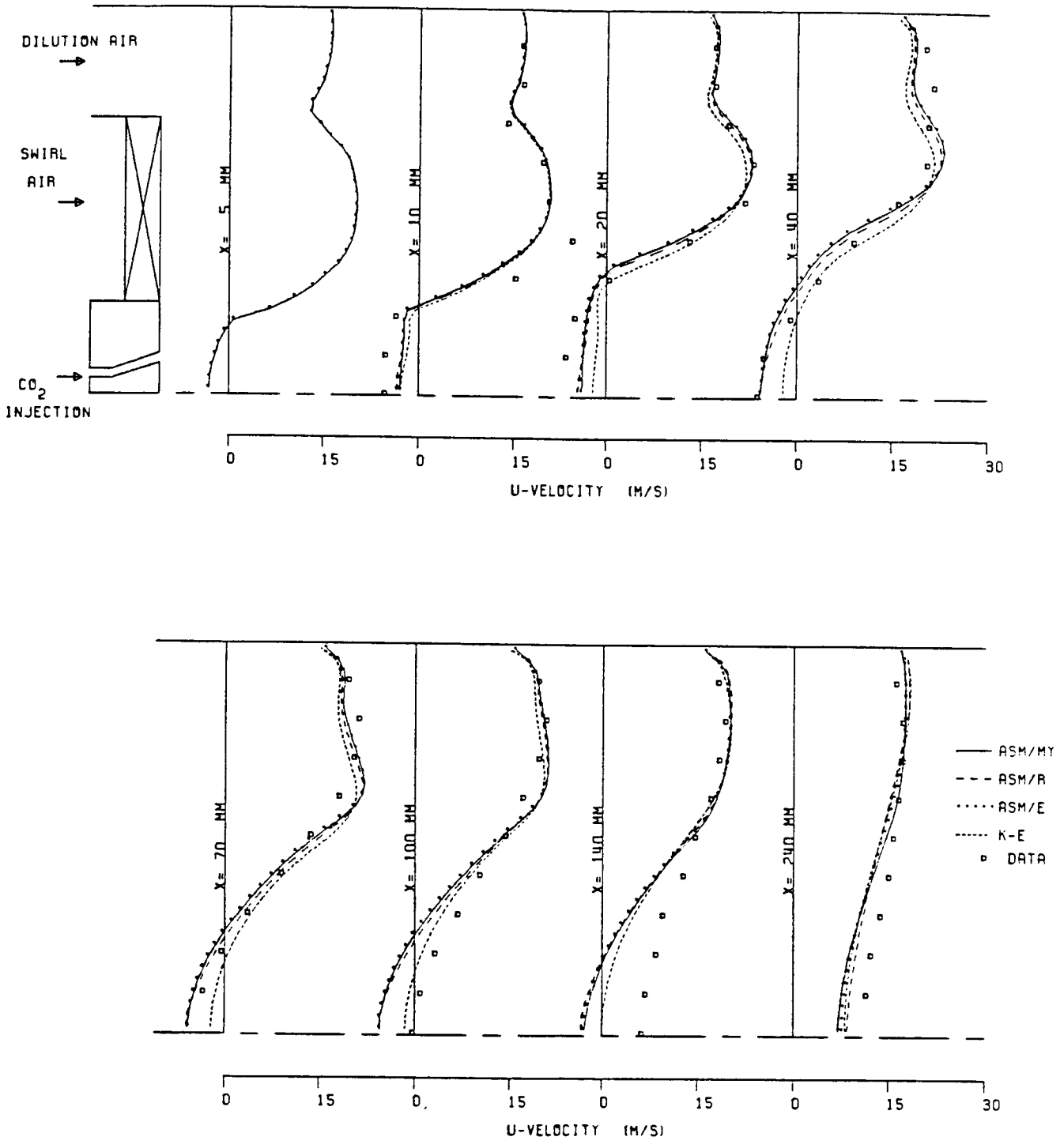

Figure 4.55 Comparison of measurements with mean axial velocity calculations (non-reacting) (Brum & Samuelsen (1982), k-ϵ, ASM)

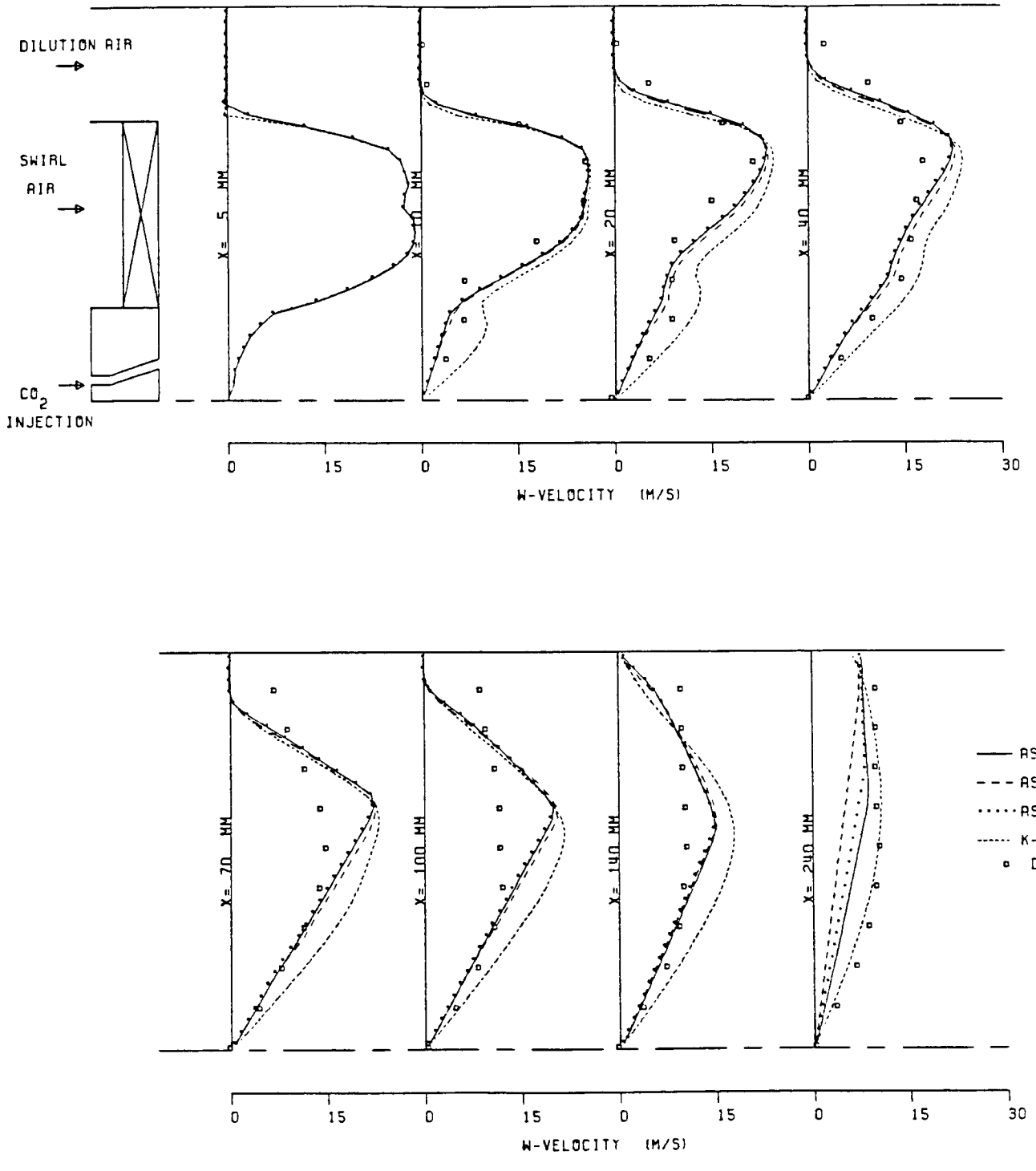

Figure 4.56 Comparison of measurements with mean tangential velocity calculations (non-reacting) (Brum & Samuelsen (1982), k-ϵ, ASM)

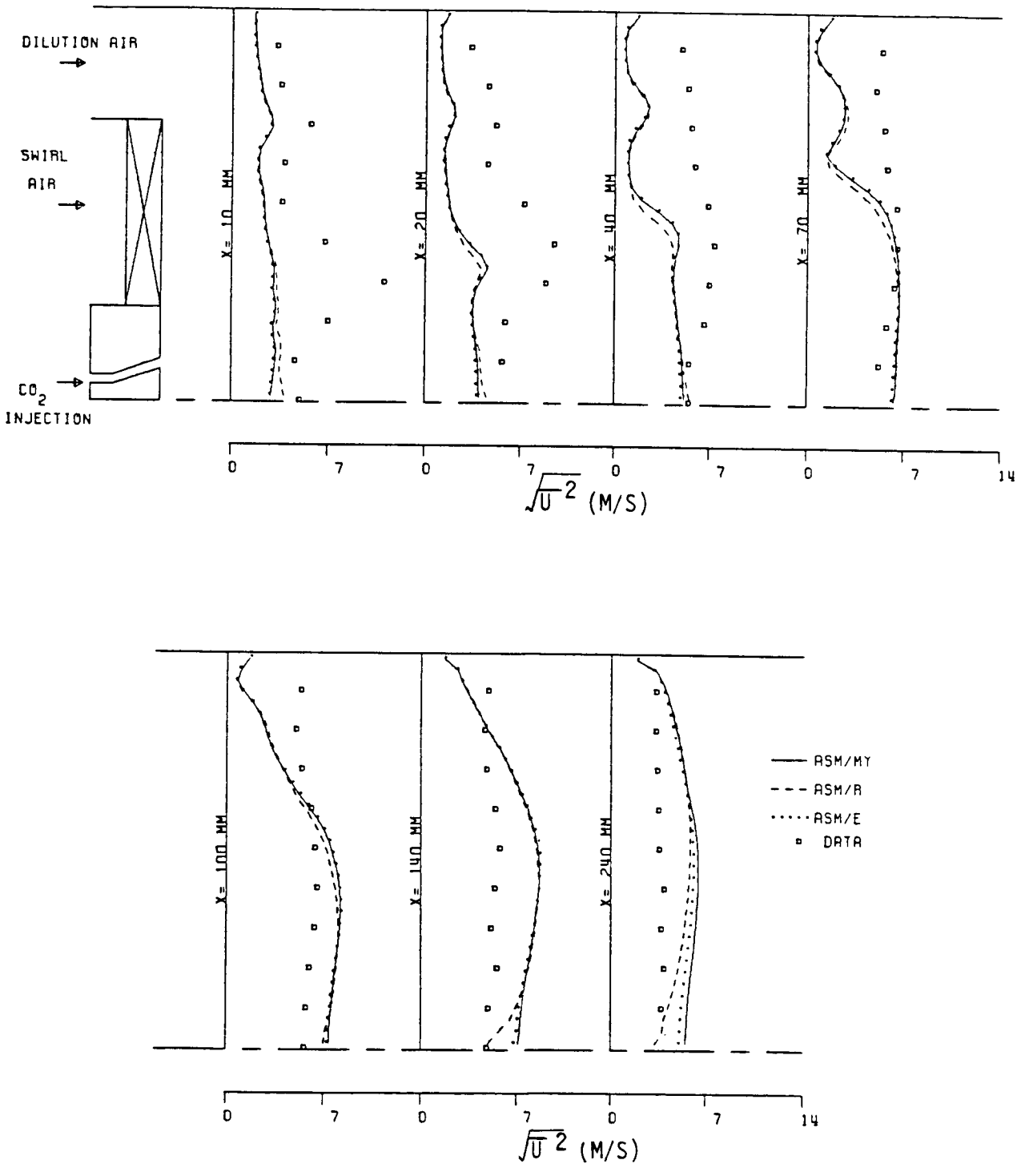

Figure 4.57 Comparison of measurements with $\sqrt{\overline{u^2}}$ calculations (non-reacting) (Brum & Samuelsen (1982), ASM)

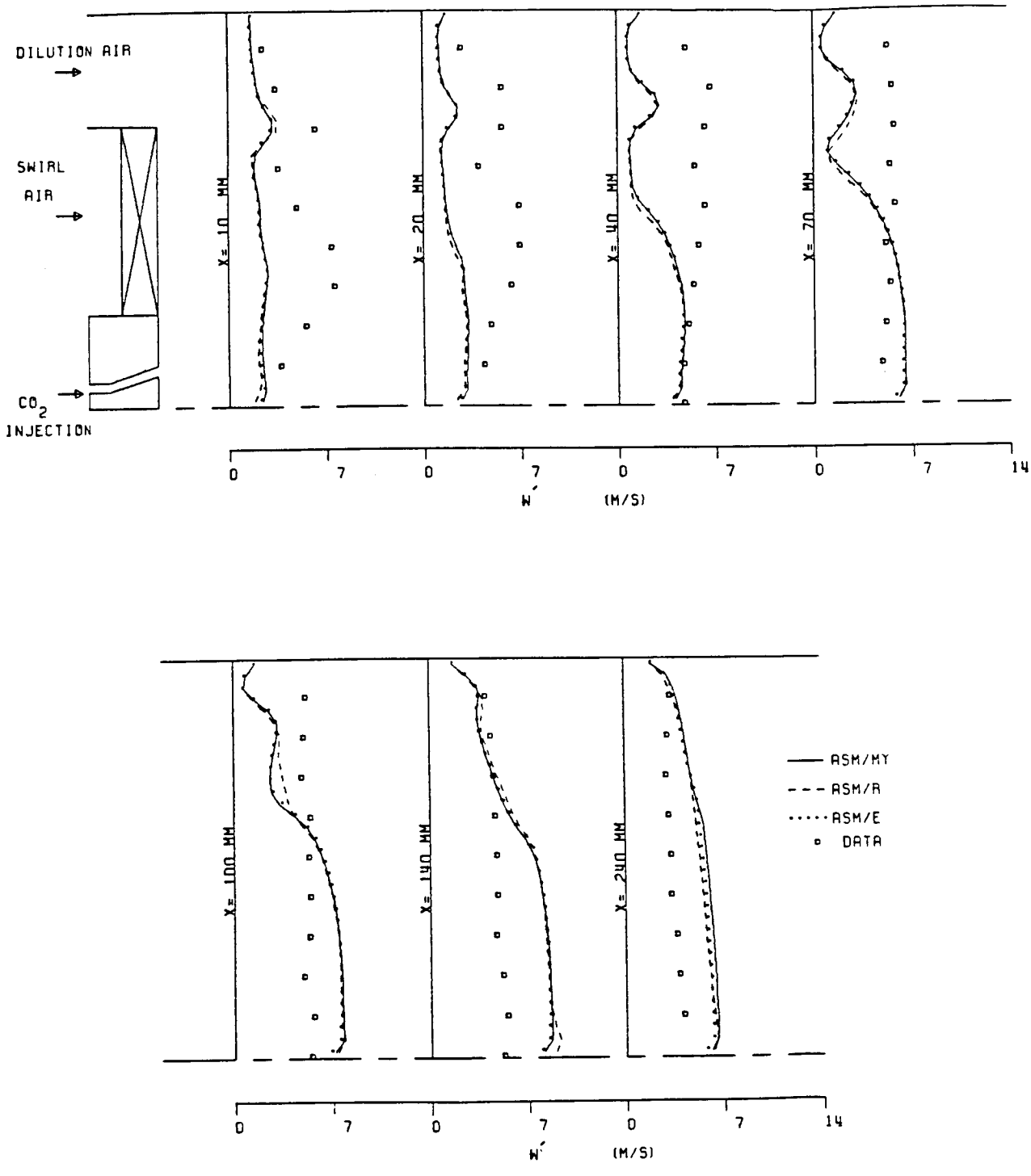

Figure 4.58 Comparison of measurements with $\sqrt{\overline{w^2}}$ calculations (non-reacting) (Brum & Samuelsen (1982), ASM)

CHAPTER 5

REACTING FLOW CALCULATIONS

This chapter presents the results of the reacting flow calculations using the constant-density turbulence models recommended in the previous chapter. There is still the basic question of whether empirical equations or models developed for constant density, non-reacting flows can be applied without modification to turbulent combustion. Models are generally required for quantities such as the turbulent eddy viscosity and the scalar dissipation function which plays an important part in turbulent chemistry (Bray, 1980). There is a widely held belief that the use of Favre averaging automatically takes account of all the effects of density fluctuations and chemical reactions, and, therefore, allows empiricism from constant-density flows to be exploited without change. While this may indeed be true in some cases, it can be justified only by actual comparison with experiments.

Another fundamental question in the modelling of reacting flows is concerned with the effects of turbulence-induced fluctuations on time-averaged reaction rate. An essentail feature of many of the practical problems is that the rate of chemical reaction is limited by the rate of

mixing of reactants. For non-premixed system, and in the limit of fast chemistry, the molecular species are instantaneously related to the conserved scalar and the statistics of all thermodynamics variables can be determined from a sufficient knowledge of the statistics of that scalar (Bilger, 1976). As a result, the need to evaluate mean reaction rate is obviated. However, the estimation of unburnt fuel and the formation of CO require consideration of finite-rate reactions. On the other hand, premixed combustion, in contrast to non-premixed combustion, requires the evaluation of mean reaction rate because the mixing is accomplished before reaction begins. Based on these differences, the results to be presented are divided into non-premixed and premixed combustion. Under non-premixed combustion, both results of fast and finite rate chemistry models are discussed for flows with and without swirl.

In view of turbulence/chemistry modelling, it would be very usefuel if isothermal and reacting flow experiments could be carried out in the same apparatus so that a natural progression in understanding could be followed. Generally, because of experimental problems, such progression has not been done. Therefore, effort is made to select the test cases which are similar to the previous isothermal flow cases in terms of the geometry, working fluids, boundary conditions and measurements technique. In addition, all data sets have to meet the criteria for acceptable measurements

in terms of adequate experimental facility, appropriate instrumentation and agreement with generally accepted flow trends. In view of the above considerations the following three experiments are chosen as the test cases:

1. Lewis and Smoot (1981)

The configuration of this experiment is very close to the configuration of Johnson and Bennet (1981).

2. Brum and Samuelsen (1982)

This experiment is used to simulate the dilute swirl-stabilized combustor. Since molecular weights of CO_2 and C_3H_8 are identical, therefore, by comparing with the non-reacting results, the effect of heat release on flow field can be assessed.

3. McDannel et al. (1982)

This experiment is used to simulate an axisymmetric opposed reacting jet combustor.

Again, the shortcoming of these experiments is the lack of well-defined inlet boundary conditions. Nevertheles, the calculations are quite beneficial because they help to illustrate the differences between the various models and their ability to calculate reacting flows.

5.1 NON-PREMIXED COMBUSTION

5.1.1 Coaxial Non-swirling Jets

In the this study, the geometry of Lewis and Smoot (1981), simulating an industrial furnance, is selected. In this experiment, coaxial streams of fuel (town gas) and air are injected into a suddenly-expanded combustion chamber (Figure 5.1). The flame is stabilized at the dividing lip between the two streams. Measurements have been made of the time mean mixture fraction and species concentration. The parameters and test conditions for this combustor are summarized in Table 5.1.

The computations for this case are made assumption a two-dimensional formulation and a standard k-ϵ model. This model is previously recommended for non-swirling, constant-density flows. Two modelling approaches have been used for the combustion process. At one condition, chemical kinetics are assumed to be rate controlling and at another, turbulent mixing is treated in detail, but infinite rate chemistry is assumed. A non-uniform grid of 61x47 is used in the computations. Uniform axial velocity profiles are prescribed for the fuel and air stream, respectively. The inlet turbulence intensities for air and fuel are given in the measurements as 6% and the length scales are assumed to be 5.7 mm for the air and 1.6 mm for the fuel jet, respectively. Along the adiabatic walls, standard wall function treatment is employed. The fuel mixture fraction is

set equal to one in the fuel stream and zero elsewhere. Because of the uniform distribution of mixture fraction in each of the streams, the fluctuation values are zero in the inlet plane.

The predictions of the mixture fraction, unburnt fuel and carbon monoxide using fast and finite-rate chemistry models are presented in Figure 5.2. The rate constants used are given in Table 5.2. It can be seen that the results are qualitatively correct. Both models over-predict the mixture fraction near the centerline in the developing region; however, the finite-rate chemistry model seems to be able to reproduce the physics better than the fast-chemistry model. A turbulent Prandtl number of 0.9 is used to obtain the results shown. In the fully developed region, the agreement is quite good. This suggests that a good prediction of mixture fraction in the developing region requires a lower turbulent Prandtl number. In the region near the inlet, the convection is dominant and the change of the Prandtl number does not have any effect on the prediction of mean mixture fraction. In the developed region, since the absolute levels of mixture fraction are low, the difference caused by changing the Prandtl number will not be significant. The middle zone is the region of very steep variation in mixture fraction and a lower Prandtl number will undoubtedly improve the prediction. Comparison of predicted and measured values of unburnt fuel is similar to that of mixture fraction. The

prediction is qualitatively correct at all planes; however, the model has over-estimated the unburnt fuel in the middle region indicating the slow reaction rate. The predicted CO levels are fair in most of the locations but beyond x =785 mm, they are significantly lower than the data. The predicted results shown in Figure 5.2 are based on the assumption of equal diffusivity for all species, enthalpy, and the mixutre fraction. It is obvious that the values of the turbulent Prandtl number are not necessarily the same for all species and may not even be uniform over the whole flow field. Therefore, further investigation regarding the scalar transport model is required.

The contour plots of temperature, mixture fraction, unburnt fuel, carbon dioxide and carbon monoxide inside the combustor are shown in Figures 5.3-5.7. The flame zone is clearly delineated by the temperature contours. The comparison clearly shows the big difference between the two combustion models, and illustrates the strong interactions between flow and chemical reactions for the finite-rate chemistry model and the relatively weak interactions shown in the fast-chemistry model (Figure 5.3). Furthermore, a sharp temperature gradient seen near the edge of the flame is a direct result of an insufficient diffusion along the radial direction. No doubt, a smaller Prandtl number will help. However, a more realistic approach would be to abandon the constant Prandtl number assumption and proceed to

evaluate the turbulent fluxes by their own transport equations. The carbon monoxide profile along the centerline behaves correctly, attaining a maximum when reaction (2.63) and (2.64) are equally competing, and subsequently falling off as the combustion products tend to their equilibrium. In general, the finite-rate chemistry model seems to give more realistic results and could be easily adopted for non-swirling combustor flow calculations.

The cold flow results are also shown in Figures 5.8-5.9 for comparison, and serve to show the effect of heat release on the mean and turbulence field. The recirculation zone in the case of reaction is: (1) more intense (higher negative velocities), and (2) more compact (shorter). Expansion effect due to heat release is amply demonstrated by the substantially lower mean axial velocity (U) in the developed region of the flow. On the other hand, turbulence activities as measured by k and uv are greatly reduced by heat release. One surprising result of the present study is given by the calculation of the fast chemistry model. Essentially, a similar behavior of U, k and $\overline{uv}$ are obtained in the reacting zone in comparison with the isothermal flow calculations. One reason for this could be due in part to unrealistic simulation of heat release effects on density fluctuations in the transport equations. It also leads to prediction of double peaks behavior for the mean axial velocity immediately after the inlet plane which is not physically

correct. Such a behavior might be attributed to the predicted scalar distribution near the inlet plane, especially in the wake region created at the dividing lip between the two streams. In a mixing controlled combustiom model, the hydrodynamic field is highly sensitive to the mixture fraction prediction. It is the only parameter that determines the amount of heat release. An incorrect prediction of mixture fraction results in incorrect temperature and density fields. Since density is strongly coupled to the flow field, an incorrect density changes the flow field completely. On the other hand, in finite rate chemistry model, the chemical heat release is determined by transport of total enthalpy and unburnt fuel which is a more realistic approach. It must be stated that neither models can provide an entirely satisfactory description of the reaction zone, however, the two-step reaction scheme has more flexibility and greater potential for application in gas turbine combustors. It needs to be further validated with simple flames to establish rate constants. In addition to Favre-averaging technique, the turbulence model has to include the heat release effect on the turbulence field in the transport equations of turbulent kinetic energy and scalar fluctuation too (Dibble et al. 1985).

C-3

5.1.2 The Dilute Swirl-Stabilized Model Combustor

The flow geometry in this case is identical to that shown in Figure 4.3. The propane-fueled combustor is operated at atmospheric pressure with an overall equivalence ratio of 0.2 and a bulk reference velocity of 15 m/s. The fuel velocity based on the nozzle area and mass flow is 28.1 m/s which is high and has a tremendous effect on the prediction of the central recirculation zone.

Computations are made over a 61x47 non-uniform grid using a standard k-ϵ and an equilibrium ASM model. The rate constants used in this calculation are given in Table 5.2 and Prandtl/Schmidt number is taken to be 0.9. Predicted velocity results from the k-ϵ and the equilibrium ASM models for isothermal and reacting flows are shown in Figures 5.10-5.12. The effect of swirl is pronounced. It produces a large recirculating region near the axis that sweeps back burnt gas products to ignite the incoming reactants. A transition occurred in the form of the recirculation zone which becomes shorter and wider. Beyond the recirculation region, the mean axial velocity profiles predicted by the ASM/E are in better agreement with data than those predicted by the k-ϵ model. However, both models failed to predict the correct location and strength of the recirculation region along the centerline. This result is attributed partly to the high vertical component of inlet fuel velocity used which tends to push the central recirculation region towards the

combustor wall. The predicted maximum flow reversal velocity is approximately -5.75 m/s, while the corresponding measured value is about -7.95 m/s. Furthermore, the location of the maximum negative velocity is predicted closer to the swirler exit compared to the data. In the developing region, the ASM/E has under-predicted the turbulent intensity, especially in the central recirculation zone; however, in the fully developed region the results are relatively better (Figure 5.11). It is also observed that, at downstream locations along the centerline, the experimental value of $\sqrt{\overline{w^2}}$ is greater than $\sqrt{\overline{u^2}}$. These excessive levels as mentioned by Brum and Samuelsen (1982) are probably produced by a spiralling action of the vortex center about the stationary laser velocimeter probe which can be considered as an experimental error. The discrepancy between prediction and measurement can be attributed to: (1) inaccurate inlet conditions, (2) the turbulence model constants, (3) experimental error and (4) the effect of heat release on the turbulence field which needs to be accounted for (Dibble et al. , 1985).

The effect of reaction is observed to double the mean axial velocity and raise the turbulence intensity in the reacting zone (Figure 5.10). However, the increase of tangential velocity near the centerline, which also stems from heat release, has not been correctly predicted. Unlike the previous test case, the fast and finite-rate chemistry

results are essentially identical. The reason is the enhanced mixing due to swirl. This increased mixing activity promotes chemical reactions between fuel and oxidant, and the net result is one of very fast reaction rates. The recirculation zone in the case of reaction is wider (16 mm) and the length of the recirculation region is shorter (38 mm). These changes are the results of gases expanding in the shear layer at the boundary of the recirculation zone. This creates a region of low pressure which tends to draw swirling air towards the centerline and close the recirculation zone (Brum and Samuelsen , 1982).

Finally, contours of unburnt fuel, temperature, mass fraction and carbon dioxide are shown in Figures 5.13-5.16. There is a strong gradient in fuel concentration in the radial direction close to the inlet, while the profile becomes more uniform as the outlet is approached. The temperature and mixture fraction distributions found by fast and finite rate chemistry models are very similar. However, the fast chemistry model shows a longer reacting zone. Both models predict the sharp temperature gradients near the perimeter where dilute air enters. This apparent suppression of radial transport could be due in part to the use of an isotropic diffusion model, unrealistic Prandtl/Schmidt number, and unrealistic simulation of heat release effects on density fluctuations in the transport equations. As mentioned before, the Prandtl number is not a significant

factor in the fully developed region because the flow is convection dominated and the axial velocity is quite uniform. However, in the developing region, the isotropic diffusion model is not valid and more realistic approach is to evaluate the turbulent fluxes by their respective transport equations.

5.2 PREMIXED COMBUSTION

Another test case selected for evaluating the kinetic scheme is the recirculating flow in an axisymmetric, opposed-reacting-jet combustor shown schematically in Figure (5.17). The incoming mainstream of premixed propane and air (U_m=7.5 m/s) is opposed by a high-velocity (U_j=135 m/s) premixed jet positioned along the longitudinal axis with an equivalence ratio of one. The jet creates a zone of recirculating flow necessary to stabilize the reaction. Computations are made over a 49x25 non-uniform grid using a k-ϵ model and the results compared to species concentration and temperature measurements reported by McDannel et al. (1982) and velocity data provided by Samuelsen (1986). The inlet turbulence intensity is assumed to be uniform with a value of 0.005 and the inlet length scale is assumed to be constant with a value of 2.5 mm. Adiabatic boundary conditions along the walls are also applied. Again, the rate constants listed in Table 5.2 are used.

The difficulty of modelling jets in a co-flowing stream is amply demonstrated by the work of Launder et al. (1973). Their results show that, of the four models, ranging from mixing-length to two-equation models, used to calculate jets in a co-flowing stream, none is capable of predicting the decay of the jet centerline velocity correctly. So and Hwang (1986) point out that there are certain inherent deficiencies in the models and these lead to a slower growth for the jet. A model for the developed region of the jet is put forward by So and Hwang (1986) and their calculations are in good agreement with measurements. For opposed-jets in a moving stream, the modelling difficulties are further compounded by the presence of a stagnation point, and the very rapid decay of the jet centerline velocity. In other words, the models may not be able to mimic the highly dissipative phenomenon occurring in the region downstream of the jet exit. In view of this, the calculated isothermal flow field of the opposed-jet experiment could not be expected to be correct. Therefore, the present comparison with measurements should be judged bearing in mind the inadequacy of the turbulence model and the inaccuracy of the isothermal flow field.

A comparison of the calculated jet centerline velocity decay with the hot- and cold-flow measurements is shown in Figure 5.18. As expected, the models under-predict the velocity decay for cold flow and the discrepancy becomes

more pronounce for the hot flow. The measurements show that the jet decays immediately downstream of the jet exit, while the models give a very small potential core region for the cold-flow jet and a much larger potential core for the hot-flow jet. The location of the stagnation point is also incorrectly predicted, and the result shows that the predicted hot-flow stagnation point is in closer agreement with the cold-flow measurement. Experimental measurements show that the hot-flow centerline velocity is always higher than the cold-flow centerline velocity. This is a consequence of flow expansion due to heat release from chemical reaction. The models cannot reproduce this behavior correctly because they over-predict the centerline velocity decay in the region $1.7<x/D<2.6$ for the hot-flow and under-predict the decay in the same region for the cold-flow. As for the region between the stagnation point and the jet exit, the k-ϵ model completely fails to reproduce the flow behavior. In the region downstream of the stagnation point, the agreement is much improved. Therefore, this points to another deficiency of the k-ϵ model; namely, it cannot properly account for the rapid dissipative phenomenon seen in the present test case.

The predicted mean axial velocity profiles for hot and cold flows are presented in Figure 5.19. Shown for comparison are the hot- and cold-flow measurements obtained by Samuelsen (1986) at one x location. The expansion effect

due to heat release is clearly apparent. The calculated recirculation zone in the case of reaction is (1) radially wider, (2) axially shorter and (3) more intense, which means higher negative velocities. This is in stark contrast to the measured profiles which show a radially wider recirculation zone for the cold flow. Reason for this could be traced to the inadequacy of the k-ϵ model and perhaps, partially, to the combustion model. The effect of reaction is also to increase the turbulent kinetic energy and shear stress considerably (Figures 5.19-5.20). In both cases, the stagnation point is incorrectly located due to deficiencies in the underlying turbulence model.

Not only does the turbulence model affect the flow field calculation, it also affects the temperature and species concentration field. A comparison of the temperature and carbon monoxide (CO) distribution for stoichiometric (ϕ=1) combustion of propane and air is shown in Figures 5.21-5.22. The flame region is indicated clearly by the temperature contours, but local agreement is not attained. As discussed before, the stagnation point error is clearly evident and so are the under-predicted axial turbulent exchange across the stagnation point and the deficient radial exchange.

5.3 CONCLUSIONS

The main conclusions emerged from this study can be summarized as follows.

1. Two-step reaction scheme performed better than fast chemistry model in predicting mean mixture fraction.

2. Satisfactory prediction of mean mixture fraction can be obtained using a turbulent Prandtl number that is constant over the flow field.

3. Finite-rate chemistry models are preferred over fast-chemistry models for determining the combustion effects in combustors. However, it needs to be further tested with simple cases to establish rate constants so that major species can be accurately predicted.

4. The constant-density k-ϵ turbulence model provides a satisfactory representation of the aerodynamics in most practical combustor flows, except in the case of jet-stabilized combustor flow. The reason is the inability of the k-ϵ model to replicate the highly dissipative phenomenon found in such flows.

5. Some improvement in complex swirling flow predictions could be obtained by using an algebraic stress model.

6. The combustion model must provide a realistic representation of heat release behavior which has the substantive effect on the flow structure.

7. In addition to Favre-averaging, the turbulence model should include some heat release effect on the turbulence field. This could be accounted for in the transport equations of turbulent kinetic energy and its dissipation and the scalar fluctuations.

TABLE 5.1 Combustor parameters and test conditions

Primary Gas		
Temperature (K)		286
Mass flow rate (Kg/s)		0.0031
Velocity (m/s)		21.7
Composition (molar %):		
CH_4	88.53%	
C_2H_6	7.44%	
N_2	2.55%	
CO_2	1.39%	
H_2	0.09%	
Secondary Air		
Temperature (K)		589
Mass flow rate (Kg/s)		0.0362
Velocity (m/s)		34.7
Composition (molar %):		
N_2	78.3	
O_2	20.8	
Ar	0.9	

TABLE 5.2 Model constants for mean reaction rates

	Town Gas	Propane
C_{R1}	= 3.	3.
C_{R2}	= 4.	4.
K_1	= 3.3×10^{14}	5.57×10^{8}
K_2	= 6.0×10^{8}	5.42×10^{9}
E1/R	= 27000	15104
E2/R	= 12500	15098
a	= 1.5	1.75
b	= 0.5	0.1
c	= 1.0	1.65
a'	= 2.0	2.0
b'	= 1.0	1.0
c'	= 1.0	0.5
d'	= 0.0	0.5

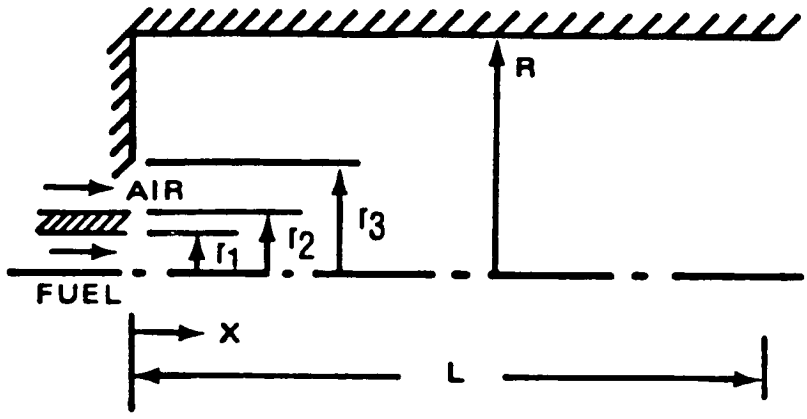

r_1 = 0.008 M
r_2 = 0.0111 M
r_3 = 0.0286 M
R = 0.1016 M
L = 1.524 M

U_{AIR} = 34.3 M/S
U_{FUEL} = 21.3 M/S

T_{AIR} = 589°K
T_{FUEL} = 300°K

Figure 5.1 Sketch of the combustor (Lewis & Smoot, 1981)

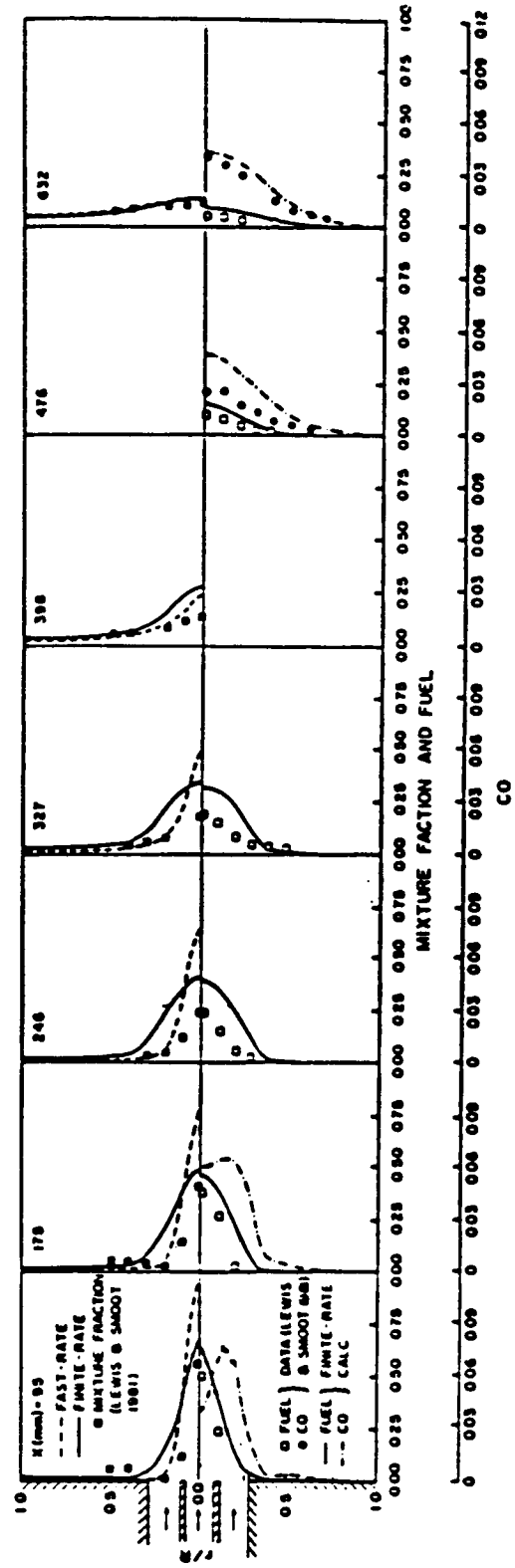

Figure 5.2 A Comparison of the calculated and measured mixture fraction, fuel and CO (Lewis & Smoot ,1981)

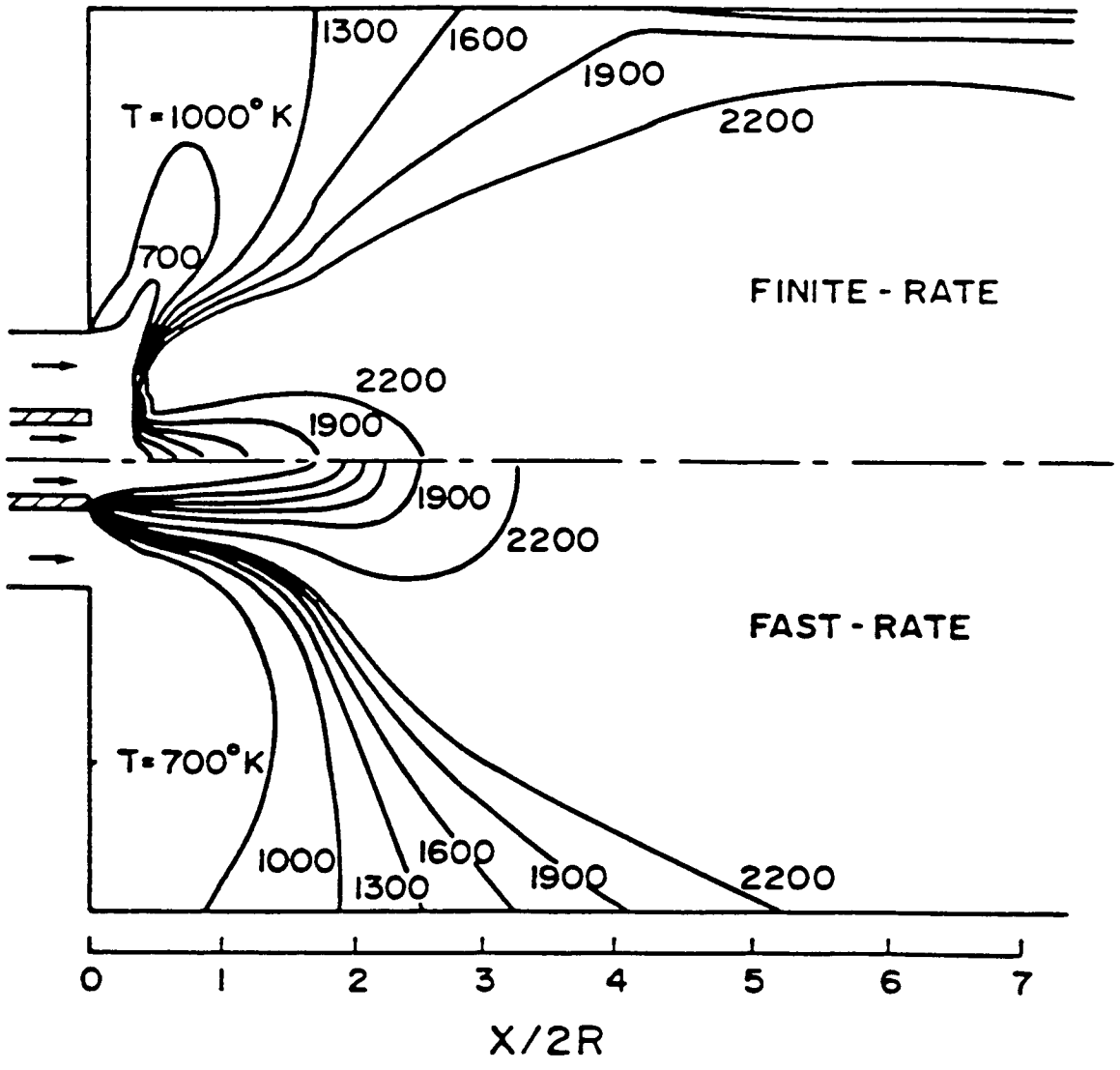

Figure 5.3 Contour plots of temperature distribution inside the combustor (Lewis & Smoot, 1981)

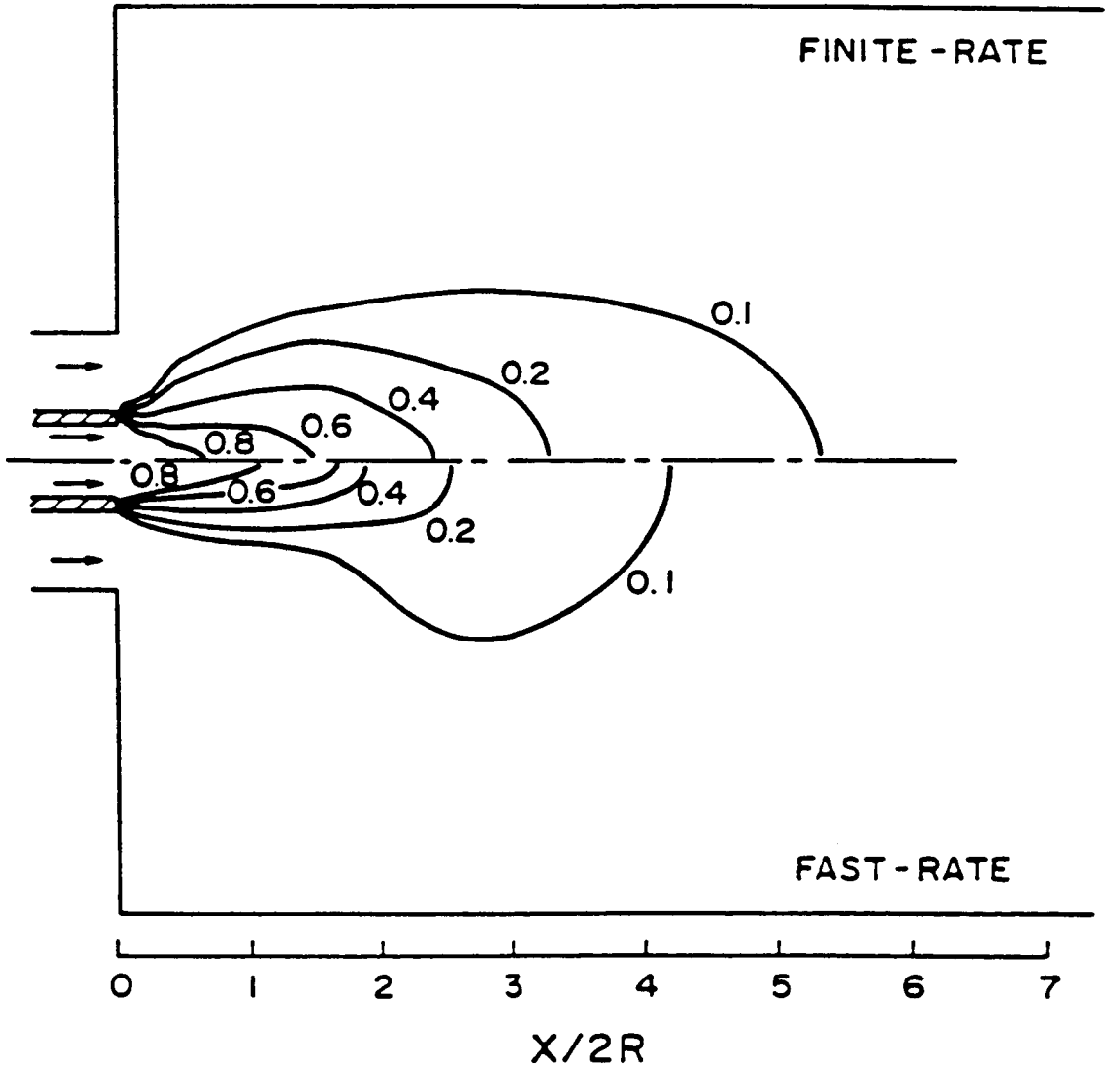

Figure 5.4 Contour plots of mixture fraction (Lewis & Smoot, 1981)

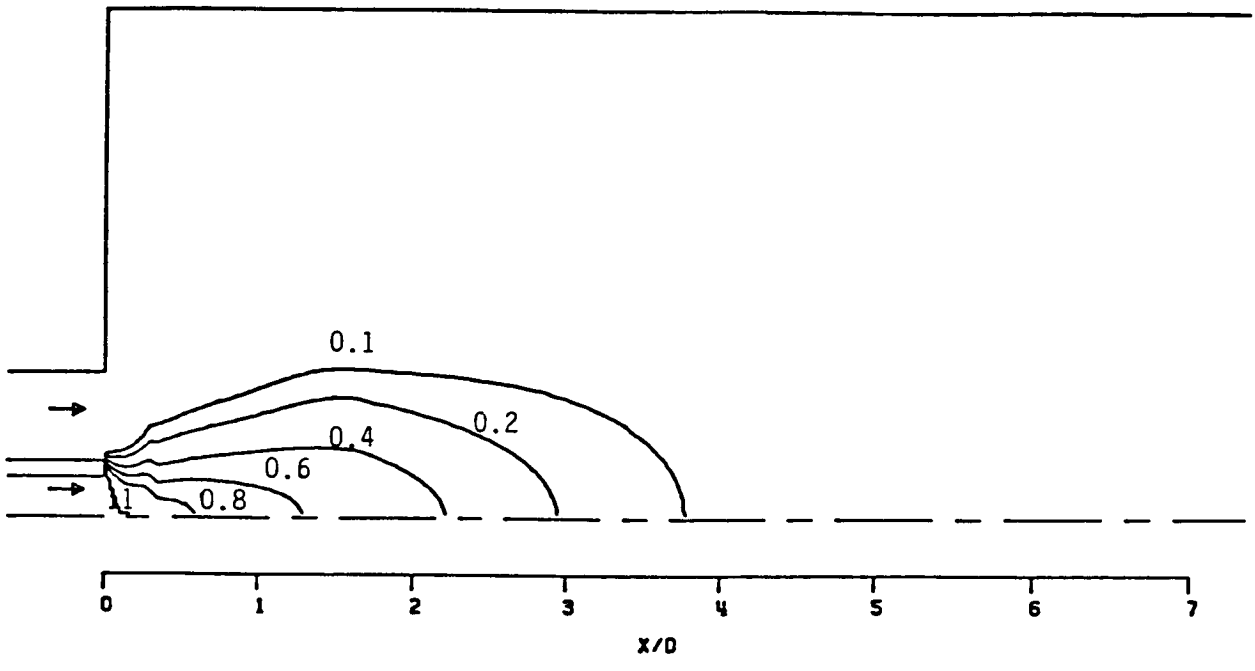

Figure 5.5 Contour plots of unburnt fuel (Lewis & Smoot, 1981)

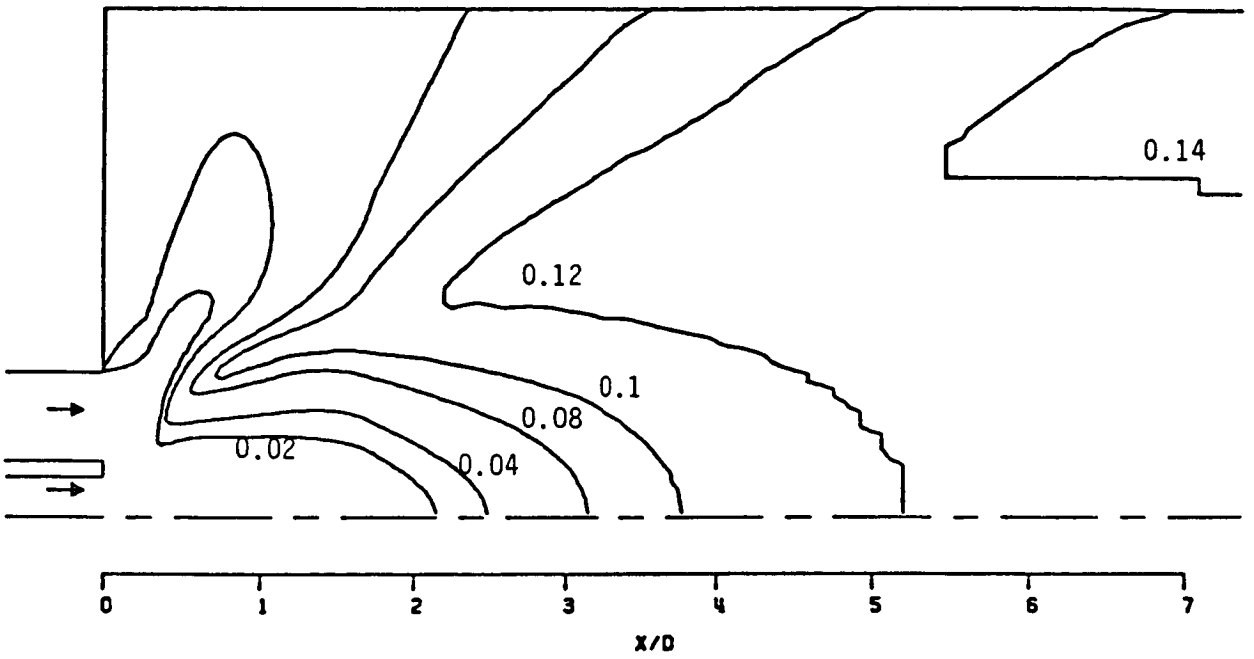

Figure 5.6 Contour plots of carbon dioxide (Lewis & Smoot, 1981)

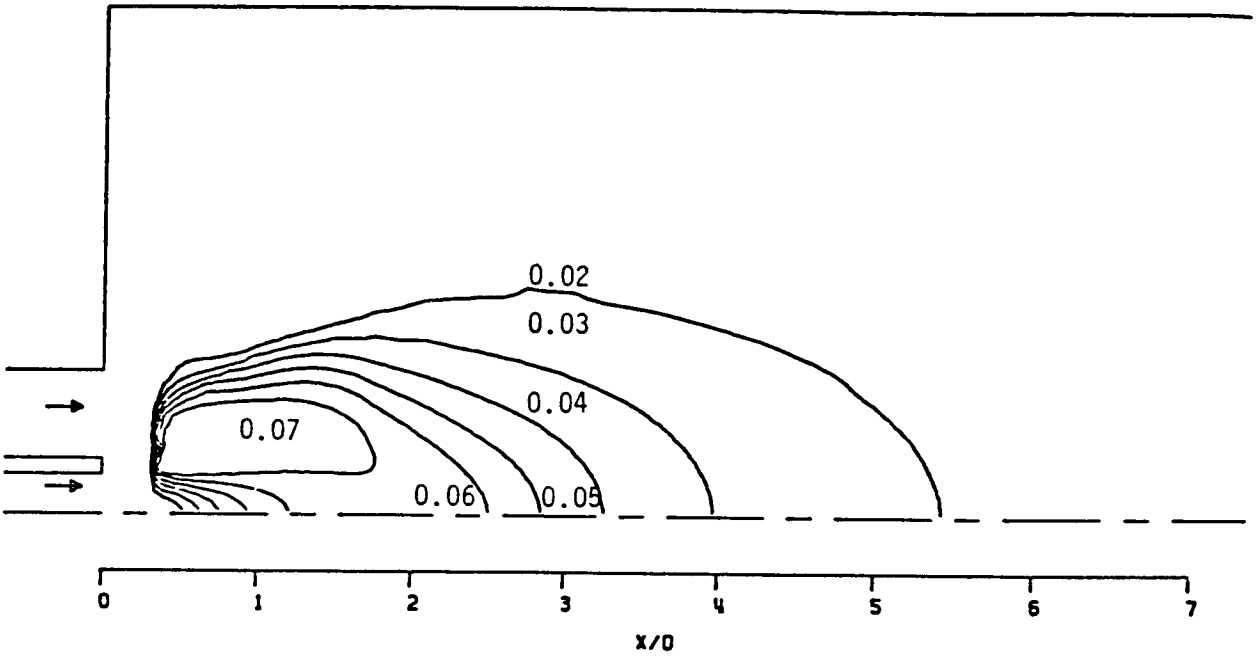

Figure 5.7 Contour plots of carbon monoxide (Lewis & Smoot, 1981)

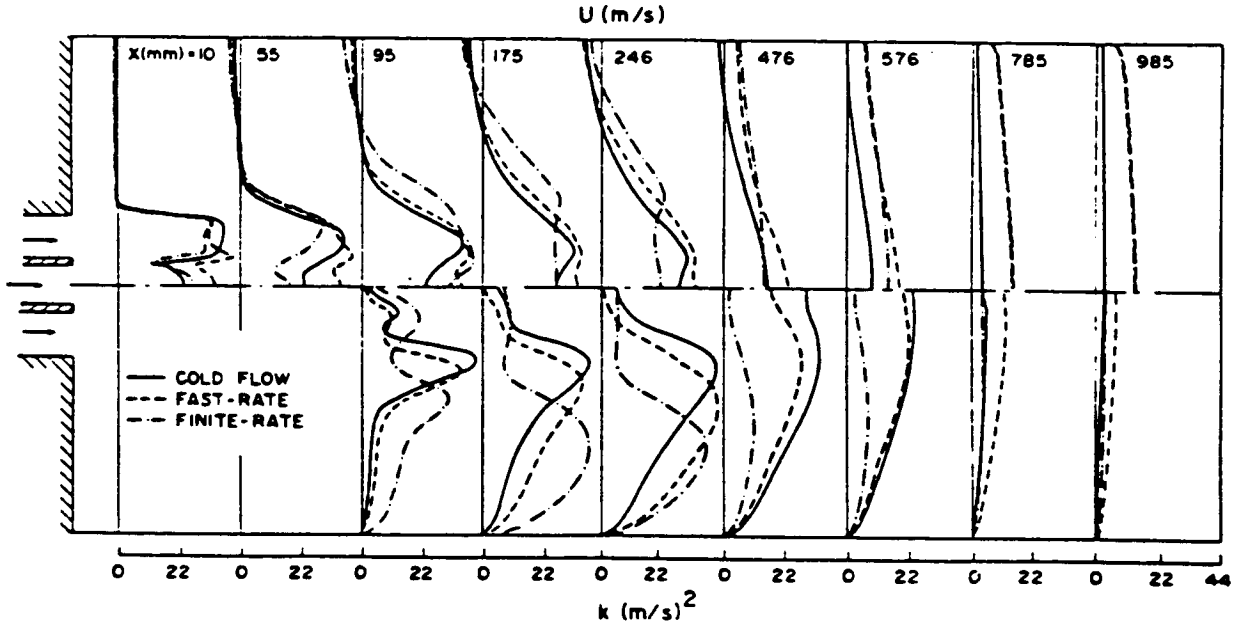

Figure 5.8 Effect of heat release on the calculated mean and turbulent flow fields (Lewis & Smoot, 1981)

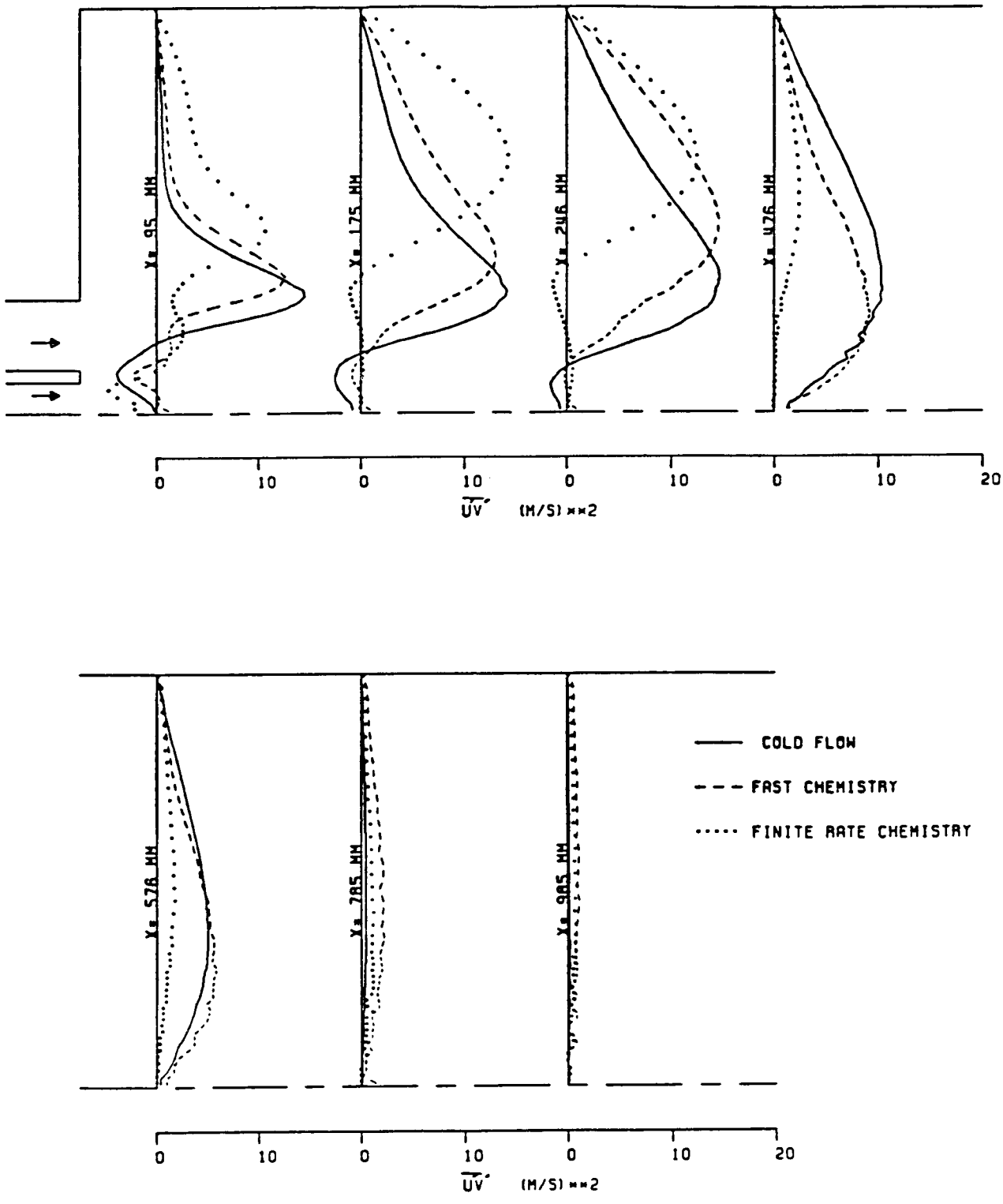

Figure 5.9 Effect of heat release on the calculated turbulent shear stress (Lewis & Smoot, 1981)

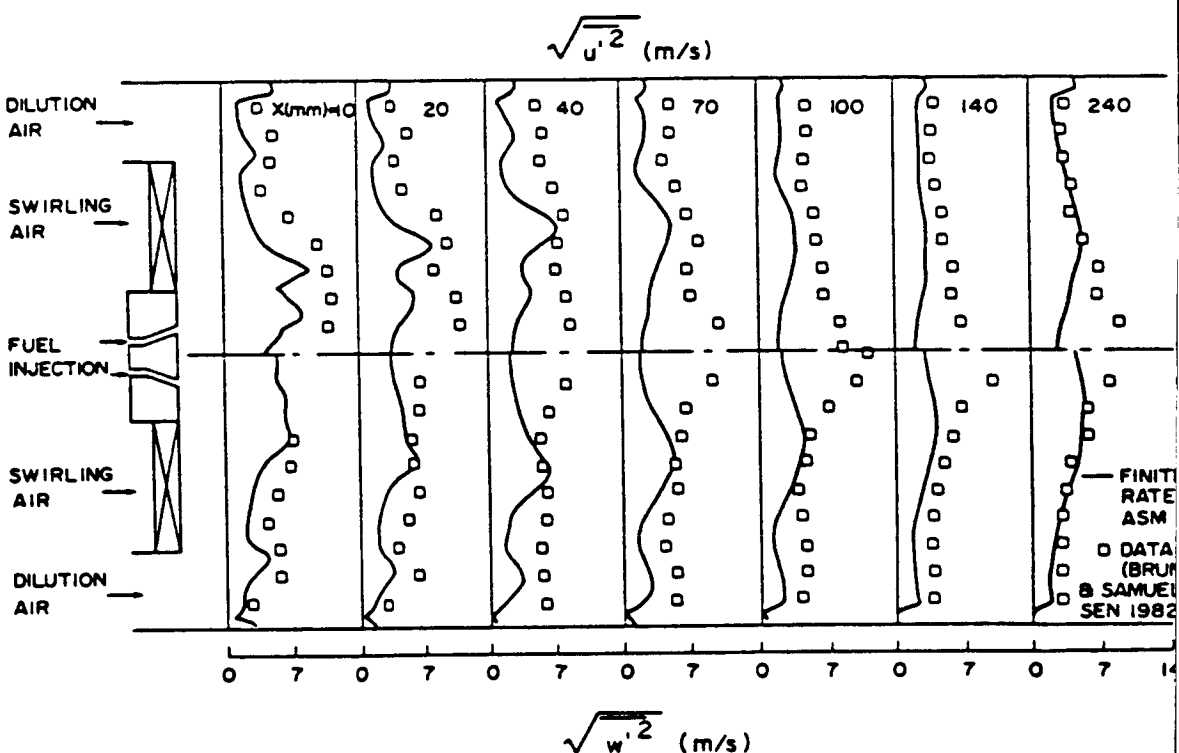

Figure 5.11 Comparison of calculated $\sqrt{u^2}$ and $\sqrt{w^2}$ with measurements (Brum & Samuelsen ,1982)

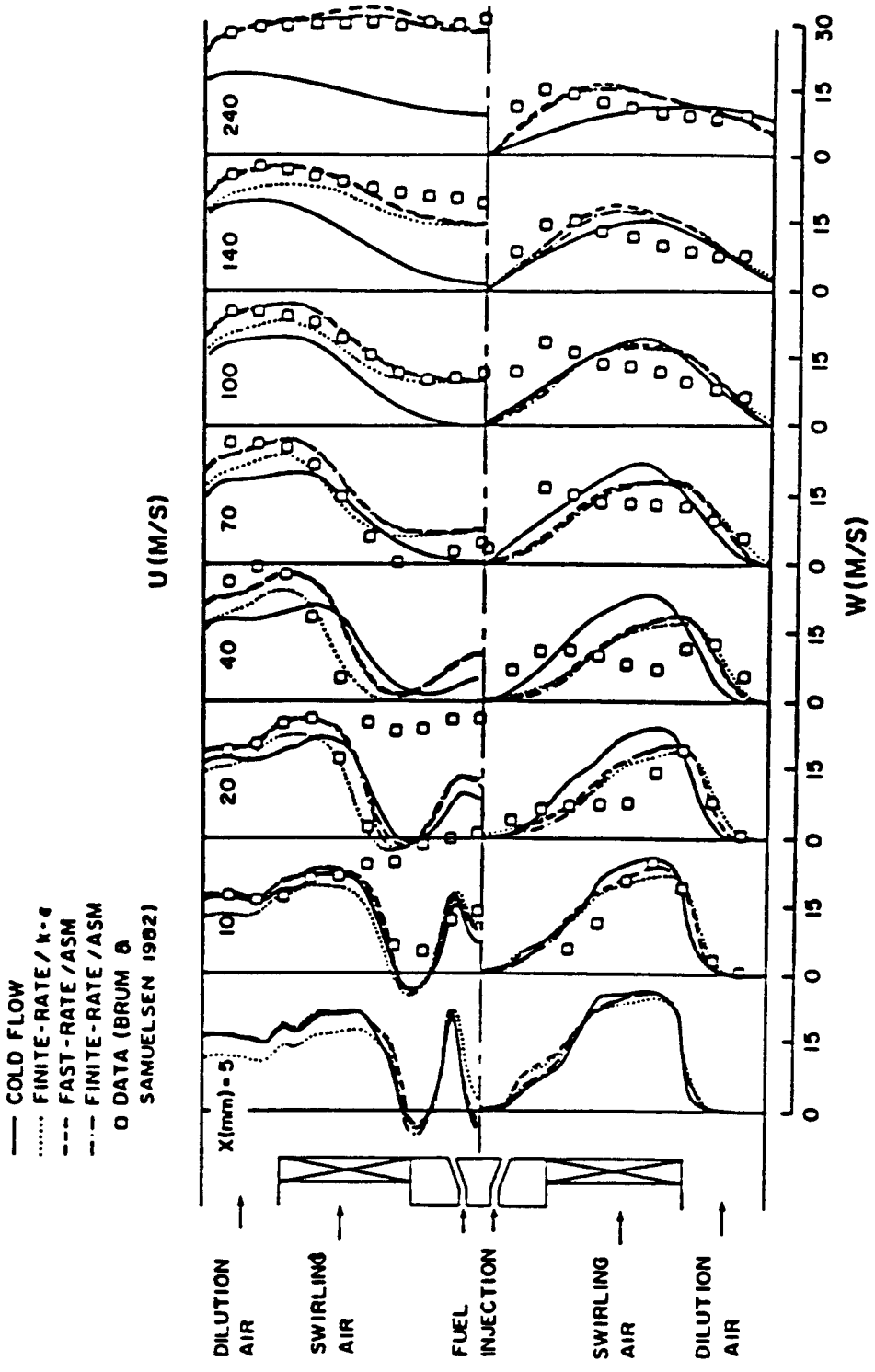

Figure 5.10 Comparison of calculated mean axial and tangential velocities with measurements (Brum & Samuelsen ,1982)

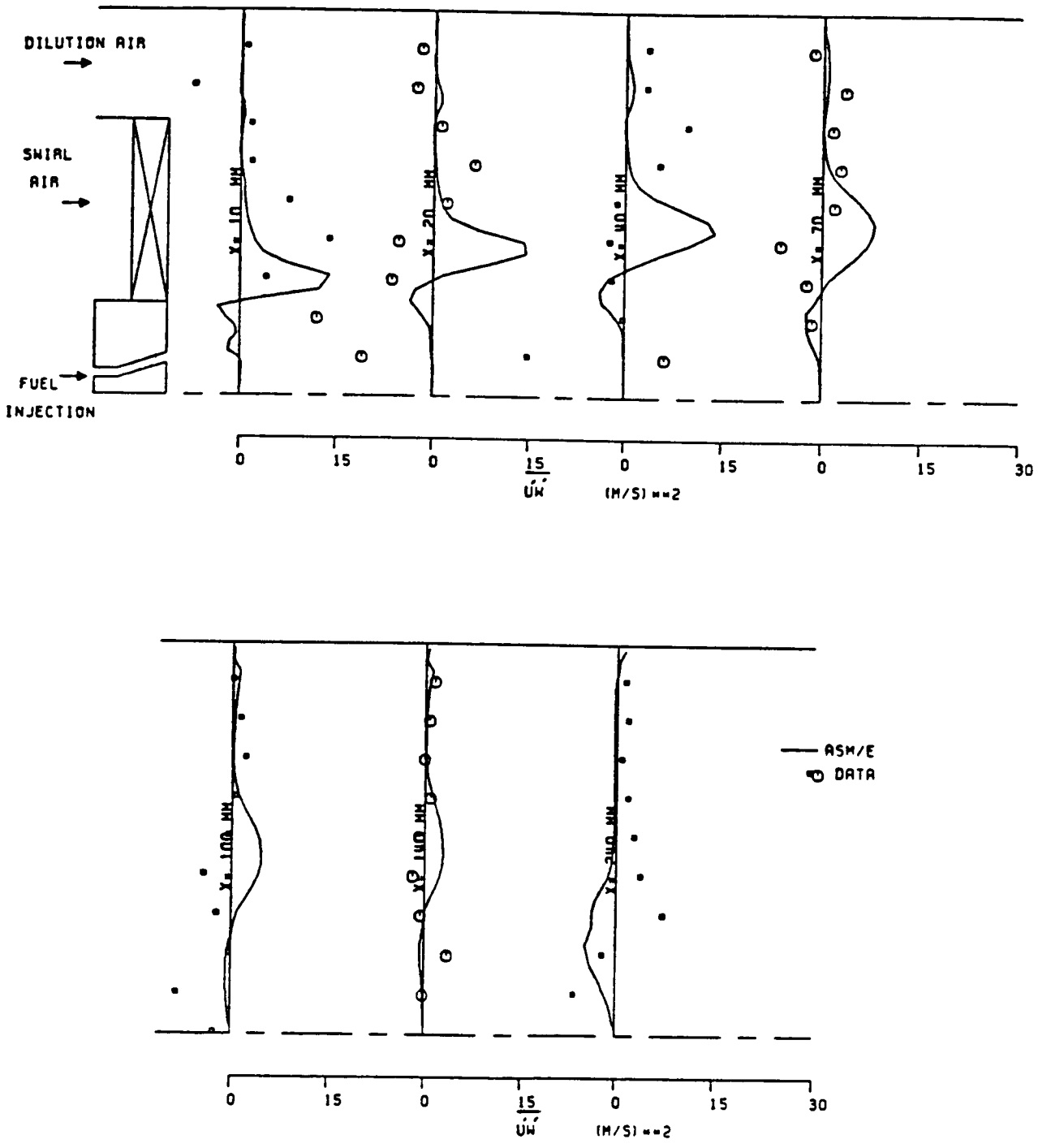

Figure 5.12 Comparison of measurements with $\overline{uw}$ calculations (Brum & Samuelsen (1982), ASM)

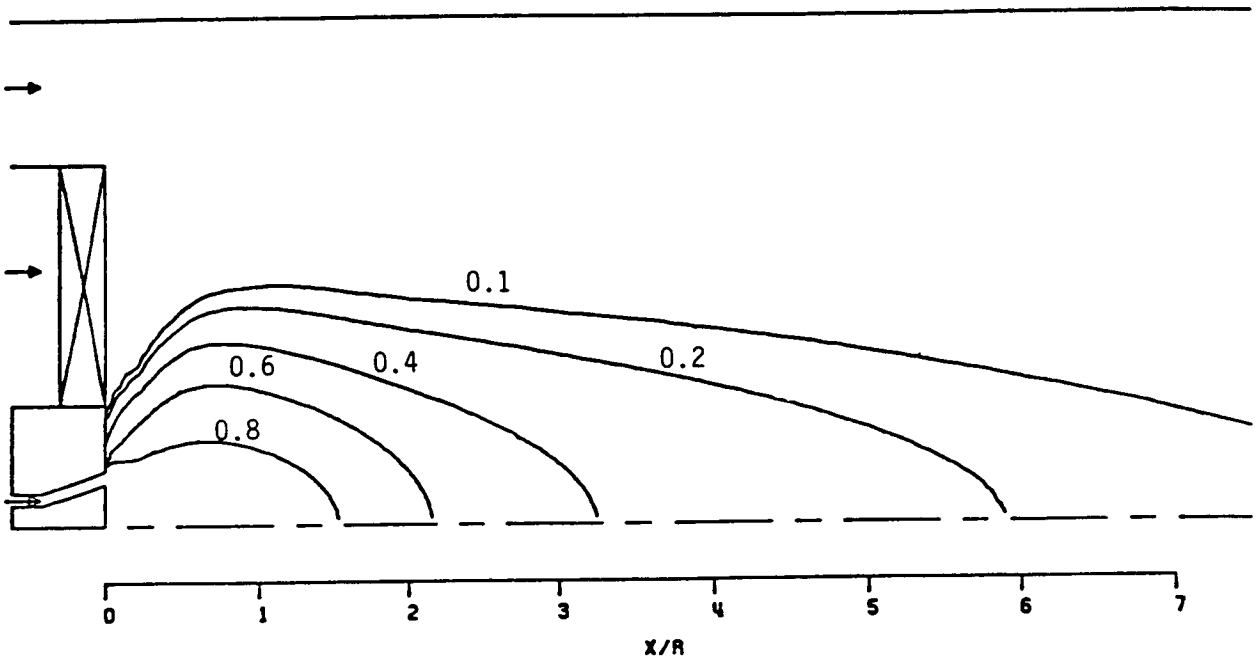

Figure 5.13 Contour plots of unburnt fuel (Brum & Samuelsen ,1982)

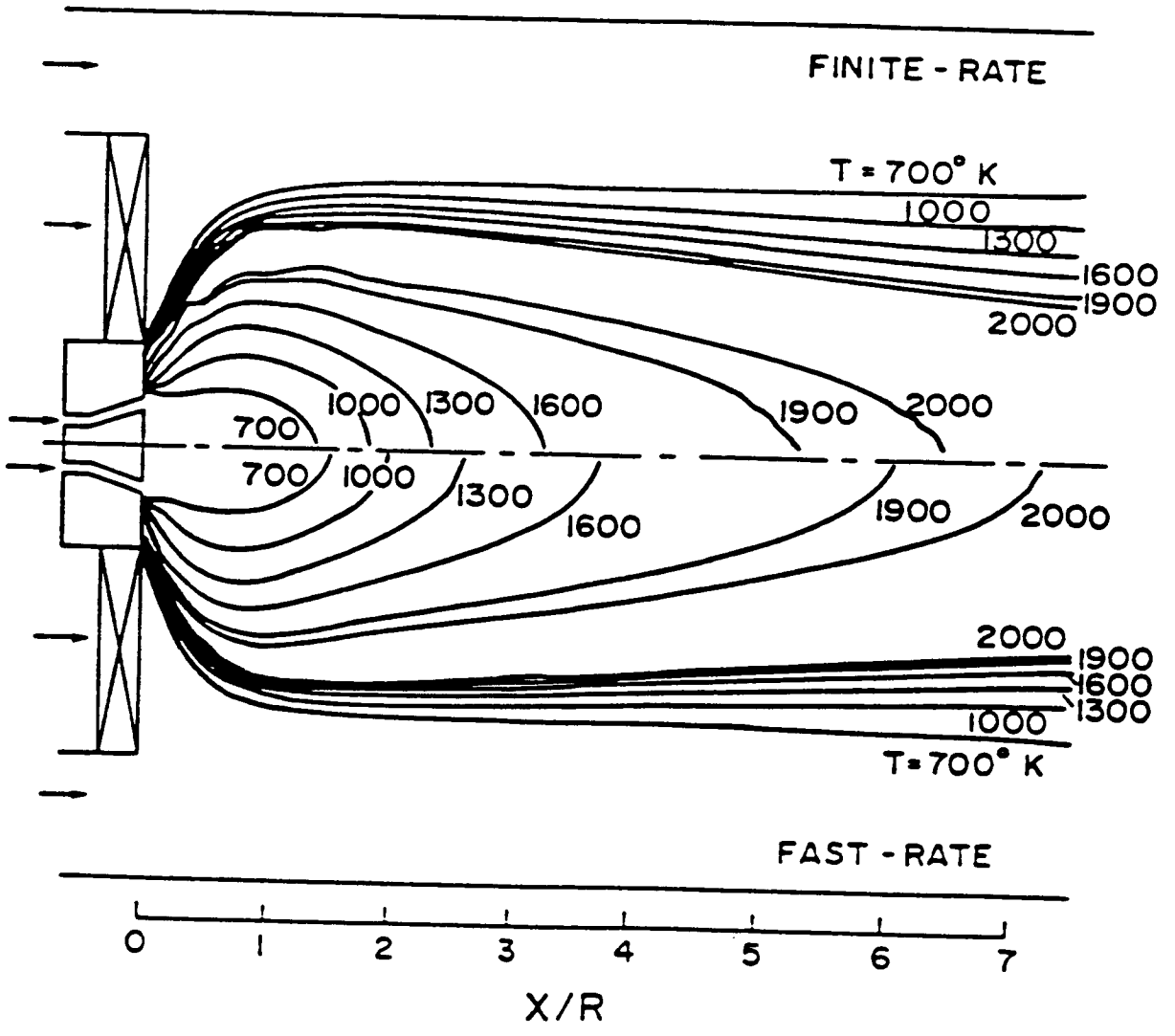

Figure 5.14 Contour plots of temperature distribution inside the combustor (Brum & Samuelsen ,1982)

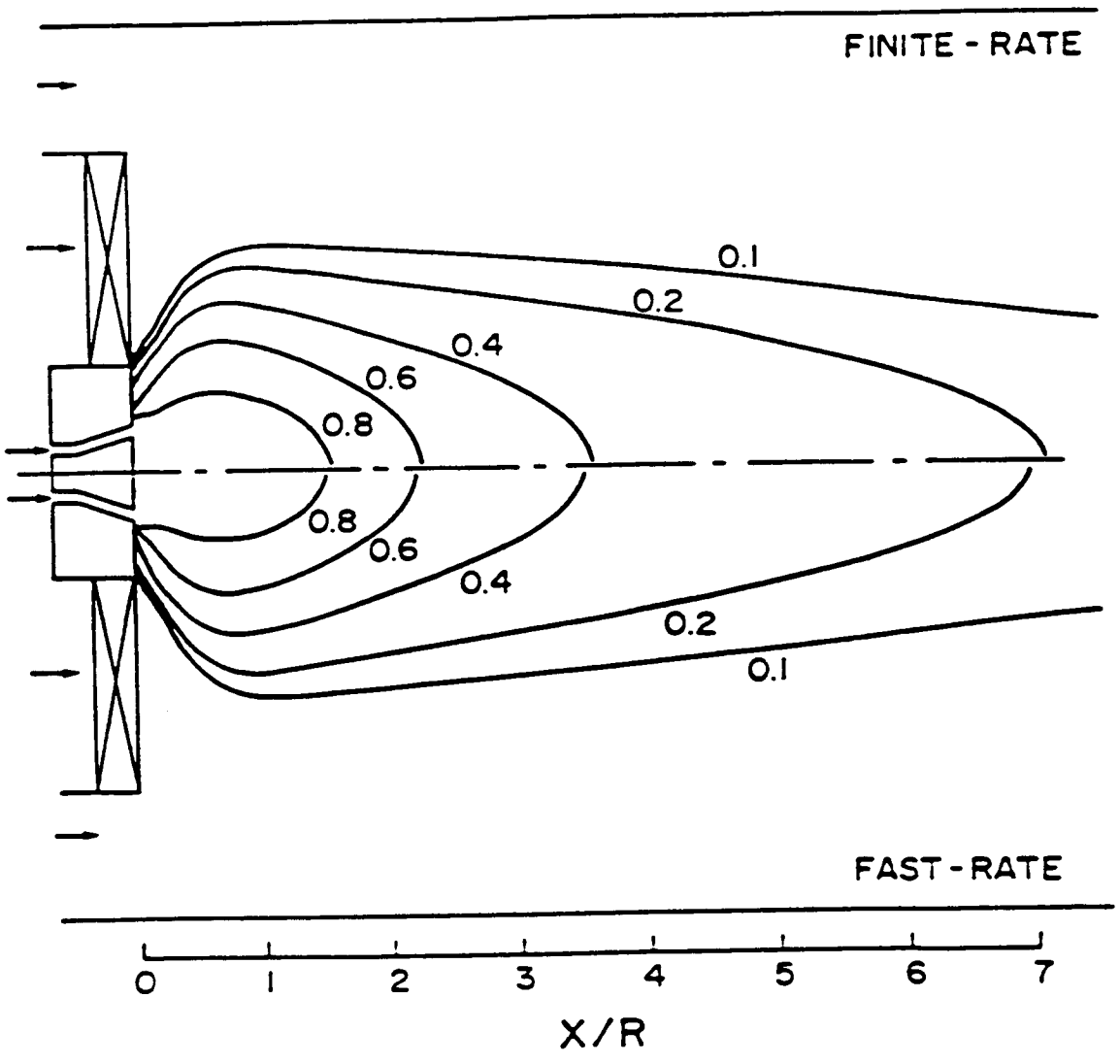

Figure 5.15 Contour plots of mixture fraction (Brum & Samuelsen ,1982)

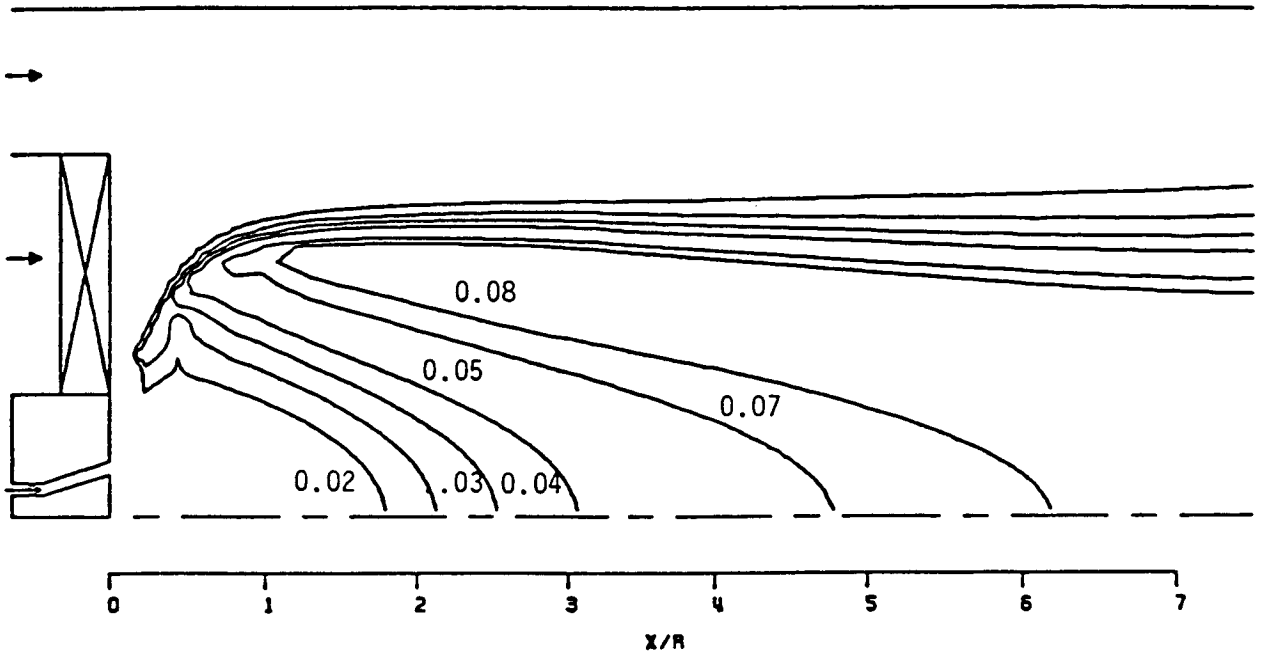

Figure 5.16 Contour plots of CO_2 (Brum & Samuelsen ,1982)

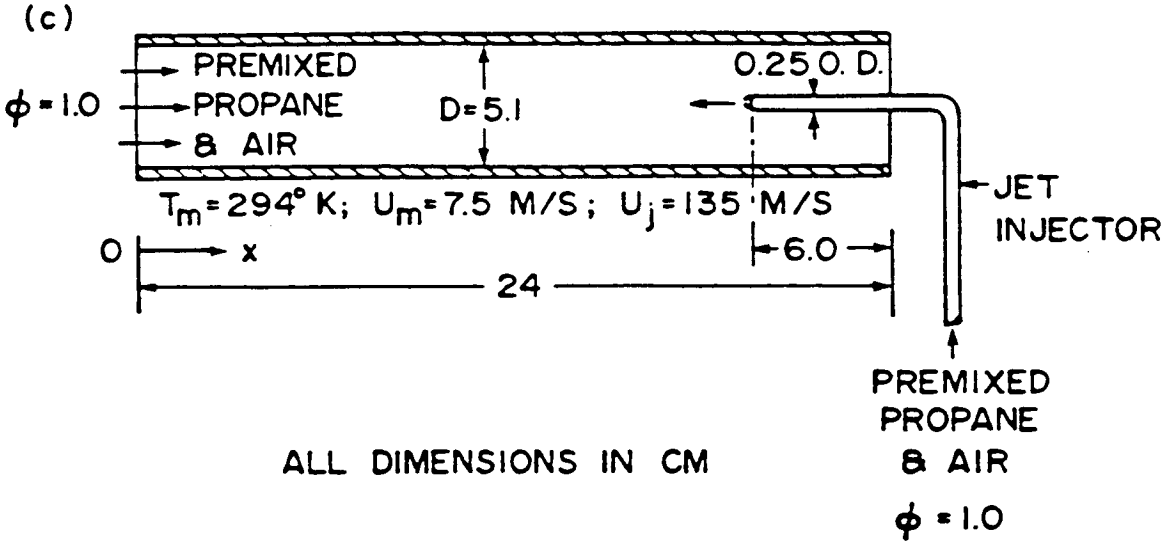

Figure 5.17 Sketch of the combustor (McDannel et al., 1982)

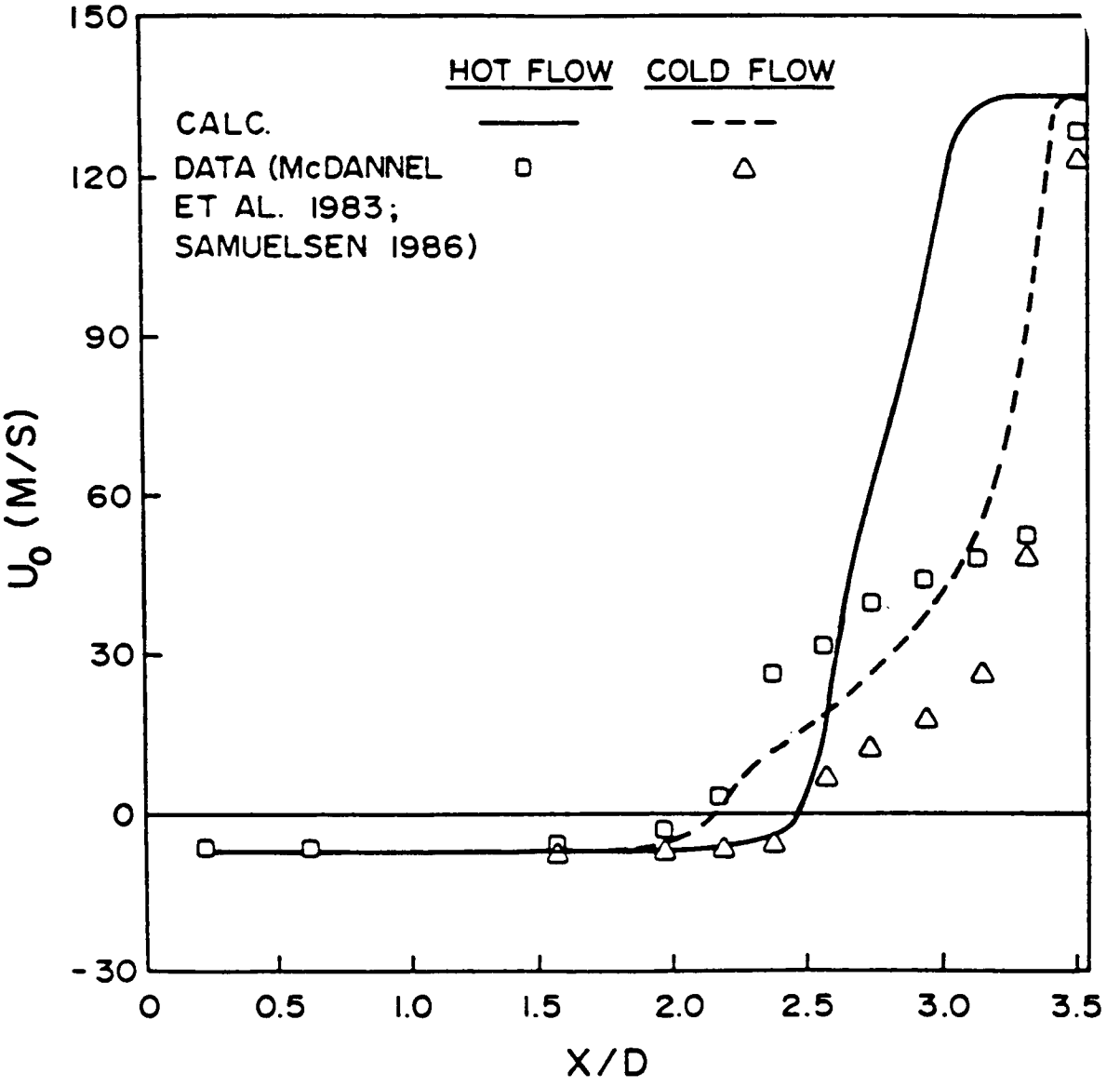

Figure 5.18 Opposed jet centerline velocity decay for hot and cold flow and their comparison with calculations (McDannel et al. ,1982)

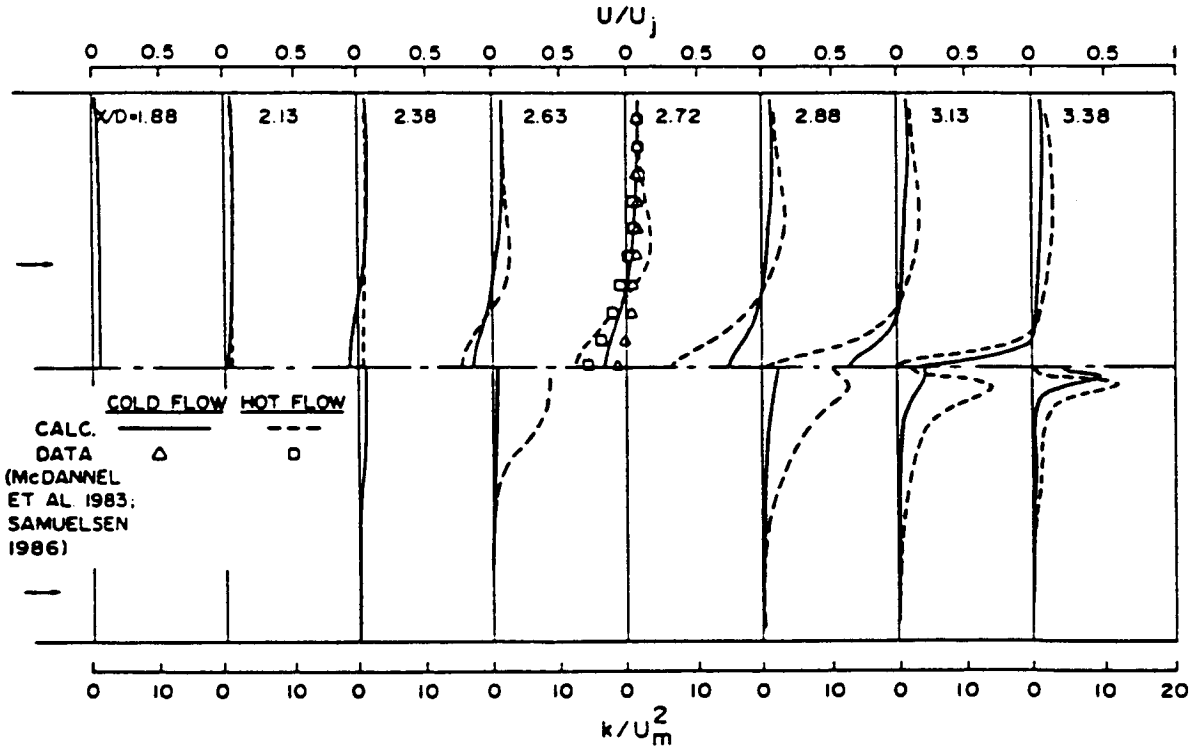

Figure 5.19 A comparison of the axial velocity profiles at different axial locations (McDannel et al. , 1982)

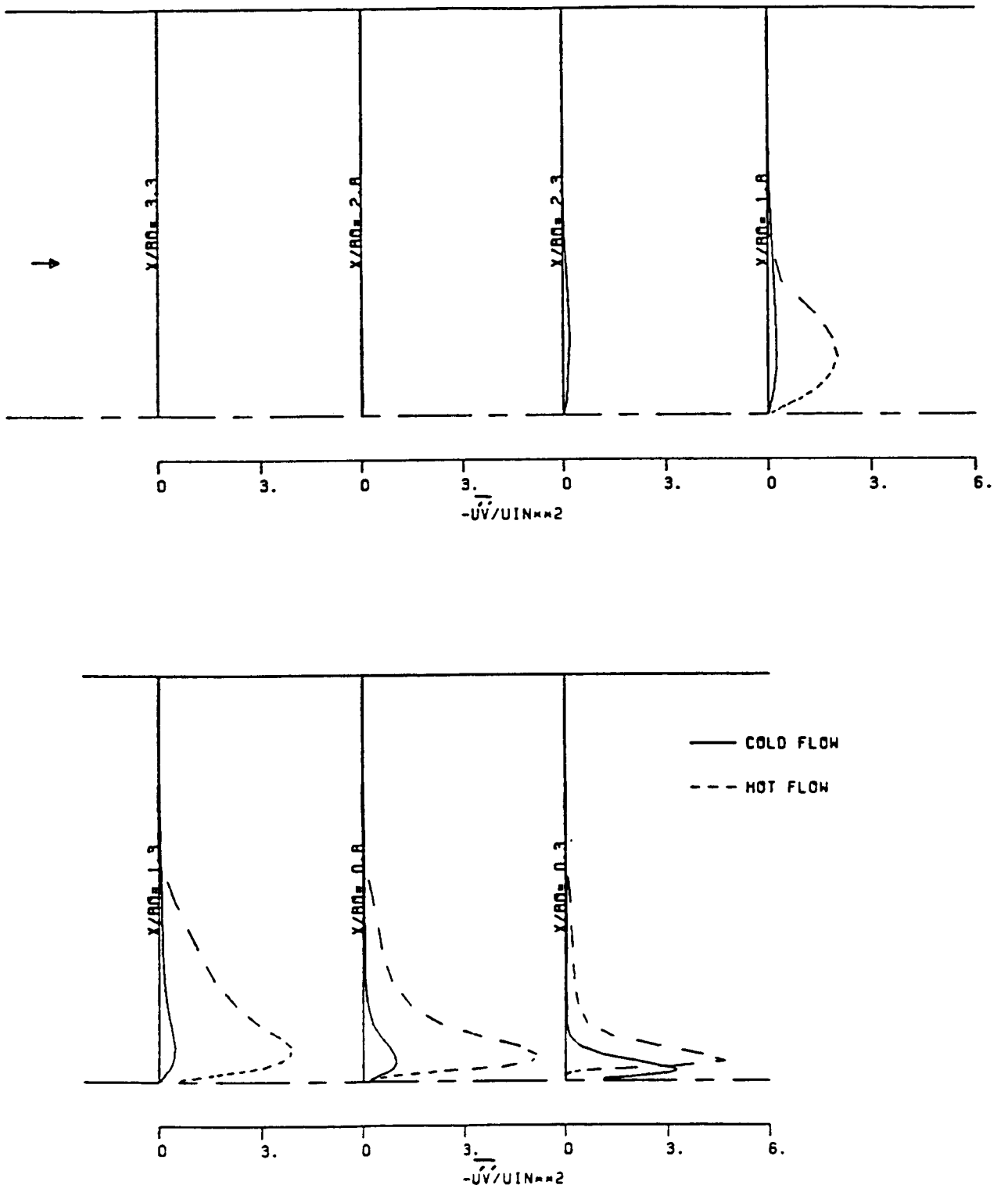

Figure 5.20 A comparison of the turbulent shear stress profiles at different axial locations. (McDannel et al. , 1982)

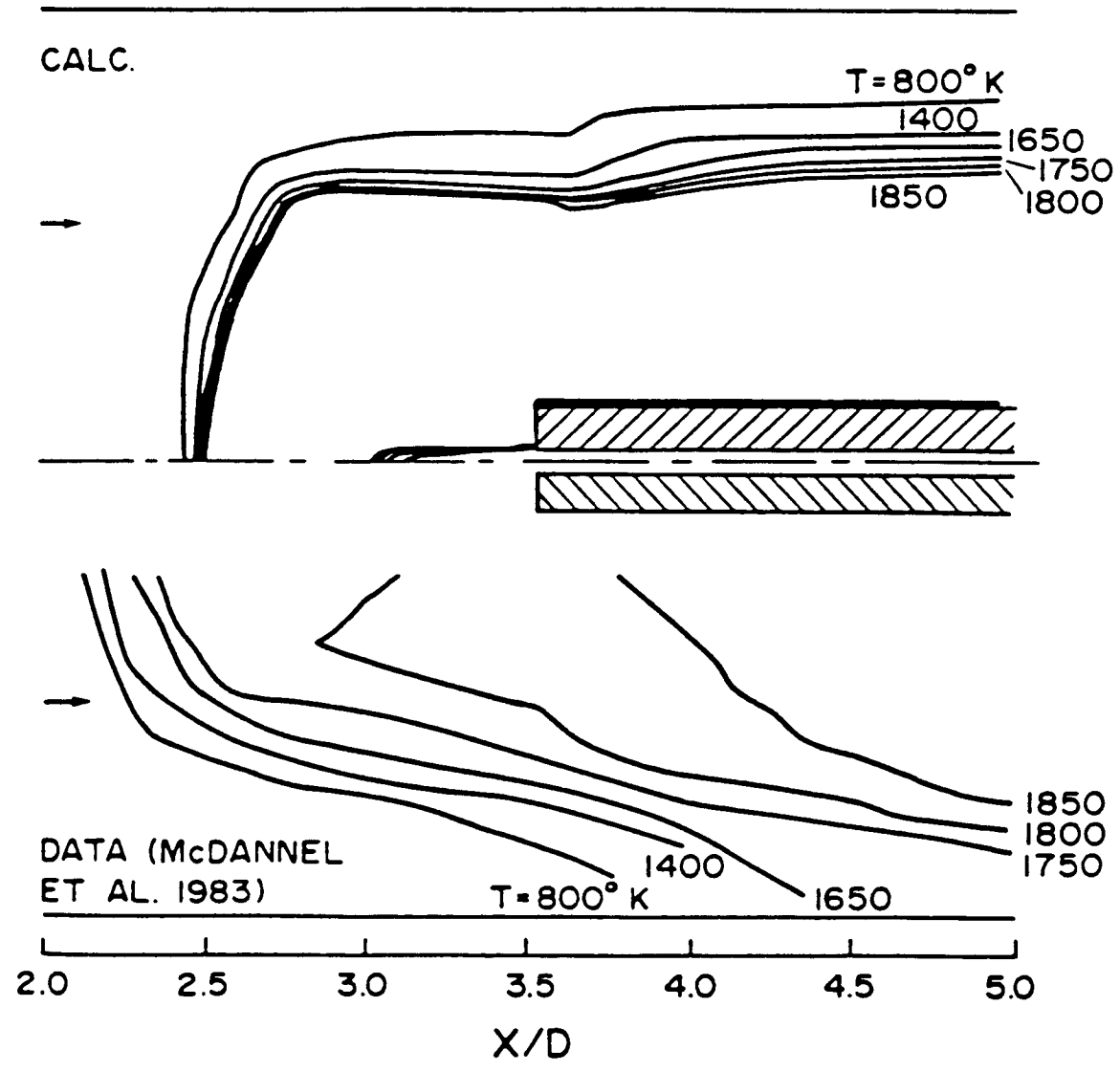

Figure 5.21 Comparison of the calculated and measured temperature contours inside combustor. (McDannel et al. , 1982)

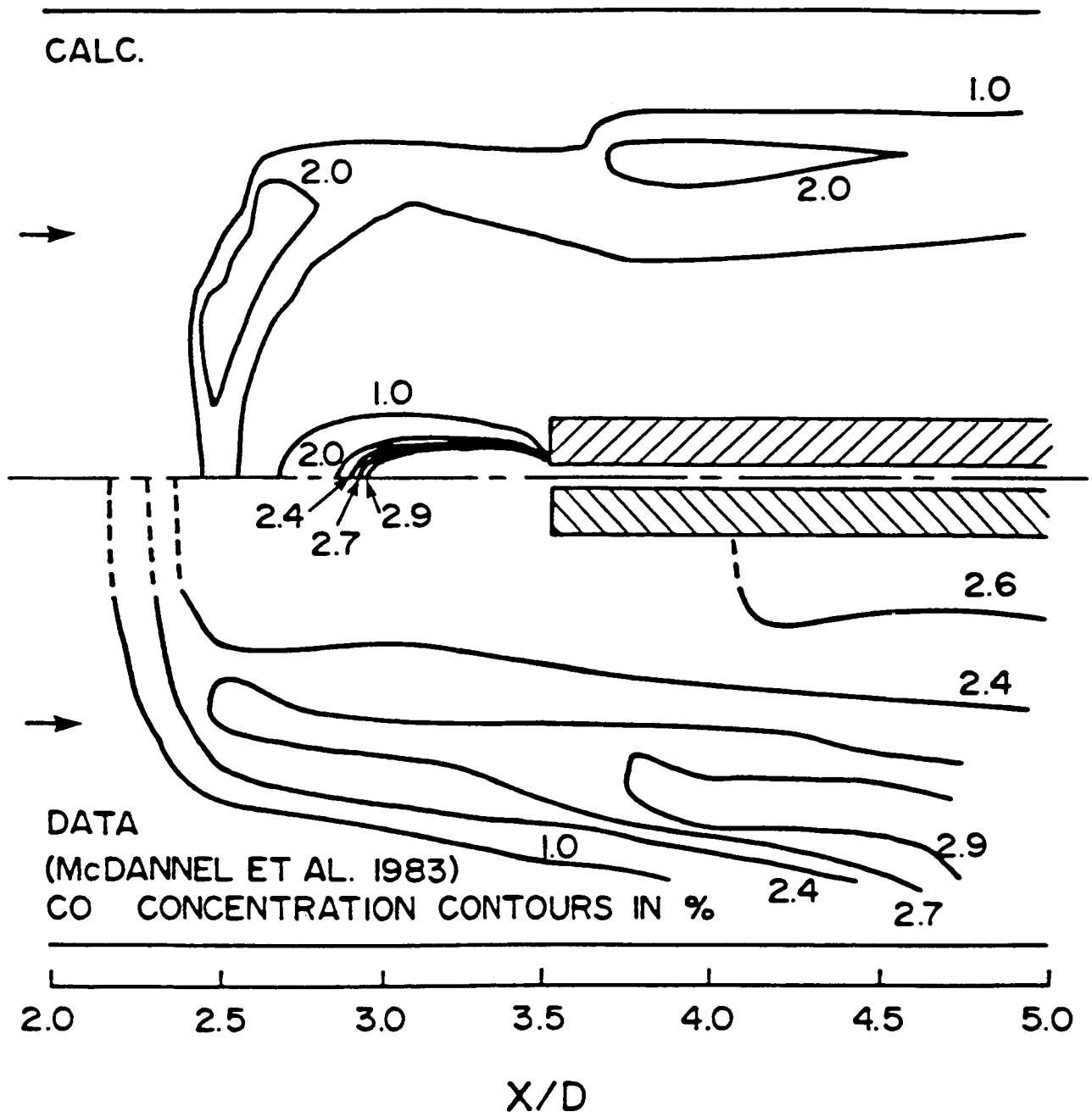

Figure 5.22 Comparison of the calculated and measured CO contours inside combustor.
(McDannel et al. , 1982)

CHAPTER 6

CONCLUDING REMARKS AND RECOMMENDATIONS

Important specific conclusions for each of the sections in chapters 4 and 5 are provided at the end of each section. This chapter, therefore, presents general conclusions of this study and makes recommendations for further work.

6.1 CONCLUSIONS

1. As far as the mean field prediction is concerned, k-ϵ closure performs just as well as any ASM or RSM in the calculation of non-swirling combustor flows.

2. The k-ϵ model gives good correlation for the developing region of complex swirling flows. However, for the far-field region the ASM provides a better prediction.

3. For swirling combustor flows, the ASM's and the full Reynolds stress models do a better job of predicting tangential velocities, while the k-ϵ model gives a good description of the centerline recirculation zone although the predictions are subject to uncertainties from the inlet boundary conditions.

4. Low-Reynolds-number model provides a better estimate of the mean and turbulence quantities in the near wall region. This model also predicts the corner recirculation zone which is observed experimentally and missed completely by all high-Reynolds-number models.

5. Models employing transport equations for the individual turbulent stress and fluxes components simulate the turbulent processes more realistically and are therefore potentially more general compared to the simpler models. However, they are not thoroughly tested and are computationally more expensive. Hence, at the present state of development, they are not very suitable for practical applications. They are important, however, as a starting point for deriving algebraic expressions for the turbulent stresses and fluxes. It seems that such expressions used in conjunction with the k and ϵ equations are sufficient for most engineering problems.

6. It should be noted that the effectiveness of turbulence model predictions could be obscured to some extent by competing factors --- boundary conditions, oscillatory phenomena and numerical diffusion. A significant contribution from any of the aforementioned factors tends to invalidate conclusions regarding the superiority or

inferiority of a given turbulence model. Numerical diffusion is a complex function of mesh size and cell aspect ratio. Inlet and boundary conditions are also of importance in strongly swirling flows. The turbulence model cannot compensate for inadequacy in this area. It is apparent that turbulence model validation must be preceeded by (1) appropriately configured and detailed experimental case studies, and (2) elimination of false diffusion considerations.

7. Favre-averaging technique is a reasonable approach for isothermal, variable density flows. However, for reacting flows, the turbulence model should also include the effects of chemical heat release on the Reynolds stress/flux components.

8. Two-step reaction scheme shows promise for application in gas turbine combustors and is preferred over fast-chemistry model for determining the combustion effects in combustors. However, they have to be further validated with simple flames to establish model constants and rate constants, so that the major species can be accurately predicted.

6.2 RECOMMENDATIONS

1. The low-Reynolds-number closure is found to provide a better estimate of the mean and the Reynolds stresses near the wall region. It is appropriate to apply a similar approach to develop a low-Reynolds-number model for the scalar transport equations too.

2. Although some of the models described in this review and in particular the k-ϵ model, have shown to work well in many situations, there is much room for further developments. The ϵ-equation in its present form appears not to be sufficiently universal and should be improved. As observed by many, this equation is the Achilles heel for most models. Ideas to use several length-scale equations for different directions or different processes are promising (Hanjalic et al. 1979) and should be developed further.

3. The model assumptions for the pressure-strain and pressure-scalr gradient correlations are also not very satisfactory and need improvement. Proposals for the behavior of $\Pi_{ij,1}$ in inhomogeneous flows have only gone further than that of Rotta (1951) by including further terms in a series expansion about the isotropic homogeneous state (Lumely and Khaheh-Nouri, 1974). However, optimization of the coefficients of the terms in the expansion on the basis

of available experimental data is a very difficult task indeed. It seems unlikely that any serious proposal for $\Pi_{ij,1}$ will be made in the near future and that emphasis should be placed on developing a better approximation for $\Pi_{ij,2}$.

4. The derivation and validation of higher-order closure schemes holds the greatest potential for turbulence model improvement for strongly swirling flows.

5. The difficulty in clearly demonstrating calculations free of numerical errors has restricted the testing of higher-order closures in recirculating flows. Efforts to find a stable and higher order (order of terms retained in an equivalent Taylor series expansion) differencing scheme that can eleminate numerical diffusion should continue. This is especilly important in the case of reacting flows because of the coupled non-linearities which exist between the chemical and fluid mechanical processes.

6. The correct solution of the potential core region is very important in analyzing the chemical heat release effects at the early stages of the reaction and obtaining the correct behavior of axial variations of turbulent velocity/scalar fluctuations in the diffusion flames.

7. An intensive submodel validation and development efforts, especially for the algebraic stress/flux model, two-step and four-step kinetic schemes, and two-step kinetic scheme in conjunction with PDF approach should be continued.

8. Unfortunately, in many instances there is a lack of quality data relevant to gas turbine combustion. Many modelling assumptions are similar to the constant-density, Reynods-stress closure. Therefore, further experiments with more emphasis on turbulent scalar fluxes and density correlations are needed to support or to improve these assumptions. In addition, more experiments with different fuels are required to assess the idealized density-mixture fraction relation and its application to turbulence modelling of diffusion flames.

REFERENCES

Bilger, R. W. (1975) A note on Favre averaging in variable density flows. Combustion Sci. and Technol. 11,215-217.

Bilger, R. W. (1976) Turbulent jet diffusion flames. Progr. Energy Combust. Sci 1,87-109.

Bilger, R. W. (1977) Comment on structure of turbulent shear flows. AIAA J. 15 , 1056.

Bilger, R. W. (1978) Reaction rates in diffusion flames. Combust. Flame 30, 277.

Bilger, R. W. (1979) discussion contribution. Acta Astronautica 6 , 987-989.

Bilger, R. W. (1980) Turbulent flows with nonpremixed reactants. in Topics in Applied Physics: Turbulent Reacting Flows (Edited bt Libby, P.A. and Williams,F.A.), pp. 65-113. Springer - Vergal, New York.

Borghi, R. (1974) Chemical reactions calculations on turbulent flows: Application to co-containing turbojet plume. Adv. Geophsics 18B , 349-365.

Bradshaw, P. , Ferriss, D.H. and Atwell, N.P. (1967) Calculation of boundary layer development using the turbulent energy equation. J. Fluid Mech. 28, p.593.

Bradshaw, P. , Dean, R.C. and McEligot, D.M. (1974) Calculations of interacting turbulent shear layer-duct flow. ASME J. Fluids Eng. 95, p. 214.

Bray, K. N. C. (1980) Turbulent flows with premixed reactants. in Topyics in Applied Physics: Turbulent Reacting Flows (Edited bt Libby, P.A. and Williams,F.A.), pp. 65-113. Springer - Vergal, New York.

Bray, K. N. C. and Moss, J. B. (1977) A unified statistical model of the premixed turbulent flame. Acta Astronaut 4,p. 291.

Brum, R.D. and Samuelsen, G.S. (1982) Assessment of a dilute swirl combustor as a bench scale, complex flow test bed for modeling, diagnostics, and fuels effects studies. AIAA-82-1263.

Butler, T.D. and O'Rourke, P.J. (1977) A numerical method for two-dimensional unsteady reacting flows. Sixteen (International) Symposium On Combustion, pp. 1503-1514.

Chien, K. Y. (1980) Predictions of channel and boundary layer flows with a low-Reynolds-number two-equation model of turbulence. AIAA-80-0134.

Chou, P. Y. (1945) On velocity correlations and the solution of the equations of turbulent fluctuations. Quart. J. Appl. Mth. 3, 38-54.

Daly, B. J. and Harlow, F. H. (1970) Transport equations of turbulence. Phys. Fluids 13 , 2634-2649.

de Vahl Davis, G. and Mallinson, G. D. (1972) False Diffusion in Numerical Fluid Mechanics. Univ. of New South Wales, School of Mech. and Ind. Eng. Rept. 1972/FMT/1.

Deardorf, J. W. (1973) The use of subgrid transport equations in a three-dimensional model of atmospheric turbulence. Trans. ASME, J. Fluid Eng. , 429-438.

Deardorf, J. W. (1974) Three-dimensional numerical study of turbulence in an entraining mixed layer. Boundary Layer Meteorology 7, 199.

Deardorf, J. W. (1975) Three-dimensional numerical study of the height and mean structur of a heated planetary boundary layer.Boundary Layer Meteorology .

Dekeyser, I. and Launder, B. E. (1983) A comparison of triple-moment temperature-velocity correlations in the axisymmetric heated jet with alternative closure models. Proceeding of fourth Turbulent Shear Flows Symposium, Karlsruhe, Germany.

Dibble, R.W. , Schefer, R.W. , Farshchi, M. and Kollman (1985) Second-order closure for turbulent nonpremixed flames. Western States Section of Combustion Institute WSS/CI - 85- 24.

Donaldson, C. du P. (1969) A computer study of boundary layer transition. AIAA J. 7 , 271.

Dwyer, H. A. and Sanders, B. R. (1977) Modeling of unsteady combustion phenomena. AIAA - 77-136.

Eaton, J. K. and Johnston, J. P. (1980) An Evaluation of Data for the Backward-Facing Step Flows. Report for the 1980/1981 conferences on complex turbulent flows, Dept. of Mechanical Engineering, Stanford University.

Favre, A. (1969) Statistical equations of turbulent gases. Problems of Hydrodynamics and Continuum Mechanics, SIAM, 231-266.

Gibson, M. M. and Launder, B. E. (1976) On the calculation of horizantal, turbulent free shear flow under gravitational influence. J. Heat Transfer, Trans. ASME 93C , 81-87.

Griffin, M.D. , Diwaker, R. , Anderson, J.D. Jr. , and Jones, E. (1978) Computational fluid dynamics applied to flows in an internal combustion engine. AIAA - 78 - 57.

Habib, M. A. and Whitelaw, J. H. (1979) Velocity characteristics of a confined coaxial jets. J. of Fluid Engineering 101 , 521-529.

Hackman, L. P. , Raithby, G. D. ,and Strong, A. B. (1984) Numerical predictions of flows over backward facing steps. Int. J. for Num. meth. in Fluids 4 , 711-724.

Han, T. Y. , Humphrey, J. A. C. ,and Launder, B. E. (1981) A comparison of hybrid and quadratic-upstream differencing in high Reynolds number elliptic flows. Computer Methods in Applied Mechanics and Engineering 29 ,81-95.

Hanjalic, K. and Launder, B. E. (1972) Asymmetric flow in a plane channel. J. Fluid Mechanics 51 ,301.

Hanjalic, K. , Launder, B. E. and Schiestel, R. (1979) Turbulence transport modelling of separating and reattaching shear flows. 2nd Symposium on Turbulent Shear Flows, London.

Hassid, S. and Poreh, M. (1978) A turbulent energy dissipation model for flows with drag reduction. J. Fluid Engng. 100 , 107-112.

Herring, J. R. (1979) Subgrid scale modeling-An introduction and overview. Turbulent Shear Flows I (Edited by Dorst, F. , Launder, B.E. , Schmidt, F.W. , Whitelaw, J.H.). Springer-Verlag, Berlin.

Hoffmann, G. H. (1975) Improved form of the low-Reynolds-number k-ϵ turbulence model. Physics of Fluids 18, 309-312.

Irwin, H. P. A. H. (1973) Measurements of a self-preserving plane wall jet in a positive pressure gradient. J. Fluid Mechanics 61 33.

Jones, W. P. (1977) Workshop on pdf methods for turbulent flows. Technische Hochschule, Aachen.

Jones, W. P. (1980) Models for turbulent flows with variable density and combustion. in Prediction Method for Turbulent Flows (Edited by Kollmann, W.), pp. 379-422. Hemisphere Publishing Corp., London.

Jones, W. P. and Launder, B. E. (1972) The prediction of laminarization with a two-equation model of turbulence. INT. J. Heat Mass Transfer 15 ,301-314.

Jones, W. P. and Whitelaw, J. H. (1982) Calculation methods for reacting turbulent flows: A Review. Combustion and Flame 48, 1-26.

Johnson, B.V. and Bennett (1981) Mass and Momentum Turbulent Transport Experiments with Confined Coaxial Jets. NASA Contractor Report NASA CR-165574.

Kim, J. (1985) Investigation of turbulence structure with a passive scalar. APS. 38th Annual Metting of The Division of Fluid Dynamics in Tucson, AZ.; Nov. 24-27

Kolmogorov, A. N. (1941) The local structure of turbulence in incompressible viscous fluid for very large Reynolds numbers. C.R. Aka. Nank. SSSR 30 , 301-305.

Kwak D. , Reynolds, W.C. and Ferzinger, J.H. (1975) Three-Dimensiona Time-Dependent Calculation of Turbulent Flow. Stanford University, Dept. Mech. Eng. Rept. TF-5.

Lam, C.K.G. and Bremhorst, K.A. (1981) Modified form of the k-ϵ model for predicting wall turbulence. J. Fluids Engng. 103, 456-460.

Launder, B. E. (1973) Turbulent Models and their Experimental Verification: 11 Scalar Property Transport by Turbulence. Imperial college, Mech Eng Dept. Rep. HTS/73/26.

Launder, B. E. (1975) On the effect of gravitational field on the turbulent transport of heat and momentum. J. Fluid Mech. 67 , 569-581.

Launder, B. E. (1976) Heat and mass transport. in Topics in Applied Physics: Turbulence (Edited by Bradshaw, P.) PP. 231-287. Springer-Verlag, New York.

Launder, B. E. (1979) Stress transport closures-into the third generation. Turbulent Shear Flows I (Edited by Dorst, F., Launder, B.E. , Schmidt, F.W. , Whitlaw, J. H.). Springer-Verlag, Berlin.

Launder, B.E. , Morse, A.P. , Rodi, W. and Spalding, D.B. (1973) The prediction of free-shear flows - a comparison of the performance of six turbulence models, Proc. NASA Langley Free Turbulent Shear Flows Conf. 1, NASA SP 320.

Launder, B. E. and Sharma, B. I. (1974) Application of the energy dissipation model of turbulence to the calculation of flow near a spinning disc. Letters in Heat and Mass transfer 1, 131-138.

Launder, B. E. , Reece, G. J. ,and Rodi, W. (1975) Progress in the development of a Reynolds-stress turbulence closure. J. Fluid Mech. 68 , 537-577.

Lavoie, G.A. , Heywood, J.B. ,and Keck, J.C. (1970) Experimental and theoritical study of nitric oxide formation in internal combustion engines. Combustion Sci. and Technol. 1, 313-326.

Leonard, B. P. (1979) A Stable and accurate convection modeling procedure based on quadratic upstream interpolation. Computer Methods in Applied Mechanics and Engineering 19 ,59-98.

Leschziner, M.A. (1980) Practical evaluation of three finite-difference schemes for the computation of unsteady-state recirculating flows. Comput. Meths. Appl. Mech. Eng. 23 , 293-312.

Lewis, M.H. and Smoot, L.D. (1981) Turbulent gaseous combustion part I: local species concentration measurements. Combustion and Flame 42, 183-196.

Libby, P. A. and Bray, K. N. C. (1980a) Counter gradient diffusion in premixed turbulent flames. AIAA - 80 -0013.

Libby, P. A. and Bray, K. N. C. (1980b) Implications of the laminar flamelet model in premixed turbulent combustion. Combustion and Flame 39, p.33.

Libby, P. A. and Williams, F. A. (1980) Turbulent Reacting Flows. Springer-Verlag, New York.

Lockwood, F. C. and Naguib, A. S. (1975) The prediction of the fluctuations in the properties of free, round-jet, turbulent, diffusion flames. Combust. and Flame 24, 109-124.

Love, M. D. and Leslie, D. C. (1979) Studies of subgrid modeling with classical closures and Burger's equation. Turbulent Shear Flows I (Edited by Dorst, F. , Launder, B.E. , Schmidt, F. W. , and Whitlaw, J. H.). Springer-Verlag, New York.

Lumley, J.L. (1970) Stochastic Tools In Turbulence. Academic Press.

Lumley, J.L. (1975a) Prediction Methods for Turbulent Flows. Lecture Series No. 26, Von Karman Inst., Belgium.

Lumley, J. L. (1975b) Pressure-strain correlations. Physics Fluids 18 , 750.

Lumley, J. L. and Khajeh-Nouri (1974) Computational modelling of turbulent transport. Advances in Geophysics 18A, 169.

Lumley, J. L. (1978) Computational modelling of turbulent flows. in Advances in Applied Mechanics 18, Acad. Press Inc.

Mansour, N. N. , Kim, J. ,and Moin, p. (1983) Computation of turbulent flows over a backward facing step. Proceeding of 4th Turbulent Shear Flows Symposium, Karlsruhe, Germany.

McDannel, M.D. , Peterson, P.R. , and Samuelsen, G.S. (1982) Species concentration and temperature measurements in a lean , premixed flow stabilized by a reverse jet. Combustion Science and Technology 28 ,211-224.

McGuirk, J.J., Taylor, A.M.K.P., and Whitelaw, J.H. (1985) The assessment of numerical diffusion in upwind difference calculations of turbulent recirculating flows. Turbulent Shear Flows III (Edited by Dorst, F. , Launder, B.E. , Schmidt, F. W. , and Whitlaw, J. H.). Springer-Verlag, New York.

Mellor, G. L. and Herring, H. J. (1973) A survey of th e mean turbulent field closure models. AIAA J. 11 , 590-599.

Mellor, G. L. and Yamada, T. (1974) A hierarchy of turbulence closure models for planetary boundary layers. J. Atmos. Sci 31 1971-1806.

Mellor, G. L. and Yamada, T. (1982) Development of a turbulence closure model for geophysical problems. Reviews of Geophysics and Space Physics 20, 851-875.

Meroney, R.N. (1976) An algebraic stress model for stratified turbulent shear flows. Computer and Fluids 4, 93-107.

Monin, A. S. (1965) On the symmetry properties of turbulence in the surface layer of air. Izvestiya Atmos. Oceanic Phys. 1 ,45-54.

Naot, D. , Shavit, A. ,and Wolfstein, M. (1973) Two-point correlation model and the redistribution of the Reynolds stresses. Phys. Fluids 16 , 738-743.

Nee, V.W. and Kovasznay, L.S.G. (1969) Calculation of the incompressible turbulent layer by a simple theory. Phys. Fluids 12, p.473.

Nikjooy, M. , So, R.M.C. and Hwang, B.C. (1985) A comparison of three algebraic stress closures for combustor flow calculations. ASME - 85-WA/FE - 3.

Otey, G. R. (1978) Numerical Methods for Solving Reaction-Diffusion Problems. Ph.D. thesis, Univerisity of California, Davis.

Patankar, S.V. (1980) Numerical Heat Transfer and Fluid Flow. McGraw Hill.

Patankar, S. V. and Spalding, D. B. (1972) A calculation procedure for heat, mass and momentum transfer in three-dimensional parabolic flows. Int. J. Heat Mass Transfer 15 ,1787-1806.

Patel, V.C. , Rodi, W. and Scheuerer (1985) Turbulence models for near-wall and low Reynolds number flows: A Review. AIAA J. 23, 1308-1319.

Pope, S. B. (1976) The probability approach to the modelling of turbulent reacting flows. Combustion and Flame 27,p. 299.

Pope, S. B. (1977) The Implications of the probability equations for turbulent combusting flows. Combustion and Flame 29,p. 235.

Pope, S. B. (1981) A Monte Carlo method for the pdf equations of turbulent reactive flow. Combustion Science and Technology 25, p.159.

Prandtl, L. (1925) Bericht uber untersuchungen zur ausgebildeten turbulenz. ZAMM 5, p.136.

Prandtl, L. (1945) Uber ein neues formelsystem fur die ausgebildete turbulenz. Nachrichten von der Akad der Wissenschaft in Gottingen.

Pratt, D. T. (1976) Calculation of Chemically Reacting Flows With Complex Chemistry. in Studies in Convection (Edited by Launder B. E.), 2 Pergamon Press, Oxford.

Pratt, D. T. (1979) Gas-phase chemical kinetics. Pulverized Coal Combustion and Gasification (Edited by Smoot, L. D. and Pratt, D. T.), Plenum, New York.

Reynolds W. C. (1976) Computation of turbulent flows. Annual Review Fluid Mech. 8 , 183-207.

Rhode, R.P. (1975) in Turbulent Mixing in Nonreactive and Reactive Flows (Edited by Murthy, S.N.B.). Plenum, New York.

Ribeiro, M. M. (1976) The Turbulent Structure of Free Jet Flows with and without swirl. University of London.

Roback, R. and Johnson, B.V. (1983) Mass and Momentum Turbulent Transport Experiments with Confined Swirling Coaxial Jets. NASA Contractor Report 168252.

Rodi, W. (1976) A new algebraic relation for calculating the Reynolds stresses. ZAMM 56 ,219-221

Rotta, J. C. (1951) Statistische theorie nichthomogener turbulenz. Zeit. fur Physik 129 , 547-572; 131, 51-77.

Rotta, J. C. (1972) Turbulente Stromungen ,B.G. Teubner, Stuttgart.

Samuelsen, G. S. (1986) Private communication

Schumann, U. (1975) Subgrid scale model for finite difference simulations of turbulent flows in plane channels and annuli. J. Comp. Phys. 18, 376-404.

Sindir, M.M. (1983a) Effects of expansion ratio on the calculation of parallel-walled backward-facing step flows: Comparison of four models of turbulence. ASME - 83-FE-10.

Sindir, M.M. (1983b) Calculation of deflected-walled backward-facing steps flows: Effects of angle of deflection on the performance of four models of turbulence. ASME-FE-16.

Smith, P.J. and Smoot, L.D. (1981) Turbulent gaseous combustion part II: theory and evaluation for local properties. Combust. Flame 42, p. 277.

Smoot, L. D. and Hill, S. C. (1983) Critical requirements in combustion research. Progr. Energy Combust. Sci. 9 ,p. 77.

So, R. M. C. (1986) Inlet centerline turbulence effects on reattachment length in axisymmetric sudden-expansion flows. Exp. in Fluid 5.

So, R. M. C. and Hwang, B. C. (1986) On incompressible, turbulent, heated round jets in a co-flowing stream. Submitted for publication.

So, R. M. C. and Yoo, G. J. (1986) On The Modelling of Low-Reynolds-Number Turbulence.NASA CR-3994.

Spalding, D. B. (1971) Concentration fluctuations in a round turbulent free jet. Chem. Eng. Sci. 26 , 95-107.

Spalding, D. B. (1975) Turbulence modelling: solved and unsolved problems. Turbulent Mixing in Nonreactive and Reactive Flows (Edited by Murthy, S. N. B.). Plenum, New York.

Spalding, D. B. (1977) The eddy break up model applied to confined turbulent steady flames. AIAA - 77 - 98.

Stevenson, W.H. , Thompson, H.D. , Gould, R.D. (1983) Laser Velocimeter Measurements and Analysis in Turbulent Flows with Combustion. AFWAL-TR-82-2076

Sturgess, G.L. , Syed, S.A. and McManus, K.R. (1983) Importance of inlet boundary conditions for numerical simulation of combustor flows. AIAA - 83 - 1263.

Taylor, A.M.K.P. and Whitelaw, J.H. (1984) Velocity characteristics in the turbulent wakes of confined axisymmetric bluff bodies. J. Fluid Mech. 139 , 391-416.

Tennekes, H. and Lumley, J. L. (1972) A First Course in Turbulence. MIT press.

Westbrook, C. K. and Dryer, F. C. (1981) Simplified reaction mechanisms for the oxidation of hydrocarbon fuels in flames. Comb. Sci. Tech. 27 , p.31.

APPENDIX A

TURBULENT FLOW EQUATIONS FOR THE k-ε MODEL

The transport equations presented in the previous sections reduce in axisymmetric coordinates (x,r) to the following

CONTINUITY EQUATION :

$$\frac{\partial \bar{\rho}}{\partial t} + \frac{1}{r}\left[\frac{\partial}{\partial x}(r\bar{\rho}U) + \frac{\partial}{\partial r}(r\bar{\rho}V)\right] = 0 \qquad (A1)$$

X - MOMENTUM EQUATION :

$$\frac{\partial}{\partial t}(\bar{\rho}U) + \frac{1}{r}\left[\frac{\partial}{\partial x}(r\bar{\rho}UU) + \frac{\partial}{\partial r}(r\bar{\rho}VU)\right] = -\frac{\partial P}{\partial x} + \frac{1}{r}\left[\frac{\partial}{\partial x}(2r\mu_T \frac{\partial U}{\partial x}) + \frac{\partial}{\partial r}\left[r\mu_T(\frac{\partial U}{\partial r} + \frac{\partial V}{\partial x})\right]\right] - \frac{2}{3}\frac{\partial}{\partial x}(\bar{\rho}k) \qquad (A2)$$

Y - MOMENTUM :

$$\frac{\partial}{\partial t}(\bar{\rho}V) + \frac{1}{r}\left[\frac{\partial}{\partial x}(r\bar{\rho}UV) + \frac{\partial}{\partial r}(r\bar{\rho}VV)\right] = -\frac{\partial P}{\partial r} - 2\mu_T \frac{V}{r^2} + \bar{\rho}\frac{W^2}{r} + \frac{1}{r}\left[\frac{\partial}{\partial x}\left[r\mu_T(\frac{\partial V}{\partial x} + \frac{\partial U}{\partial r})\right] + \frac{\partial}{\partial r}(2r\mu_T \frac{\partial V}{\partial r})\right] - \frac{2}{3}\frac{\partial}{\partial r}(\bar{\rho}k) \qquad (A3)$$

θ - MOMENTUM :

$$\frac{\partial}{\partial t}(\bar{\rho}W) + \frac{1}{r}\left[\frac{\partial}{\partial x}(r\bar{\rho}UW) + \frac{\partial}{\partial r}(r\bar{\rho}VW)\right] = -\mu_T \frac{W}{r^2} - \bar{\rho}\frac{VW}{r} - \frac{W}{r}\frac{\partial}{\partial r}\mu_T \tag{A4}$$

k - TRANSPORT EQUATION :

$$\frac{\partial}{\partial t}(\bar{\rho}k) + \frac{1}{r}\left[\frac{\partial}{\partial x}(r\bar{\rho}Uk) + \frac{\partial}{\partial r}(r\bar{\rho}Vk)\right] = \bar{\rho}P_k - \bar{\rho}\varepsilon + \tag{A5}$$

$$\frac{1}{r}\left[\frac{\partial}{\partial x}\left[r\left(\frac{\mu_t}{\sigma_k} + \mu\right)\frac{\partial k}{\partial x}\right] + \frac{\partial}{\partial r}\left[r\left(\frac{\mu_t}{\sigma_k} + \mu\right)\frac{\partial k}{\partial r}\right]\right]$$

ε - TRANSPORT EQUATION :

$$\frac{\partial}{\partial t}(\bar{\rho}\varepsilon) + \frac{1}{r}\left[\frac{\partial}{\partial x}(r\bar{\rho}U\varepsilon) + \frac{\partial}{\partial r}(r\bar{\rho}V\varepsilon)\right] = \bar{\rho}C_{\varepsilon 1}\frac{\varepsilon}{k}P_k - C_{\varepsilon 2}\rho\frac{\varepsilon^2}{k} + \tag{A6}$$

$$\frac{1}{r}\left[\frac{\partial}{\partial x}\left[r\left(\frac{\mu_t}{\sigma_\varepsilon} + \mu\right)\frac{\partial \varepsilon}{\partial x}\right] + \frac{\partial}{\partial r}\left[r\left(\frac{\mu_t}{\sigma_\varepsilon} + \mu\right)\frac{\partial \varepsilon}{\partial r}\right]\right]$$

TURBULENCE MODEL :

$$\mu_t = C_\mu \bar{\rho}\frac{k^2}{\varepsilon} \tag{A7}$$

$$\sigma_k = \frac{3}{2}C_\mu/C_s \tag{A8}$$

$$\sigma_\varepsilon = \frac{\kappa^2}{(C_{\varepsilon 2} - C_{\varepsilon 1})\sqrt{C_\mu}} \tag{A9}$$

where

$$\mu_T = \mu_t + \mu$$

$$P_k = \frac{\mu_t}{\rho}\left[2\left[\left(\frac{\partial U}{\partial x}\right)^2 + \left(\frac{\partial V}{\partial r}\right)^2 + \left(\frac{V}{r}\right)^2\right] + \left(\frac{\partial U}{\partial r} + \frac{\partial V}{\partial x}\right)^2 + \left(\frac{\partial W}{\partial x}\right)^2 + \left[r\frac{\partial}{\partial r}\left(\frac{W}{r}\right)\right]^2\right]$$

APPENDIX B

TURBULENT FLOW EQUATIONS FOR THE ASM MODEL

The governing equations under the gradient diffusion assumption in the cylindrical coordinate system are reduced to the following

CONTINUITY EQUATION :

$$\frac{\partial \bar{\rho}}{\partial t} + \frac{1}{r}\left[\frac{\partial}{\partial x}(r\bar{\rho}U) + \frac{\partial}{\partial r}(r\bar{\rho}V)\right] = 0 \qquad (B1)$$

X-MOMENTUM EQUATION :

$$\frac{\partial}{\partial t}(\bar{\rho}U) + \frac{1}{r}\left[\frac{\partial}{\partial x}(r\bar{\rho}UU) + \frac{\partial}{\partial r}(r\bar{\rho}UV)\right] - \frac{1}{r}\left[\frac{\partial}{\partial x}(r\mu_{1e}\frac{\partial U}{\partial x}) + \frac{\partial}{\partial r}(r\mu_{4e}\frac{\partial U}{\partial r})\right] =$$

$$-\frac{\partial P}{\partial x} + S^u \qquad (B2)$$

where

$$S^u = \frac{1}{r}\left[\frac{\partial}{\partial x}(r\mu_{1e}\frac{\partial U}{\partial x}) + \frac{\partial}{\partial r}(r\mu_{4e}\frac{\partial V}{\partial x})\right] - \frac{\partial}{\partial x}(\frac{2}{3}\bar{\rho}k) - \frac{\partial}{\partial x}(\frac{2}{3}\mu_{11}\frac{\partial U_m}{\partial x_m})$$

Y-MOMENTUM EQUATION :

$$\frac{\partial}{\partial t}(\bar{\rho}V) + \frac{1}{r}\left[\frac{\partial}{\partial x}(r\bar{\rho}UV) + \frac{\partial}{\partial r}(r\bar{\rho}VV)\right] - \frac{1}{r}\left[\frac{\partial}{\partial x}(r\mu_{4e}\frac{\partial V}{\partial x}) + \frac{\partial}{\partial r}(r\mu_{2e}\frac{\partial V}{\partial r})\right] =$$

$$-\frac{\partial P}{\partial r} + S^v \qquad (B3)$$

where

$$S^v = \frac{1}{r}\left[\frac{\partial}{\partial x}\left(r\mu_{4e}\frac{\partial U}{\partial r}\right) + \frac{\partial}{\partial r}\left(r\mu_{2e}\frac{\partial V}{\partial r}\right)\right] + \frac{1}{2}\bar{\rho}W^2 - 2\mu_{3e}\frac{V}{r^2}$$

$$- \frac{\partial}{\partial r}\left(\frac{2}{3}\bar{\rho}k\right) - \frac{1}{r}\frac{\partial}{\partial r}\left(\frac{2}{3}r\mu_{22}\frac{\partial U_m}{\partial x_m}\right) + \frac{2}{3}\frac{\mu_{33}}{r}\frac{\partial U_m}{\partial x_m}$$

θ-MOMENTUM EQUATION :

$$\frac{\partial}{\partial t}(\bar{\rho}W) + \frac{1}{r}\left[\frac{\partial}{\partial x}(r\bar{\rho}UW) + \frac{\partial}{\partial r}(r\bar{\rho}VW)\right] - \frac{1}{r}\left[\frac{\partial}{\partial x}\left(r\mu_{6e}\frac{\partial W}{\partial x}\right) + \frac{\partial}{\partial r}\left(r\mu_{5e}\frac{\partial W}{\partial r}\right)\right] =$$

$$\mu_{5e}\frac{\partial}{\partial r}\left(\frac{W}{r}\right) - \frac{1}{r}\frac{\partial}{\partial r}(\mu_{5e}W) - \frac{\bar{\rho}}{r}VW \qquad (B4)$$

k-TRANSPORT EQUATION :

$$\frac{\partial \bar{\rho}k}{\partial t} + \frac{1}{r}\left[\frac{\partial}{\partial x}(r\bar{\rho}Uk) + \frac{\partial}{\partial r}(r\bar{\rho}Vk)\right] - \frac{1}{r}\left[\frac{\partial}{\partial x}\left(r(\mu+\mu_{1k})\frac{\partial k}{\partial x}\right) + \frac{\partial}{\partial r}\left(r(\mu+\mu_{2k})\frac{\partial k}{\partial r}\right)\right]$$

$$= P_k - \bar{\rho}\varepsilon - \frac{\partial}{\partial x}\left(\mu_{4k}\frac{\partial k}{\partial r}\right) - \frac{1}{r}\frac{\partial}{\partial r}\left(r\mu_{4k}\frac{\partial k}{\partial x}\right) \qquad (B5)$$

ε-TRANSPORT EQUATION :

$$\frac{\partial \bar{\rho}\varepsilon}{\partial t} + \frac{1}{r}\left[\frac{\partial}{\partial x}(r\bar{\rho}U\varepsilon) + \frac{\partial}{\partial r}(r\rho V\varepsilon)\right] - \frac{1}{r}\left[\frac{\partial}{\partial x}\left(r(\mu+\mu_{1\varepsilon})\frac{\partial \varepsilon}{\partial x}\right) + \frac{\partial}{\partial r}\left(r(\mu+\mu_{2\varepsilon})\frac{\partial \varepsilon}{\partial r}\right)\right]$$

$$C_{\varepsilon 1}\bar{\rho}\frac{\varepsilon}{k}P_k - C_{\varepsilon 2}\bar{\rho}\frac{\varepsilon^2}{k} - \frac{\partial}{\partial x}\left(\mu_{4\varepsilon}\frac{\partial \varepsilon}{\partial r}\right) - \frac{1}{r}\frac{\partial}{\partial r}\left(r\mu_{4\varepsilon}\frac{\partial \varepsilon}{\partial x}\right) \qquad (B6)$$

where

$$P_k = \left(\overline{uu}\frac{\partial U}{\partial x} + \overline{uv}\frac{\partial U}{\partial r} + \overline{uv}\frac{\partial V}{\partial x} + \overline{vv}\frac{\partial V}{\partial r} + \overline{vw}\frac{\partial W}{\partial r} - \overline{vw}\frac{W}{r} + \overline{uw}\frac{\partial W}{\partial x} + \overline{ww}\frac{V}{r}\right) \qquad (B7)$$

$$\mu_{11}=(\frac{2}{3}\bar{\rho}k-\bar{\rho}\overline{uu})/2(\frac{\partial U}{\partial x}+\frac{1}{3}(\frac{U}{\bar{\rho}}\frac{\partial\bar{\rho}}{\partial x}+\frac{V}{\bar{\rho}}\frac{\partial\bar{\rho}}{\partial r})) \quad (B8)$$

$$\mu_{22}=(\frac{2}{3}\bar{\rho}k-\rho\overline{vv})/2(\frac{\partial V}{\partial r}+\frac{1}{3}(\frac{U}{\bar{\rho}}\frac{\partial\bar{\rho}}{\partial x}+\frac{V}{\bar{\rho}}\frac{\partial\bar{\rho}}{\partial r})) \quad (B9)$$

$$\mu_{33}=(\frac{2}{3}\bar{\rho}k-\bar{\rho}\overline{ww})/2(\frac{V}{r}+\frac{1}{3}(\frac{U}{\bar{\rho}}\frac{\partial\bar{\rho}}{\partial x}+\frac{V}{\bar{\rho}}\frac{\partial\bar{\rho}}{\partial r})) \quad (B10)$$

$$\mu_{12}=-\bar{\rho}\ \overline{uv}/(\frac{\partial U}{\partial r}+\frac{\partial V}{\partial x}) \quad (B11)$$

$$\mu_{23}=-\bar{\rho}\ \overline{vw}/(\frac{\partial W}{\partial r}-\frac{W}{r}) \quad (B12)$$

$$\mu_{31}=-\bar{\rho}\ \overline{uw}/(\frac{\partial W}{\partial x}) \quad (B13)$$

$$\mu_{1e}=\mu_{11}+\mu \quad (B14)$$

$$\mu_{2e}=\mu_{22}+\mu \quad (B15)$$

$$\mu_{3e}=\mu_{33}+\mu \quad (B16)$$

$$\mu_{4e}=\mu_{12}+\mu \quad (B17)$$

$$\mu_{5e}=\mu_{23}+\mu \quad (B18)$$

$$\mu_{6e}=\mu_{31}+\mu \quad (B19)$$

$$\mu_{1k}=C_s\bar{\rho}\frac{k}{\varepsilon}\overline{uu} \quad (B20)$$

$$\mu_{2k}=C_s\bar{\rho}\frac{k}{\varepsilon}\overline{vv} \quad (B21)$$

$$\mu_{4k}=-C_s\bar{\rho}\frac{k}{\varepsilon}\overline{uv} \quad (B22)$$

$$\mu_{1\varepsilon}=C_\varepsilon\bar{\rho}\frac{k}{\varepsilon}\overline{uu} \quad (B23)$$

$$\mu_{2\varepsilon}=C_\varepsilon\bar{\rho}\frac{k}{\varepsilon}\overline{vv} \quad (B24)$$

$$\mu_{4\varepsilon}=-C_\varepsilon\bar{\rho}\frac{k}{\varepsilon}\overline{uv} \quad (B25)$$

APPENDIX C

ALGEBRAIC-STRESS CLOSURE IN AXISYMMETRIC COORDINATES (x,r)

The Reynolds stresses are obtained by the following algebraic expression

$$P_{ij} - \frac{2}{3} B\delta_{ij}\varepsilon - C_1 \frac{\varepsilon}{k}(\overline{u_i u_j} - \frac{2}{3}\delta_{ij}k) - \alpha(P_{ij} - \frac{2}{3}\delta_{ij}P_k - \frac{2}{3}\overline{u_i u_j}\frac{\partial U_m}{\partial x_m}) \tag{C1}$$

$$-\beta(D_{ij} - \frac{2}{3}\delta_{ij}P_k - \frac{2}{3}\overline{u_i u_j}\frac{\partial U_m}{\partial x_m}) - \gamma k S_{ij} - \frac{A}{k}\overline{u_i u_j}(P_k - \varepsilon) = 0.$$

Constants A and B are equal to 1 for Rodi's model. Mellor and Yamada's model is obtained by assigining A=0 and $B=P_k/\varepsilon$ and for the equilibrium model A=0 and B=1 . In the cylindrical coordinates system, production of the Reynolds stresses and the mean strain rate are expressed as

$$P_{11} = -2(\overline{u^2}\frac{\partial U}{\partial x} + \overline{uv}\frac{\partial U}{\partial r}) \tag{C2}$$

$$P_{22} = -2(\overline{uv}\frac{\partial V}{\partial x} + \overline{v^2}\frac{\partial V}{\partial r} - \overline{vw}\frac{W}{r}) \tag{C3}$$

$$P_{33} = -2(\overline{uw}\frac{\partial W}{\partial x} + \overline{vw}\frac{\partial W}{\partial r} + \overline{w^2}\frac{V}{r}) \tag{C4}$$

$$P_{12} = -(\overline{u^2}\frac{\partial V}{\partial x} + \overline{uv}\frac{\partial V}{\partial r} - \overline{uw}\frac{W}{r} + \overline{uv}\frac{\partial U}{\partial x} + \overline{v^2}\frac{\partial U}{\partial r}) \tag{C5}$$

$$P_{23} = -(\overline{uv}\frac{\partial W}{\partial x} + \overline{v^2}\frac{\partial W}{\partial r} + \overline{vw}\frac{V}{r} + \overline{uw}\frac{\partial V}{\partial x} + \overline{vw}\frac{\partial V}{\partial r} - \overline{w^2}\frac{W}{r}) \tag{C6}$$

$$P_{13} = -(\overline{u^2}\frac{\partial W}{\partial x} + \overline{uv}\frac{\partial W}{\partial r} + \overline{uw}\frac{V}{r} + \overline{uw}\frac{\partial U}{\partial x} + \overline{vw}\frac{\partial U}{\partial r}) \tag{C7}$$

$$D_{11}=-2(\overline{u^2}\ \frac{\partial U}{\partial x}+\overline{uv}\ \frac{\partial V}{\partial x}+\overline{uw}\ \frac{\partial W}{\partial x}) \tag{C8}$$

$$D_{22}=-2(\overline{uv}\ \frac{\partial U}{\partial r}+\overline{v^2}\ \frac{\partial V}{\partial r}+\overline{vw}\ \frac{\partial W}{\partial r}) \tag{C9}$$

$$D_{33}=2(\overline{vw}\ \frac{W}{r}-\overline{w^2}\ \frac{V}{r}) \tag{C10}$$

$$D_{12}=-(\overline{u^2}\ \frac{\partial U}{\partial r}+\overline{uv}\ \frac{\partial V}{\partial r}+\overline{uw}\ \frac{\partial W}{\partial r}+\overline{uv}\ \frac{\partial U}{\partial x}+\overline{v^2}\ \frac{\partial V}{\partial x}+\overline{vw}\ \frac{\partial W}{\partial x}) \tag{C11}$$

$$D_{23}=-(\overline{w^2}\ \frac{\partial W}{\partial r}+\overline{vw}\ \frac{\partial V}{\partial r}+\overline{uw}\ \frac{\partial U}{\partial r}+\overline{vw}\ \frac{V}{r}-\overline{v^2}\ \frac{W}{r}) \tag{C12}$$

$$D_{13}=-(\overline{w^2}\ \frac{\partial W}{\partial x}+\overline{vw}\ \frac{\partial V}{\partial x}+\overline{uw}\ \frac{\partial U}{\partial x}+\overline{uw}\ \frac{V}{r}-\overline{uv}\ \frac{W}{r}) \tag{C13}$$

$$S_{11}=\frac{\partial U}{\partial x} \tag{C14}$$

$$S_{22}=\frac{\partial V}{\partial r} \tag{C15}$$

$$S_{33}=\frac{V}{r} \tag{C16}$$

$$S_{12}=.5(\frac{\partial U}{\partial r}+\frac{\partial V}{\partial x}) \tag{C17}$$

$$S_{23}=.5(\frac{\partial W}{\partial r}-\frac{W}{r}) \tag{C18}$$

$$S_{13}=.5(\frac{\partial W}{\partial x}) \tag{C19}$$

$$P_{11}=0. \tag{C20}$$

$$P_{22}=2\overline{vw}\ \frac{W}{r} \tag{C21}$$

$$P_{33}=-2\overline{vw}\ \frac{W}{r} \tag{C22}$$

$$P_{12}=\overline{uw}\ \frac{W}{r} \tag{C23}$$

$$P_{23}=(\overline{w^2}-\overline{v^2})\frac{W}{r} \tag{C24}$$

$$P_{33} = -\overline{uv}\,\frac{W}{r} \tag{C25}$$

$$P_k = -\overline{u}^2\frac{\partial U}{\partial x} - \overline{uv}\left(\frac{\partial U}{\partial r} + \frac{\partial V}{\partial x}\right) - \overline{v}^2\frac{\partial V}{\partial r} + \overline{vw}\,\frac{W}{r} - \overline{uw}\,\frac{\partial W}{\partial x} - \overline{vw}\,\frac{\partial W}{\partial r} - \overline{w}^2\,\frac{V}{r} \tag{C26}$$

APPENDIX D

ALGEBRAIC FLUX MODEL IN AXISYMMETRIC COORDIANRES (x,r)

The turbulent fluxes are obtained by the following algebraic expressions

$$-C_{1\theta}\frac{\varepsilon}{k}\overline{u\theta}-\overline{u^2}\frac{\partial\Theta}{\partial x}-\overline{uv}\frac{\partial\Theta}{\partial r}+(C_{2\theta}-1)\left(\overline{u\theta}\frac{\partial U}{\partial x}+\overline{v\theta}\frac{\partial U}{\partial r}\right)-A\frac{\overline{u\theta}}{2k}(P_k-\varepsilon)=0 \tag{D1}$$

$$-C_{1\theta}\frac{\varepsilon}{k}\overline{v\theta}-\overline{uv}\frac{\partial\Theta}{\partial x}-\overline{v^2}\frac{\partial\Theta}{\partial r}+(C_{2\theta}-1)\left(\overline{u\theta}\frac{\partial V}{\partial x}+\overline{v\theta}\frac{\partial V}{\partial r}-2\overline{w\theta}\frac{W}{r}\right)$$

$$+\overline{w\theta}\frac{W}{r}+A\frac{\overline{v\theta}}{2k}(P_k-\varepsilon)=0 \tag{D2}$$

$$-C_{1\theta}\frac{\varepsilon}{k}\overline{w\theta}-\overline{uw}\frac{\partial\Theta}{\partial x}-\overline{vw}\frac{\partial\Theta}{\partial r}+(C_{2\theta}-1)\left(\overline{u\theta}\frac{\partial W}{\partial x}+\overline{v\theta}\frac{\partial W}{\partial r}+\overline{w\theta}\frac{V}{r}+\overline{v\theta}\frac{W}{r}\right)$$

$$+A\frac{\overline{w\theta}}{2k}(P_k-\varepsilon)=0 \tag{D3}$$

Constant A is equal to 0 for Mellor and Yammada's model; and is equal to 1 for Launder and Gibson'model.

APPENDIX E

REYNOLDS-STRESS CLOSURE IN AXISYMMETRIC COORDINATES (x,r)

The Reynolds-stress transport equations are represented by

$$C_{ij} = D_{ij} + P_{ij} - \tilde{\varepsilon}_{ij} + \Pi_{ij}$$

convection = diffusion + production - dissipation + redistribution

where $\tilde{\varepsilon}_{ij} = \varepsilon_{ij} + \frac{2\nu\ \delta_{in}\ \delta_{jm}\ \overline{u_n u_m}}{(\delta_{2k}\ x_k)^2}$

In the following equations, constant A is equal to 0 for Daly and Harlow's diffusion model (Eq. 2.2.10) and for Hanjalic and Launder's model (Eq. 2.2.11) is equal to 2 for normal stresses and 1 for shear stresses.

Equation for $\overline{u^2}$:

(E1)

$$\frac{1}{r}\left[\frac{\partial(\bar{\rho} r U \overline{u^2})}{\partial x} + \frac{\partial(\bar{\rho} r V \overline{u^2})}{\partial r}\right] - \frac{1}{r}\left[\frac{\partial}{\partial x}\left[r(\mu + (A+1)C_s \bar{\rho}\frac{k}{\varepsilon}\overline{u^2})\frac{\partial \overline{u^2}}{\partial x}\right]\right.$$

$$\left. + \frac{\partial}{\partial r}\left[r(\mu + \bar{\rho} C_s \frac{k}{\varepsilon}\overline{v^2})\frac{\partial \overline{u^2}}{\partial r}\right]\right] = \frac{1}{r}\frac{\partial}{\partial r}\left[A\ r C_s \bar{\rho}\frac{k}{\varepsilon}\left(\overline{u^2}\frac{\partial \overline{uv}}{\partial x} + \right.\right.$$

$$\overline{uv}\,\frac{\partial\overline{uv}}{\partial r} - \left(\frac{\overline{uw}}{r}\right)^2\Big) + rC_s\bar{\rho}\,\frac{k}{\varepsilon}\,\overline{uv}\,\frac{\partial\overline{u^2}}{\partial x}\Big] + \frac{\partial}{\partial x}\Big[(A+1)\bar{\rho}\,C_s\,\frac{k}{\varepsilon}\,\overline{uv}\,\frac{\partial\overline{u^2}}{\partial r}\Big]$$

$$- \alpha(-2\bar{\rho}\overline{u^2}\,\frac{\partial U}{\partial x} - 2\bar{\rho}\,\overline{uv}\,\frac{\partial U}{\partial r} - \frac{2}{3}\,P_k) - \beta(-2\bar{\rho}\overline{u^2}\,\frac{\partial U}{\partial x} - 2\bar{\rho}\,\overline{uv}\,\frac{\partial V}{\partial x} -$$

$$2\bar{\rho}\,\overline{uw}\,\frac{\partial W}{\partial x} - \frac{2}{3}\,P_k) - 2\bar{\rho}\,(\overline{u^2}\,\frac{\partial U}{\partial x} + \overline{uv}\,\frac{\partial U}{\partial r}) - \gamma\bar{\rho}k\,\frac{\partial U}{\partial x} - \frac{2}{3}\,\bar{\rho}\varepsilon$$

$$- C_1\bar{\rho}\,\frac{\varepsilon}{k}\,(\overline{u^2} - \frac{2}{3}k) - \frac{2\mu\overline{u^2}}{(R-r)^2}$$

Equation for $\overline{v^2}$:

(E2)

$$\frac{1}{r}\Big[\frac{\partial(r\bar{\rho}U\overline{v^2})}{\partial x} + \frac{\partial(r\bar{\rho}V\overline{v^2})}{\partial r}\Big] - \frac{1}{r}\Big[\frac{\partial}{\partial x}\Big[r(\mu + C_s\bar{\rho}\,\frac{k}{\varepsilon}\,\overline{u^2})\,\frac{\partial\overline{v^2}}{\partial x}\Big] +$$

$$\frac{\partial}{\partial r}\Big[r(\mu + (A+1)C_s\bar{\rho}\,\frac{k}{\varepsilon}\,\overline{v^2})\,\frac{\partial\overline{v^2}}{\partial r}\Big]\Big] = \frac{\partial}{\partial x}\Big[C_s\bar{\rho}\,\frac{k}{\varepsilon}\,(\overline{uv}\,\frac{\partial\overline{v^2}}{\partial r} -$$

$$2\overline{uw}\,\frac{\overline{vw}}{r}) + A\,\bar{\rho}\,C_s\,\frac{k}{\varepsilon}\,(\overline{uv}\,\frac{\partial\overline{uv}}{\partial x} + \overline{v^2}\,\frac{\partial\overline{uv}}{\partial r} - \overline{vw}\,\frac{\overline{uw}}{r})\Big] +$$

$$\frac{1}{r}\,\frac{\partial}{\partial r}\Big[(A+1)r\,\bar{\rho}\,C_s\,\frac{k}{\varepsilon}\Big[\overline{uv}\,\frac{\partial\overline{v^2}}{\partial x} - 2\,(\frac{\overline{vw}}{r})^2\Big]\Big] - \frac{2+A}{r}\,\bar{\rho}\,C_s\,\frac{k}{\varepsilon}\Big[\overline{uw}\,\frac{\partial\overline{vw}}{\partial x}$$

$$+\overline{vw}\,\frac{\partial\overline{vw}}{\partial r} + \overline{w^2}\,(\frac{\overline{v^2} - \overline{w^2}}{r})\Big] - \frac{A}{r}\,C_s\bar{\rho}\,\frac{k}{\varepsilon}\Big[\overline{uv}\,\frac{\partial\overline{w^2}}{\partial x} + \overline{v^2}\,\frac{\partial\overline{w^2}}{\partial r} +$$

$$2\left(\frac{\overline{vw}}{r}\right)^2\Big] - 2\bar{\rho}\left(\overline{uv}\,\frac{\partial V}{\partial x} + \overline{v^2}\,\frac{\partial V}{\partial r} - \overline{vw}\,\frac{W}{r}\right) - C_1\bar{\rho}\,\frac{\varepsilon}{k}\left(\overline{v^2} - \frac{2}{3}k\right) -$$

$$\alpha\left(-2\bar{\rho}\,\overline{uv}\,\frac{\partial V}{\partial x} - 2\bar{\rho}\,\overline{v^2}\,\frac{\partial V}{\partial r} + 2\bar{\rho}\,\overline{vw}\,\frac{W}{r} - \frac{2}{3}P_k\right) - \beta\left(-2\bar{\rho}\,\overline{uv}\,\frac{\partial U}{\partial r} -\right.$$

$$\left.2\bar{\rho}\,\overline{v^2}\,\frac{\partial V}{\partial r} - 2\bar{\rho}\,\overline{vw}\,\frac{\partial W}{\partial r} - \frac{2}{3}P_k\right) - \gamma\bar{\rho}k\,\frac{\partial V}{\partial r} - \frac{2}{3}\bar{\rho}\varepsilon + 2\bar{\rho}\,\overline{vw}\,\frac{W}{r} - \frac{2\mu\overline{v^2}}{(R-r)^2}$$

Equation for $\overline{w^2}$:

(E3)

$$\frac{1}{r}\left[\frac{\partial(r\bar{\rho}U\overline{w^2})}{\partial x} + \frac{\partial(r\bar{\rho}V\overline{w^2})}{\partial r}\right] - \frac{1}{r}\left[\frac{\partial}{\partial x}\left[r\left(\mu + C_s\bar{\rho}\,\frac{k}{\varepsilon}\,\overline{u^2}\right)\frac{\partial\overline{w^2}}{\partial x}\right] +\right.$$

$$\left.\frac{\partial}{\partial r}\left[r\left(\mu + C_s\bar{\rho}\,\frac{k}{\varepsilon}\,\overline{v^2}\right)\frac{\partial\overline{w^2}}{\partial r}\right]\right] = \frac{\partial}{\partial x}\left[C_s\bar{\rho}\,\frac{k}{\varepsilon}\left(\overline{uv}\,\frac{\partial\overline{w^2}}{\partial r} + 2\overline{uw}\,\frac{\overline{vw}}{r}\right) +\right.$$

$$\left.A\,C_s\bar{\rho}\,\frac{k}{\varepsilon}\left(\overline{uw}\,\frac{\partial\overline{uw}}{\partial x} + \overline{vw}\,\frac{\partial\overline{uw}}{\partial r} + \overline{w^2}\,\frac{\overline{uv}}{r}\right)\right] +$$

$$\frac{1}{r}\frac{\partial}{\partial r}\left[r\bar{\rho}C_s\,\frac{k}{\varepsilon}\left[\left(\overline{uv}\,\frac{\partial\overline{w^2}}{\partial x} + 2\,\frac{(\overline{vw})^2}{r}\right) + A\left(\overline{uw}\,\frac{\partial\overline{vw}}{\partial x} + \overline{vw}\,\frac{\partial\overline{vw}}{\partial r} +\right.\right.\right.$$

$$\left.\left.\left.\overline{w^2}\,\frac{\overline{v^2} - \overline{w^2}}{r}\right)\right]\right] + \frac{1}{r}C_s\bar{\rho}\,\frac{k}{\varepsilon}\left[(2+A)\left[\overline{uw}\,\frac{\partial\overline{vw}}{\partial x} + \overline{vw}\,\frac{\partial\overline{vw}}{\partial r} +\right.\right.$$

$$\left.\left.\overline{w^2}\,\frac{\overline{v^2} - \overline{w^2}}{r}\right] + A\left[\overline{uv}\,\frac{\partial\overline{w^2}}{\partial x} + \overline{v^2}\,\frac{\partial\overline{w^2}}{\partial r} + 2\,\frac{(\overline{vw})^2}{r}\right]\right] - \bar{\rho}\gamma k\,\frac{V}{r} -$$

$$-2\bar{\rho}\ (\overline{uw}\ \frac{\partial W}{\partial x} + \overline{vw}\ \frac{\partial W}{\partial r} + \overline{w^2}\ \frac{V}{r}) - C_1\bar{\rho}\ \frac{\varepsilon}{k}\ (\overline{w^2} - \frac{2}{3}k) - \alpha(-2\bar{\rho}\ \overline{uw}\ \frac{\partial W}{\partial x} -$$

$$2\bar{\rho}\ \overline{vw}\ \frac{\partial W}{\partial r} - 2\bar{\rho}\ \overline{w^2}\ \frac{V}{r} - \frac{2}{3}\ P_k) - \beta(2\bar{\rho}\ \overline{vw}\ \frac{W}{r} - 2\bar{\rho}\ \overline{w2}\ \frac{V}{r} - \frac{2}{3}\ P_k) -$$

$$\frac{2}{3}\ \bar{\rho}\ \varepsilon - 2\bar{\rho}\ \overline{vw}\ \frac{W}{r} - \frac{2\mu\overline{w^2}}{(R-r)^2}$$

Equation for $\overline{uv}$:

(E4)

$$\frac{1}{r}\left[\ \frac{\partial(r\bar{\rho}U\overline{uv})}{\partial x} + \frac{\partial(r\bar{\rho}V\overline{uv})}{\partial r}\ \right] - \frac{1}{r}\left[\ \frac{\partial}{\partial x}\left[r(\mu + (A+1)\bar{\rho}C_s\ \frac{k}{\varepsilon}\ \overline{u^2})\frac{\partial\overline{uv}}{\partial x}\ \right]\right.$$

$$\left. + \frac{\partial}{\partial r}\left[r(\mu + (A+1)\bar{\rho}C_s\ \frac{k}{\varepsilon}\ \overline{v^2})\ \frac{\partial\overline{uv}}{\partial r}\ \right]\right] = \frac{\partial}{\partial x}\left[\bar{\rho}\ C_s\ \frac{k}{\varepsilon}\left[(A+1)(\overline{uv}\ \frac{\partial\overline{uv}}{\partial r}\right.\right.$$

$$\left. - (\frac{\overline{uw}}{r})^2) + A(\overline{uv}\ \frac{\partial\overline{u^2}}{\partial x} + \overline{v^2}\ \frac{\partial\overline{u^2}}{\partial r}\ )\right]\right] + \frac{1}{r}\ \frac{\partial}{\partial r}\left[rC_s\bar{\rho}\ \frac{k}{\varepsilon}\left[(A+1)(\overline{uv}\ \frac{\partial\overline{uv}}{\partial x}\right.\right.$$

$$\left. - \overline{vw}\ \frac{\overline{uw}}{r}\ ) + A(\overline{u^2}\ \frac{\partial\overline{v^2}}{\partial x} + \overline{uv}\ \frac{\partial\overline{v^2}}{\partial r} - 2\overline{uw}\ \frac{\overline{vw}}{r}\ )\right]\right] - \frac{1}{r}\ \bar{\rho}C_s\ \frac{k}{\varepsilon}$$

$$\left[(A+1)\left[\overline{uw}\ \frac{\partial\overline{uw}}{\partial x} + \overline{vw}\ \frac{\partial\overline{uw}}{\partial r} + \overline{w^2}\ \frac{\overline{uv}}{r}\right] + A\left[\overline{u^2}\ \frac{\partial\overline{w^2}}{\partial x} + \overline{uv}\ \frac{\partial\overline{w^2}}{\partial r} + 2\overline{uw}\ \frac{\overline{vw}}{r}\right]\right]$$

$$+\bar{\rho}\ \overline{uw}\ \frac{W}{r} - \bar{\rho}(\overline{u^2}\ \frac{\partial V}{\partial x} + \overline{uv}\ \frac{\partial V}{\partial r} - \overline{uw}\ \frac{W}{r} + \overline{uv}\ \frac{\partial U}{\partial x} + \overline{v^2}\ \frac{\partial U}{\partial r}\ ) - C_1\bar{\rho}\ \frac{\varepsilon}{k}\ \overline{uv}$$

$$- \alpha\ \bar{\rho}(-\ \overline{u^2}\ \frac{\partial V}{\partial x} - \overline{uv}\ \frac{\partial V}{\partial r} + \overline{uw}\ \frac{W}{r} - \overline{uv}\ \frac{\partial U}{\partial x} - \overline{v^2}\ \frac{\partial U}{\partial r}\ )$$

$$-\beta\bar{\rho}\left[-\overline{u^2}\,\frac{\partial U}{\partial r}-\overline{uw}\,\frac{\partial W}{\partial r}-\overline{v^2}\,\frac{\partial V}{\partial x}-\overline{vw}\,\frac{\partial W}{\partial x}-\overline{uv}\left(\frac{\partial V}{\partial r}+\frac{\partial U}{\partial x}\right)\right]$$

$$-\bar{\rho}\,\gamma\,\frac{k}{2}\left(\frac{\partial U}{\partial r}+\frac{\partial V}{\partial x}\right)-\frac{2\mu\overline{uv}}{(R-r)^2}$$

Equation for $\overline{vw}$:

(E5)

$$\frac{1}{r}\left[\frac{\partial(r\bar{\rho}U\overline{vw})}{\partial x}+\frac{\partial(r\bar{\rho}V\overline{vw})}{\partial r}\right]-\frac{1}{r}\left[\frac{\partial}{\partial x}\left[r\left(\mu+C_s\bar{\rho}\,\frac{k}{\varepsilon}\,\overline{u^2}\right)\frac{\partial\overline{vw}}{\partial x}\right]+\right.$$

$$\left.\frac{\partial}{\partial r}\left[r\left(\mu+(A+1)\,C_s\bar{\rho}\,\frac{k}{\varepsilon}\,\overline{v^2}\right)\frac{\partial\overline{vw}}{\partial r}\right]\right]=\frac{\partial}{\partial x}\left[C_s\bar{\rho}\,\frac{k}{\varepsilon}\left[\overline{uv}\,\frac{\partial\overline{vw}}{\partial r}+\right.\right.$$

$$\overline{uw}\,\frac{\overline{v^2}-\overline{w^2}}{r}+A\left(\overline{uv}\,\frac{\partial\overline{uw}}{\partial x}+\overline{v^2}\,\frac{\partial\overline{uw}}{\partial r}+\overline{vw}\,\frac{\overline{uv}}{r}+\overline{uw}\,\frac{\partial\overline{uv}}{\partial x}+\overline{vw}\,\frac{\partial\overline{uv}}{\partial r}-\right.$$

$$\left.\left.\left.\overline{w^2}\,\frac{\overline{uw}}{r}\right)\right]\right]+\frac{1}{r}\,\frac{\partial}{\partial r}\left[C_s\bar{\rho}\,r\,\frac{k}{\varepsilon}\left[(A+1)\left(\overline{vw}\,\frac{\overline{v^2}-\overline{w^2}}{r}+\overline{uv}\frac{\partial\overline{vw}}{\partial x}\right)+A\left(\overline{vw}\,\frac{\partial\overline{v^2}}{\partial r}-\right.\right.\right.$$

$$\left.\left.\left.2\overline{w^2}\,\frac{\overline{vw}}{r}+uw\frac{\partial\overline{v^2}}{\partial x}\right)\right]\right]+\frac{1}{r}\,C_s\bar{\rho}\,\frac{k}{\varepsilon}\left[\overline{vw}\,\frac{\partial}{\partial r}(\overline{v^2}-\overline{w^2})-4\overline{w^2}\,\frac{\overline{vw}}{r}+\overline{uw}\frac{\partial}{\partial x}(\overline{v^2}-\overline{w^2})\right.$$

$$+2A\left[-\overline{uw}\,\frac{\partial\overline{w^2}}{\partial x}-\overline{vw}\,\frac{\partial\overline{w^2}}{\partial r}-\overline{w^2}\,\frac{2\overline{vw}}{r}+\overline{uv}\,\frac{\partial\overline{vw}}{\partial x}+\overline{v^2}\,\frac{\partial\overline{vw}}{\partial r}+\right.$$

$$\left.\left.\overline{vw}\,\frac{\overline{v^2}-\overline{w^2}}{r}\right]\right]+\bar{\rho}\left(-\overline{uv}\,\frac{\partial W}{\partial x}-\overline{v^2}\,\frac{\partial W}{\partial r}+\overline{vw}\,\frac{\partial U}{\partial x}+\overline{w^2}\,\frac{W}{r}-\overline{uw}\,\frac{\partial V}{\partial x}\right)-C_1\bar{\rho}\,\frac{\varepsilon}{k}\,\overline{vw}-$$

$$\alpha\bar{\rho}\left(-\overline{uv}\frac{\partial W}{\partial x}-\overline{v^2}\frac{\partial W}{\partial r}+\overline{vw}\frac{\partial U}{\partial x}+\overline{w^2}\frac{W}{r}-\overline{uw}\frac{\partial V}{\partial x}\right)-\bar{\rho}\beta\left(\overline{v^2}\frac{W}{r}+\overline{vw}\frac{\partial U}{\partial x}-\overline{uw}\frac{\partial U}{\partial r}-\overline{w^2}\frac{\partial W}{\partial r}\right)$$

$$-\gamma\bar{\rho}\,\frac{k}{2}\,r\,\frac{\partial}{\partial r}\left(\frac{W}{r}\right)-\bar{\rho}\left(\overline{v^2}-\overline{w^2}\right)\frac{W}{r}-\frac{2\mu vw}{(R-r)^2}$$

Equation for $\overline{uw}$:

(E6)

$$\frac{1}{r}\left[\frac{\partial(r\bar{\rho}U\overline{uw})}{\partial x}+\frac{\partial(r\bar{\rho}V\overline{uw})}{\partial r}\right]-\frac{1}{r}\left[\frac{\partial}{\partial x}\left[r\left(\mu+(A+1)C_s\bar{\rho}\,\frac{k}{\varepsilon}\overline{u^2}\right)\frac{\partial\overline{uw}}{\partial x}\right]\right.$$

$$\left.+\frac{\partial}{\partial r}\left[r\left(\mu+C_s\bar{\rho}\,\frac{k}{\varepsilon}\,\overline{v^2}\right)\frac{\partial\overline{uw}}{\partial r}\right]\right]=\frac{\partial}{\partial x}\left[C_s\bar{\rho}\,\frac{k}{\varepsilon}\left[(A+1)\left(\overline{uv}\,\frac{\partial\overline{uw}}{\partial r}+\overline{uw}\,\frac{\overline{uv}}{r}\right)+\right.\right.$$

$$\left.\left.A\left(\overline{uw}\frac{\partial\overline{u^2}}{\partial x}+\overline{vw}\,\frac{\partial\overline{u^2}}{\partial r}\right)\right]\right]+\frac{1}{r}\,\frac{\partial}{\partial r}\left[rC_s\bar{\rho}\,\frac{k}{\varepsilon}\left[\overline{uv}\frac{\partial\overline{uw}}{\partial x}+\overline{vw}\frac{\overline{uv}}{r}+A\left(\overline{u^2}\frac{\partial\overline{vw}}{\partial x}+\overline{uv}\frac{\partial\overline{vw}}{\partial r}+\right.\right.\right.$$

$$\left.\left.\left.\overline{uw}\frac{\overline{v^2}-\overline{w^2}}{r}+\overline{uw}\frac{\partial\overline{uv}}{\partial x}+\overline{vw}\frac{\partial\overline{uv}}{\partial r}-\overline{w^2}\frac{\overline{uw}}{r}\right)\right]\right]+\frac{1}{r}\,C_s\bar{\rho}\frac{k}{\varepsilon}\left[\overline{uw}\frac{\partial\overline{uv}}{\partial x}+\overline{vw}\frac{\partial\overline{uv}}{\partial r}-\overline{w^2}\frac{\overline{uw}}{r}\right.$$

$$\left.+A\left[\overline{uv}\frac{\partial\overline{uw}}{\partial x}+\overline{v^2}\frac{\partial\overline{uw}}{\partial r}+\overline{vw}\frac{\overline{uv}}{r}+\overline{u^2}\frac{\partial\overline{vw}}{\partial x}+\overline{uv}\frac{\partial\overline{vw}}{\partial r}+\overline{uw}\frac{\overline{v^2}-\overline{w^2}}{r}\right]\right]+\bar{\rho}\left(-\overline{u^2}\frac{\partial W}{\partial x}\right.$$

$$\left.-\overline{uv}\frac{\partial W}{\partial r}-\overline{vw}\frac{\partial U}{\partial r}+\overline{uw}\frac{\partial V}{\partial r}\right)(1-\alpha)-\beta\bar{\rho}\left(\overline{uv}\frac{W}{r}+\overline{uw}\frac{\partial V}{\partial r}-\overline{w^2}\frac{\partial W}{\partial x}-\overline{vw}\frac{\partial V}{\partial x}\right)$$

$$-\frac{1}{2}\gamma\bar{\rho}k\frac{\partial W}{\partial x}-C_1\bar{\rho}\,\frac{\varepsilon}{k}\,\overline{uw}-\bar{\rho}\,\overline{uv}\,\frac{W}{r}-\frac{2\mu\overline{uw}}{(R-r)^2}$$

APPENDIX F

THE SCALAR FLUX TRANSPORT CLOSURE

Equation for $\overline{u\theta}$:

(F1)

$$\frac{1}{r}\left[\frac{\partial(r\bar{\rho}U\overline{u\theta})}{\partial x}+\frac{\partial(r\bar{\rho}V\overline{u\theta})}{\partial r}\right]-\frac{1}{r}\left[\frac{\partial}{\partial x}\left(2r\bar{\rho}C_{s\theta}\frac{k}{\varepsilon}\overline{u^2}\frac{\partial\overline{u\theta}}{\partial x}\right)+\right.$$

$$\left.\frac{\partial}{\partial r}\left(r\bar{\rho}C_{s\theta}\frac{k}{\varepsilon}\overline{v^2}\frac{\partial\overline{u\theta}}{\partial r}\right)\right]=\frac{\partial}{\partial x}\left(2\bar{\rho}C_{s\theta}\frac{k}{\varepsilon}\overline{uv}\frac{\partial\overline{u\theta}}{\partial r}\right)$$

$$+\frac{1}{r}\frac{\partial}{\partial r}\left[r\bar{\rho}C_{s\theta}\frac{k}{\varepsilon}\left(\overline{uv}\frac{\partial\overline{u\theta}}{\partial x}+\overline{uv}\frac{\partial\overline{v\theta}}{\partial r}+\overline{u^2}\frac{\partial\overline{v\theta}}{\partial x}-\overline{uw}\frac{\overline{w\theta}}{r}\right)\right]$$

$$-\bar{\rho}\left[\overline{u^2}\frac{\partial\Theta}{\partial x}+\overline{uv}\frac{\partial\Theta}{\partial r}+\overline{u\theta}\frac{\partial U}{\partial x}+\overline{v\theta}\frac{\partial U}{\partial r}\right]-C_{1\theta}\bar{\rho}\frac{\varepsilon}{k}\overline{u\theta}$$

Equation for $\overline{v\theta}$:

(F2)

$$\frac{1}{r}\left[\frac{\partial(r\bar{\rho}U\overline{v\theta})}{\partial x}+\frac{\partial(r\bar{\rho}V\overline{v\theta})}{\partial r}\right]-\frac{1}{r}\left[\frac{\partial}{\partial x}\left(r\bar{\rho}C_{s\theta}\frac{k}{\varepsilon}\overline{u^2}\frac{\partial\overline{v\theta}}{\partial x}\right)+\right.$$

$$\left.\frac{\partial}{\partial r}\left(2r\bar{\rho}C_{s\theta}\frac{k}{\varepsilon}\overline{v^2}\frac{\partial\overline{v\theta}}{\partial r}\right)\right]=\frac{\partial}{\partial x}\left[\bar{\rho}C_{s\theta}\frac{k}{\varepsilon}\left(\overline{uv}\frac{\partial\overline{v\theta}}{\partial r}-\overline{uv}\frac{\overline{w\theta}}{r}+\right.\right.$$

$$\overline{uv}\,\frac{\partial \overline{u\theta}}{\partial x} + \overline{v^2}\,\frac{\partial \overline{u\theta}}{\partial r}\Big)\Big] + \frac{1}{r}\frac{\partial}{\partial r}\Big[r\bar{\rho}C_{s\theta}\,\frac{k}{\varepsilon}\,\Big(2\overline{uv}\,\frac{\partial \overline{v\theta}}{\partial x} - \overline{w\theta}\,\frac{\overline{v^2}}{r} -$$

$$\overline{vw}\,\frac{\overline{w\theta}}{r}\Big)\Big] + \frac{W}{r}\,\overline{w\theta}\,\bar{\rho} - \bar{\rho}\Big[\overline{u\theta}\,\frac{\partial V}{\partial x} + \overline{v\theta}\,\frac{\partial V}{\partial r} - 2\overline{w\theta}\,\frac{W}{r} + \overline{uv}\,\frac{\partial \Theta}{\partial x} + \overline{v^2}\,\frac{\partial \Theta}{\partial r}\Big]$$

$$- C_{1\theta}\,\frac{\varepsilon}{k}\,\overline{v\theta}$$

Equation for $\overline{w\theta}$:

(F3)

$$\frac{1}{r}\Big[\frac{\partial(r\bar{\rho}U\overline{w\theta})}{\partial x} + \frac{\partial(r\bar{\rho}V\overline{w\theta})}{\partial r}\Big] - \frac{1}{r}\Big[\frac{\partial}{\partial x}(r\bar{\rho}C_{s\theta}\,\frac{k}{\varepsilon}\,\overline{u^2}\,\frac{\partial \overline{w\theta}}{\partial x}) +$$

$$\frac{\partial}{\partial r}(r\bar{\rho}C_{s\theta}\,\frac{k}{\varepsilon}\,\overline{v^2}\,\frac{\partial \overline{w\theta}}{\partial r})\Big] = \frac{\partial}{\partial x}\Big[\bar{\rho}C_{s\theta}\,\frac{k}{\varepsilon}\,(\overline{uv}\,\frac{\partial \overline{w\theta}}{\partial r} + \overline{uw}\,\frac{\overline{v\theta}}{r} +$$

$$\overline{uw}\,\frac{\partial \overline{u\theta}}{\partial x} + \overline{vw}\,\frac{\partial \overline{u\theta}}{\partial r})\Big] + \frac{1}{r}\frac{\partial}{\partial r}\Big[r\bar{\rho}C_{s\theta}\,\frac{k}{\varepsilon}\,(\overline{uv}\,\frac{\partial \overline{w\theta}}{\partial x} + \overline{vw}\,\frac{\overline{v\theta}}{r} +$$

$$\overline{uw}\,\frac{\partial \overline{v\theta}}{\partial x} + \overline{vw}\,\frac{\partial \overline{v\theta}}{\partial r} - \overline{w^2}\,\frac{\overline{w\theta}}{r})\Big] - \bar{\rho}\Big[\overline{uw}\,\frac{\partial \Theta}{\partial x} + \overline{vw}\,\frac{\partial \Theta}{\partial r} + \overline{u\theta}\,\frac{\partial W}{\partial x} +$$

$$\overline{v\theta}\,\frac{\partial W}{\partial r} + \overline{w\theta}\,\frac{V}{r} + \overline{v\theta}\,\frac{W}{r}\Big] - C_{1\theta}\,\bar{\rho}\,\frac{\varepsilon}{k}\,\overline{w\theta}$$

APPENDIX G

BOUNDARY CONDITIONS FOR HIGH REYNOLDS-NUMBER MODELS

Differential transport equations for various turbulence quantities were introduced in chapter two. There exist an infinite number fields that satisfy the same set of equations, and only the boundary conditions distinguish one type of flow from another. Thus consideration of boundary conditions is very important. Most turbulence models are devised for high Reynolds number flows. However, in the vicinity of the solid boundaries the low Reynolds number effects become significant and must be accounted for. This can be performed either by solving the low Reynolds number version of the transport equations or by developing wall functions that introduce these effects into the existing high Reynolds number models. The first option predicts the near wall region better but it needs vast amount of computer time. In the high Reynolds models, it is assumed that the distribution of mean velocity and turbulence quantities throughout the main part of the flow is weakly dependent on the model of the turbulent transport in the immediate wall vicinity and the conventional logarithmic law which is based on the local equilibrium is applied. Details of this sort of

bounadary condition for high Reynolds number models are given in the following sub-sections.

G.1 NEAR-WALL VELOCITY PROFILE

In general, near the wall, one dimensional couette flow analysis is made. In this region shear stress is assumed to be constant. This condition is true only for an impermeable wall, with negligible streamwise pressure gradient. The wall region is made up of three zones: The viscous sublayer, transition or buffer zone, and inertial sublayer. Our approach is to dispose of the buffer layer by defining a point $y^+=11.63$ below which the flow is assumed to be purely viscous and above which it is purely turbulent. The law of the wall may be expressed as

$$\begin{aligned} &\overset{+}{y} \quad 11.63 && \overset{+}{u} = \overset{+}{y} \\ &\overset{+}{y} > 11.63 && \overset{+}{u} = \frac{1}{\kappa} \ell n(\overset{*}{E}\, \overset{+}{y}) \end{aligned} \tag{G1}$$

where

$$\overset{+}{y} = \frac{u_\tau y}{\nu} \quad ; \quad \overset{+}{u} = \frac{U}{u_\tau} \quad ; \quad u_\tau^2 = \frac{\tau_w}{\rho}$$

κ = Van Karman conastant = .4187

$\overset{*}{E}$ = Roughness Parameter = 9.973

G.2 NEAR-WALL TURBULENCE KINETIC ENERGYY BUDGET AND DISSIPATION RATE

The near-wall kinetic energy levels are obtained from the solution of the k transport equation. The convection and diffusion terms are treated by hybrid differencing while the production and dissipation terms need to be changed to include the near wall effects. The approach is based on one dimensional, constant shear stress couette layer. In the inertial sublayer and in the absence of buoyancy effects, the local rate of production of turbulence is balanced by the viscous dissipation rate ϵ which, together with eddy viscosity and the fact that the shear stress is approximately equall to the wall shear stress τ_w ,leads to

$$k = \frac{u_\tau^2}{\sqrt{C_\mu}} \qquad \text{(G2)}$$

From equation (G2) the surface shear stress may be found as

$$\tau_s = \frac{\bar{\rho}\ \kappa\ \sqrt{k}\ U\ C_\mu^{.25}}{\ell n(\overset{*}{E}\ \overset{+}{y})} \qquad \text{(G3)}$$

The mean production rate of k per unit volume can then be found as

$$\text{MEAN PRODUCTION RATE} = \tau_s \, U_p / y_p \qquad \text{(G4)}$$

where y_p being the distance of the near wall grid point from the the wall and U_p is the velocity at that point.

In wall-flows, unlike turbulent kinetic energy which falls to zero at the wall , ϵ reaches its highest value at the wall. With local equilibrium assumption

$$\epsilon = u_\tau^2 \frac{\partial U}{\partial y}$$

and $\partial U/\partial y$ from (G3), there results the following boundary condition for ϵ:

$$\epsilon = \frac{u_\tau^3}{\kappa y} \qquad \text{(G5)}$$

G.3 NEAR-WALL SCALAR PROFILE

For an impermeable wall with zero streamwise pressure gradient, the scalar flux at pont P near the wall can be written as

$$J_{\theta,s} = - \frac{\Theta_p \sqrt{(\tau_s \rho)}}{\theta^+} \qquad \text{(G6)}$$

where

$$\theta^+ = \sigma_{\theta,t} \, (u^+ + PF) \qquad (G7)$$

The quantity PF in Eq. (G7) is a following Van Driest Function:

$$PF = (.25\pi/\mathrm{Sin}(\pi/4)) \; (\kappa/26)^{-.5} \, (-1 + \sigma/\sigma_t)(\sigma/\sigma_t)^{-.25} \qquad (G8)$$

where σ and σ_t are the the molecular and turbulent prndtl number for scalar

G.4 SYMMETRY CONDITIONS

At symmetry plane, the normal gradients are zero for all quantities with symmetrical behavior such as scalar quantities and velocity components parallel to the symmetry plane or line

G.5 INLET CONDITIONS

For flows without swirl, the radial component of velocity is set to zero and axial velocity can be specified either by a fully developed pipe flow condition or by information from expeimental data. In swirl flows, howevere, an accurate specification of velocities is required for a better comaprison with measurement. The turbulent kinetic energy profile either is calculated by the mixing length

hypothesis or is determined from the experimental data. The inlet dissipation rate is calculated from the following expression

$$\epsilon = \frac{k^{1.5}}{\ell}$$

where ℓ is the turbulent length scale.

1. Report No.	2. Government Accession No.	3. Recipient's Catalog No.
NASA CR-4041		

4. Title and Subtitle	5. Report Date
On the Modelling of Non-Reactive and Reactive Turbulent Combustor Flows	April 1987
	6. Performing Organization Code

7. Author(s)	8. Performing Organization Report No.
Mohammad Nikjooy and Ronald M. C. So	CR-R86091 (E-3451)
	10. Work Unit No. 505-62-21

9. Performing Organization Name and Address	11. Contract or Grant No.
Arizona State University Mechanical and Aerospace Engineering Tempe, Arizona 85287	NAG3-167 and NAG3-260
	13. Type of Report and Period Covered Contractor Report Final
12. Sponsoring Agency Name and Address NASA Lewis Research Center Cleveland, Ohio 44135 and Defense Advanced Research Project Agency Arlington, Virginia 22209	14. Sponsoring Agency Code

15. Supplementary Notes

Project Managers, James D. Holdeman, Internal Fluid Mechanics Division, NASA Lewis Research Center and F. Zarlingo, Naval Weapons Center, China Lake, California 92555 (cofunded under NWC Contract N60530-85-C-0191).

16. Abstract

A numerical study of non-reactive and reactive axisymmetric combustor flows with and without swirl is presented. Closure of the Reynolds equations is achieved by three different levels of models; k-ε, algebraic stress and Reynolds stress closure. Performance of two locally non-equilibrium and one equilibrium algebraic stress models is analyzed assuming four different pressure-strain models. A comparison is also made of the performance of a high and a low Reynolds number model for combustor flow calculations using Reynolds stress closures. Effects of diffusion and pressure-strain models on these closures are also investigated. Two different models for the scalar transport are presented. One employs the second-moment closure which solves the transport equations for the scalar fluxes, while the other solves the algebraic equations for the scalar fluxes. In addition, two cases of non-premixed and one case of premixed combustion are considered. Fast- and finite-rate chemistry models are applied to non-premixed combustion. Both models show promise for application in gas turbine combustors. However, finite rate chemistry models, which are more realistic, need to be further examined to establish a suitable coupling of the heat release effects on the turbulence field and the rate constants.

17. Key Words (Suggested by Author(s))	18. Distribution Statement
Combustor flows; Turbulent flow modelling; Reactive flow modelling; Reynolds-stress closures; Algebraic stress closures; Premixed flames; Non-premixed flames	Unclassified - unlimited STAR Category 07

19. Security Classif. (of this report)	20. Security Classif. (of this page)	21. No. of pages	22. Price*
Unclassified	Unclassified	269	A12

*For sale by the National Technical Information Service, Springfield, Virginia 22161

NASA-Langley, 1987